Measuring and Thermodynamic Modeling of De-Mixing CO2 Capture Systems

Arshad, Muhammad Waseem; Thomsen, Kaj; von Solms, Nicolas

Publication date:
2014

Document Version
Publisher's PDF, also known as Version of record

Measuring and Thermodynamic Modeling of De-Mixing CO_2 Capture Systems

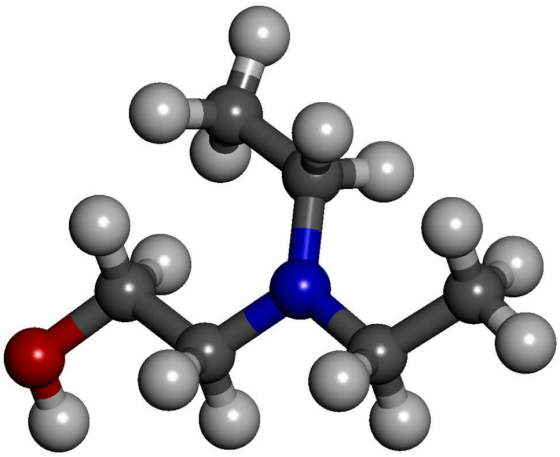

2–(Diethylamino)ethanol (DEEA)

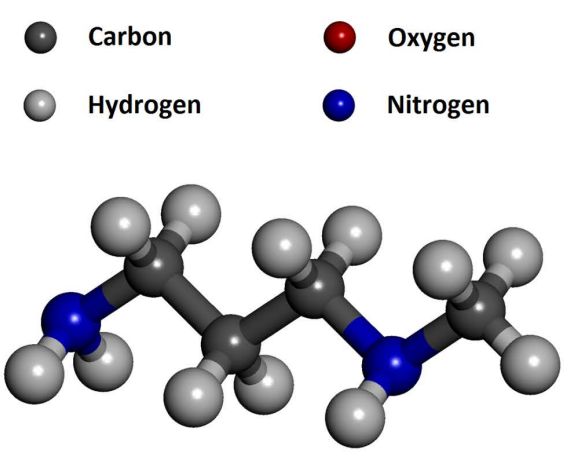

3–(Methylamino)propylamine (MAPA)

Muhammad Waseem Arshad
Ph.D. Thesis
June 2014

DTU Chemical Engineering
Department of Chemical and Biochemical Engineering

Measuring and Thermodynamic Modeling of De-Mixing CO_2 Capture Systems

Muhammad Waseem Arshad

PhD Thesis

June, 2014

Center for Energy Resources Engineering
Department of Chemical and Biochemical Engineering
Technical University of Denmark
DK-2800 Kongens Lyngby
Denmark

DTU Chemical Engineering
Department of Chemical and Biochemical

Address: Center for Energy Resources Engineering
Department of Chemical and
Biochemical Engineering
Technical University of Denmark
Søltofts Plads, Building 229
DK-2800 Kgs. Lyngby
Denmark
Phone: +45 4525 2800
Fax: +45 4525 4588
Web: www.cere.dtu.dk

Print: J&R Frydenberg A/S
København
December 2014

ISBN: 978-87-93054-55-4

Preface

This thesis is submitted to the Technical University of Denmark (DTU) as a partial fulfillment of the requirements for obtaining the degree of Doctor of Philosophy (PhD). This work has been carried out at the Center for Energy Resources Engineering (CERE), Department of Chemical and Biochemical Engineering at DTU under the supervision of Associate Professor Kaj Thomsen as a main supervisor and Associate Professor Nicolas von Solms as a co-supervisor. As a part of external research, six months of work has been carried out at the Department of Chemical Engineering at Norwegian University of Science and Technology (NTNU) under the supervision of Professor Hallvard Fjøsne Svendsen.

The present work, *Measuring and Thermodynamic Modeling of De-Mixing CO_2 Capture Systems*, also presents a contribution to the European research project iCap - Innovative CO_2 Capture. The project was financially supported by European Commission under the 7th Framework Program (Grant Agreement No. 241393) through the iCap project.

The iCap Project:

"iCap is an R&D project whose objective is to develop new CO_2 capture technologies that individually and combined will enable highly efficient and cost effective production of electrical power from fossil fuels with near zero emissions. The target is to reduce the CO_2 capture energy penalty to 4-5% points, about half of the penalty today, and to reduce the associated CO_2 avoidance cost to 15 €/tonne CO_2. iCap focuses on post combustion technologies that can be used both for retrofit and for green field plants.

iCap is a 4 years project consisting of a consortium of 15 partners, including European R&D organisations, an industrial group, and partners from Australia and China. The project is supported by the European Commission under the 7th Framework Program Contract No: 241393 and is coordinated by the Norwegian University of Science and Technology."

http://icapco2.org/0/31/home/ (June, 2014)

Muhammad Waseem Arshad
Kongens Lyngby, Denmark
13 June, 2014

Acknowledgements

First and foremost, I would like to thank my supervisor Kaj Thomsen and express my deep gratitude for his guidance and support throughout my thesis work. I am also grateful to him for allowing me the freedom in my research work. I feel fortunate to have had the opportunity to work with such a wonderful person both in my MSc and PhD. I found him very humble, friendly and supportive. I am grateful to my co-supervisor Nicolas von Solms for his support and for presenting my work in the iCap technical meetings. Besides the research work, it was always nice to talk to you about Cricket.

I would like to acknowledge the iCap consortium for financially supporting the project. I also wish to thank Erling H. Stenby and Philip L. Fosbøl for their efforts in establishing the funding and making DTU a part of the iCap project.

I am very grateful to Assistant Professor Philip L. Fosbøl for his support in the experimental work at CERE and thank you for the nice traveling and sightseeing together. I would like to thank all my colleagues for the nice research and social environment at CERE. Thanks to Victor Darde for the valuable support in the Electrolyte course. I would also like to thank Karin Petersen, Zacarias Tecle, Povl V. Andersen, and Thoung Dang for their assistance in the laboratory work. Special thanks to the CERE secretaries Louise and Patricia for their administrative support and Christian for the IT support.

During my PhD, I had the opportunity to visit NTNU for six months external research. A very special thanks to Professor Hallvard Svendsen for hosting this visit and giving access to the NTNU and SINTEF labs. I would also like to thank him for the good collaboration between DTU and NTNU through the iCap project. Inna Kim and Anastasia Trollebø are acknowledged for their support in the experimental work. Thanks to Hanna Knuutila, Ardi Hartono, Nina, Hamid, Mehdi, and Naveed for their support during my stay at NTNU.

I wish to thank all my friends at CERE who share a great and memorable time during my work. I want to thank my close friends, Muhammad Shafique Bashir, Pir Adeel Zahid Saifi, and Muhammad Riaz, for maintaining an excellent friendship for more than twelve years. I greatly acknowledge your support during all those years we have been together. Thanks to Azeem and Qasim for their support and having good time at DTU.

I want to pay heartfelt thanks and humble gratitude to my mother and grandfather (Ghulam Hussain), my brothers and sisters in Pakistan for their love, prayers and unconditional support at every stage of my life. Especially, it was the vision of my late father (Muhammad Arshad), and guidance, support, and prayers of my mother and grandfather, that bring me this far in my life.

Finally, thanks to my lovely wife Anam. Your love, care, patience, and understanding made it easy for me to complete this work.

پیاری ماں کے نام۔۔۔

بڑی محبت و صد احترام کے ساتھ

محمد وسیم ارشد
کوپن ھیگن، ڈنمارک
جمعۃ المبارک، ۱۳جون، ۲۰۱۴ء
۱۵شعبان المعظم، ۱۴۳۵ھ

Abstract

Carbon dioxide (CO_2) is a well-known greenhouse gas playing a major role in the global warming and changing the global climate. Fossil fuel power generation, cement production, and other industrial activities are the major point sources of anthropogenic CO_2 emissions worldwide. To mitigate the climate change, it is critical to reduce the CO_2 emissions. Amine based absorption-desorption process is a mature and commercially available technology for the post combustion capture and monoethanolamine (MEA) is a very well-studied solvent. However, it is well-know that the MEA based scrubbing is an energy intensive process. This Ph.D. work presents a de-mixing solvent system consisting of two amines, 2-(diethylamino)ethanol (DEEA) and 3-(methylamino)propylamine (MAPA), for CO_2 capture with a potential to reduce the energy penalty of the capture process.

The development of de-mixing solvents in this work involved experimental investigations and thermodynamic modeling of the aqueous DEEA, MAPA, and DEEA-MAPA mixtures which form liquid-liquid phase change (de-mixing). The experimental work consisted of freezing point depression (FPD) measurements in the binary and ternary aqueous solution of DEEA and MAPA. FPD measurements were also performed for the CO_2 loaded aqueous DEEA and MAPA solutions. A calorimetric study was performed to measure, simultaneously, the heat of absorption of CO_2 and equilibrium total pressures in aqueous solution of DEEA, MAPA and DEEA-MAPA mixtures. The examined systems were the binary aqueous solutions of 5 M DEEA, 2 M MAPA, and 1 M MAPA, and the ternary aqueous mixtures of 5 M DEEA + 2 M MAPA and 5 M DEEA + 1 M MAPA. The latter two solvent systems gave biphasic liquid-liquid phase change (de-mixing). The CO_2 partial pressures were estimated from the measured equilibrium total pressure data for all the tested solvent systems. The experimental measurements were done in a wide range of temperature, pressure, amine concentration, and CO_2 loading. All the experimental data measured in this work were compared with the 30 mass % MEA as a benchmark.

The Extended UNIQUAC thermodynamic framework was implemented to describe the thermodynamics of the de-mixing H_2O-DEEA-MAPA-CO_2 system and the two sub-systems, H_2O-DEEA-CO_2 and H_2O-MAPA-CO_2. The aqueous-phase activity coefficients (γ) were calculated from the Extended UNIQUAC model and the vapor-phase fugacity coefficients (ϕ) were estimated from the Soave-Redlich-Kwong (SRK) cubic equation of state. Different types of experimental equilibrium data and thermal property data, previously measured in this work together with the data available in the literature, were used for the parameter estimation. 94 model parameters and 6 thermodynamic properties were fitted to approximately 1500 experimental data consisting of pure amine vapor pressure, vapor-liquid equilibrium, solid-liquid equilibrium, liquid-liquid equilibrium, excess enthalpy, and heat of absorption of CO_2 in aqueous amine solutions. Using a single unique set of parameters, the model developed in this work can reproduce almost all the data points and can describe all the data types satisfactorily.

Résumé på Dansk

Kuldioxid (CO_2) er en velkendt drivhusgas som spiller en vigtig rolle i den globale opvarmning og påvirker det globale klima. Fossil elproduktion, cementproduktion, og andre industrielle aktiviteter er de vigtigste punktkilder af menneskeskabt CO_2-udledning på verdensplan. For at mindske klimaændringer, er det vigtigt at reducere CO_2-udledningen. Amin baseret absorption-desorption er en moden og kommercielt tilgængelig teknologi til fjernelse af kuldioksid fra gasser. Vandig monoethanolamin (MEA) er et meget velundersøgt opløsningsmiddel. Det er dog velkendt, at MEA baseret scrubbing er en energiintensiv proces. Dette Ph.D. arbejde præsenterer et opløsningsmiddel for CO_2 opsamling, som efter absorption af CO_2 splitter i to separate faser. Opløsningsmidlet består af vand og to aminer, 2-(diethylamino)ethanol (DEEA) og 3-(methylamino)propylamin (MAPA). Dette opløsningsmiddel for CO_2-opsamling kan have potentiale til at reducere processens energi behov.

Udviklingen af de specielle opløsningsmidler i dette arbejde er baseret på eksperimentelle undersøgelser og termodynamisk modellering af vandige DEEA, MAPA, og DEEA-MAPA blandinger, som danner væske-væske fase split. Det eksperimentelle arbejde bestod af målinger af frysepunktsænkninger (FPD) i binære og ternære vandige opløsninger af DEEA og MAPA. FPD målinger blev også udført for CO_2 holdige vandige DEEA og MAPA løsninger. Et kalorimetrisk studium blev udført for samtidig at måle absorptionsvarmen, opløseligheden af CO_2 og ligevægtstrykket i vandige opløsning af DEEA, MAPA, og DEEA-MAPA blandinger. De undersøgte systemer var de binære vandige opløsninger af 5 M DEEA, 2 M MAPA, og 1 M MAPA, og ternære vandige blandinger af 5 M DEEA + 2 M MAPA og 5 M DEEA + 1 M MAPA. Sidstnævnte to opløsningsmiddelsystemer gav tofaset væske-væske split. CO_2 partialtrykket blev estimeret ud fra de målte ligevægts totaltryk for alle de testede opløsningsmiddel-systemer. De eksperimentelle målinger blev udført ved en lang række temperaturer, tryk, amin-koncentrationer, og CO_2-indhold. Alle de eksperimentelle data målt i dette arbejde blev sammenlignet med tilsvarende målinger for en standard 30 masse % MEA.

Den termodynamiske model Extended UNIQUAC blev anvendt til at beskrive termodynamikken af fase-split i H_2O-DEEA-MAPA-CO_2-systemer og de to sub-systemer, H_2O-DEEA-CO_2 og H_2O-MAPA-CO_2. Aktivitetskoefficienter (γ) for den vandige fase blev beregnet ud fra Extended UNIQUAC modellen og damp-fase fugacitet koefficienter (ϕ) blev estimeret fra Soave-Redlich-Kwongs (SRK) kubiske tilstandsligning. Forskellige typer af eksperimentelle ligevægtsdata og standard termodynamiske egenskaber, der tidligere er målt i dette arbejde sammen med de tilgængelige data i litteraturen, blev anvendt til parameterestimering. 94 modelparametre og 6 termodynamiske egenskaber blev bestemt fra cirka 1500 eksperimentelle data. De eksperimentelle data bestod af damptryk for rene aminer, dampvæskeligevægtsdata, data for fast-flydende ligevægt, væske-væske ligevægt, excess enthalpi, og absorptionsvarme for CO_2 i vandige aminopløsninger. Ved hjælp af et enkelt unikt sæt af parametre, kan modellen der er udviklet i dette arbejde gengive næsten alle datapunkter og kan beskrive alle datatyper tilfredsstillende.

Table of Contents

List of Figures

List of Tables

1. Introduction

1.1 Background

There is a general consensus that the anthropogenic carbon dioxide (CO_2, a greenhouse gas) emissions are the major contributor to the global warming and drastically changing the global climate.[1] To mitigate this global problem, it is critical to develop cost and energy effective technologies. One potential solution to this problem is Carbon Capture and Storage (CCS).[2] The CCS approach is to capture CO_2 from an emitting source such as a power plant, transport the captured CO_2 to an injection site for example via a pipeline, and sequestrate it into a geological formation (e.g., a deep saline formation) for a long time storage. The potential injection site may also be a petroleum reservoir, and the captured CO_2 can be used for the enhanced oil and/ or gas production from the petroleum reservoirs.[3]

Over 60 % of the total electricity generated worldwide comes through the combustion of fossil fuels mainly coal and natural gas.[4] Coal is a cheap and abundantly available fossil fuel. Only coal fired power plants generate about 42 % of the total electricity worldwide.[5] It is expected that the power generation dependency on the coal as a main fuel will continue to increase due to increased energy demand and energy security in the future.[6] Coal can also be a strategic fuel in future power generation due to its low cost, security and sustainability in the supply. However, the use of coal for power generation is associated with high CO_2 emissions.[7] Natural gas, on the other hand, is a relatively cleaner fuel. In United States, around 30 % of the total electricity generation comes from natural gas fired power plants in 2012.[6] The projected future electricity generation in United States suggests that the coal and natural gas will represent 34 % each (68 % together) of the total generation in 2035 and 67 % of the total generation by 2040 (32 % coal and 37 % natural gas generation).[6] It is essential to develop CCS technologies that can lead to near zero emissions from power plants based on fossil fuel (coal and natural gas). Therefore, CO_2 capture is likely to be an important part of the future power generation.

1.2 CO_2 Emissions

CO_2 emissions from different sources are reported in the open literature.[7-10] CO_2 capture from mobile sources, such as transportation, and small sources, such as small industrial plants and residential sector, is likely to be very expensive and difficult compared to the large stationary sources such as fossil fuel fired power plants and big industrial units (e.g., cement, steel, refineries, and petrochemical plants etc.). CO_2 emissions from the large stationary sources worldwide emitting more than 0.1 million ton CO_2 per year have been reported in the IPCC special report on CCS.[10] These emissions are presented graphically in Figure 1.1 and show the percentage contribution of different emitting sources. The left side pie chart presents the CO_2 emissions of different sources for the total CO_2 emissions of 13468 Mt per year. It can be seen that the power generation sector contributes about 78.3 % of the total CO_2 emissions (i.e., 10539 Mt CO_2 per year).

Cement production contributes the second largest CO_2 emissions of around 6.9% (932 Mt CO_2 per year) followed by 5.9 % emissions from refineries (798 Mt CO_2 per year), 4.8 % from iron and steel industry (646 Mt CO_2 per year), 2.8 % from petrochemical industry (379 Mt CO_2 per year), 0.7 % from bioethanol and bioenergy (91 Mt CO_2 per year), 0.4 % from oil and gas processing (50 Mt CO_2 per year), and 0.2 % from other miscellaneous sources (33 Mt CO_2 per year). The CO_2 emissions from the power generation are further categorized on the right side pie chart in Figure 1.1. It shows that the coal based power generation contributes about 76 % of the total power sector emissions (7984 Mt CO_2 per year) and the remaining 24 % power sector emissions (2555 Mt CO_2 per year) come from the natural gas, fuel oil, and other fuels based power generation.

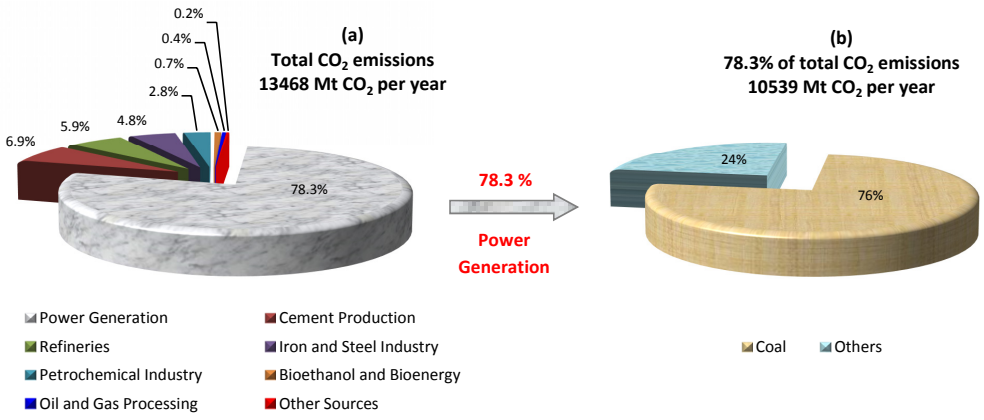

Figure 1.1: A profile of stationary point sources emitting more than 0.1 Mt CO_2 per year. a, CO_2 emissions in percentages of different sources for the total CO_2 emissions of 13468 Mt per year; and b, CO_2 emission contributions from coal and other fuels (natural gas, fuel oil, and other fuels) to the 78.3 % emissions (10539 Mt CO_2 per year) from power generation.

1.3 CO_2 Capture Systems

Three basic CO_2 capture systems are reported in the literature for the fossil fuel based power generation; pre-combustion capture, oxy-fuel combustion capture and post-combustion capture.[10] A process description of the pre-combustion capture system is given in Figure 1.2 along with the particulates and sulfur removal equipment. A fuel is mixed with air or oxygen and steam to produce a gas mixture of carbon monoxide and hydrogen called synthesis gas (or syngas or water gas). Carbon monoxide in the syngas is then reacted with steam in a catalytic reactor (shift reactor) to produce CO_2 and hydrogen. Finally, CO_2 is captured from this gas mixture to produce hydrogen rich gas stream which is used to run a gas turbine to produce electricity.

The basic idea in oxy-fuel combustion capture is to burn the fuel with pure oxygen which produces a flue gas stream containing mainly CO_2 and water vapors which can easily be removed by condensation to produce pure CO_2 streams. Cryogenic (low temperature) separation of air is used to produce pure oxygen which is used to burn the fuel in a boiler to generate steam for electricity generation via steam turbines. Figure 1.3 presents the oxy-fuel capture system with some additional equipment for the removal of particulates and sulfur.

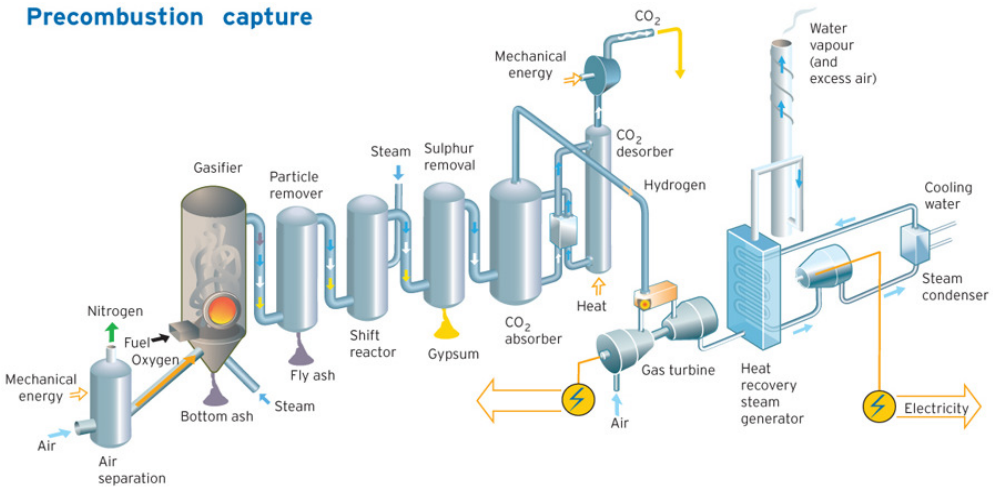

Figure 1.2: Process diagram of pre-combustion capture system (Photo courtesy of Vattenfall).

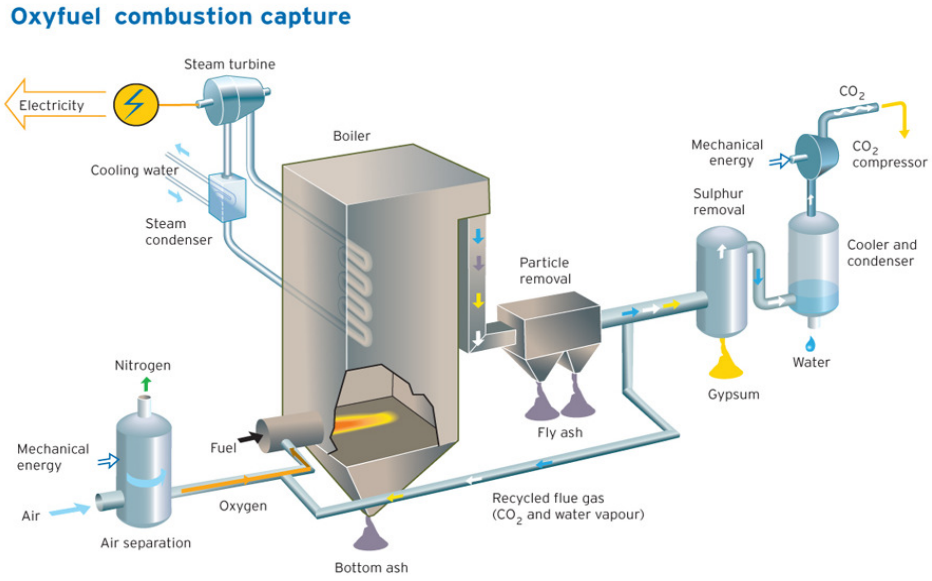

Figure 1.3: Process diagram of oxy-fuel combustion capture system (Photo courtesy of Vattenfall).

In post-combustion capture, the fuel is burnt with air in a boiler to produce steam for electricity generation. The flue gas coming out of the boiler is treated to remove the particulates and sulfur compounds, and finally send to the CO_2 capture unit. A general post-combustion capture system is illustrated in Figure 1.4. The CO_2 contents in the flue gas depend on the type of fuel used i.e., typically 3 % by volume in the natural gas fired boilers and 12-15 % by volume in the coal-based combustion. A low thermodynamic driving force for capturing CO_2 from the flue gas due to the low CO_2 partial pressure poses technical challenges in developing the energy and cost effective capture processes. In these conditions, chemical absorption of CO_2 in amines is an attractive choice. However, it is associated with high energy requirements in stripping off CO_2 during solvent regeneration. Therefore, new energy efficient solvent systems are essential. Experimental and thermodynamic study of one such solvent system is presented in this work.

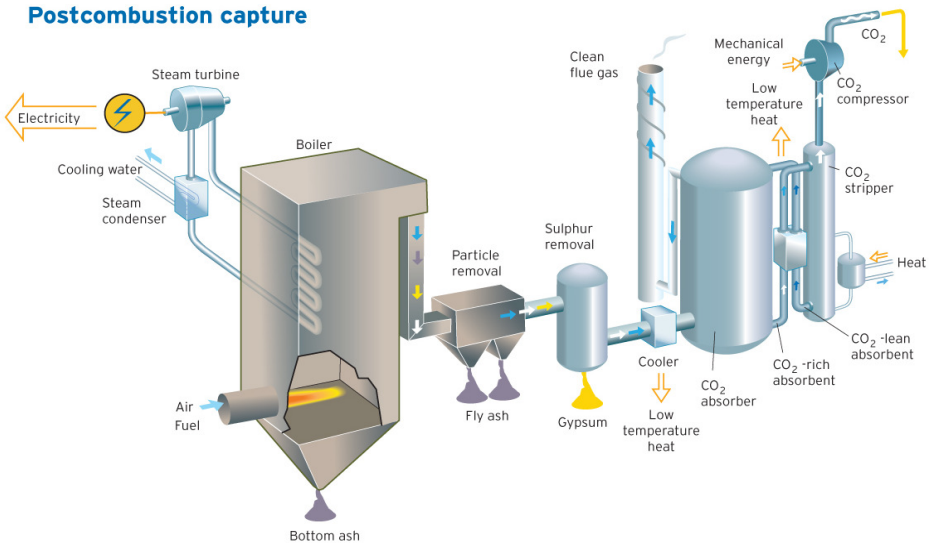

Figure 1.4: Process diagram of post-combustion capture system (Photo courtesy of Vattenfall).

1.4 De-mixing CO_2 Capture Solvents

Amine based absorption-desorption is a well-established and commercially available technology for the postcombustion CO_2 capture.[11] Monoethanolamine (MEA) is the most commonly studied amine solvent and used as a benchmark. The main disadvantage of MEA (30 mass %) as a capture solvent is the high energy demand of the reboiler which is around 3.7 GJ.(ton CO_2)$^{-1}$.[12,13] There is a need to develop energy efficient solvent systems. A de-mixing solvent system[14] consists of two amines, 2-(diethylamino)ethanol (DEEA) and 3-(methylamino)propylamine (MAPA), is presented in this work. When a mixture of DEEA and MAPA at certain concentrations reacts with CO_2, it forms a biphasic liquid-liquid phase change (de-mixing) giving an upper liquid phase lean in CO_2 and a lower liquid phase rich in CO_2. The CO_2 lean phase is sent back to the absorber without regeneration and only the CO_2 rich phase is sent to stripper for regeneration. Due to a low liquid circulation rate in the stripper, one can reduce the solvent regeneration energy. A

recent process simulation study shows a reboiler duty of 2.4 GJ.(ton CO_2)$^{-1}$ at a desorber pressure of 400 kPa for an aqueous mixture of DEEA-MAPA which can further reduced to 2.2 GJ.(ton CO_2)$^{-1}$ at a lower desorber pressures.[15] These values are significantly lower than the 30 mass % MEA reference case with a reboiler duty of 3.5 GJ/ ton CO_2 at a desorber pressure of 200 kPa[15] showing a potential for energy efficient CO_2 capture.

A typical amine based post-combustion capture system consists of an absorber and a stripper column as shown in Figure 1.5. The flue gas rich in CO_2 enters at bottom of the absorber and comes in contact with the lean amine solution entering at the top of absorber. CO_2 in the flue gas is get absorbed in the amine solution and the flue gas lean in CO_2 leaves the absorber from the top. The CO_2 rich amine solution from bottom of the absorber is sent to the top of the stripper via a heat exchanger where it is heated up by the regenerated amine solvent (lean amine). CO_2 is stripped off in the desorber (or stripper) and the regenerated solvent from bottom of the stripper is sent to the top of absorber for another run. The CO_2 stream coming out at top of the stripper is cooled to separate the water vapors and pure CO_2 is compressed and transported to the storage site. However, the process diagram for the de-mixing solvents based absorption-desorption system is slightly different as shown in Figure 1.6.[14] The only difference between the two processes is that the CO_2 rich solution (both liquid phases) from the absorber is sent to the decanter to separate the two liquid phases. The lower CO_2 rich liquid phase is sent to the stripper for regeneration and the upper CO_2 lean liquid phase is mixed with the regenerated rich phase from the stripper and sent to the top of absorber.

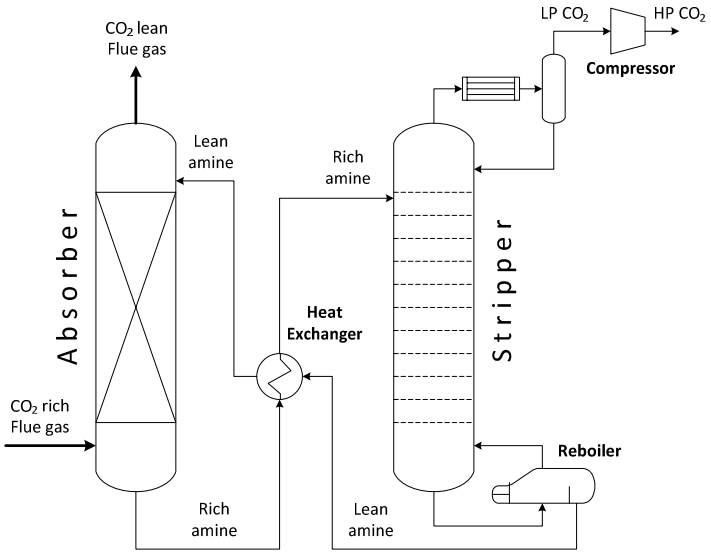

Figure 1.5: Simplified flow diagram of conventional amine based absorption-desorption process for CO_2 capture.

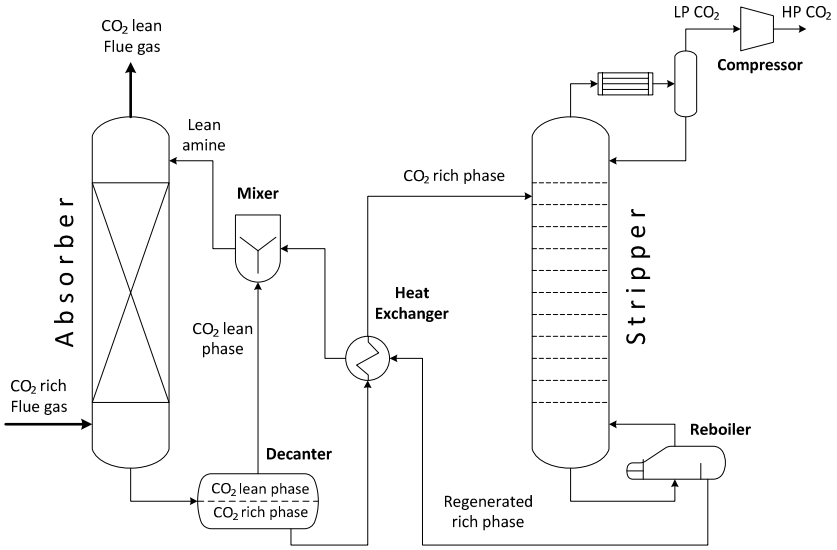

Figure 1.6: Simplified flow diagram of de-mixing solvents based absorption-desorption process for CO_2 capture.

1.5 Thesis Objectives

The main objectives of this Ph.D. work can be divided into the experimental measurements and the thermodynamic modeling, and elaborated as follows:

1) Experimental measurements of freezing point depression for the unloaded and CO_2 loaded aqueous DEEA and MAPA solutions, and unloaded aqueous DEEA-MAPA mixtures.
2) Calorimetric measurements for the heat of absorption of CO_2 in binary and ternary aqueous solutions of DEEA and MAPA (H_2O-DEEA, H_2O-MAPA, and H_2O-DEEA-MAPA).
3) Measurements of equilibrium total pressures and CO_2 solubility in H_2O-DEEA-CO_2, H_2O-MAPA-CO_2, and H_2O-DEEA-MAPA-CO_2 solutions.
4) Thermodynamic modeling of the de-mixing H_2O-DEEA-MAPA-CO_2 system, and the two sub-systems H_2O-DEEA-CO_2 and H_2O-MAPA-CO_2.

1.6 Thesis Layout

The work related to different objectives of the thesis is presented in separate chapters. A brief overview of these chapters is given by:

Chapter 2 presents the freezing point depression (FPD) measurements in the de-mixing (or phase change) solvents containing DEEA and MAPA using a modified Beckmann apparatus. These measurements were

performed for the binary aqueous DEEA and MAPA solutions at different concentrations of amine and for the ternary aqueous DEEA-MAPA solutions for different molar ratios of DEEA/MAPA. The experimental method was extended to the freezing point measurements in the CO_2 loaded systems based on the saturation of amine solution by CO_2 and then dilution by using a batch of the original unloaded amine solution in order to get the solutions with different CO_2 loadings. Measurements for the CO_2 loaded systems were performed for different concentration of DEEA and MAPA solutions at different CO_2 loadings. The measured freezing point data were compared with monoethanolamine (MEA) and methyl diethanolamine (MDEA) found in the literature. A correlation for the freezing points as a function of solution composition was formulated for the unloaded binary and ternary systems.

Chapter 3 covers the measurements of heat of absorption of CO_2 in the de-mixing solvents as a function of CO_2 loading at different temperatures using a commercially available reaction calorimeter. The tested systems were aqueous single amines (5 M DEEA, 2 M MAPA, and 1 M MAPA) and aqueous amine mixtures (5 M DEEA + 2 M MAPA and 5 M DEEA + 1 M MAPA) which give two liquid phases (de-mixing) on reacting with CO_2. The measurements were taken isothermally at three different temperatures 40, 80, and 120 ^{o}C. The measured differential heat of absorption values were converted into integral values by integration. All the measured heat of absorption data reported in this chapter were compared with 30 mass % MEA used as a base case.

Chapter 4 covers the measurements of equilibrium total pressures and estimation of CO_2 partial pressures from the measured total pressure data in the aqueous solutions of DEEA, MAPA, and their mixture (de-mixing solvents). The measurements were carried out in a commercially available calorimeter used as an equilibrium cell. The examined systems were the binary aqueous solutions of 5 M DEEA, 2 M MAPA, and 1 M MAPA, and the ternary aqueous mixtures of 5 M DEEA + 2 M MAPA and 5 M DEEA + 1 M MAPA which gave liquid-liquid phase split upon CO_2 absorption. The measurements were also carried out for the 30 mass % MEA solutions in order to validate the experimental method. The total pressures were measured and the CO_2 partial pressures were estimated as a function of CO_2 loading at three different temperatures 40, 80, and 120 ^{o}C. All the measured data reported in this chapter were compared with the results of 30 mass % MEA as a reference case.

Chapter 5 presents the thermodynamic modeling of the de-mixing aqueous DEEA-MAPA solvent system for CO_2 capture. The Extended UNIQUAC thermodynamic framework was implemented to describe the thermodynamics of the two sub-systems, H_2O-DEEA-CO_2 and H_2O-MAPA-CO_2, followed by the H_2O-DEEA-MAPA-CO_2 system which gives liquid-liquid phase split (de-mixing or phase change). Different types of experimental equilibrium data and thermal property data were used for the parameter estimation. 94 model parameters and 6 thermodynamic properties were fitted to approximately 1500 experimental data consisting of pure amine vapor pressure, vapor-liquid equilibrium, solid-liquid equilibrium, liquid-liquid equilibrium, excess enthalpy, and heat of absorption of CO_2 in aqueous amine solutions. Most of these experimental data were measured in this Ph.D. work. The model developed in this work reproduces almost all the data points and describes all the data types satisfactorily with a single unique set of parameters.

Finally, chapter 6 presents the overall summary of the experimental and thermodynamic modeling results together with some recommendations for the future work.

1.7 References

(1) Stocker, T. F.; Qin, D.; Plattner, G.-K.; Tignor, M. M. B.; Allen, S. K.; Boschung, J.; Nauels, A.; Xia, Y.; Bex, V.; Midgley, P. M. Eds. *Climate Change 2013 - The Physical Science Basis*. Working Group I Contribution to the Fifth Assessment Report of the Intergovernmental Panel on Climate Change, Cambridge University Press, U.K., 2013.

(2) Introduction to Carbon Capture and Storage (CCS), CSIRO & Global CCS Institute, 2012. Available online: http://cdn.decarboni.se/sites/default/files/publications/43276/introduction-carbon-capture-and-storage.pdf (accessed April 2014).

(3) *The Global Status of CCS: 2012*, Global CCS Institute: Canberra, Australia, 2012.

(4) Birol, F.; Argiri, M. World energy prospects to 2020. *Energy* 1999, 24 (11), 905-918.

(5) *Power Generation from Coal*. International Energy Agency (IEA): Paris, France, 2010. Available online at http://www.iea.org/ciab/papers/power_generation_from_coal.pdf (accessed April 2014).

(6) *Annual Energy Outlook 2014* early release overview, IEA, DOE/IEA-0383ER, December 2013. Available online at http://www.eia.gov/forecasts/aeo/er/early_elecgen.cfm (accessed April 2014).

(7) *CO_2 Emissions from Fuel Combustion - Highlights*, International Energy Agency (IEA) Statistic: Paris, France, 2013. Available online at http://www.iea.org/co2highlights/co2highlights.pdf (accessed April 2014).

(8) International Energy Statistics - Total Carbon dioxide Emissions from the Consumption of Energy. http://www.eia.gov/cfapps/ipdbproject/iedindex3.cfm?tid=90&pid=44&aid=8 (accessed April 2014).

(9) *World Energy Outlook 2013 (WEO-2013)*, International Energy Agency (IEA), 2013. Available online at http://www.worldenergyoutlook.org/publications/weo-2013/#d.en.36200 (accessed April 2014).

(10) Metz, B.; Davidson, O.; de Coninck, H.; Loos, M.; Meyer, L. Eds. *IPCC Special Report on Carbon Dioxide Capture and Storage*. Prepared by Working Group III of the Intergovernmental Panel on Climate Change (IPCC), Cambridge University Press, U.K., 2005.

(11) Kohl, A. L.; Nielsen, R. B. *Gas Purification*, 5th ed.; Gulf Publishing Co.: Houston, TX, USA, 1997.

(12) Knudsen, J.; Jensen, J. N.; Vilhelmsen, P.-J.; Biede, O. Experience with CO_2 capture from coal flue gas in pilot-scale: testing of different amine solvents. *Energy Procedia* 2009, 1, 783-790.

(13) Abu-Zahra, M.; Schneiders, L. H. J.; Niederer, J. P. M.; Feron, P. H. M.; Versteeg, G. F. CO_2 capture from power plants. Part I. A parametric study of the technical performance based on monoethanolamine. *Int. J. Greenhouse Gas Control* 2007, 1, 37-46.

(14) Raynal, L.; Pascal, A.; Bouillon, P.-A.; Gomez, A.; le Febvre de Nailly, M.; Jacquin, M.; Kittel, J.; di Lella, A.; Mougin, P.; Trapy, J. The DMX™ process: an original solution for lowering the cost of post-combustion carbon capture. *Energy Procedia* 2011, 4, 779-786.

(15) Liebenthal, U.; Pinto, D. D. D.; Monteiro, J. G. M.-S.; Svendsen, H. F.; Kather, A. Overall Process Analysis and Optimisation for CO_2 Capture from Coal Fired Power Plants based on Phase Change Solvents Forming Two Liquid Phases. *Energy Procedia* 2013, 37, 1844-1854.

2. Freezing Point Depression

2.1 Introduction

Reactive absorption using amines is one of the most common industrial technologies available today for the post-combustion CO_2 capture. These processes have been considered as the most feasible route to capture CO_2 from power plant flue gases. This is due to their use in many industrial applications such as CO_2 removal from reformer gases, acid gas removal from natural gas, etc.[1] The amine based scrubbing selectively removes CO_2 from the flue gases and releases a high-purity CO_2 offgas stream upon heating in a stripper column which is suitable for storage without any further treatment. However, the energy requirement for solvent regeneration is very high in these processes.[2,3] Therefore, the development of new solvent systems with improved energy efficiency, innovative process design, and technological improvements are necessary in order to reduce the high capital cost and energy requirements for the capture process.[4,5]

Primary and secondary amines are known for their fast reaction rates and high heat of reaction due to formation of carbamates with CO_2.[6] Consequently they require high energy for the reaction reversion. Tertiary amines, on the other hand, have low heat of reactions due to formation of bicarbonates by base catalysis of CO_2 hydration[7] and require relatively low energy for solvent regeneration. These amines generally have high CO_2 loading capacity and low reaction rate.[8,9] None of the amine types have ideal properties for CO_2 absorption, so mixed amine systems have become very popular in order to exploit the favorable properties of all types of amines.

A new set of solvents have recently emerged, which may be called phase change solvents. They have shown potential to reduce the energy requirements for solvent regeneration. These solvents either form precipitate, for example, the Alstom chilled ammonia (CAP) process[10] or form two liquid phases, for example, the DMX™ process[11] and thermomorphic biphasic solvents (TBS) systems.[12] The TBS solvent systems release the absorbed CO_2 in the desorber at a much lower temperature of 80 ^oC or even below compared to the conventional aqueous alkanolamine solutions, which is typically 120 ^oC. They form two liquid phases during solvent regeneration and become one phase again during absorption and revert back to two phases upon heating and agitating in the desorber.[13-15] In the DMX™ process developed by IFP Energies nouvelles, on the other hand, the single phase solvent splits into two liquid phases after CO_2 absorption. The amine-rich phase with very low CO_2 loading recycles back to the absorber without regeneration and only the water-rich phase with very high CO_2 loading goes to the stripper for the thermal regeneration. Therefore, the energy consumption for solvent regeneration can be lowered due to reduced liquid flow rate in the stripper.[11]

Two different amines, 2-(diethylamino)ethanol (DEEA) and 3-(methylamino)propylamine (MAPA), are under investigation in this study. DEEA is a tertiary alkanolamine and MAPA has two amine functional groups, a primary and a secondary. Molecular structures of both DEEA and MAPA are shown in Figure 2.1. Therefore, we can exploit the favorable properties of amines by blending DEEA and MAPA. Their blends have an additional advantage of making liquid-liquid split when reacted with CO_2. Previous studies have shown that the single phase aqueous blend of DEEA-MAPA turns into two liquid phases upon CO_2 absorption with an upper phase lean in CO_2 and a lower phase rich in CO_2, and only the CO_2 rich phase needs to be regenerated.[16,17] This solvent system has also shown lower heat of absorption at solvent regeneration temperature (120 °C) compared to 30 mass % MEA[17] making it a potential solvent system with low regeneration heat requirement in the stripper.

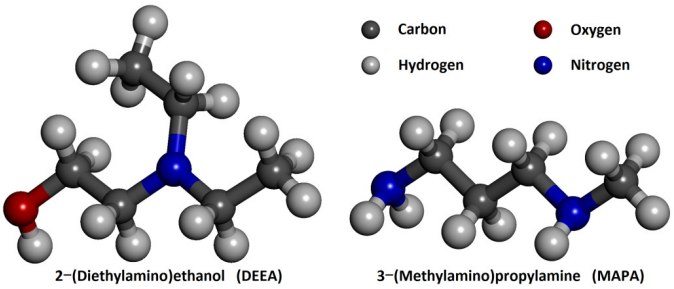

Figure 2.1: Molecular structures of DEEA (left) and MAPA (right).

Water activity is a key parameter for the amount of water evaporated in the desorber during the solvent regeneration step in CO_2 capture processes. If the water activity is low, less water will evaporate and consequently less amount of energy will be consumed during CO_2 desorption. Water activity data can be very accurately computed from freezing point depression (FPD) data by considering the temperature dependent equilibrium constant, $K_T = a_{\mathrm{H_2O(l)}}$, for the reaction given in Equation 1.

$$\mathrm{H_2O}(s) \rightleftarrows \mathrm{H_2O}\ (l) \tag{1}$$

The equilibrium constant as a function of temperature can be calculated as described by Thomsen[18] from Gibbs-Helmholtz equation (Equation 2), change in standard state enthalpy with temperature (Equation 3) and a three-parameter temperature dependent heat capacity correlation (Equation 4), also used in the Extended UNIQUAC model by Thomsen et al.[19]

$$\frac{d\ln K}{dT} = \frac{d\left(\Delta G^{\circ}/RT\right)}{dT} = \frac{\Delta H^{\circ}}{RT^2} \tag{2}$$

$$\frac{d\Delta H^{\circ}}{dT} = \Delta C_p^{\circ} \tag{3}$$

$$C_{p,i}^{o} = a_i + b_i T + \frac{c_i}{T - T_{\Theta,i}} \tag{4}$$

Integrating equations 2 & 3 and using equation 4 leads to a form of equilibrium constant given in Equation 5.

$$\begin{aligned} R \ln K_T = R \ln K_{T_o} - \Delta H_{T_o}^{o} \left(\frac{1}{T} - \frac{1}{T_o} \right) + \Delta a \left(\ln \frac{T}{T_o} + \frac{T_o}{T} - 1 \right) \\ + 0.5 \Delta b \left(\frac{(T - T_o)^2}{T} \right) + \frac{\Delta c}{T_\Theta} \left(\frac{T - T_\Theta}{T} \ln \frac{T - T_\Theta}{T_o - T_\Theta} - \ln \frac{T}{T_o} \right) \end{aligned} \tag{5}$$

where, T_Θ = 200 K and standard state temperature, T_o = 298.15 K. Δa, Δb, and Δc represent the difference in values of correlation parameters for the system considered (ice and water in this case). The standard state formation properties for water and ice, and correlation parameters (a_i, b_i, and c_i) for the heat capacity in Equation 4 have been reported earlier by Thomsen et al.[19] and Fosbøl et al.[20] and are presented here in Table 2.1 (All the tables are presented in the Appendix at the end of this chapter). A revised value of a = 49.627 J.(mol K)$^{-1}$ for ice is suggested which has not been previously published.

Chang et al.[21] reported freezing point measurements for aqueous MDEA (methyl diethanolamine). The data are not conclusive because it divided into two series forming a curve that separates into two branches. Using Equation 5, Fosbøl et al.[22] determined the water activity from the freezing point data of aqueous MDEA by Chang et al.[21] They reported a difference in water activity up to 3.5 % due to uncertainty in the freezing point data for the two branches. Such an error can considerably affect the estimation of water evaporated during the solvent regeneration process in the stripper. Therefore, accurate FPD measurement is very important to accurately determine the water activity data needed for the thermodynamic modeling of CO_2 capture systems.

The main focus in this work has been to measure accurate FPD for aqueous DEEA, MAPA, and their mixtures with and without CO_2 loading because no data have been found in the literature for these systems. The freezing point measurement method developed earlier by Fosbøl et al.[22,23] can be used for FPD and solubility measurements. An important aim in this work has been to extend this FPD method to CO_2 loaded systems. This was done by using a simple approach. Additionally, there is a need to determine the molecular interaction between DEEA and MAPA in aqueous solutions in order to understand the system containing these solvents. This can be done by measuring freezing points in the binary DEEA-water and MAPA-water and the ternary DEEA-MAPA-water systems. The interaction between CO_2 and the solvents can be deduced from the measured freezing points in the CO_2 loaded systems.

2.2 Experimental Section

DEEA (pale yellow to yellowish-orange) was purchased from Merck with a purity of > 99 % and MAPA (colorless) with a purity of 97-98 % was purchased from Sigma-Aldrich. Both are clear liquids at room temperature. Sodium chloride used for the calibration of Pt100 thermometer was purchased from Merck with a purity of 99.5 %. Carbon dioxide used for loading amine solutions was purchased from AGA, purity

≥99.99 %. The solutions were made with deionized water using an analytical balance with an accuracy of ±0.1 mg. No measurements were made for the density or purities of the amines. All chemicals were used as received with no further purification.

The FPD measurements were carried out by using a modified Beckmann apparatus as described by Fosbøl et al.[22] This setup has also been used by Fosbøl et al.[23] to measure the aqueous solubility of amines using a different experimental method. A brief overview of the experimental setup and working procedure is given here. A schematic diagram of the setup is shown in Figure 2.2.

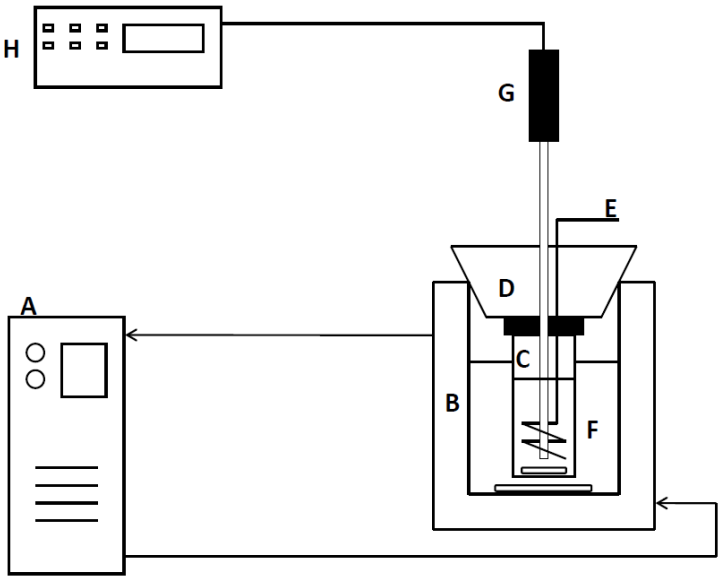

Figure 2.2: Experimental setup for measuring freezing point. A, Thermostatic bath with ethanol; B, Cooling jacket; C, Sample glass with magnetic stirrer; D, Rubber stopper with sample glass lid; E, Device for manual stirring; F, Controlled temperature ethanol bath with magnetic stirrer; G, Pt100 Thermometer; H, Data acquisition unit.

Approximately 5 to 10 gram of amine solution to be tested was taken in the sample glass (C), see Figure 2.2. The sample glass was then taken into the controlled temperature ethanol bath (F). Constant temperature was maintained in the ethanol bath (F) by the cooling jacket (B) which is connected to the thermostatic bath (A) with ethanol as refrigerant. Temperature in the thermostatic ethanol bath (A) was kept about 5 to 15 ^{o}C below the expected freezing point of the solution in the sample glass (C) in order to provide necessary thermal gradient for the solution to freeze. This depends on the concentration of the solution i.e. high temperature difference for the solutions with high concentrations and vice versa. The temperature of solution in the sample glass was recorded by a Pt100 thermometer (G) which is attached to Agilent data acquisition unit (H) which was calibrated against the recommended freezing point values of aqueous NaCl from Clarke and Glew.[24] The solution in the sample glass was continuously stirred with a magnetic stirrer

and a device for manual stirring (E) for homogeneous temperature condition in the sample solution. Once the solution in the glass sample froze and the freezing point was determined from the temperature logging against time (one point every 4 seconds), it was taken out and heated up externally by placing the sample glass in an ethanol beaker at room temperature. Stirring was continued both during freezing and melting the solution. When micro-ice crystals were left in the solution, the sample glass was again taken back into the controlled temperature ethanol bath (F), and the procedure was repeated for at least five times to get consecutive freezing point readings. Average values of these five consecutive freezing point readings along with the standard deviation are reported in this study.

An example of the freezing temperature profile logged as a function of time for the 15 mass % MAPA solutions is presented in Figure 2.3. The five red diamond points (♦) were reported as the measured freezing points. It can be noticed that the freezing point (268.46 K) for this solution was reached after about 92 s but the ice did not form at this point. The solution was subcooled down to 265.69 K and then suddenly at this point (188 s), the ice formed stochastically. The large subcooling resulted in excess formation of ice which noticeably changed the liquid phase concentration of the solution, thus giving an inaccurate freezing point measurement. The first freezing point measurements in all the experiments were considered inaccurate and not reported in the results.

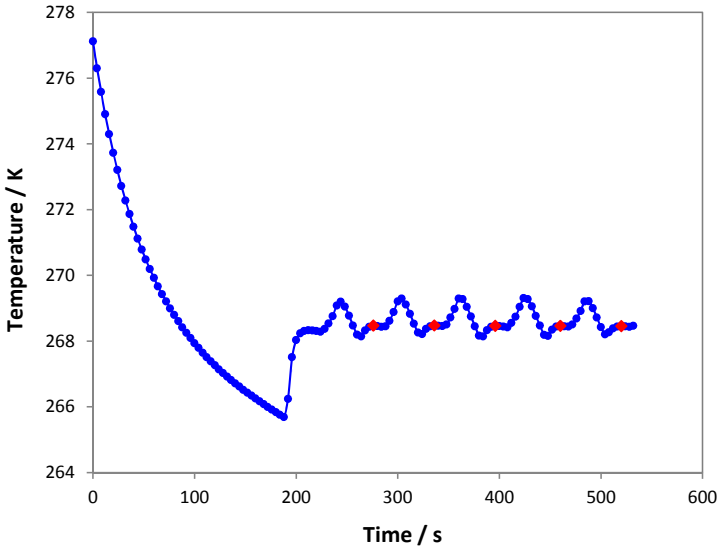

Figure 2.3: Example of freezing temperature profile logged as a function of time for the 15 mass % MAPA solutions. Data points were recorded after every 4 seconds. The red diamond points (♦) were reported as the measured freezing points.

A magnified view of freezing point measurements from Figure 2.3 for the time ranging from 252 to 332 s and temperature from 268 to 269.4 K is shown in Figure 2.4. The curve from 252 to 284 s represents the cooling after the last external heating cycle with a red diamond point as the registered freezing point. The

increase in temperature after 264 s represents the heat of crystallization and a slight decrease in temperature after the registered freezing point represents a slight increase in the solution concentration. The sample glass was then taken out of the ethanol bath and heated externally as represented by the dashed red line from 284 to 304 s. The external heating was done to melt the ice crystals and preparing for the next freezing cycle with a few microcrystals left in the solution. This was done by visual inspection of the solution. These microcrystals act as seed crystals and help avoiding the subcooling in the next freezing point measurement cycle. The curve starting from 304 s onward represents the cooling cycle for the next freezing point measurement.

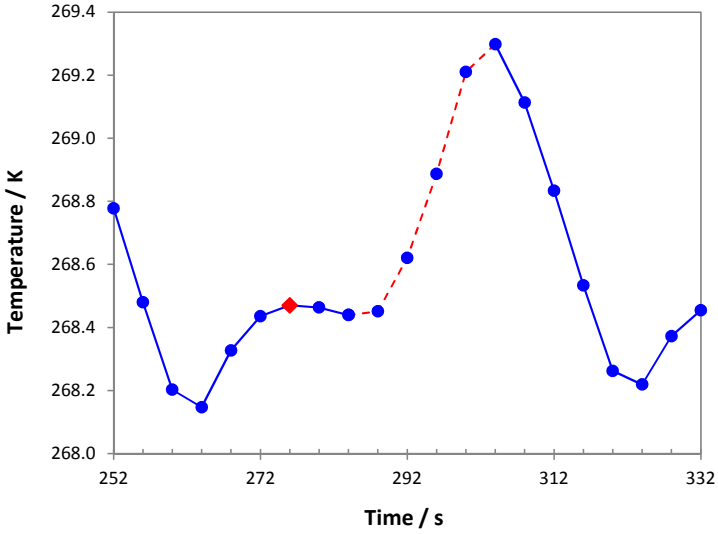

Figure 2.4: Magnified view of freezing point measurements from Figure 2.3 for the time ranging from 252 to 332 s and temperature from 268 to 269.4 K. The red diamond point (♦) was reported as the measured freezing point. The solid blue line represents the course of cooling in the ethanol bath and dashed red line of the curve represents the period when sample was heated externally.

The freezing point measurements were carried out by maintaining a constant temperature in the cooling jacket surrounding the sample glass. The first measurement was carried out to indicate the order of magnitude of the freezing point and then a constant sub cooling was applied. This means that speed of cooling was higher far away from the freezing point, but low, close to the freezing point. The speed of cooling is therefore not constant during the experiment. It is in the order of 0.01 to 0.1 ^{o}C.(sec)$^{-1}$.

It was noticed that the amine solutions with high concentrations had the tendency to make foam. This might be due to increased viscosity of the solutions at very low temperatures. It was also observed during the experiments that the foam formation was due to stirring. If the stirring rate is higher, more air is drawn into the solution to make foam. This foam was in the form of tiny air bubbles trapped into the solutions. Also, the solutions with high concentrations took a relatively longer time to complete 5-fold measurements

due to lower freezing temperatures and stirring these solutions for long times trapped more air bubbles into the solutions at low temperatures. This foaming tendency was low in the first couple of measurements and obviously it increased when the solutions were stirred for long time. Because of this formation of foam, it was difficult to distinguish between the tiny trapped air bubbles and micro-ice crystals in the solution during external heating of the glass sample. However, freezing points were measured by carefully controlling the stirring rate so that it trapped relatively less air bubbles without compromising the homogeneous temperature condition in the sample solutions. The repeatability of the measurements was ensured and a high degree of accuracy was obtained. For each sample, five measurements were made with a standard deviation of equal or less than 0.05 K.

A schematic diagram for loading CO_2 in amine solutions is given in Figure 2.5.

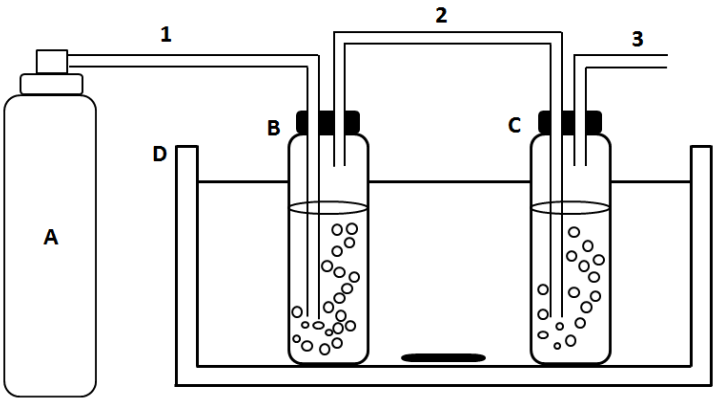

Figure 2.5: Experimental setup for CO_2 loading in amine solutions. A, CO_2 cylinder; B, Gas humidifier; C, Gas absorber; D, Water bath with a magnetic stirrer. 1, Dry CO_2 to gas humidifier; 2, Water saturated CO_2 to gas absorber; 3, Water saturated CO_2 to exit.

The amine solution to be loaded with CO_2 was filled in a gas humidifier (B) and a gas absorber (C), which were placed in a water bath (D) with a magnetic stirrer. The same composition and quantity of amine solution was taken both in the gas humidifier and the gas absorber. The temperature of the water bath was kept at 25 ^{o}C. Dry gas (CO_2) from CO_2 cylinder (A) was injected to the gas humidifier through gas line 1. The water saturated CO_2 was then transferred from the gas humidifier to the gas absorber through gas line 2 and exited from the system through gas line 3. Since dry CO_2 was used and the reaction between CO_2 and amine solutions is exothermic, water (or solution) was lost both from the gas humidifier and the gas absorber. It was assumed that the water (or solution) lost from the gas humidifier and the gas absorber is the same, so the net loss from the gas absorber was zero. CO_2 was allowed to flow through the system and the solution was assumed to be fully loaded when no significant change in weight of the gas absorber (C) was observed for at least five minutes. The difference in weight before and after CO_2 loading gave the amount of CO_2 loaded in the amine solution. To check any amine loss during the loading process, the amine contents in the solutions were analyzed by a standard titration procedure with aqueous 0.1 M H_2SO_4 using

potentiometric titrator Titrando-809 (Metrohm AG, Switzerland).[25,26] The loaded solutions containing CO_2 were analyzed by the barium chloride ($BaCl_2$) method described in details by Ma'mun et al.[27] Using this information the amine contents in the loaded solutions were determined on CO_2 free basis. The results of unloaded and loaded solutions has shown a deviation of less than ± 0.8 %, which is within the limit of experimental error.

Freezing point measurements were carried out for the binary aqueous DEEA solutions (concentration range of 0 to 55 mass percent) and aqueous MAPA solutions (concentration range of 0 to 32.5 mass percent). Measurements in the ternary aqueous DEEA-MAPA solutions were made by first preparing binary mixtures of DEEA and MAPA with fixed molar ratios of 5:1, 3:1, 1:1, 1:3, and 1:5 for DEEA/MAPA. These mixtures were then diluted with water to prepare the ternary aqueous DEEA/MAPA solutions in a concentration range of 0 to 45 mass percent of total amine. For the CO_2 loaded solutions, freezing point measurements were carried out for aqueous DEEA solutions (12, 20, 30, and 33 mass percent) and aqueous MAPA solutions (10, 20, and 27 mass percent). Aqueous solutions of DEEA and MAPA with known compositions were first fully loaded with CO_2 and then diluted with the corresponding unloaded solutions to get a range of zero to maximum CO_2 loading in that solution with a specific composition. For example, a batch of 12 mass % DEEA solution was prepared. A known portion of this solution was fully loaded with CO_2 and then diluted with the remaining unloaded 12 mass % DEEA solution to get different CO_2 loadings in 12 mass % DEEA solution. In order to avoid any CO_2 evaporation from the solutions, the freezing point measurements were carried out right after preparation of the solutions.

2.3 Results and Discussion

Experimental results of freezing points as a function of amine composition for the binary aqueous DEEA and MAPA solutions are given in Table 2.2 and Table 2.3, respectively. These results are graphically presented in Figure 2.6 as mole percent of amine. The freezing points results for the ternary aqueous DEEA-MAPA solutions for the mixtures with molar ratios of 5:1, 3:1, 1:1, 1:3, and 1:5 for DEEA/MAPA are presented in Figure 2.7 and the values are tabulated in Table 2.4. Standard deviations of 5-fold measurements for each data point are also given in the tables for all the systems. With the exception of few data points, all freezing point measurements for unloaded systems have standard deviation of equal or less than 0.05 K. Generally, the standard deviation has shown a tendency to increase with increase in amine concentration in this work. This might be a result of relatively less efficient mixing of sample due to increased viscosity of concentrated solutions at lower temperatures.

The MAPA-water system has shown a greater decrease in the freezing points as a function of amine composition compared to DEEA-water system as can be seen in Figure 2.6. It can also be noticed in Figure 2.7 that the increase in MAPA concentration in the DEEA/MAPA mixtures decreases the freezing points and the curves get closer to the MAPA-water curve. The MAPA-water system represents the low freezing points both on mole and mass percent basis.

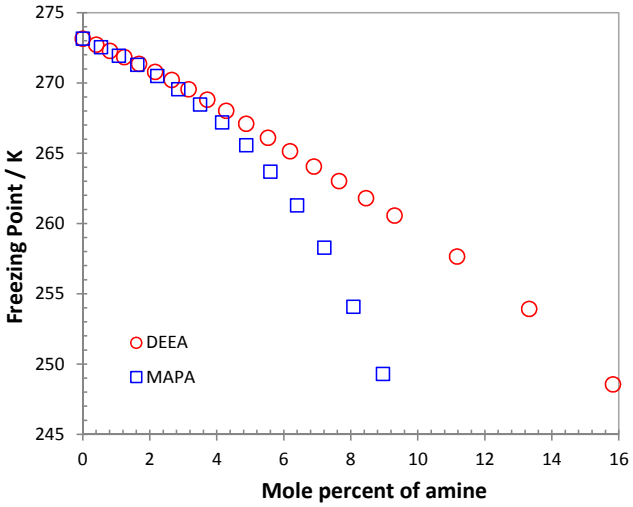

Figure 2.6: Freezing points of DEEA-water and MAPA-water systems measured in this work.

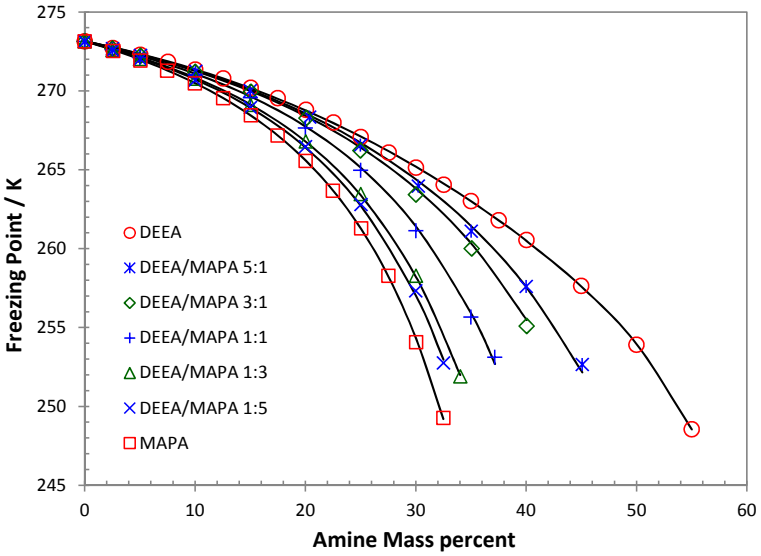

Figure 2.7: Freezing points of DEEA-MAPA-water system at different molar ratios of DEEA/MAPA. Freezing points of DEEA-water and MAPA-water are also shown. The lines were calculated by using Equations 6 to 8.

Freezing points data of binary aqueous DEEA and MAPA solutions on molal basis (mol.(kg H_2O)$^{-1}$) from this work are compared with MEA and MDEA data found in the literature. All these results are plotted against the freezing points of an ideal solution as shown in Figure 2.8. The ideal solution curve was calculated by

using Equation 5 and the data are given in Table 2.1. It can be seen that the DEEA (a tertiary alkanolamine) freezing point values are close to that of MEA data from Chang et al.[21] and Fosbøl et al.[22] MDEA has slightly low freezing points than DEEA and the difference increases at high concentrations. The MAPA-water system has shown the greatest deviation from ideality among all the compared amine systems. This indicates that the MAPA-water interaction is higher than the interaction of DEEA-water, MEA-water and MDEA-water systems.

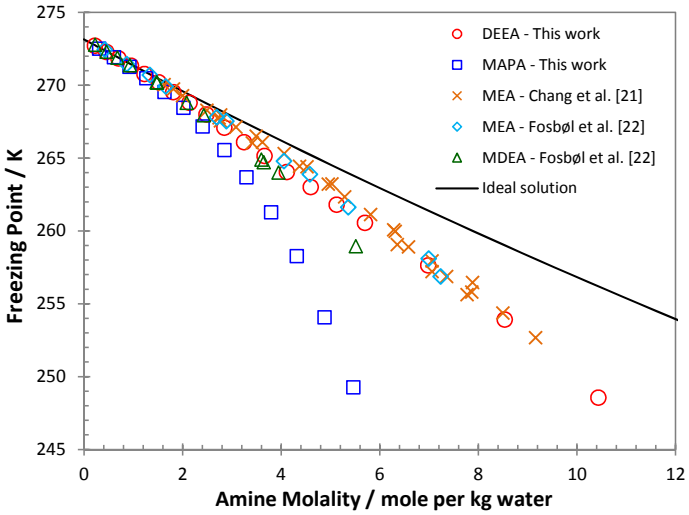

Figure 2.8: Freezing point measurements from this work compared with MEA and MDEA found in the literature. All the data are also compared with the freezing points of an ideal solution calculated by using Equation 5 and the data given in Table 2.1.

For CO_2 loaded systems, freezing points were measured for the ternary DEEA-CO_2-H_2O and MAPA-CO_2-H_2O systems. The measurements were carried out for 12, 20, 30, and 33 mass percent DEEA solutions at different CO_2 loadings, and the results are given in Figure 2.9 and Table 2.5. For MAPA, the measurements were taken for 10, 20, and 27 mass percent MAPA solutions at different CO_2 loadings. The results of MAPA-CO_2-H_2O system are given in Figure 2.10 and Table 2.6. For CO_2 loaded systems, all freezing point data are presented as a function of CO_2 loading. Standard deviations of freezing point data are also given in the tables for all the CO_2 loaded systems. Similar to the unloaded systems, freezing point measurements for the CO_2 loaded systems have a standard deviation of equal or less than 0.05 K with the exception of only a few data points. The method developed to measure freezing point for the CO_2 loaded systems has shown good accuracy.

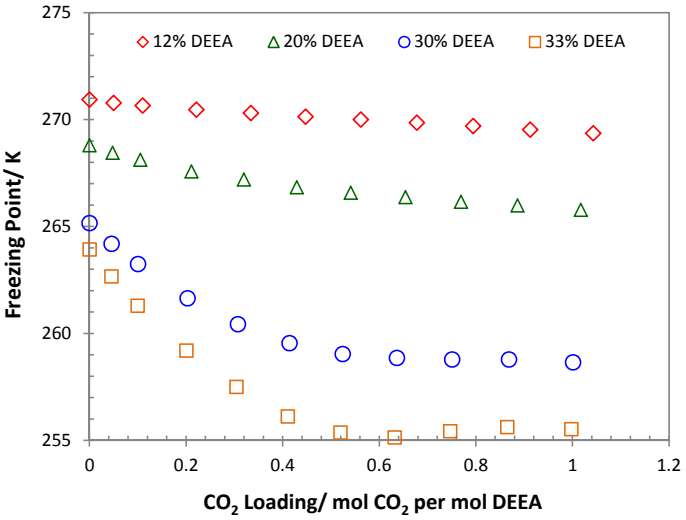

Figure 2.9: Freezing points of different mass percent DEEA solutions as a function of CO_2 loading.

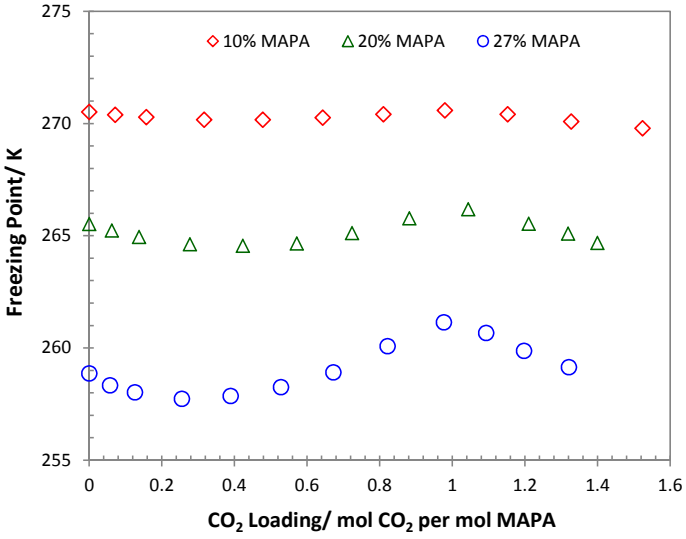

Figure 2.10: Freezing points of different mass percent MAPA solutions as a function of CO_2 loading.

In the ternary DEEA-CO_2-H_2O system, freezing points first decrease almost linearly up to CO_2 loading of around 0.6 (mol CO_2.(mol DEEA)$^{-1}$) and then become almost constant as can be seen in Figure 2.9. This effect is more pronounced at high DEEA concentrations i.e. 30 and 33 mass percent DEEA. On the other hand, ternary MAPA-CO_2-H_2O system behaves very differently. The freezing points first decrease, then

increase, and again decrease as a function of CO_2 loading and give a wave-like curve as shown in Figure 2.10. This wave-like behavior increases with the concentration of MAPA. There is a change in pH when the MAPA solutions were loaded with CO_2 and this change in pH changes the speciation which resulted in changing the freezing point of the solutions. MAPA is a diamine and there are possibilities of formation of several species in the solution. So, this wave-like behavior in MAPA solutions at higher concentrations may be explained by the formation of different species with loading.

2.3.1 Freezing Point Correlation

A correlation for the estimation of FPD as a function of amine composition was formulated for the amine systems studied in this work. The equations of the correlation are given by

$$\Delta T_{DEEA} = c_1 b_{DEEA} + c_2 b_{DEEA}^2 + c_3 b_{DEEA}^3 + c_4 b_{DEEA}^4 \quad (6)$$

$$\Delta T_{MAPA} = c_5 b_{MAPA} + c_6 b_{MAPA}^2 + c_7 b_{MAPA}^4 \quad (7)$$

$$\Delta T_{Mix} = \Delta T_{DEEA} + \Delta T_{MAPA} + b_{DEEA} b_{MAPA} \left(c_8 b_{DEEA} + c_9 b_{MAPA} \right) \quad (8)$$

where b_i is the molality of amine i in mol amine.(kg water)$^{-1}$, ΔT_i is the calculated freezing points in Kelvin and c_1 to c_9 are the parameters to be fitted. Equation 6 with four parameters, c_1 to c_4, and Equation 7 with three parameters, c_5 to c_7, represent the freezing point correlation for the two binary systems DEEA-water and MAPA-water respectively. A correlation for the ternary DEEA-MAPA-water system is proposed in Equation 8. The first two terms in Equation 8 are the freezing point contribution from DEEA and MAPA with a linear mixing rule based on Equations 6 and 7. The last term in Equation 8 with two parameters, c_8 and c_9, describes the interaction due to deviation from the linear mixing rule. Least square fitting between the experimental and calculated freezing points was used to obtain the values of model parameters, c_1 to c_9, used in the Equations 6 to 8. The values of these parameters along with their units are given in Table 2.7. For CO_2 loaded systems, a detailed thermodynamic modeling is needed.

The isothermal freezing point curves calculated from the model Equations 6 to 8 are shown in Figure 2.11 represented by the lines. The shown experimental data points are the selected freezing points from all the measured data which lay in the close neighborhood to the calculated isotherms. The scatter in the figure is due to the small difference in calculation and experimental conditions. The selected data points for the isotherms are ± 0.8 K from the experimental conditions. There is an acceptable agreement between the experimental and the calculated freezing points. The triangular diagram in Figure 2.11 shows the solubility of ice in the ternary mixture of DEEA-MAPA-H_2O for water mass percent > 50. It can also be noticed that there is almost a linear trend in the water saturated isothermal phase boundary lines.

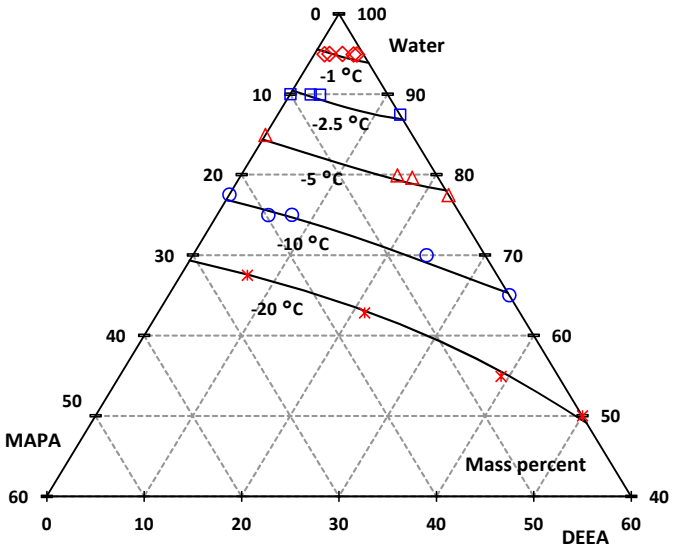

Figure 2.11: Isothermal freezing points of ice in DEEA-MAPA-H_2O solutions at -1, -2.5, -5, -10, and -20°C. Different symbols are the selected freezing point measurements of this work with ± 0.8 K from the selected isothermal temperatures. Equations 6 to 8 were used to calculate the lines at constant temperatures.

The model is valid in a molality range from 0 to 10.5 mol.(kg H_2O)$^{-1}$ for DEEA (0 to 55 mass percent) and 0 to 5.5 mol.(kg H_2O)$^{-1}$ for MAPA (0 to 32.5 mass percent). A parity plot is given in Figure 2.12 which shows the experimental and calculated freezing points evenly distributed on the diagonal line. The mean absolute deviation for the correlation is 0.1 K.

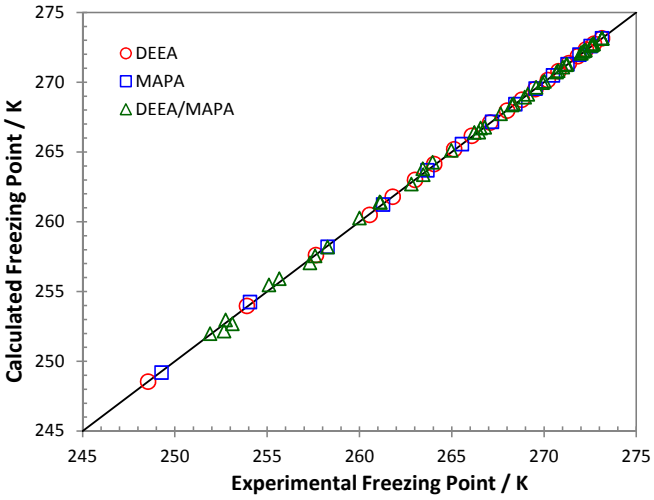

Figure 2.12: Parity plot with experimental and calculated values of freezing points in this work.

2.4 Conclusions

Freezing points for the phase change (or de-mixing) CO_2 solvents were measured using a modified Beckmann apparatus. The measurements were performed in the concentration range of 0 to 55 and 0 to 32.5 mass percent of amine respectively for the binary aqueous DEEA and MAPA solutions. Measurements in the ternary aqueous DEEA-MAPA solutions were made for the mixtures with molar ratios of 5:1, 3:1, 1:1, 1:3, and 1:5 for DEEA/MAPA. These mixtures were diluted with deionized water and the measurements were taken in a concentration range of 0 to 45 mass percent of total amine. A method was developed for easy and accurate measurement of freezing point in the CO_2 loaded systems. It is based on saturation of the solution by CO_2 and then dilution by using a batch of the original unloaded solution in order to get the solutions with different CO_2 loadings. For CO_2 loaded systems, freezing point measurements were carried out for 12, 20, 30, and 33 mass percent DEEA solutions and 10, 20, and 27 mass percent MAPA solutions. The apparatus and the experimental method used have shown good repeatability and accuracy.

The measured freezing point data for the binary aqueous DEEA and MAPA solutions are compared with MEA and MDEA data available in the literature. The experimental values indicate that the DEEA-water interaction is almost similar to that of MEA-water interaction. MAPA has shown a stronger non-ideal behavior compared to DEEA. A correlation for the freezing points as a function of solution composition was formulated for unloaded systems which is valid from 0 to 55 mass percent of DEEA and 0 to 32.5 mass percent of MAPA.

The measured freezing point data can be used for thermodynamic modeling of CO_2 absorption-desorption systems when aqueous blends of DEEA-MAPA are used as solvents. Water activity data can very accurately be determined from the measured freezing point data which can enhance the prediction of water loss, energy efficiency and the energy requirements for solvent regeneration in the desorber.

2.5 References

(1) Kohl, A. L.; Nielsen, R. B. Gas Purification, 5th ed. Gulf Publishing Company, Houston, TX, **1997**.

(2) Davison, J. Performance and costs of power plants with capture and storage of CO_2. *Energy* **2007**, 32, 1163-1176.

(3) Davidson, R. M. Post-combustion Carbon Capture from Coal Fired Plants - Solvent Scrubbing. IEA Clean Coal Centre, CCC/125, **2007**.

(4) IEA report, Technology Roadmap - CCS, **2009**, via: http://www.iea.org/papers/2009/CCS_Roadmap.pdf (accessed September 2012)

(5) Wang, M.; Lawal, A.; Stephenson, P.; Sidders, J.; Ramshaw, C. Post-combustion CO_2 capture with chemical absorption: A state-of-the-art review. *Chem. Eng. Res. Des.* **2011**, 89, 1609-1624.

(6) Versteeg, G. F.; Van Swaaij, W. P. M. On the kinetics between CO_2 and alkanolamines both in aqueous and non-aqueous solutions - I. Primary and secondary amines. *Chem. Eng. Sci.* **1988**, 43 (3), 573-585.

(7) Donaldson, T. L.; Nguyen, Y. N. Carbon dioxide reaction kinetics and transport in aqueous amine membranes. *Ind. Eng. Chem. Fundam.* **1980**, 19, 260-266.

(8) Versteeg, G. F.; Van Swaaij, W. P. M. On the kinetics between CO_2 and alkanolamines both in aqueous and non-aqueous solutions - II. Tertiary amines. *Chem. Eng. Sci.* **1988**, 43 (3), 587-591.

(9) Versteeg, G. F.; Van Dijck, L. A. J.; Van Swaaij, W. P. M. On the kinetics between CO_2 and alkanolamines both in aqueous and non-aqueous solutions. An overview. *Chem. Eng. Commun.* **1996**, 144, 113-158.

(10) Kozak, F.; Petig, A.; Morris, E.; Rhudy, R.; Thimsen, D. Chilled ammonia process for CO_2 capture, *Energy Procedia* **2009**, 1, 1419-1426.

(11) Raynal, L.; Pascal, A.; Bouillon, P.-A.; Gomez, A.; le Febvre de Nailly, M.; Jacquin, M.; Kittel, J.; di Lella, A.; Mougin, P.; Trapy, J. The DMX^{TM} process: an original solution for lowering the cost of post-combustion carbon capture, *Energy Procedia* **2011**, 4, 779-786.

(12) Agar, D. W.; Tan, Y.; Zhang, X. CO_2 removal processes by means of absorption using thermomorphic biphasic aqueous amine solutions. Patent WO/2008/015217, **2008**.

(13) Zhang, J.; Agar, D. W.; Zhang, X.; Geuzebroek, F. CO_2 absorption in biphasic solvents with enhanced low temperature solvent regeneration. *Energy Procedia* **2011**, 4, 67-74.

(14) Zhang, J.; Nwani, O.; Tan, Y.; Agar, D. W. Carbon dioxide absorption into biphasic amine solvent with solvent loss reduction. *Chem. Eng. Res. Des.* **2011**, 89, 1190-1196.

(15) Zhang, J.; Misch, R.; Tan, Y.; Agar, D. W. Novel thermomorphic biphasic amine solvents for CO_2 absorption and low-temperature extractive regeneration. *Chem. Eng. Technol.* **2011**, 34 (9), 1481-1489.

(16) Pinto, D. D. D.; Monteiro, J. G. M.-S.; Bruder, P.; Zaidy, S. A. H.; Jonassen, Ø.; Hartono, A.; Svendsen, H. F. Correlation and Prediction of Vapor-Liquid-Liquid Equilibrium using the e-NRTL model applied to the MAPA-DEEA-CO_2-Water System. *TCCS-6 Trondheim*, 2011.

(17) Arshad, M. W.; von Solms, N.; Thomsen, K.; Svendsen, H. F. Heat of Absorption of CO_2 in Aqueous Solutions of DEEA, MAPA and their Mixture. *GHGT-11 Kyoto*, November 2012, Paper 496.

(18) Thomsen, K. Aqueous Electrolytes, Model Parameters and Process Simulation. Ph.D. Thesis, IVC-SEP, Technical University of Denmark, Kgs. Lyngby, Denmark, **1997**.

(19) Thomsen, K.; Rasmussen, P.; Gani, R. Correlation and prediction of thermal properties and phase behaviour for a class of aqueous electrolyte systems. *Chem. Eng. Sci.* **1996**, 51 (14), 3675-3683.

(20) Fosbøl, P. L.; Thomsen, K.; Stenby, E. H. Modeling of the Mixed Solvent Electrolyte System CO_2-Na_2CO_3-$NaHCO_3$-Monoethylene Glycol-Water. *Ind. Eng. Chem. Res.* **2009**, 48 (4), 4565-4578.

(21) Chang, H.; Posey, M.; Rochelle, G. T. Thermodynamics of alkanolamine-water solutions from freezing point measurements. *Ind. Eng. Chem. Res.* **1993**, 32, 2324-2335.

(22) Fosbøl, P. L.; Pedersen, M. G.; Thomsen, K. Freezing Point Depressions of Aqueous MEA, MDEA, and MEA-MDEA Measured with a New Apparatus. *J. Chem. Eng. Data* **2011**, 56, 995-1000.

(23) Fosbøl, P. L.; Neerup, R.; Arshad, M. W.; Tecle, Z.; Thomsen, K. Aqueous Solubility of Piperazine and 2-Amino-2-methyl-1-propanol plus Their Mixtures Using an Improved Freezing-Point Depression Method. *J. Chem. Eng. Data* **2011**, 56, 5088-5093.

(24) Clarke, E.C.W.; Glew, D. N. Evaluation of the thermodynamic functions for aqueous sodium chloride from equilibrium and calorimetric measurements below 154^{o}C. *J. Phys. Chem. Ref. Data* **1985**, 14, 489-610.

(25) Kim, I.; Svendsen, H.F.; Borresen, E. Ebulliometric Determination of Vapor-Liquid Equilibria for Pure Water, Monoethanolamine, N-Methyldiethanolamine, 3-(Methylamino)-propylamine, and Their Binary and Ternary Solutions. *J. Chem. Eng. Data* **2008**, 53 (11), 2521-2531.

(26) Alkalinity of Amine-Containing Gas Washing Solutions. Titration Application Note No. T-27; Metrohm AG: Switzerland.

(27) Ma'mun, S.; Jakobsen, J. P.; Svendsen, H. F. Experimental and Modeling Study of the Solubility of Carbon Dioxide in Aqueous 30 Mass % 2-((2-Aminoethyl)amino)ethanol Solution. *Ind. Eng. Chem. Res.* **2006**, 45(8), 2505-2512.

2.6 Appendix

Table 2.1: Standard state formation properties and correlation parameter for the heat capacity (Equation 4).

	$\Delta_f G^o$	$\Delta_f H^o$	a_i	b_i	c_i
	kJ.mol^{-1}	kJ.mol^{-1}	J.(mol K)$^{-1}$	J.(mol K^2)$^{-1}$	J.mol^{-1}
Water	-237.129[20]	-285.83[20]	58.370[19]	0.03896[19]	523.88[19]
Ice	-236.538[20]	-292.624[20]	49.627[A]	0[20]	0[20]

[A] Revised value estimated by Kaj Thomsen, not previously published.

Table 2.2: Experimental measurements of freezing point for DEEA–Water system.[a]

DEEA Concentration	Freezing Point	Standard Deviation
Mass Percent	K	K
2.54	272.71	0.01
5.05	272.28	0.009
7.543	271.84	0.006
10.012	271.35	0.008
12.551	270.79	0.005
15.053	270.21	0.003
17.506	269.54	0.008
20.061	268.80	0.02
22.536	268.01	0.02
25.010	267.09	0.008
27.552	266.09	0.02
30.024	265.14	0.02
32.529	264.05	0.02
35.010	263.01	0.03
37.524	261.80	0.03
40.034	260.55	0.02
44.988	257.64	0.03
49.991	253.91	0.05
55.010	248.56	0.05

[a] The standard uncertainty for the composition of the solutions is 0.00008 mass fraction, except for the first two solutions for which it is 0.0003 mass fraction. The standard uncertainty for the temperatures is estimated to be $u(T) = 0.03$ K.

Table 2.3: Experimental measurements of freezing point for MAPA–Water system.[a]

MAPA Concentration	Freezing Point	Standard Deviation
Mass Percent	K	K
2.59	272.53	0.004
5.05	271.93	0.005
7.493	271.28	0.005
9.998	270.49	0.005
12.550	269.55	0.003
15.073	268.46	0.007
17.495	267.18	0.003
20.042	265.56	0.02
22.497	263.68	0.01
25.056	261.29	0.03
27.536	258.28	0.04
30.050	254.07	0.04
32.501	249.28	0.08

[a] The standard uncertainty for the composition of the solutions is 0.00008 mass fraction, except for the first two solutions for which it is 0.0003 mass fraction. The standard uncertainty for the temperatures is estimated to be $u(T) = 0.03$ K.

Table 2.4: Experimental measurements of freezing point for DEEA–MAPA–Water system.[a]

Amine Mixture	DEEA Concentration	MAPA Concentration	Freezing Point	Standard Deviation
Molar Ratio	Mass Percent	Mass Percent	K	K
DEEA/MAPA	2.19	0.33	272.69	0.004
5:1	4.40	0.66	272.25	0.004
	8.750	1.318	271.25	0.009
	13.044	1.965	270.03	0.01
	17.711	2.668	268.35	0.02
	21.725	3.272	266.56	0.02
	26.278	3.958	263.97	0.05
	30.445	4.585	261.11	0.03
	34.777	5.238	257.60	0.06
	39.184	5.902	252.67	0.07
DEEA/MAPA	2.02	0.51	272.68	0.007
3:1	4.06	1.02	272.22	0.005
	8.011	2.009	271.21	0.008
	12.047	3.021	269.93	0.008
	16.071	4.031	268.27	0.01
	19.988	5.013	266.23	0.03
	24.002	6.020	263.43	0.04
	28.049	7.035	260.00	0.03
	32.020	8.031	255.10	0.08
DEEA/MAPA	1.44	1.08	272.63	0.01
1:1	2.86	2.15	272.13	0.003
	5.722	4.308	271.02	0.01
	8.576	6.456	269.58	0.01
	11.416	8.594	267.66	0.005
	14.272	10.744	264.98	0.02
	17.132	12.897	261.15	0.03
	19.966	15.030	255.67	0.04
	21.209	15.966	253.12	0.06
DEEA/MAPA	0.78	1.75	272.59	0.005
1:3	1.54	3.48	272.02	0.008
	3.096	6.981	270.78	0.008
	4.615	10.409	269.12	0.01
	6.155	13.882	266.80	0.01
	7.685	17.332	263.47	0.01
	9.226	20.806	258.29	0.03
	10.453	23.574	251.91	0.06
DEEA/MAPA	0.54	2.01	272.57	0.003
1:5	1.06	3.99	272.03	0.002
	2.108	7.920	270.69	0.001
	3.157	11.858	268.95	0.01
	4.205	15.795	266.48	0.02
	5.262	19.767	262.81	0.01
	6.304	23.682	257.33	0.02
	6.836	25.678	252.76	0.06

[a] The mass percent of the amines are listed. The remaining mass percent is made up of water. The standard uncertainty for the composition of the solutions in each amine mixture is 0.00007 mass fraction, except for the first two solutions in each mixture for which it is 0.0003 mass fraction. The standard uncertainty for the temperatures is estimated to be $u(T) = 0.03$ K.

Table 2.5: Experimental measurements of freezing point for DEEA–CO_2–Water system.[a]

Solution	CO_2 Loading	Freezing Point	Standard Deviation
Mass Percent	mol CO_2.(mol DEEA)$^{-1}$	K	K
12.00% DEEA	0	270.93	0.01
	0.050	270.78	0.02
	0.110	270.65	0.02
	0.221	270.46	0.02
	0.334	270.30	0.007
	0.447	270.13	0.01
	0.562	270.00	0.01
	0.678	269.85	0.02
	0.794	269.69	0.01
	0.912	269.52	0.007
	1.043	269.35	0.005
20.00% DEEA	0	268.80	0.02
	0.048	268.44	0.02
	0.105	268.11	0.02
	0.211	267.57	0.02
	0.319	267.19	0.03
	0.429	266.83	0.01
	0.541	266.58	0.03
	0.654	266.37	0.03
	0.769	266.15	0.03
	0.887	265.99	0.02
	1.017	265.78	0.03
30.00% DEEA	0	265.16	0.01
	0.046	264.19	0.03
	0.100	263.24	0.02
	0.203	261.64	0.05
	0.307	260.42	0.02
	0.414	259.54	0.04
	0.524	259.04	0.06
	0.637	258.85	0.03
	0.751	258.78	0.04
	0.869	258.78	0.04
	1.001	258.64	0.04
33.00% DEEA	0	263.92	0.02
	0.045	262.66	0.05
	0.100	261.29	0.02
	0.200	259.19	0.03
	0.304	257.50	0.05
	0.411	256.11	0.05
	0.520	255.35	0.04
	0.632	255.12	0.05
	0.747	255.42	0.08
	0.865	255.62	0.04
	0.997	255.51	0.05

[a] The standard uncertainty for the temperatures is estimated to be $u(T) = 0.03$ K.

Table 2.6: Experimental measurements of freezing point for MAPA–CO_2–Water system.[a]

Solution	CO_2 Loading	Freezing Point	Standard Deviation
Mass Percent	mol CO_2.(mol MAPA)$^{-1}$	(K)	(K)
10.00% MAPA	0	270.51	0.005
	0.072	270.38	0.006
	0.157	270.27	0.02
	0.317	270.16	0.01
	0.478	270.16	0.01
	0.643	270.26	0.01
	0.811	270.40	0.01
	0.980	270.57	0.02
	1.153	270.41	0.008
	1.328	270.08	0.01
	1.524	269.78	0.008
20.00% MAPA	0	265.52	0.04
	0.063	265.23	0.02
	0.137	264.94	0.02
	0.278	264.62	0.04
	0.423	264.55	0.03
	0.572	264.65	0.04
	0.724	265.12	0.02
	0.882	265.78	0.02
	1.044	266.18	0.03
	1.211	265.53	0.02
	1.319	265.09	0.03
	1.399	264.68	0.008
27.00% MAPA	0	258.87	0.07
	0.057	258.33	0.03
	0.126	258.02	0.04
	0.255	257.73	0.04
	0.390	257.86	0.02
	0.528	258.25	0.07
	0.672	258.91	0.05
	0.822	260.07	0.05
	0.977	261.14	0.04
	1.093	260.67	0.06
	1.198	259.86	0.05
	1.321	259.14	0.05

[a] The standard uncertainty for the temperatures is estimated to be $u(T) = 0.03$ K.

Table 2.7: Parameters of equations 6 to 8 for freezing point correlation.

Model Parameter	Parameter value	Parameter unit
c_1	-1.685	$K.(mol.kg^{-1})^{-1}$
c_2	-0.2449	$K.(mol.kg^{-1})^{-2}$
c_3	0.03741	$K.(mol.kg^{-1})^{-3}$
c_4	-0.001929	$K.(mol.kg^{-1})^{-4}$
c_5	-1.781	$K.(mol.kg^{-1})^{-1}$
c_6	-0.249	$K.(mol.kg^{-1})^{-2}$
c_7	-0.00763	$K.(mol.kg^{-1})^{-4}$
c_8	-0.06612	$K.(mol.kg^{-1})^{-3}$
c_9	-0.2098	$K.(mol.kg^{-1})^{-3}$

3. Heat of Absorption of CO_2

3.1 Introduction

Amine scrubbing is one of the most common postcombustion CO_2 capture technologies available today. Owing to its extensive use in different industrial applications e.g., CO_2 removal from reformer gases, natural gas sweetening etc.[1], it has been considered as the most feasible route for the post-combustion capture. These amine scrubbing processes selectively absorb CO_2 from the flue gases and release a high-purity CO_2 offgas stream upon heating in a stripper which is suitable for storage without any further treatment. However, it is well-known that these processes are energy intensive.[2,3] Innovative process design and technological improvements are necessary in order to reduce the high capital cost and energy requirements for the capture processes.[4] Besides this, it is also essential to develop solvent systems with improved energy efficiency while retaining the desirable properties of fast reaction rate, high loading, and cyclic capacities, low solvent degradation, low corrosiveness, and being environmental friendly, etc. For energy efficient solvent systems, besides reasonable heat of absorption, the equilibrium temperature sensitivity should also be high in order to reduce the need for stripping steam.[5]

Single amine solvent systems for CO_2 capture were extensively studied and reported in the open literature. Primary and secondary amines are very reactive toward CO_2 as they form carbamates. They have high heats of reaction and fast reaction rates.[6] Consequently, high energy is required for the solvent regeneration. Tertiary amines, on the other hand, form bicarbonates due to base catalysis of CO_2 hydration.[7] They have low heats of reaction leading to low energy requirements for the reaction reversion. These amines generally have high CO_2 loading capacity and a low reaction rate.[8,9] Each type of amine group is associated with its own merits and demerits. Therefore, amine blends have become an attractive choice to exploit the favorable properties of both amine types. Various amine blends (e.g., MEA + MDEA) have been studied and reported in the literature.[10,11]

Recently, a new class of mixed amine solvent systems is emerging, which may be called phase change solvents. They have shown a potential to reduce the solvent regeneration energy. These phase change solvents either form precipitates on CO_2 absorption such as the Alstom chilled ammonia process (CAP)[12] or make a liquid-liquid split e.g., the DMX^{TM} process[13,14] and Thermomorphic Biphasic Solvents (TBS) systems.[15] The TBS systems, after CO_2 absorption, regenerate at relatively lower temperature of 80 ^{o}C compared to the regeneration temperature of conventional alkanolamine solutions (~ 120 ^{o}C). They give liquid-liquid split upon heating and agitation during the regeneration and become single phase during absorption. The main advantage of these systems is lower regeneration temperature which can be achieved without using steam.[16-18] In the DMX^{TM} process, on the other hand, the single phase solvent splits into two liquid phases after CO_2 absorption. The CO_2 lean phase recycles back to the absorber without regeneration and only the

CO_2 rich phase goes to the stripper for thermal regeneration. Therefore, the energy consumption for solvent regeneration can be lowered due to reduced flow rate of the liquid in the stripper.[13]

In the present work, we are investigating a solvent system consisting of two different amines, 2-(diethylamino)ethanol (DEEA) and 3-(methylamino)propylamine (MAPA). DEEA is a tertiary alkanolamine and MAPA has two amine functional groups, a primary and a secondary (see Figure 3.1). Therefore, we can exploit the favorable properties of amines by blending DEEA and MAPA. Their mixtures have an additional benefit of making liquid-liquid split when reacted with CO_2. Previous studies have shown that the single phase aqueous blends of DEEA-MAPA turn into two liquid phases upon CO_2 absorption with an upper phase lean in CO_2 and the lower phase rich in CO_2.[19] If only the lower phase is regenerated, these blends have the potential to reduce the energy requirements for the solvent regeneration.

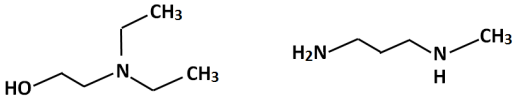

DEEA MAPA

Figure 3.1: Structures of DEEA and MAPA.

Heat of absorption is an important parameter to design unit operations in the gas treating processes. The energy requirements for solvent regeneration in the capture process are directly related to it. The magnitude of heat of absorption gives a direct measure of heat requirements in the stripper.[20] Experimental data in the literature[21-25] have shown a difference of about 25-30 % between the enthalpy of absorption at 40 ^{o}C (absorption condition) and 120 ^{o}C (desorption condition). Therefore, the effect of temperature on heat of absorption is an important parameter to be determined, which is generally ignored, and a constant value of enthalpy of absorption is assumed both for the absorption and desorption conditions.[1] Direct calorimetric measurements give accurate heat of absorption values, reflecting the combined effect of heat due to the reaction between solvent and CO_2, and the physical dissolution of gas in the solvent. Since, it is possible to perform the heat of absorption measurements isothermally in the calorimeters, temperature dependency can be observed.

The main objective in this work is to measure the heats of absorption of CO_2 in aqueous DEEA, MAPA, and their mixtures. Since, these phase change solvent systems are relatively new, no heat of absorption data were found in the literature except some data published by Kim.[25] However, these data do not cover the concentration range where the liquid-liquid phase split occurs. Therefore, an important objective in this work is to measure the data for the aqueous amine mixtures of DEEA-MAPA within the target concentration range where the solvent systems give two liquid phases. The experimental measurements for the solutions with different amine compositions were made by using a reaction calorimeter as a function of CO_2 loading in the temperature range of 40-120 ^{o}C.

3.2 Experimental Section

DEEA (purity ≥ 99 %), MAPA (purity 99 %) and MEA (purity ≥ 99 %) were purchased from Sigma-Aldrich. All chemicals were clear liquids at room temperature. Carbon dioxide (CO_2) was purchased from AGA (a

member of The Linde Group, Linde AG) with purity ≥ 99.99 %. The amine solutions were made with deionized water using an analytical balance. All chemicals were used as received with no further purification.

The amine systems studied in this work with experimental conditions of temperature and pressure are listed in Table 3.1 (All the tables are presented in the Appendix at the end of this chapter). The experimental setup is given schematically in Figure 3.2. The details of reaction calorimeter, working procedure and experimental uncertainties have already been described elsewhere.[23,25] A very brief description of the setup and the procedure is given here.

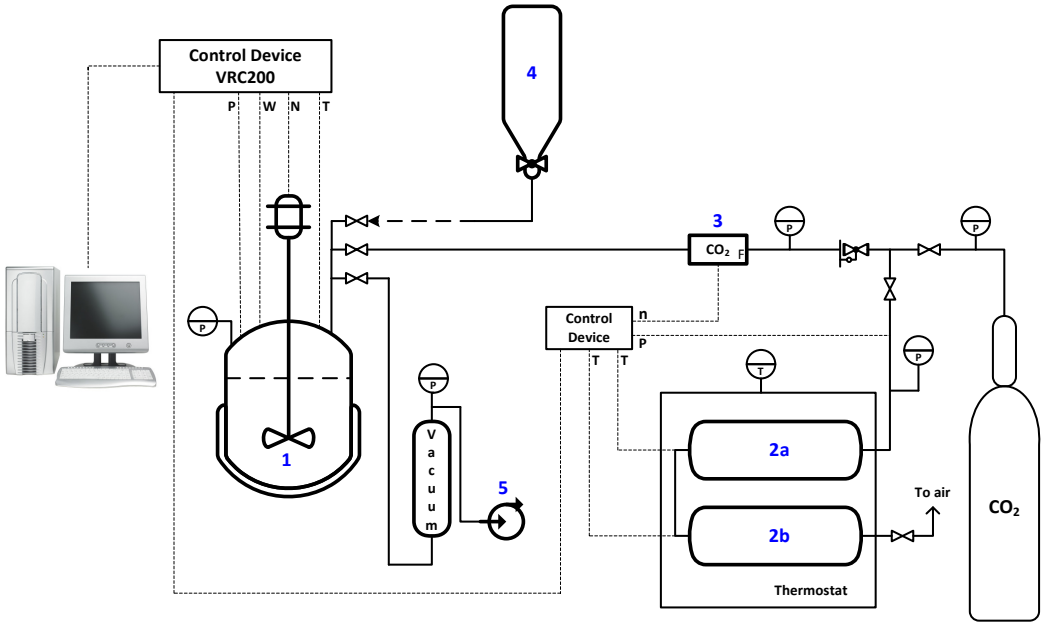

Figure 3.2: Experimental setup for measuring heat of absorption: 1 - reaction calorimeter; 2a, 2b - CO_2 storage cylinders; 3 - CO_2 mass flow controller; 4 - amine solution feed bottle; 5 - vacuum pump.

The reaction calorimeter (model CPA 122) used in this work is a stainless steel reactor from ChemiSens AB, Lund, Sweden. The volume of the reactor is 2000 cm^3 and it has a mechanical agitator. The insulated jacketed reactor is suitable for working in a temperature range of -20 to 200 ^oC and pressure range of -1 to 100 bar. All the units are connected to a computer through a control device (VRC200) which records heat production rate (online Heat Balance), reactor and jacket temperatures, CO_2 storage cylinders and reactor pressure, stirring speed, and other operating parameters as a functions of time.

Before starting the experiment, the reactor was evacuated to a pressure between 40-50 mbar and then filled with CO_2 to a pressure of ~ 3 bar and then evacuated again. This CO_2 flushing was done in order to ensure the complete removal of any inert gas present in the reactor. After evacuation about 1200-1500 cm^3 of amine solution was fed into the reactor from an amine solution feed bottle. The solution was then heated at a preset temperature and the system was allowed to reach the equilibrium. When the change in temperature or pressure of the reactor is respectively within ± 0.01 ^oC or ± 0.01 bar, the system was

assumed to be at equilibrium. Also at equilibrium, no heat transfer took place between the outer heating jacket of the reactor and the reaction system inside the reactor i.e. $\Delta T = T_{in}^{jacket} - T_{out}^{jacket} = constant$. Once the equilibrium is ensured, about 0.1-0.3 mol of CO_2 was injected into the reactor via a precalibrated mass flow controller from CO_2 storage cylinders by monitoring their pressure difference. The injected CO_2 got absorbed in the amine solution and produced heat. The thermostat medium (reactor jacket) added or removed heat from the system to keep the isothermal conditions in the reactor. All the operating parameters were logged against time. The system took about 60-90 min (with some exceptions where it took more time) to reach the new equilibrium and the reactor was fed again with CO_2 for another cycle. The reactor was continuously fed with CO_2 until no more gas could enter in it at a preset pressure (the absorption rate nearly became zero). The temperature and pressure of the reactor and CO_2 storage cylinders were recorded before and after every CO_2 feeding cycle. The amount of CO_2 added to the reactor in each feeding cycle was calculated from the Peng-Robinson equation of state by using the data of pressure difference in the CO_2 storage cylinders (recorded earlier). The heat released in each feeding cycle was determined by integration of the heat flux curve. Finally, the ratio of heat released in a given feeding cycle (Q_{total}) to the amount of CO_2 absorbed (n_{CO_2}) gave the molar heat of absorption for that feeding cycle.

The heat of absorption measurements were taken isothermally at three different temperatures 40, 80 and, 120 ^{o}C. The initial total pressure at a given temperature before feeding any CO_2 to the reactor at the start of each experiment was the amine plus water vapor pressure and it changes after each CO_2 feeding cycle to a maximum final total pressure (amine + water vapors + CO_2) of 6 bar during the last feeding (CO_2 feed pressure). In calculations, it is assumed that the initial total pressure (amine + water vapors) remains constant. Previous work by Kim and Svendsen[23] found no effect of CO_2 feed pressure while performing experiments at different feed pressures of 3 and 10 bar. However, higher loadings could be achieved at very high CO_2 feed pressures. The CO_2 was injected in the reactor in several small steps by keeping a low loading span (about 0.015-0.07 mol CO_2.(mol amine)$^{-1}$) which gives differential heat of absorption values that are semi differential in loading (integral within each feeding interval). These differential heats of absorption values were then converted into integral values by integration.

The main uncertainty sources in the measured heat of absorption data were the calculated amount of CO_2 fed to the reactor from CO_2 storage cylinders, the change of CO_2 amount in the gas phase of the reactor and integration of the heat flux curves to calculate the heat released in each CO_2 feeding cycle (for details see Kim and Svendsen[23] and Kim[25]). The uncertainty can be determined as[23]:

$$\frac{\sigma_{\Delta H_{abs}}}{\Delta H_{abs}} = \sqrt{\left(\frac{\sigma_{Q_{total}}}{Q_{total}}\right)^2 - \left(\frac{\sigma_{n_{CO_2}}}{n_{CO_2}}\right)^2} \qquad (1)$$

As described earlier, the amount of CO_2 injected to the reactor in each feeding cycle was calculated from the Peng-Robinson equation of state. However, it may also be taken from the precalibrated mass flow controller readings. Kim and Svendsen[23] reported an estimated uncertainty of ± 1.2 % for the amount of CO_2 fed to the reactor based on difference between the two methods. The main uncertainty in integrating the heat flux curves stems from selection of the integration borders and setting of the baseline. Since the baseline was not very stable, the heat flux curves were integrated by using the trapezoidal method with the

assumption of linear change in the baseline. Also, each curve was integrated thrice and an average value of heat released was used in the calculations. The uncertainty in the amount of released heat was then determined to be ± 1.7 %. Finally, the estimated uncertainty in the molar heat of absorption was ± 2.1 %.

3.3 Results and Discussion

Aqueous solutions of single amines (5 M DEEA, 2 M MAPA, and 1 M MAPA) and amine mixtures (5 M DEEA + 2 M MAPA and 5 M DEEA + 1 M MAPA) were studied in this work in the temperature range of 40-120 °C. The selected composition of amine blends gave two liquid phases upon CO_2 absorption. The experimental measurements of heat of absorption of CO_2 were carried out with 30 mass % MEA solution and used as a reference case to compare with the systems studied in this work. The results for 30 mass % MEA at temperatures 40, 80 and, 120 °C are presented in Figure 3.3 which shows a good agreement in the data measured in this work, feed pressure of 6 bar, and from Kim[25], feed pressure of 3 bar. No effect of CO_2 feed pressure was observed on heat of absorption.

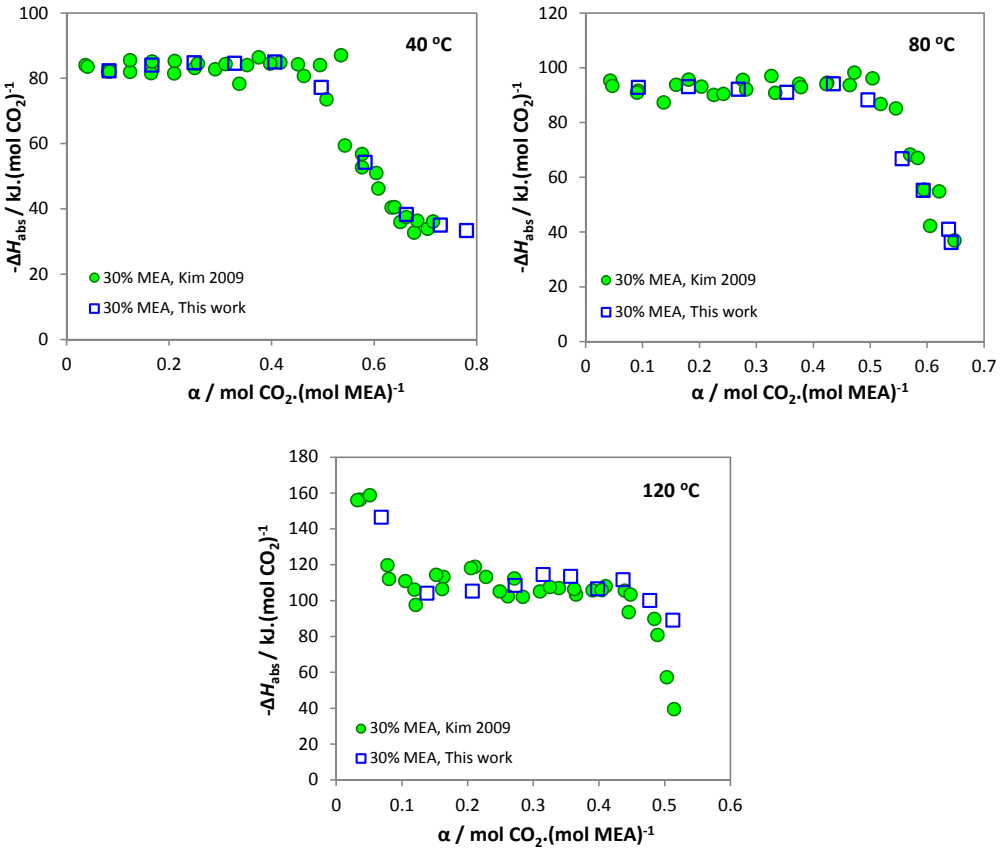

Figure 3.3: Differential enthalpy of absorption of CO_2 with 30 mass % MEA at 40, 80, and 120 °C.

3.3.1 DEEA System

The differential enthalpies of absorption of CO_2 in 5 M (~ 61.1 mass %) DEEA solutions were measured in the temperature ranging from 40-120 °C and converted to integral values by integration. The results are given in Table 3.2, Table 3.3, and Table 3.4. These measurements were taken at a CO_2 feed pressure of 6 bar and compared with 32 and 37 mass % DEEA data from Kim[23] (CO_2 feed pressure of 3 bar). The results are shown in Figure 3.4 which shows disagreement between the two sets of data except at 40 °C up to CO_2 loading of 0.35 mol CO_2.(mol DEEA)$^{-1}$. The repeatability in this work is fairly good, whereas there is some scatter in Kim's data (at 80 and 120 °C). The experimental data show that the heat of absorption is dependent on temperature, that is, increases by increasing the temperature. However, CO_2 loading capacity, on the other hand, decreases significantly by increasing the temperature, for example, the loading capacity at 120 °C decreases by an order of magnitude from the values at 40 °C at the given experimental conditions in this work. Differential heats of absorption values are almost constant for 5 M DEEA at 40 °C up to the saturation loading point of ~ 0.9 mol CO_2.(mol amine)$^{-1}$ in this work. However, it shows strong dependency on CO_2 loading at 80 and 120 °C.

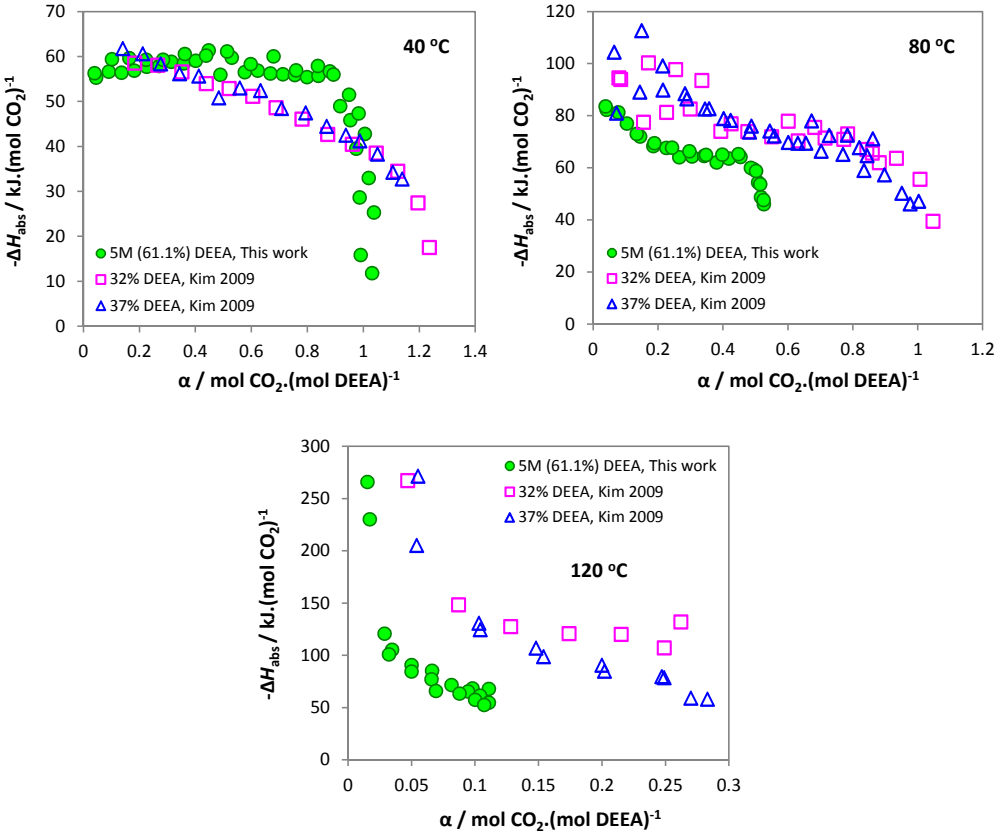

Figure 3.4: Differential enthalpy of absorption of CO_2 with 5M (61.1 mass %) DEEA at 40, 80, and 120 °C.

According to Kim and Svendsen,[23] amine concentration has almost negligible effect on heat of absorption. Contrary to this, Merkley et al.[26] reported that the heat of absorption of CO_2 has dependency on the concentration of amine (MDEA) in the solution. However, there is an agreement between Kim and Merkley that the heat of absorption is independent of partial pressure of CO_2 above the solution. But, this may only be true when one parameter (solvent concentration) is fixed and the other parameter (CO_2 feed pressure) is changed as can be seen in Figure 3.3 where 30 mass % MEA (fixed concentration) is used for two different feed pressures i.e., 6 bar (this work) and 3 bar (Kim's work). Similarly, there is no effect on heat of absorption by fixing the second parameter (CO_2 feed pressure) and changing the first one (solvent concentration). This can be seen in the results of MAPA where no effect on heat of absorption was observed when two different concentrations of MAPA, 2M (~ 17.9 mass %) and 1M (~ 8.9 mass %), were tested at a fixed CO_2 feed pressure of 6 bar (see Figure 3.10). It can also be seen that Kim's findings of negligible concentration effect on heat of absorption may only be valid for small changes in concentration of the solvent e.g., a difference of only 5 mass % between 37 mass % and 32 mass % DEEA solutions. But this may not be true if higher changes in solvent concentration are used, such as 5M (~61.1 mass%) DEEA used in this work compared to 32 mass % and 37 mass % DEEA from Kim. After this discussion, one can argue that changing both parameters, solvent concentration (large difference in concentration) and CO_2 feed pressure, simultaneously can affect the heat of absorption. This argument can explain the disagreement between two sets of data presented in Figure 3.4 in which a comparison is given for different concentrations of DEEA tested at different CO_2 feed pressures.

3.3.2 MAPA System

For MAPA, the differential heats of absorption of CO_2 were measured in 2 M (~ 17.9 mass %) and 1 M (~ 8.9 mass %) MAPA solutions at a CO_2 feed pressure of 6 bar and temperatures 40, 80 and, 120 ^{o}C. These results along with the integrated heat of absorption values are given respectively in Table 3.5, Table 3.6, and Table 3.7 for for 2 M MAPA, and Table 3.8, Table 3.9, and Table 3.10 for 1 M MAPA. The experimental data from this work are compared with 3 and 8 mass % MAPA (feed pressure of 3 bar) data from Kim[25] as presented in Figure 3.5 and Figure 3.6 for 2 M and 1 M MAPA respectively. A very good repeatability can be seen in our results. However, there is large scatter in Kim's data except for the results at 40 ^{o}C. Since MAPA is a diamine, a high CO_2 loading is achieved. The heats of absorption show an increase with increase in the temperature. Contrary to DEEA, MAPA shows high CO_2 loading capacity at higher temperatures. It can also be noticed that the differential heat of absorption is almost constant up to a loading of ~ 1 mol CO_2.(mol amine)$^{-1}$ (the saturation point). After the saturation loading point is reached, the carbamate reversion reaction starts to take place. This can be indicated by a relatively sharp drop in the heat of absorption after the saturation point. Very high heats of absorption values can be seen for lower CO_2 loadings at 120 ^{o}C. This effect was reproduced in all parallel experiments as well as for all the single amine systems studied (5 M DEEA, 2 M MAPA, 1 M MAPA and 30 mass % MEA). Kim and Svendsen[23] also reported this effect for single amine solvent systems. The reason for this behavior is not clear, so these points were omitted in calculating the integral heat of absorption. However, this effect was not observed in the amine mixture systems studied in this work.

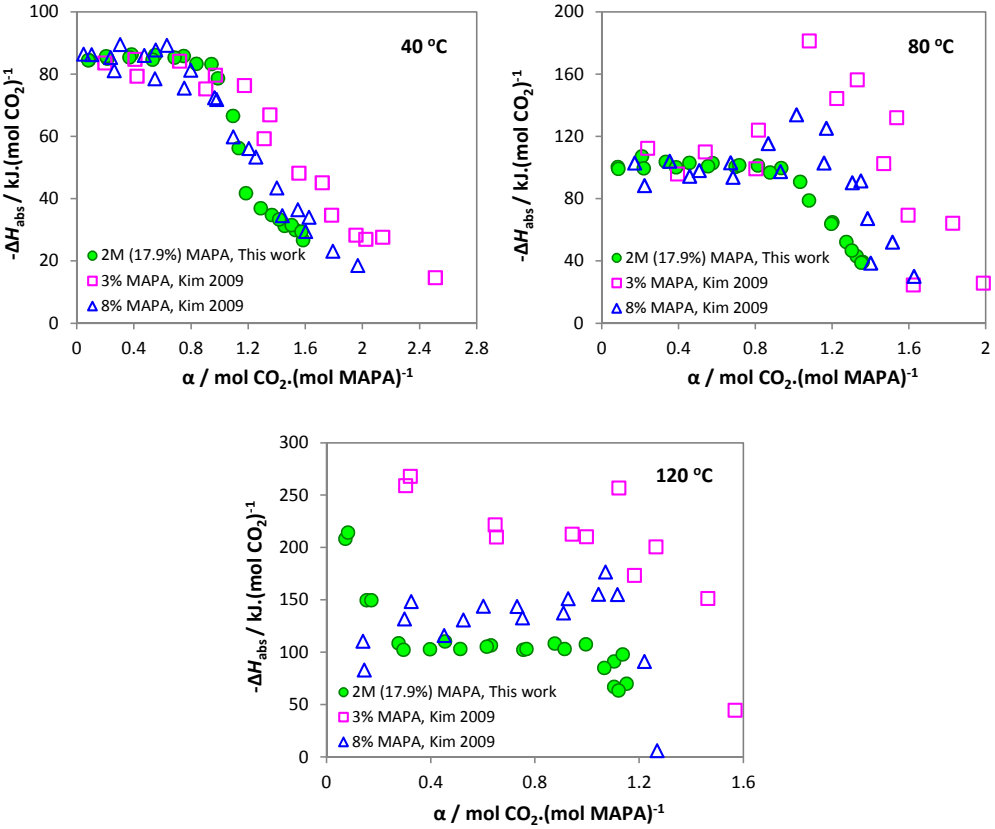

Figure 3.5: Differential enthalpy of absorption of CO_2 with 2M (17.9 mass %) MAPA at 40, 80, and 120 °C.

The two sets of data in Figure 3.5 and Figure 3.6 have fairly good agreement at low CO_2 loadings. It can be seen that 1 M (~ 8.9 mass %) MAPA results from this work and 8 mass % MAPA from Kim have comparatively better agreement which support our argument as discussed earlier. However, 3 mass % MAPA from Kim also shows a fairly good agreement at lower loadings and temperatures 40 and 80 °C. This may be explained by the different effect for different types of amines. For example, Merkley et al.[26] reported solvent concentration dependency of the heat of absorption of CO_2 when MDEA, a tertiary alkanolamine, is used. On the other hand, Kim and Svendsen[23] reported negligible effect of solvent concentration on heat of absorption by using MEA (primary amine) and AEEA (diamine, both primary and secondary amine functionalities). Our results for DEEA (tertiary alkanolamine) and MAPA (diamine, both primary and secondary amine functionalities), and taking into account the earlier discussed argument, are consistent both with Merkley and Kim. Thus, for the studied systems in this work, it can be postulated that the heat of absorption of CO_2 with single amine solutions can be affected by changing solvent composition (maybe large concentration differences) and CO_2 feed pressure simultaneously in combination with type of

amine used. However, further experimental investigations are proposed to see the effect of these parameters on heat of absorption.

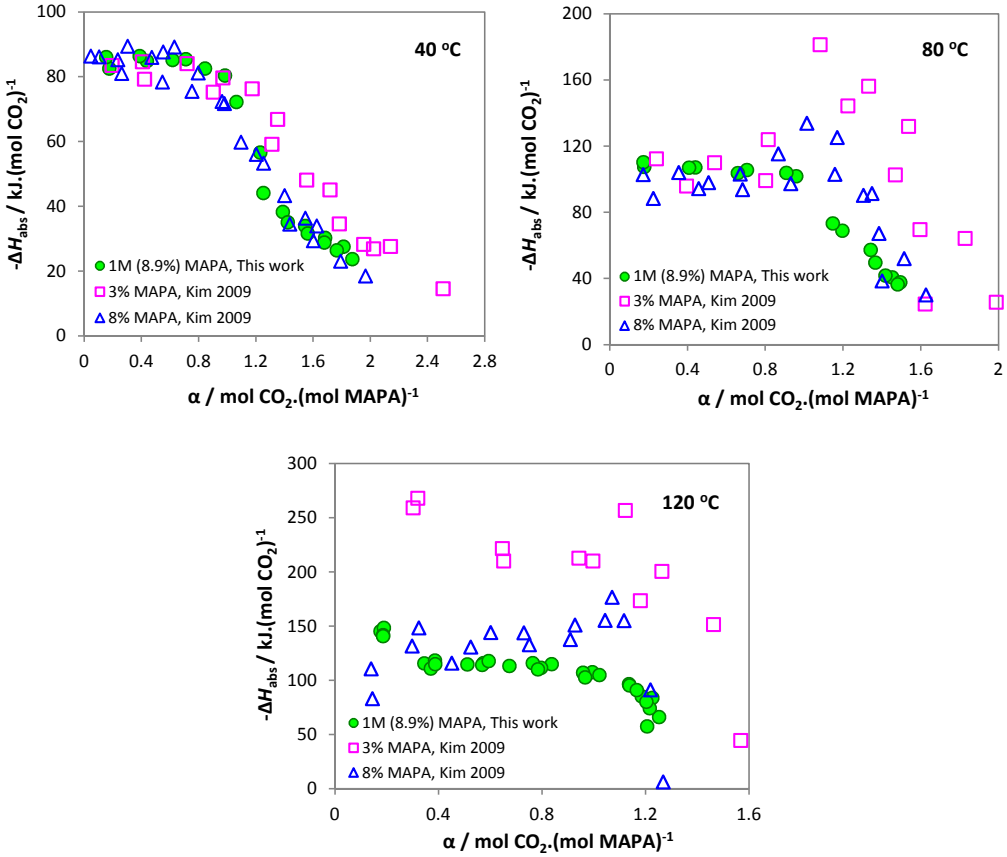

Figure 3.6: Differential enthalpy of absorption of CO_2 with 1M (8.9 mass %) MAPA at 40, 80, and 120 °C.

Heat of absorption results can also be presented as integral values per mole of amine in the solution against CO_2 loading. Mathonat et al.[27] have used this representation to measure the solubility limit of CO_2 in 30 mass % MEA solution when the heat of absorption (kJ.(mol MEA)$^{-1}$) data are measured at very high CO_2 loadings (α = 4 mol CO_2.(mol MEA)$^{-1}$). The results of our work are presented in Figure 3.7 for 5 M DEEA, 2 M MAPA, and 1 M MAPA in the temperature range of 40-120 °C. It may be seen that the integral values heat of absorption first increases almost linearly with CO_2 loading as an almost straight line until the saturation point is reached and then the slope of the line decreases. The heat of absorption is constant along this straight line. It can also be seen that the slope of the line increases with temperature which indicates that the heat of absorption increases with temperature. The slopes of these lines give the values of heats of

absorption in kJ.(mol CO_2)$^{-1}$ which are similar to the measured values. For example, the calculated slopes of the lines for 2 M MAPA give values of 84.9, 101.7 and 122.8 kJ.(mol CO_2)$^{-1}$ for 40, 80 and, 120°C respectively, which are similar to the measured values.

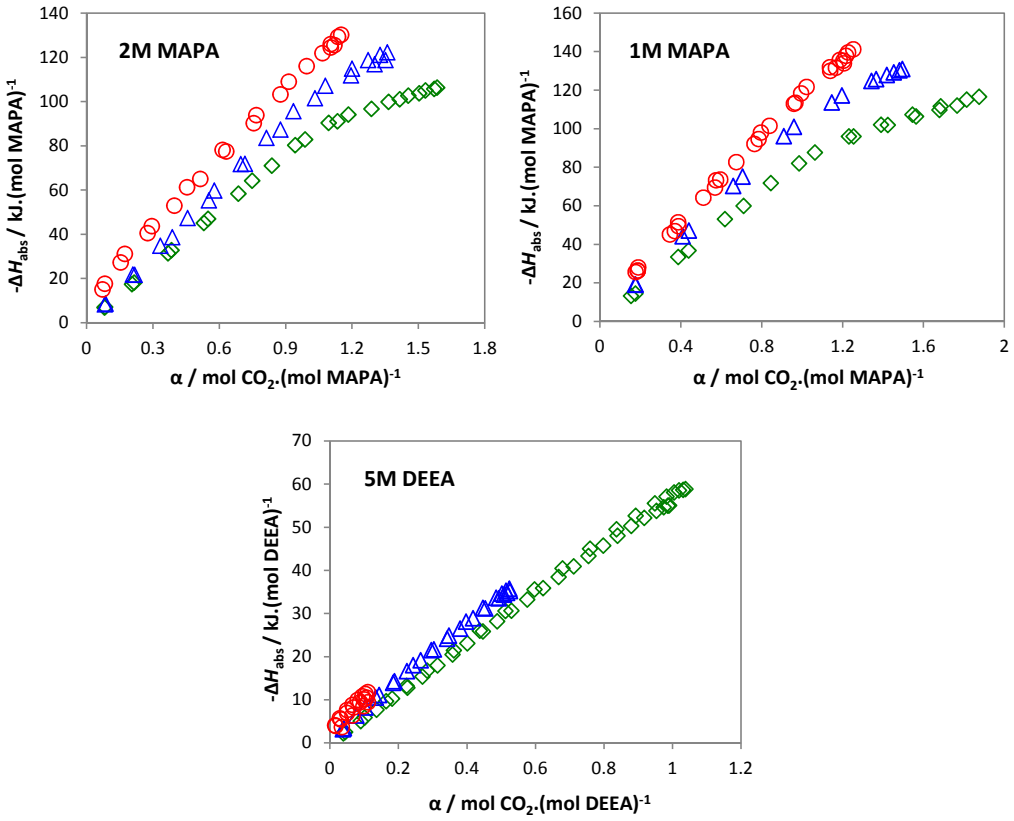

Figure 3.7: Integral heat of absorption of CO_2 with 5M DEEA, 2M MAPA and 1M MAPA at temperatures 40 °C (◊), 80 °C (Δ), and 120 °C (○).

3.3.3 Amine Mixtures

The results of heat of absorption of CO_2 in 5 M DEEA + 2 M MAPA (~ 63.5 mass % DEEA + 19.1 mass % MAPA) and 5 M DEEA + 1 M MAPA (~ 62 mass % DEEA + 9.3 mass % MAPA) at 6 bar CO_2 feed pressure in the temperature range 40-120 °C are presented graphically in Figure 3.8 and Figure 3.9, respectively. For simplicity, 5 M DEEA + 2 M MAPA and 5 M DEEA + 1 M MAPA are abbreviated as 5D2M and 5D1M, respectively. The measured data are tabulated in Table 3.11, Table 3.12, and Table 3.13 for 5D2M, and Table 3.14, Table 3.15, and Table 3.16 for 5D1M. The results in this work are compared with the data from Kim[25] measured at 3 bar CO_2 feed pressure (Figure 3.8 and Figure 3.9). The results indicate that the heat of absorption of CO_2 in amine mixtures is a function of temperature and CO_2 loading. This functionality is more

pronounced in 5D1M than in 5D2M. Our results again show very good repeatability. The differential heat of absorption data for amine mixtures is very scarce in the literature. Kim and Svendsen[24] reported that the heat of absorption profile against loading depends on the composition of the amine mixture. This can also be seen in comparison of our results with Kim's data (Figure 3.8 and Figure 3.9).

In the selected concentration range, these amine blends give two liquid phases upon CO_2 absorption. However, the two liquid phases may become one phase again above a certain CO_2 loading. This was observed when fully loaded amine mixtures, at the given experimental conditions, were taken out from the calorimeter after finishing the experiments. The loaded amine mixtures were transferred into a separating funnel and analyzed visually for the two phases at 25 °C.

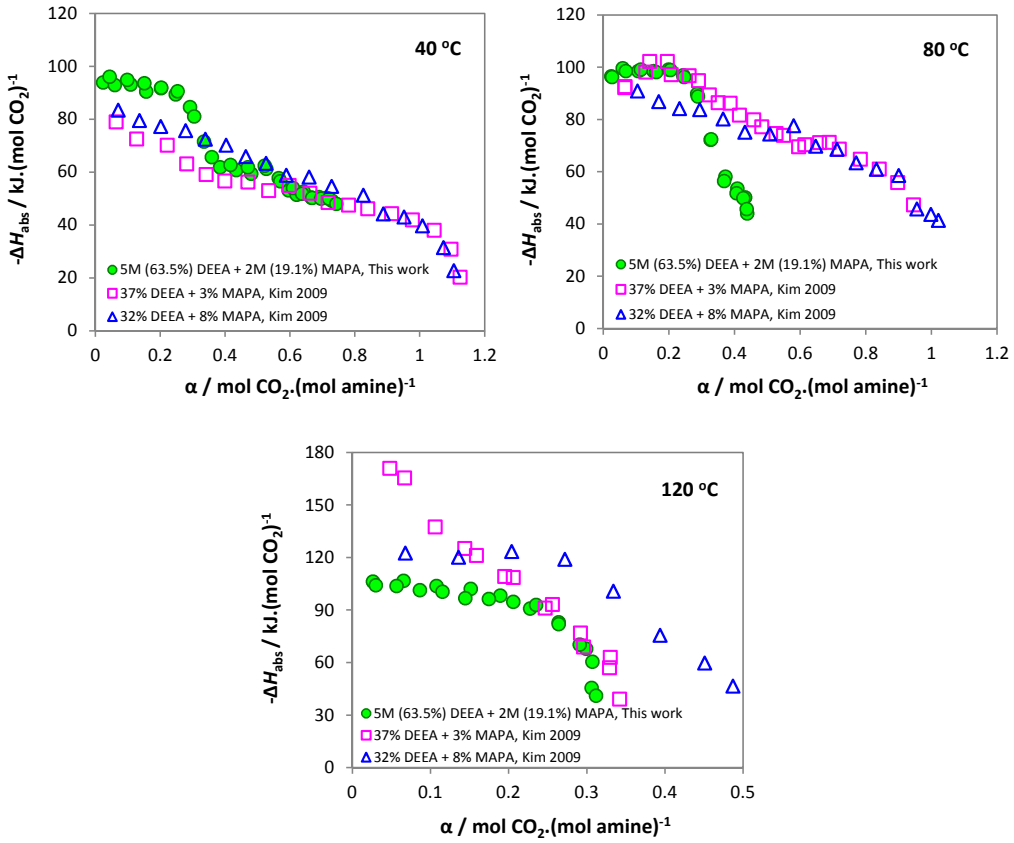

Figure 3.8: Differential enthalpy of absorption of CO_2 with 5M (63.5 mass %) DEEA + 2M (19.1 mass %) MAPA at 40, 80, and 120 °C.

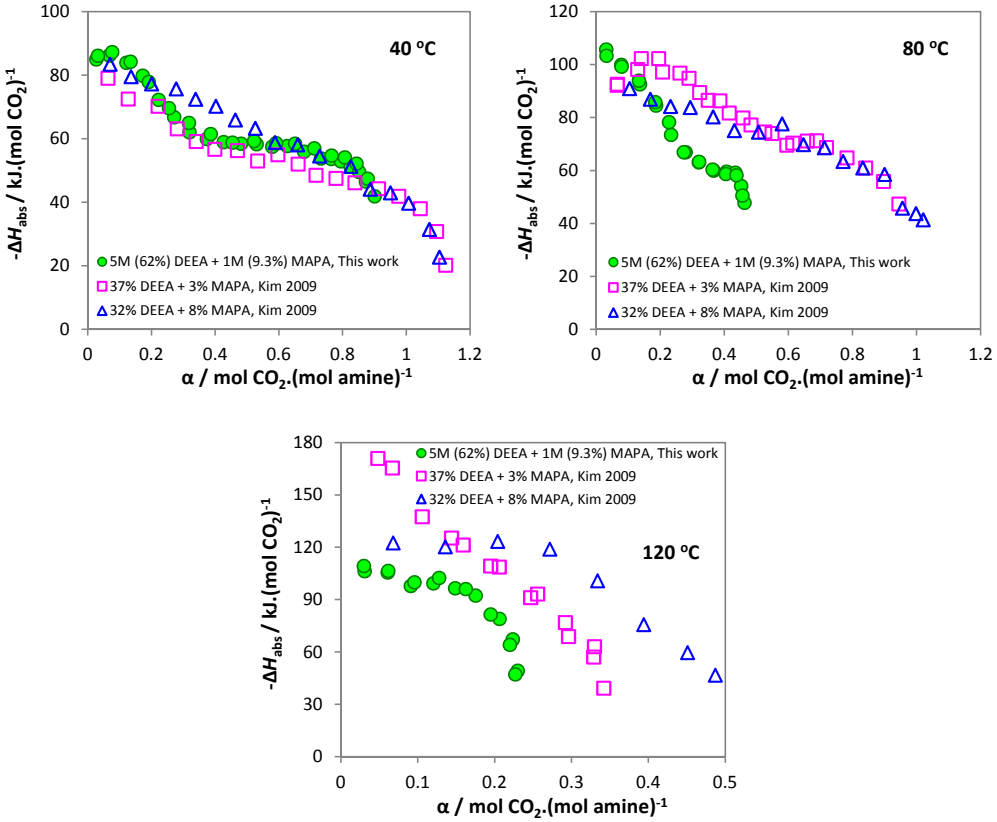

Figure 3.9: Differential enthalpy of absorption of CO_2 with 5M (62 mass %) DEEA + 1M (9.3 mass %) MAPA at 40, 80, and 120 °C.

Table 3.17 gives an overview of maximum loading achieved against final total pressure in the reactor at the end of experiments along with number of phases formed and volume percentages of upper and lower phases (at 25 °C) for all the experiments of amine mixtures in the temperature range of 40-120 °C. Both 5D2M and 5D1M systems gave one viscous phase at 40 °C. However, 5D2M system gave two phases at 80 and 120 °C with upper phase/lower phase volume % of around 50/50 (α = 0.44) and 64/36 (α = 0.31), respectively. The 5M1D system, on the other hand, gave one phase at 80°C and two phases at 120°C with upper phase/lower phase volume % of around 67/33 (α = 0.23). It was observed that the lower phase rich in CO_2 was relatively more viscous compared to the upper phase lean in CO_2. The parallel experiments gave similar results for all cases. These results show that the volume of relatively viscous lower phase (CO_2 rich phase) increases with an increase in CO_2 loading and becomes one CO_2 rich viscous phase after a certain loading as shown by results of 5D2M and 5D1M systems at 40 °C. The 5D1M system has shown relatively lower heat of absorption compared to that of the 5D2M system (Figure 3.8 and Figure 3.9). However, it becomes one phase from two liquid phases at certain loading above α = 0.23. The phase change behavior of these solvents as a function of CO_2 loading and possibly other parameters requires further examination in

order to find the critical CO_2 loading range where these solvents give two liquid phases at a reasonably high loading in combination with low heat of absorption of CO_2 for the solvent system.

An overall comparison of differential enthalpies of absorption of CO_2 for all the studied systems and 30 mass % MEA (base case) at 40, 80 and, 120 °C is given in Figure 3.10. The MAPA solutions of 2 M and 1 M have similar heats of absorption as that of 30 mass % MEA at 40 °C but these values are higher at temperatures 80 and 120 °C. However, a high CO_2 loadings were achieved in both 2 M and 1 M MAPA solutions compared to the results of 30 mass % MEA which is obviously due to the presence of two amine functionalities on the MAPA molecules. On the other hand, 5 M DEEA, a tertiary alkanolamine, has shown the lowest heat of absorption (as expected) among all the studied systems. It can also be seen that DEEA shows the lowest absorption capacity at 120 °C which indicates that less energy may be needed for the reaction reversion between DEEA and CO_2 in the stripper.

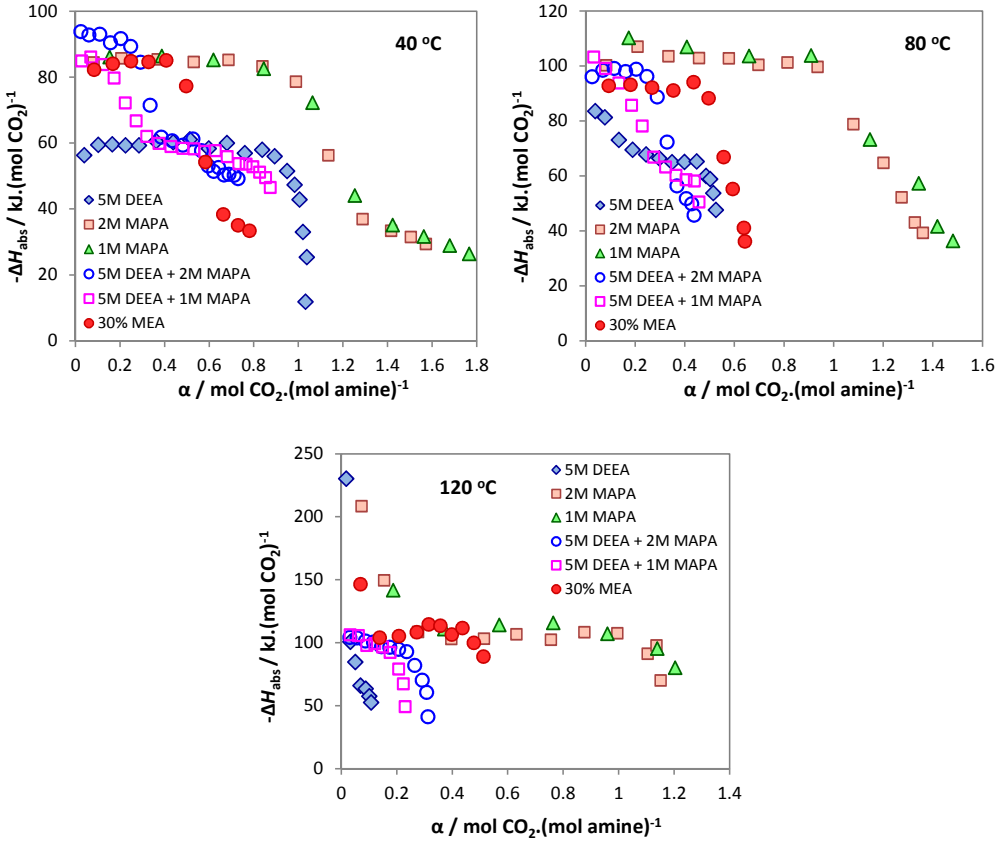

Figure 3.10: Overall comparison of differential enthalpy of absorption of CO_2 for all studied systems and 30 mass % MEA at 40, 80, and 120 °C.

In amine mixtures, primary and secondary amines are expected to react first with CO_2 due to their fast reaction rates followed by the tertiary amines which have comparatively slower reaction rate. This can be seen at temperature 40 ^{o}C in Figure 3.10. Both 5D2M and 5D1M systems show that MAPA reacts first in the mixture due to its fast reaction rate and its values are close to that of single MAPA solution values and then DEEA start reacting and reaches close to values of single DEEA solution. The length of this transition and consequently the heat of absorption depends on the concentration of the promoter (MAPA in this case), that is, increases by increasing the amount of promoter. Therefore, 5D1M has shown relatively lower heat of reaction compared to 5D2M. However, at higher temperatures, MAPA appears to be the main reacting component in the emulsion due to the low CO_2 absorption capacity of DEEA at higher temperatures especially at 120 ^{o}C. Therefore, both 5D2M and 5D1M systems have almost the same heat of absorption at 120 ^{o}C but lower than the single MAPA solutions values. On comparison with 30 mass % MEA, 5D2M has slightly higher heats of absorption and 5D1M has the same as that of 30 mass % MEA at 40 ^{o}C and lower loadings. However, it drops quickly with increase in loading. These mixtures have high loading capacities compared to 30 mass % MEA at 40 ^{o}C. However, they show much lower absorption capacities at 120 ^{o}C compared to 30 mass % MEA.

It can be noticed that the mixtures have shown relatively low CO_2 absorption capacities compared to the constituent amines when they were used as single solvents. It was also observed that the CO_2 loaded amine mixtures were relatively more viscous than the original unloaded feed solutions when they were taken out from the calorimeter after finishing the experiments. This increase in viscosity during CO_2 absorption may have an effect on CO_2 absorption capacity.

3.4 Conclusions

Heat of absorption of CO_2 in phase change solvents containing DEEA and MAPA were measured as a function of CO_2 loading at different temperatures using a commercially available reaction calorimeter. The tested systems were 5 M DEEA, 2 M MAPA, 1 M MAPA, 5 M DEEA + 2 M MAPA, and 5 M DEEA + 1 M MAPA. The selected amine composition in the mixtures gave two liquid phases on reacting with CO_2. All experiments were repeated and have shown good repeatability. The measurements were taken isothermally over a temperature range of 40-120 ^{o}C. The measured differential heat of absorption values were converted into integral values by integration. Since CO_2 was injected in the reactor in several small steps by keeping a low loading span, the measured enthalpy of absorption data are semi differential in loading. Heat of absorption is a function of temperature, that is, increases with temperature.

For the studied solvent systems, the heat of absorption of CO_2 in single amine solutions can be affected by changing the solvent composition (large difference in concentration) and CO_2 feed pressure simultaneously in combination with type of amine used. This effect is more pronounced in tertiary alkanolamine (DEEA) compared to diamine (MAPA) consisting of primary and secondary amine functional groups. However, further experimental investigations are proposed to fully understand the effect of these parameters on heat of absorption. In aqueous amine mixtures, heat of absorption depends on CO_2 loading, temperature, and composition of the constituent amines in the mixture.

DEEA showed the lowest heat of absorption among all the studied systems and MAPA has values close to that of 30 mass % MEA. 5D1M showed a lower heat of absorption compared to the 5D2M system.

However, it becomes one liquid phase at certain loading above α = 0.23 mol CO_2.(mol amine)$^{-1}$. Further experimental work is suggested to fully investigate the phase change behavior of these solvent systems against CO_2 loading.

3.5 References

(1) Kohl, A. L.; Nielsen, R. B. Gas Purification, 5th ed. Gulf Publishing Company, Houston, TX, **1997**.

(2) Davison, J. Performance and costs of power plants with capture and storage of CO_2. *Energy* **2007**, 32, 1163-1176.

(3) Davidson, R. M. Post-combustion Carbon Capture from Coal Fired Plants - Solvent Scrubbing. IEA Clean Coal Centre, CCC/125, **2007**.

(4) IEA report, Technology Roadmap - CCS, **2009**, via: http://www.iea.org/papers/2009/CCS_Roadmap.pdf (accessed November 2012)

(5) Svendsen, H. F.; Hessen, E. T.; Mejdell, T. Carbon dioxide capture by absorption, challenges and possibilities. *Chem. Eng. J.* **2011**, 171, 718-724.

(6) Versteeg, G. F.; Van Swaaij, W. P. M. On the kinetics between CO_2 and alkanolamines both in aqueous and non-aqueous solutions - I. Primary and secondary amines. *Chem. Eng. Sci.* **1988**, 43 (3), 573-585.

(7) Donaldson, T. L.; Nguyen, Y. N. Carbon dioxide reaction kinetics and transport in aqueous amine membranes. *Ind. Eng. Chem. Fundam.* **1980**, 19, 260-266.

(8) Versteeg, G. F.; Van Swaaij, W. P. M. On the kinetics between CO_2 and alkanolamines both in aqueous and non-aqueous solutions - II. Tertiary amines. *Chem. Eng. Sci.* **1988**, 43 (3), 587-591.

(9) Versteeg, G. F.; Van Dijck, L. A. J.; Van Swaaij, W. P. M. On the kinetics between CO_2 and alkanolamines both in aqueous and non-aqueous solutions. An overview. *Chem. Eng. Commun.* **1996**, 144, 113-158.

(10) Glasscock, D. A.; Critchfield, J. E.; Rochelle, G. T. CO_2 absorption/ desorption in mixtures of methyldiethanolamine with monoethanolamine or diethanolamine. *Chem. Eng. Sci.* **1991**, 46(11), 2829-2845.

(11) Zhu, D.; Fang, M.; Lv, Z.; Wang, Z.; Luo, Z. Selection of Blended Solvents for CO_2 Absorption from Coal-Fired Flue Gas. Part 1: Monoethanolamine (MEA)-Based Solvents. *Energy & Fuels* **2012**, 26, 147-153.

(12) Kozak, F.; Petig, A.; Morris, E.; Rhudy, R.; Thimsen, D. Chilled ammonia process for CO_2 capture. *Energy Procedia* **2009**, 1, 1419-1426.

(13) Raynal, L.; Pascal, A.; Bouillon, P.-A.; Gomez, A.; le Febvre de Nailly, M.; Jacquin, M.; Kittel, J.; di Lella, A.; Mougin, P.; Trapy, J. The DMX™ process: an original solution for lowering the cost of post-combustion carbon capture. *Energy Procedia* **2011**, 4, 779-786.

(14) Aleixo, M.; Prigent, M.; Gibert, A.; Porcheron, F.; Mokbel, I.; Jose, J.; Jacquin, M. Physical and Chemical Properties of DMX™ Solvents. *Energy Procedia* **2011**, 4, 148-155.

(15) Agar, D. W.; Tan, Y.; Zhang, X. CO_2 removal processes by means of absorption using thermomorphic biphasic aqueous amine solutions. Patent WO/2008/015217, **2008**.

(16) Zhang, J.; Agar, D. W.; Zhang, X.; Geuzebroek, F. CO_2 absorption in biphasic solvents with enhanced low temperature solvent regeneration. *Energy Procedia* **2011**, 4, 67-74.

(17) Zhang, J.; Nwani, O.; Tan, Y.; Agar, D. W. Carbon dioxide absorption into biphasic amine solvent with solvent loss reduction. *Chem. Eng. Res. Des.* **2011**, 89, 1190-1196.

(18) Zhang, J.; Misch, R.; Tan, Y.; Agar, D. W. Novel thermomorphic biphasic amine solvents for CO_2 absorption and low-temperature extractive regeneration. *Chem. Eng. Technol.* **2011**, 34 (9), 1481-1489.

(19) Pinto, D. D. D.; Monteiro, J. G. M.-S.; Bruder, P.; Zaidy, S. A. H.; Jonassen, Ø.; Hartono, A.; Svendsen, H. F. Correlation and Prediction of Vapor-Liquid-Liquid Equilibrium using the e-NRTL model applied to the MAPA-DEEA-CO_2-Water System. *TCCS-6 Trondheim*, 2011.

(20) Kim, I.; Hoff, K. A.; Hessen, E. T.; Haug-Warberg, T.; Svendsen, H. F. Enthalpy of absorption of CO_2 with alkanolamine solutions predicted from reaction equilibrium constants. *Chem. Eng. Sci.* **2009**, 64, 2027-2038.

(21) Oscarson, J. L.; Van Dam, R. H.; Christensen, J. J.; Izatt, R. M. Enthalpies of absorption of carbon dioxide in aqueous diethanolamine solutions. *Thermochim. Acta* **1989**, 146, 107-114.

(22) Mathonat, C.; Majer, V.; Mather, A. E.; Grolier, J. P. E. Enthalpies of absorption and solubility of CO_2 in aqueous solutions of methyldiethanolamine. *Fluid Phase Equilib.* **1997**, 140, 171-182.

(23) Kim, I.; Svendsen, H. F. Heat of absorption of carbon dioxide (CO_2) in monoethanolamine (MEA) and 2-(aminoethyl)ethanolamine (AEEA) solutions. *Ind. Eng. Chem. Res.* **2007**, 46, 5803-5809.

(24) Kim, I.; Svendsen, H. F. Comparative study of the heats of absorption of post combustion CO_2 absorbents. *Int. J. of Greenhouse Gas Control* **2011**, 5, 390-395.

(25) Kim, I. Heat of reaction and VLE of post combustion CO_2 absorbents. PhD Thesis. Norwegian University of Science and Technology, Trondheim, Norway, **2009**.

(26) Merkley, K. E.; Christensen, J. J.; Izatt, R. M. Enthalpies of absorption of carbon dioxide in aqueous methyldiehtanolamine solutions. *Thermochim. Acta* **1987**, 121, 437-446.

(27) Mathonat, C.; Majer, V.; Mather, A. E.; Grolier, J. P. E. Use of flow calorimetry for determining enthalpies of absorption and the solubility of CO_2 in aqueous monoethanolamine solutions. *Ind. Eng. Chem. Res.* **1998**, 37, 4136-4141.

3.6 Appendix

Table 3.1: List of amine systems studied in this work.

Amine	CAS No.	Concentration	T/ °C	P/ kPa
Aqueous single amines				
2-(Diethylamino)ethanol (DEEA)	100-37-8	5M (~61.1 mass%)	40, 80, 120	600
3-(Methylamino)propylamine (MAPA)	6291-84-5	2M (~17.9 mass%), 1M (~8.9 mass%)	40, 80, 120	600
Monoethanolamine (MEA)	141-43-5	30 mass%	40, 80, 120	600
Aqueous amine mixtures*				
DEEA+MAPA	-	5M + 2M ~(63.5 mass% + 19.1 mass%)	40, 80, 120	600
DEEA+MAPA	-	5M + 1M ~(62 mass% + 9.3 mass%)	40, 80, 120	600

* The selected concentrations of amine mixtures give liquid-liquid split on CO_2 absorption.

Table 3.2: Heat of Absorption of CO_2 with 5 M (~ 61.1 mass %) DEEA Solutions at 40 °C.

α	$-\Delta H_{diff}$	$-\Delta H_{int}$	$-\Delta H_{int}$
mol CO_2.(mol DEEA)$^{-1}$	kJ.(mol CO_2)$^{-1}$	kJ.(mol DEEA)$^{-1}$	kJ.(mol CO_2)$^{-1}$
40 °C (1)			
0.045	55.308	2.483	55.308
0.090	56.643	5.051	55.979
0.136	56.387	7.653	56.117
0.182	56.840	10.239	56.298
0.226	57.720	12.798	56.577
0.271	57.917	15.364	56.796
0.314	58.840	17.939	57.081
0.358	58.481	20.497	57.252
0.401	59.019	23.053	57.443
0.447	61.369	25.861	57.845
0.489	55.916	28.197	57.680
0.530	59.760	30.657	57.841
0.576	56.532	33.264	57.736
0.622	56.852	35.888	57.671
0.668	56.200	38.454	57.570
0.712	56.024	40.941	57.474
0.755	55.889	43.330	57.384
0.798	55.430	45.725	57.278
0.840	55.720	48.037	57.201
0.880	56.687	50.309	57.178
0.918	48.924	52.156	56.838
0.954	45.837	53.814	56.421
0.975	39.473	54.652	56.052
0.987	28.674	54.986	55.729
0.990	15.863	55.044	55.582
40 °C (2)			
0.039	56.271	2.213	56.271
0.101	59.384	5.902	58.177
0.164	59.601	9.649	58.722
0.224	59.287	13.214	58.873
0.284	59.276	16.754	58.958
0.362	60.532	21.453	59.296
0.438	60.197	26.049	59.453
0.513	61.098	30.619	59.693
0.598	58.315	35.560	59.497
0.679	59.998	40.463	59.558
0.759	56.886	45.015	59.276
0.837	57.898	49.523	59.148
0.893	55.957	52.651	58.948
0.949	51.510	55.524	58.511
0.983	47.319	57.129	58.125
1.005	42.780	58.080	57.786
1.020	32.980	58.556	57.434
1.031	11.818	58.695	56.915
1.038	25.315	58.867	56.708

Table 3.3: Heat of Absorption of CO_2 with 5 M (~ 61.1 mass %) DEEA Solutions at 80 °C.

α	$-\Delta H_{diff}$	$-\Delta H_{int}$	$-\Delta H_{int}$
mol CO_2.(mol DEEA)$^{-1}$	kJ.(mol CO_2)$^{-1}$	kJ.(mol DEEA)$^{-1}$	kJ.(mol CO_2)$^{-1}$
80 °C (1)			
0.041	82.234	3.404	82.234
0.104	76.961	8.224	79.059
0.144	71.997	11.121	77.089
0.185	68.304	13.915	75.148
0.225	67.683	16.615	73.825
0.265	64.020	19.177	72.345
0.304	64.368	21.680	71.324
0.342	64.509	24.144	70.564
0.380	62.049	26.492	69.716
0.418	63.592	28.894	69.162
0.454	64.166	31.217	68.764
0.493	59.476	33.561	68.022
0.508	54.382	34.355	67.629
0.517	48.745	34.804	67.293
0.526	45.989	35.200	66.945
80 °C (2)			
0.038	83.516	3.179	83.516
0.077	81.271	6.364	82.377
0.134	73.045	10.498	78.431
0.189	69.458	14.316	75.819
0.243	67.747	17.995	74.016
0.296	66.372	21.528	72.643
0.348	64.918	24.849	71.506
0.398	65.072	28.116	70.693
0.447	65.222	31.335	70.089
0.485	59.956	33.631	69.290
0.502	58.808	34.599	68.946
0.515	53.724	35.286	68.568
0.525	47.610	35.757	68.172

Table 3.4: Heat of Absorption of CO_2 with 5 M (~ 61.1 mass %) DEEA Solutions at 120 °C.

α	$-\Delta H_{diff}$	$-\Delta H_{int}$	$-\Delta H_{int}$
mol CO_2.(mol DEEA)$^{-1}$	kJ.(mol CO_2)$^{-1}$	kJ.(mol DEEA)$^{-1}$	kJ.(mol CO_2)$^{-1}$
120 °C (1)			
0.035	105.415	3.658	105.415
0.066	85.232	6.337	95.822
0.098	68.455	8.523	86.911
0.111	67.899	9.396	84.707
120 °C (2)			
0.015	265.834	4.044	*a*
0.029	120.766	5.680	120.766
0.050	90.659	7.595	102.428
0.066	77.082	8.814	94.485
0.081	71.615	9.942	89.049
0.095	65.490	10.799	85.161
0.104	61.474	11.369	82.680
0.111	54.825	11.752	80.645
120 °C (3)			
0.017	230.233	3.932	*a*
0.032	100.768	5.450	100.768
0.050	84.614	6.962	92.001
0.069	65.880	8.221	82.414
0.088	63.383	9.403	77.392
0.100	57.493	10.106	74.457
0.107	52.535	10.486	72.697

[a] The first point was omitted from the integration.

Table 3.5: Heat of Absorption of CO_2 with 2 M (~ 17.9 mass %) MAPA Solutions at 40 °C.

α	$-\Delta H_{diff}$	$-\Delta H_{int}$	$-\Delta H_{int}$
mol CO_2.(mol MAPA)$^{-1}$	kJ.(mol CO_2)$^{-1}$	kJ.(mol MAPA)$^{-1}$	kJ.(mol CO_2)$^{-1}$
40 °C (1)			
0.084	84.454	7.058	84.454
0.214	84.960	18.170	84.763
0.384	86.232	32.768	85.411
0.549	86.115	46.989	85.623
0.749	85.756	64.161	85.658
0.943	83.169	80.324	85.146
1.094	66.493	90.369	82.571
1.184	41.694	94.103	79.479
1.365	34.758	99.877	73.144
1.455	31.210	102.665	70.570
1.532	29.883	104.982	68.511
1.584	26.683	106.369	67.139
40 °C (2)			
0.081	84.460	6.851	84.460
0.205	85.667	17.463	85.190
0.368	85.369	31.419	85.269
0.530	84.582	45.103	85.060
0.686	85.252	58.373	85.103
0.838	83.227	71.040	84.763
0.988	78.644	82.840	83.833
1.134	56.241	91.050	80.282
1.288	36.930	96.744	75.093
1.416	33.339	101.008	71.323
1.504	31.485	103.782	68.990
1.572	29.383	105.781	67.275

Table 3.6: Heat of Absorption of CO_2 with 2 M (~ 17.9 mass %) MAPA Solutions at 80 °C.

α	$-\Delta H_{diff}$	$-\Delta H_{int}$	$-\Delta H_{int}$
mol CO_2.(mol MAPA)$^{-1}$	kJ.(mol CO_2)$^{-1}$	kJ.(mol MAPA)$^{-1}$	kJ.(mol CO_2)$^{-1}$
80 °C (1)			
0.083	100.290	8.293	100.290
0.209	107.061	21.803	104.381
0.334	103.525	34.739	104.060
0.456	102.939	47.343	103.759
0.577	102.800	59.735	103.559
0.696	100.438	71.744	103.023
0.813	101.300	83.567	102.776
0.935	99.670	95.696	102.372
1.079	78.804	107.095	99.213
1.200	64.735	114.929	95.737
1.273	52.209	118.722	93.253
1.327	43.070	121.051	91.209
1.359	39.274	122.313	89.982
80 °C (2)			
0.086	99.184	8.561	99.184
0.218	99.504	21.640	99.377
0.387	100.111	38.594	99.698
0.553	100.749	55.325	100.014
0.716	101.394	71.835	100.328
0.876	96.749	87.335	99.673
1.033	90.819	101.552	98.331
1.195	63.743	111.883	93.639
1.302	46.593	116.882	89.763
1.351	38.885	118.797	87.908

Table 3.7: Heat of Absorption of CO_2 with 2 M (~ 17.9 mass %) MAPA Solutions at 120 °C.

α	$-\Delta H_{diff}$	$-\Delta H_{int}$	$-\Delta H_{int}$
mol CO_2.(mol MAPA)$^{-1}$	kJ.(mol CO_2)$^{-1}$	kJ.(mol MAPA)$^{-1}$	kJ.(mol CO_2)$^{-1}$
120 °C (1)			
0.072	208.383	15.075	*a*
0.154	149.583	27.259	*a*
0.276	108.512	40.529	108.512
0.397	102.917	52.924	105.736
0.514	103.108	65.013	104.880
0.631	106.652	77.506	105.315
0.755	102.335	90.252	104.698
0.876	108.432	103.311	105.321
0.995	107.568	116.102	105.639
1.104	91.328	126.064	103.996
1.137	97.930	129.262	103.794
1.151	69.934	130.300	103.290
120 °C (2)			
0.082	214.410	17.620	*a*
0.172	149.657	31.105	*a*
0.295	102.375	43.670	102.375
0.455	110.371	61.284	106.894
0.615	105.361	78.213	106.338
0.767	103.262	93.861	105.554
0.913	103.216	108.987	105.092
1.066	84.982	121.949	101.659
1.104	67.054	124.514	100.239
1.121	63.449	125.571	99.593

a The first two points were omitted from the integration.

Table 3.8: Heat of Absorption of CO_2 with 1 M (~ 8.9 mass %) MAPA Solutions at 40 °C.

α	$-\Delta H_{diff}$	$-\Delta H_{int}$	$-\Delta H_{int}$
mol CO_2.(mol MAPA)$^{-1}$	kJ.(mol CO_2)$^{-1}$	kJ.(mol MAPA)$^{-1}$	kJ.(mol CO_2)$^{-1}$
40 °C (1)			
0.175	82.522	14.433	82.522
0.438	84.859	36.728	83.925
0.710	85.402	59.957	84.491
0.984	80.390	82.013	83.348
1.231	56.607	95.997	77.981
1.389	38.287	102.055	73.460
1.544	33.919	107.318	69.488
1.684	30.291	111.559	66.230
1.813	27.579	115.112	63.484
1.875	23.669	116.563	62.181
40 °C (2)			
0.153	86.100	13.210	86.100
0.387	86.365	33.393	86.260
0.618	85.195	53.093	85.862
0.845	82.543	71.763	84.973
1.063	72.255	87.571	82.356
1.253	44.098	95.953	76.554
1.423	35.085	101.907	71.610
1.563	31.616	106.331	68.029
1.678	28.863	109.663	65.335
1.766	26.395	111.968	63.410

Table 3.9: Heat of Absorption of CO_2 with 1 M (~ 8.9 mass %) MAPA Solutions at 80 °C.

α	$-\Delta H_{diff}$	$-\Delta H_{int}$	$-\Delta H_{int}$
mol CO_2.(mol MAPA)$^{-1}$	kJ.(mol CO_2)$^{-1}$	kJ.(mol MAPA)$^{-1}$	kJ.(mol CO_2)$^{-1}$
80 °C (1)			
0.177	107.384	18.957	107.384
0.440	107.009	47.136	107.160
0.705	105.463	75.067	106.522
0.959	101.754	100.931	105.258
1.196	68.895	117.259	98.052
1.365	49.593	125.654	92.043
1.452	40.664	129.191	88.965
1.495	37.598	130.913	87.595
80 °C (2)			
0.173	110.238	19.118	110.238
0.408	106.952	44.215	108.348
0.659	103.691	70.212	106.576
0.908	103.849	96.138	105.827
1.146	73.234	113.561	99.062
1.342	57.308	124.789	92.968
1.418	41.648	127.926	90.241
1.481	36.335	130.235	87.929

Table 3.10: Heat of Absorption of CO_2 with 1 M (~ 8.9 mass %) MAPA Solutions at 120 °C.

α	$-\Delta H_{diff}$	$-\Delta H_{int}$	$-\Delta H_{int}$
mol CO_2.(mol MAPA)$^{-1}$	kJ.(mol CO_2)$^{-1}$	kJ.(mol MAPA)$^{-1}$	kJ.(mol CO_2)$^{-1}$
120 °C (1)			
0.176	145.357	25.615	*a*
0.345	115.542	45.153	115.542
0.512	114.746	64.223	115.148
0.674	113.206	82.644	114.513
0.838	114.962	101.462	114.624
0.995	107.413	118.314	113.242
1.136	96.384	131.967	110.755
1.227	83.689	139.517	108.431
1.252	66.190	141.211	107.426
120 °C (2)			
0.189	148.542	28.062	*a*
0.387	118.273	51.480	118.273
0.574	115.920	73.210	117.129
0.796	111.549	97.964	115.090
1.022	104.885	121.640	112.325
1.186	85.301	135.627	107.881
1.216	74.261	137.865	106.895
120 °C (3)			
0.186	141.748	26.435	*a*
0.370	110.821	46.816	110.821
0.569	114.161	69.456	112.554
0.764	115.783	92.084	113.647
0.959	107.144	112.962	112.006
1.139	95.286	130.078	108.852
1.204	80.204	135.312	107.014
120 °C (4)			
0.186	140.740	26.247	*a*
0.388	114.894	49.420	114.894
0.594	117.798	73.688	116.361
0.785	110.203	94.670	114.401
0.967	102.806	113.424	111.691
1.166	91.103	131.572	107.505
1.206	57.394	133.883	105.527

[a] The first point was omitted from the integration.

Table 3.11: Heat of Absorption of CO_2 with 5 M (~ 63.5 mass %) DEEA + 2 M (~ 19.1 mass %) MAPA Solutions at 40 °C.

α	$-\Delta H_{diff}$	$-\Delta H_{int}$	$-\Delta H_{int}$
mol CO_2.(mol amine)$^{-1}$	kJ.(mol CO_2)$^{-1}$	kJ.(mol amine)$^{-1}$	kJ.(mol CO_2)$^{-1}$
40 °C (1)			
0.024	93.781	2.208	93.781
0.060	92.799	5.603	93.184
0.109	93.049	10.111	93.124
0.156	90.380	14.419	92.287
0.202	91.678	18.658	92.148
0.247	89.347	22.678	91.638
0.292	84.490	26.425	90.552
0.335	71.434	29.505	88.091
0.385	61.814	32.571	84.701
0.434	60.713	35.558	81.981
0.481	59.334	38.341	79.770
0.527	61.201	41.150	78.152
0.565	57.655	43.374	76.753
0.595	53.045	44.978	75.549
0.620	51.361	46.244	74.587
0.642	52.540	47.401	73.831
0.666	50.273	48.605	72.983
0.689	50.513	49.764	72.235
0.712	50.194	50.912	71.527
0.729	49.155	51.746	71.006
40 °C (2)			
0.044	95.994	4.247	95.994
0.098	94.813	9.347	95.346
0.151	93.574	14.333	94.722
0.203	91.823	19.072	93.985
0.253	90.508	23.636	93.293
0.304	80.994	27.769	91.231
0.359	65.582	31.369	87.312
0.416	62.631	34.928	83.941
0.470	61.766	38.267	81.392
0.522	62.399	41.503	79.505
0.570	56.463	44.197	77.575
0.609	53.936	46.328	76.042
0.637	51.792	47.783	74.973
0.668	50.239	49.346	73.822
0.695	49.919	50.683	72.902
0.720	49.945	51.926	72.108
0.743	47.984	53.018	71.369

Table 3.12: Heat of Absorption of CO_2 with 5 M (~ 63.5 mass %) DEEA + 2 M (~ 19.1 mass %) MAPA Solutions at 80 °C.

α	$-\Delta H_{diff}$	$-\Delta H_{int}$	$-\Delta H_{int}$
mol CO_2.(mol amine)$^{-1}$	kJ.(mol CO_2)$^{-1}$	kJ.(mol amine)$^{-1}$	kJ.(mol CO_2)$^{-1}$
80 °C (1)			
0.024	96.510	2.357	96.510
0.059	99.535	5.821	98.287
0.107	98.509	10.496	98.386
0.153	98.461	15.063	98.409
0.199	99.037	19.590	98.553
0.243	96.877	23.882	98.248
0.286	89.741	27.747	96.967
0.327	72.132	30.705	93.854
0.372	58.078	33.326	89.518
0.408	53.531	35.253	86.345
0.432	50.128	36.450	84.343
0.439	43.960	36.746	83.723
80 °C (2)			
0.026	96.160	2.523	96.160
0.068	98.445	6.676	97.569
0.114	99.104	11.223	98.185
0.161	98.027	15.824	98.139
0.204	98.846	20.064	98.288
0.247	96.202	24.164	97.927
0.288	88.720	27.849	96.601
0.328	72.346	30.748	93.641
0.368	56.360	32.982	89.627
0.406	51.756	34.949	86.080
0.427	49.840	35.997	84.296
0.437	45.667	36.449	83.422

Table 3.13: Heat of Absorption of CO_2 with 5 M (~ 63.5 mass %) DEEA + 2 M (~ 19.1 mass %) MAPA Solutions at 120 °C.

α	$-\Delta H_{diff}$	$-\Delta H_{int}$	$-\Delta H_{int}$
mol CO_2.(mol amine)$^{-1}$	kJ.(mol CO_2)$^{-1}$	kJ.(mol amine)$^{-1}$	kJ.(mol CO_2)$^{-1}$
120 °C (1)			
0.027	106.295	2.819	106.295
0.066	106.755	6.997	106.569
0.108	103.682	11.352	105.443
0.152	102.077	15.853	104.465
0.189	98.215	19.543	103.225
0.228	90.906	23.036	101.146
0.264	83.033	26.069	98.643
0.299	67.864	28.434	95.057
0.306	45.542	28.757	93.910
120 °C (2)			
0.030	104.153	3.154	104.153
0.057	103.700	5.908	103.941
0.087	101.320	8.922	103.041
0.115	100.475	11.814	102.401
0.145	96.829	14.637	101.277
0.175	96.336	17.552	100.421
0.206	94.771	20.512	99.565
0.235	92.943	23.217	98.745
0.264	81.932	25.600	96.894
0.291	70.254	27.487	94.436
0.307	60.522	28.468	92.646
0.312	41.102	28.658	91.884

Table 3.14: Heat of Absorption of CO_2 with 5 M (~ 62 mass %) DEEA + 1 M (~ 9.3 mass %) MAPA Solutions at 40 °C.

α	$-\Delta H_{diff}$	$-\Delta H_{int}$	$-\Delta H_{int}$
mol CO_2.(mol amine)$^{-1}$	kJ.(mol CO_2)$^{-1}$	kJ.(mol amine)$^{-1}$	kJ.(mol CO_2)$^{-1}$
40 °C (1)			
0.027	84.892	2.331	84.892
0.068	86.119	5.833	85.624
0.121	83.830	10.289	84.838
0.173	79.747	14.398	83.320
0.223	72.200	18.017	80.820
0.271	66.710	21.244	78.304
0.320	62.025	24.240	75.844
0.374	59.883	27.518	73.510
0.427	58.907	30.631	71.703
0.481	58.428	33.792	70.211
0.531	58.220	36.677	69.092
0.579	57.468	39.451	68.123
0.626	57.699	42.173	67.338
0.680	55.901	45.170	66.436
0.732	53.753	47.986	65.529
0.765	53.562	49.740	65.016
0.795	52.848	51.343	64.552
0.825	51.164	52.872	64.068
0.852	49.498	54.207	63.607
0.873	46.505	55.192	63.192
40 °C (2)			
0.032	86.089	2.729	86.089
0.077	87.170	6.640	86.723
0.135	84.177	11.533	85.624
0.191	77.842	15.950	83.317
0.255	69.563	20.385	79.881
0.318	64.963	24.442	76.948
0.386	61.413	28.642	74.196
0.455	58.762	32.698	71.855
0.522	59.226	36.690	70.226
0.592	58.605	40.754	68.864
0.651	58.397	44.204	67.914
0.711	56.919	47.647	66.979
0.766	54.649	50.634	66.099
0.808	54.123	52.890	65.481
0.844	52.090	54.795	64.901
0.879	47.368	56.456	64.202
0.901	41.829	57.375	63.657

Table 3.15: Heat of Absorption of CO_2 with 5 M (~ 62 mass %) DEEA + 1 M (~ 9.3 mass %) MAPA Solutions at 80 °C.

α	$-\Delta H_{diff}$	$-\Delta H_{int}$	$-\Delta H_{int}$
mol CO_2.(mol amine)$^{-1}$	kJ.(mol CO_2)$^{-1}$	kJ.(mol amine)$^{-1}$	kJ.(mol CO_2)$^{-1}$
80 °C (1)			
0.031	105.657	3.316	105.657
0.078	99.871	8.019	102.185
0.137	92.526	13.388	98.079
0.187	84.460	17.658	94.398
0.234	73.415	21.115	90.179
0.279	66.903	24.127	86.426
0.320	63.064	26.731	83.415
0.366	59.878	29.472	80.473
0.407	59.479	31.900	78.367
0.435	59.096	33.523	77.150
0.453	54.144	34.515	76.219
0.463	47.750	34.987	75.610
80 °C (2)			
0.032	103.277	3.287	103.277
0.079	99.173	7.988	100.822
0.133	93.888	13.072	98.006
0.184	85.765	17.443	94.622
0.227	78.208	20.815	91.510
0.274	66.835	23.914	87.333
0.321	63.264	26.925	83.769
0.364	60.278	29.472	81.040
0.405	58.603	31.872	78.768
0.438	58.131	33.824	77.187
0.457	50.498	34.767	76.096

Table 3.16: Heat of Absorption of CO_2 with 5 M (~ 62 mass %) DEEA + 1 M (~ 9.3 mass %) MAPA Solutions at 120 °C.

α	$-\Delta H_{diff}$	$-\Delta H_{int}$	$-\Delta H_{int}$
mol CO_2.(mol amine)$^{-1}$	kJ.(mol CO_2)$^{-1}$	kJ.(mol amine)$^{-1}$	kJ.(mol CO_2)$^{-1}$
120 °C (1)			
0.031	106.259	3.278	106.259
0.061	105.608	6.444	105.938
0.091	97.901	9.391	103.277
0.120	99.274	12.298	102.302
0.149	96.555	15.034	101.206
0.175	92.281	17.514	99.839
0.206	79.016	19.953	96.723
0.223	67.273	21.109	94.459
0.230	49.177	21.423	93.199
120 °C (2)			
0.030	109.350	3.271	109.350
0.062	106.447	6.666	107.852
0.096	99.872	10.071	105.015
0.128	102.432	13.345	104.370
0.163	96.051	16.675	102.595
0.195	81.435	19.318	99.072
0.220	64.126	20.921	95.102
0.227	47.212	21.254	93.614

Table 3.17: Volume distribution in upper and lower phases

T	5 M DEEA + 2 M MAPA				5 M DEEA + 1 M MAPA			
	α	Final P_{total}	No. of phases	UP/LP*	α	Final P_{total}	No. of phases	UP/LP*
°C	mol CO_2. (mol amine)$^{-1}$	kPa		vol%.(vol%)$^{-1}$	mol CO_2. (mol amine)$^{-1}$	kPa		vol%.(vol%)$^{-1}$
40 (1)	0.729	265.6	1	-	0.873	235.9	1	-
40 (2)	0.743	288.1	1	-	0.901	266.9	1	-
80 (1)	0.439	556.6	2	50/50	0.463	568.9	1	-
80 (2)	0.437	543.1	2	50.2/49.8	0.457	550.9	1	-
120 (1)	0.306	589.2	2	64.3/35.7	0.230	582.9	2	67.1/32.9
120 (2)	0.312	584.5	2	64.1/35.9	0.227	582.3	2	67.2/32.8

*UP = upper phase and LP = lower phase

4. Vapor-Liquid Equilibrium

4.1 Introduction

Carbon dioxide (CO_2) is a well-known greenhouse gas and a major contributor to the global warming.[1] Fossil fuel based power generation is one of the major sources of CO_2 emissions worldwide.[2] The other large CO_2 emitting point sources are iron and steel industry, cement production plants, refineries, natural gas processing plants, and petrochemicals production plants.[3] Carbon capture and storage (CCS) is considered as a potential solution to reduce the CO_2 emissions and to mitigate the climate change.[4] Among the available CCS technologies, the amine based absorption-desorption capture process is considered as the most mature technology due to its extensive use in different industrial application such as acid gas removal from natural gas.[5] This technology can be retrofitted to the existing power generation plants, and the techno-economic feasibility studies indicate that the technology will remain competitive in the coming future.[6,7] However, the major challenge with the amine scrubbing is the high energy requirements of the process.[8] Technical improvements in the capture process and improved process design are one way to reduce the high energy demand of the process, the other being the design of energy efficient solvent systems.[9]

On the basis of the characteristics of different groups of amines, several amine-based solvent systems have been studied and reported in the literature. A few examples are (a) aqueous single alkanolamine solutions such as primary (monoethanolamine, MEA), secondary (diethanolamine, DEA), and tertiary (triethanolamine, TEA, and methyldiethanolamine, MDEA) alkanolamines,[5] (b) aqueous amine blends (tertiary amine blended with primary or secondary amines as a promoter such as MEA + MDEA and DEA + MDEA)[10] to exploit the favorable properties of different types of amines, and (c) sterically hindered amines[11] and cyclic amine (e.g., piperazine)[12] both as single aqueous solutions[13-15] or as a blend of both together[16-18] or a blend of each with other amines.[19-21] One of the basic purposes of these and many other studies reported in the literature is to get the best solvent system with the characteristics of high CO_2 loading and cyclic capacity, fast reaction kinetics, low heat of absorption, low thermal and chemical degradation, low corrosion tendency, environmentally benign, and possibility of operating at elevated desorber pressures etc. High equilibrium temperature sensitivity is also advantageous which can reduce the stripping steam requirement in the desorber.[22]

A new generation of mixed amine solvent systems has recently received attention which can form two liquid phases e.g., the thermomorphic biphasic solvents (TBS) systems[23] and the DMX process.[24,25] In the DMX process by IFPEN, the solvents form two immiscible phases after CO_2 absorption and only the CO_2 rich phase is sent to stripper for regeneration whereas the CO_2 lean phase is sent back to the absorber without regeneration. Due to low liquid circulation rate in the stripper, one can reduce the solvent regeneration energy. This process has claimed to reduce the reboiler duty down to 2.1 GJ.(ton CO_2)$^{-1}$ compared to 3.7

GJ.(ton CO_2)$^{-1}$ for the reference 30 mass % MEA process. On the other hand, the TBS systems absorb CO_2 and regenerate at a much lower temperature of 80 ^{o}C compared to the regeneration temperature of 120 ^{o}C for the conventional alkanolamine solutions. They give a liquid-liquid phase split during regeneration and become one liquid phase again during absorption. A lower solvent regeneration temperature is the main advantage of these systems which can be done without the use of steam.[26,27] In this work a blend of amines, 2-(diethylamino)ethanol (DEEA) and 3-(methylamino)propylamine (MAPA), is under investigation. This system has the characteristics of biphasic liquid-liquid phase change solvents. MAPA is a diamine having a primary and a secondary amine functional group whereas DEEA is a tertiary alkanolamine.

The equilibrium solubility data of CO_2 in aqueous amine solutions are essential for the design and modeling of the absorption-desorption capture processes. Such data are generally measured by using equilibrium cells. Extensive CO_2 solubility data are available in the literature for various amine systems measured with different equilibrium cells.[28-32] These data are generally measured by using either static or dynamic (circulation) methods.[33] In the static method, an amine solution of known weight is taken in the equilibrium cell, CO_2 is injected, and the system is allowed to reach the equilibrium. When the equilibrium is established, the equilibrium pressure is recorded and compositions of the two phases (liquid and gas phases) are analyzed for CO_2 content. In the dynamic or circulation method, the amine solution is taken in the equilibrium cell followed by the injection of nitrogen and the system is equilibrated at a preset temperature. The equilibrium pressure (nitrogen pressure + amine and water vapor pressure) is recorded and CO_2 is injected to the equilibrium cell. Then the vapor phase is circulated with the help of a circulating pump and the gas is bubbled through the liquid phase. When equilibrium is achieved, the total pressure of the system is recorded and the CO_2 partial pressure is calculated from the difference between the total pressure and the equilibrium pressure before introducing any CO_2 in the system.[33] Calorimeters have rarely been used for the solubility measurements. Xu and Rochelle presented total pressure measurements in aqueous amines at elevated temperatures by using the calorimeter and autoclave as the equilibrium cell.[34,35] In the present work, the solubility measurements were carried out in a calorimeter that is generally used for the measurement of heat of absorption. The experimental method, in principle, resembles to the static method with some differences. The advantage of using a calorimeter is the measurement of both CO_2 equilibrium solubility and heat of absorption in aqueous amine solutions at the same time. Our previous work presented the heat of absorption measurements in all the solvent systems studied in the present work.[36,37]

The main objective of this work is the experimental measurements of equilibrium total pressure and the estimation of CO_2 solubility from the measured total pressure data in aqueous solutions of DEEA, MAPA, and their mixtures. The selected concentration range of the aqueous amine mixtures gives liquid-liquid phase split upon CO_2 absorption. Although some CO_2 solubility data were found in the literature for the binary aqueous DEEA solutions, there is a complete lack of CO_2 solubility data for the aqueous MAPA and mixed aqueous DEEA-MAPA systems. Another objective of this work is to validate the experimental method used for the measurements. For this, CO_2 solubility data were measured in 30 mass % MEA solutions and compared with the literature data. For all the amine systems studied in this work, the equilibrium total pressure measurements were carried out by using the calorimeter as a function of amine composition, CO_2 loading and the temperature ranging between 40-120 ^{o}C.

4.2 Experimental Section

MEA (clear colorless liquid with a purity of ≥ 99 mass %), DEEA (clear pale yellow liquid with a purity of ≥ 99 mass %), and MAPA (clear colorless liquid with a purity of 99 mass %) were supplied by Sigma-Aldrich. Carbon dioxide (CO_2) with a purity of ≥ 99.99 mol % was purchased from AGA Gas GmbH. All amines were used as received with no further purification. The amine sample solutions (mostly 2000 cm^3 and a few cases with 1000 cm^3) were prepared with deionized water by using an analytical balance (accuracy of ± 0.01 g) with standard uncertainty *u(x)* = 0.00003 mass fraction for the composition of the solutions.

A schematic diagram of the experimental setup is shown in Figure 4.1. The equipment details and the experimental method are similar to those described in the previous studies.[37,38] Only the main features related to the total pressure measurements are highlighted here, which were not explained earlier.

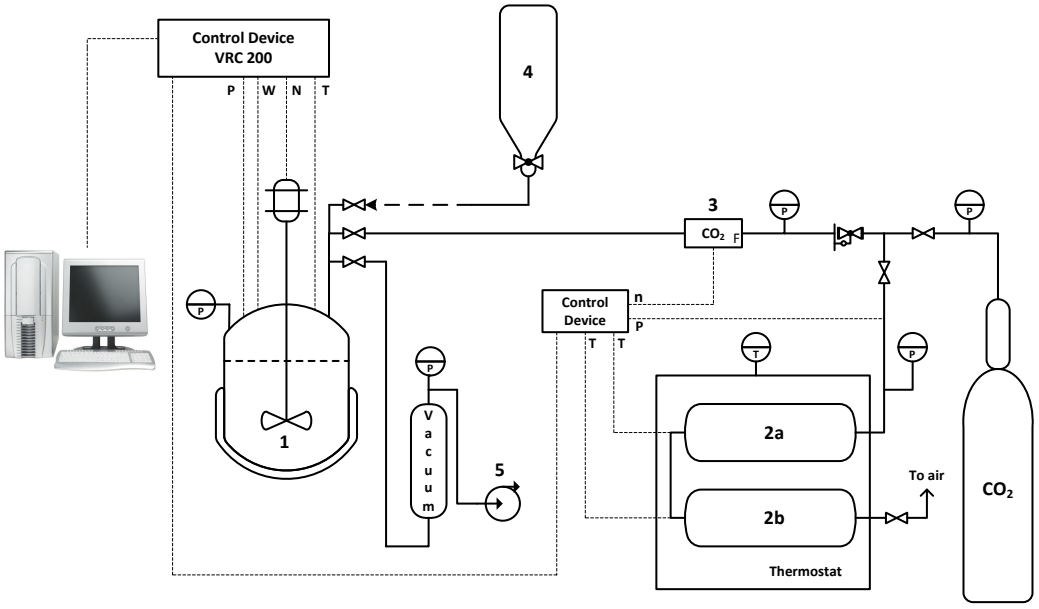

Figure 4.1: Schematic diagram of the experimental setup: 1 - reaction calorimeter; 2a and 2b - CO_2 storage cylinders; 3 - CO_2 mass flow controller; 4 - amine solution feed bottle; 5 - vacuum pump.

The experimental setup consists of a thermally insulated jacked reaction calorimeter (model CPA 122 from ChemiSens AB, Sweden), with a reactor volume of 2000 cm^3, connected to two CO_2 storage cylinders (placed in a thermostatic water bath) through a precalibrated mass flow controller, amine solution feed bottle, and a vacuum pump. A data acquisition unit (VRC 200), connected to all the equipment and a computer, recorded all the operating parameters as a function of time.

Before feeding the amine sample solution into the reactor, it was evacuated and flushed with CO_2 to remove air and any inert gas present in the reactor. A known amount of amine solution (about 1200-1500 cm^3) was then injected into the reactor and heated at a preset temperature to reach the equilibrium that was assured when the pressure and temperature of the reactor changed respectively within ± 0.01 bar and ± 0.01 °C. The equilibrium total pressure was recorded before injecting any CO_2 into the reactor. This total pressure before feeding any CO_2 into the reactor was the sum of partial pressures of amine and water vapors and represented as P_0. Then a known small amount of CO_2 (0.1-0.3 mol) was fed to the reactor by recording the pressure difference in the CO_2 storage cylinders (the Peng-Robinson equation of state was used to calculate the amount of CO_2 fed to the reactor). The exothermic reaction between CO_2 and amine solution produced heat and the temperature increased inside the reactor, which was kept to isothermal conditions by the thermostatic jacket of the reactor. The system reached to a new equilibrium in 60-90 min. The new equilibrium total pressure was also recorded, which is the sum of partial pressures of CO_2, amine, and water vapors, represented as P_t. The partial pressure of CO_2 (P_{CO_2}) was then calculated from the difference between the two total pressures as $P_{CO_2} = P_t - P_0$. CO_2 was continuously fed to the reactor until the amine solution was fully saturated. The corresponding CO_2 partial pressures were also calculated for each CO_2 feeding cycle by assuming that the P_0 remained constant throughout the experiment. All the necessary operating parameters were logged against time. An example of logged data for one complete experiment of 1 M MAPA at 80 °C is shown in Figure 4.2.

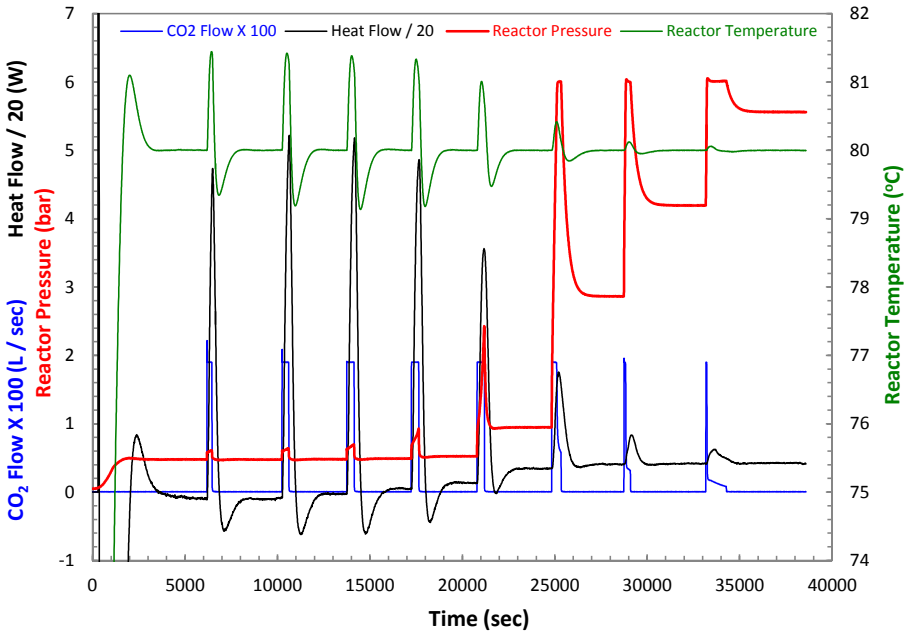

Figure 4.2: Example of different parameters (reactor temperature and pressure, heat flow and CO_2 flow in the reactor) recorded as a function of time for one complete experiment of 1 M MAPA at 80 °C. In order to plot the multiple logged data on the left ordinate, CO_2 flow values were multiplied by 100 and heat flow values were divided by 20.

The blue line indicates the injection of CO_2 into the reactor (eight times) and the black, green, and red lines, respectively, represent the corresponding heat flow, reactor temperature, and reactor pressure. The equilibrium total pressure in the reactor increased up to approximately 6 bar at the end of the experiment. The measurements were made isothermally at 40, 80, and 120 ^{o}C for all the systems studied in this work. The measured equilibrium total pressure and the calculated CO_2 partial pressure data are presented as a function of CO_2 loading.

The total pressure data were measured with an estimated uncertainty of ± 1 % for P_{total} below 50 kPa (with corresponding uncertainty of ± 2 % for the calculated P_{CO_2} from the total pressure data), ± 0.7 % for P_{total} ranging between 51-100 kPa (with corresponding uncertainty of ± 1.7 % for P_{CO_2}), and ± 0.5 % for P_{total} ranging between 101-600 kPa (with corresponding uncertainty of ± 1.5 % for P_{CO_2}).

4.3 Results and Discussion

Equilibrium total pressures were measured and CO_2 partial pressures were estimated from the total pressure measurements in binary and ternary aqueous solutions of DEEA and MAPA (H_2O-DEEA-CO_2, H_2O-MAPA-CO_2 and H_2O-DEEA-MAPA-CO_2) at different amine concentrations as a function of CO_2 loading in the temperature ranging from 40-120 ^{o}C. The experimental method described in this work was first validated by carrying out measurements with 30 mass % MEA solutions and comparing it with the literature data at three different temperatures 40, 80, and 120 ^{o}C. For 30 mass % MEA solutions, the measured total pressures and the calculated CO_2 partial pressures as a function of CO_2 loading are tabulated in Table 4.1 (All the tables are presented in the Appendix at the end of this chapter). These results are also presented graphically in Figure 4.3, which illustrates a good agreement between the data measured in this work and the literature data[28-32,34,35] in the whole temperature range of 40-120 ^{o}C.

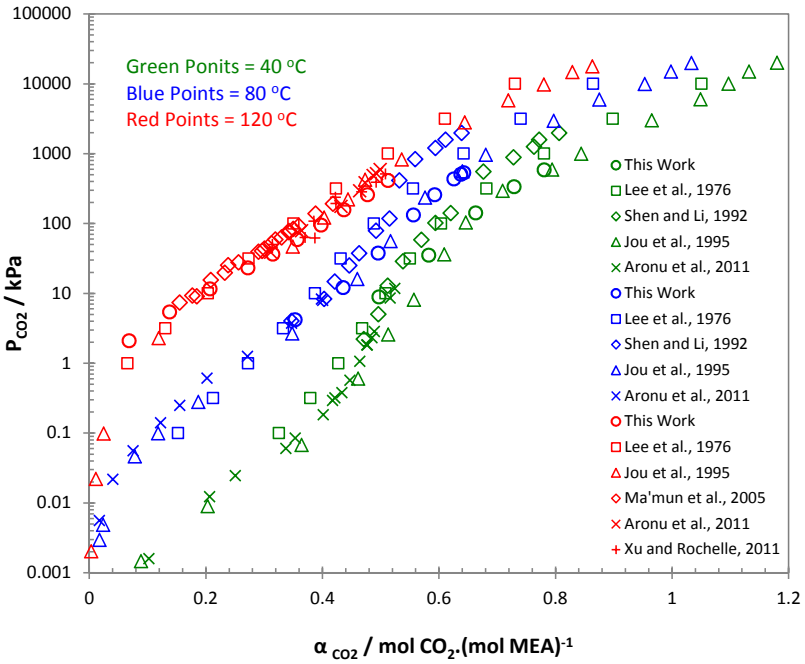

Figure 4.3: Comparison of partial pressure of CO_2 in 30 mass % MEA solutions as a function of CO_2 loading at 40, 80, and 120 °C from this work and the data from Lee et al.[28], Shen and Li[29], Jou et al.[30], Ma'mun et al.[31], Aronu et al.[32], and Xu and Rochelle.[34]

4.3.1 H_2O-DEEA-CO_2 System

For DEEA, the equilibrium total pressures were measured in 5 M (~ 61.1 mass %) DEEA solutions as a function of CO_2 loading in the temperature range of 40-120 °C. The results are presented in Table 4.2. Total pressure data measured in this work as a function of CO_2 loading were compared with the data from Monteiro et al.,[39] as shown in Figure 4.4. The two sets of data are in good agreement. The data measured in this work have good repeatability with a little scatter at 40 °C at high CO_2 loadings. The estimated CO_2 partial pressure data from this work and Monteiro et al.[39] are also compared and presented graphically in Figure 4.5. Again, a very good agreement between two sets of data can be observed.

It should be noted that the isotherm at 40 °C shows a high CO_2 loading capacity at relatively low CO_2 partial pressures. However, the CO_2 loading capacity of 5 M DEEA at 120 °C is very low and gives high CO_2 partial pressures. The cyclic capacity obtained from the difference in CO_2 loading between 40 °C (rich loading) and 120 °C (lean loading) is large. Therefore, DEEA with its high cyclic capacity and low heat of absorption[37] can be an attractive candidate for the energy efficient CO_2 absorbent. However, DEEA (a tertiary alkanolamine) has low reaction kinetics which can lead to a very large size of the absorber.

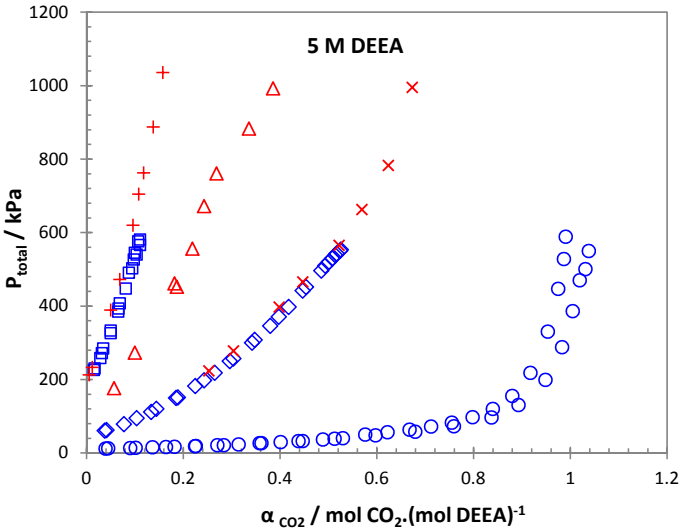

Figure 4.4: Comparison of total pressure in 5 M (~ 61.1 mass %) DEEA solutions as a function of CO_2 loading. This work (blue points): O, 40 °C; ◊, 80 °C; and □, 120 °C. Monteiro et al.[39] (red points): X, 80 °C; Δ, 100 °C; and +, 120 °C.

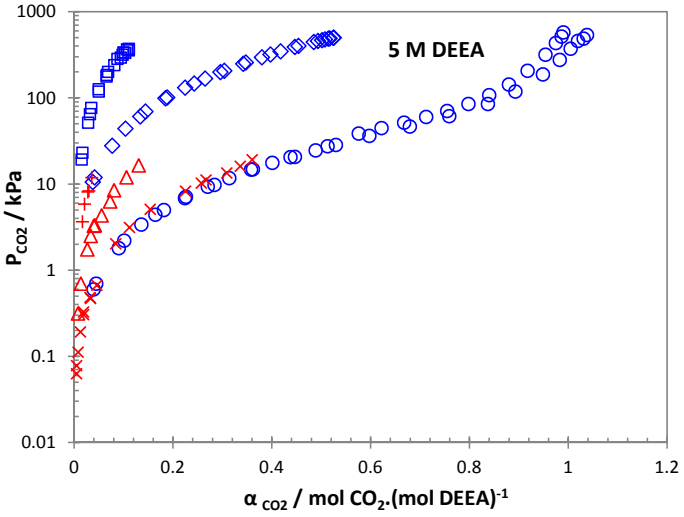

Figure 4.5: Comparison of partial pressure of CO_2 in 5 M (~ 61.1 mass %) DEEA solutions as a function of CO_2 loading. This work (blue points): O, 40 °C; ◊, 80 °C; and □, 120 °C. Monteiro et al.[39] (red points): X, 40 °C; Δ, 60 °C; and +, 80 °C.

4.3.2 H_2O-MAPA-CO_2 Systems

The equilibrium total pressure measurements were performed for two different concentrations, 2 M (~ 17.9 mass %) and 1 M (~ 8.9 mass %), of aqueous MAPA solutions as a function of CO_2 loading at three different temperatures 40, 80, and 120 °C. The results for 2 M and 1 M MAPA solutions are respectively given in Table 4.3 and Table 4.4. Both total pressure (right ordinate) and CO_2 partial pressure (left ordinate) data as a function of CO_2 loading are presented graphically in Figure 4.6 for 2 M MAPA and Figure 4.7 for 1 M MAPA solutions. A good reproducibility can be observed in the data for both systems.

MAPA, being a diamine, shows a very high CO_2 loading capacity for both the tested concentrations (2 M and 1 M) at 40 °C. It also gives high CO_2 loading capacity at 120 °C which results in relatively low cyclic capacity for MAPA compared to that of DEEA. MAPA has high heats of absorption[37] and this can lead to high regeneration energy requirements. However, the fast reaction kinetics of MAPA can lead to a reasonable size of the absorber.

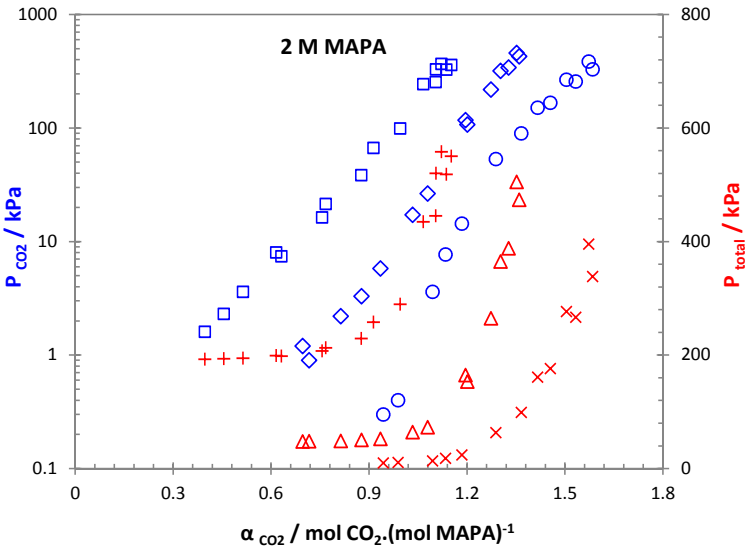

Figure 4.6: Total pressures and solubility of CO_2 in 2 M (~ 17.9 mass %) MAPA solutions as a function of CO_2 loading in this work. Total pressure (red points): X, 40 °C; Δ, 80 °C; and +, 120 °C. Partial pressure of CO_2 (blue points): O, 40 °C; ◊, 80 °C; and □, 120 °C.

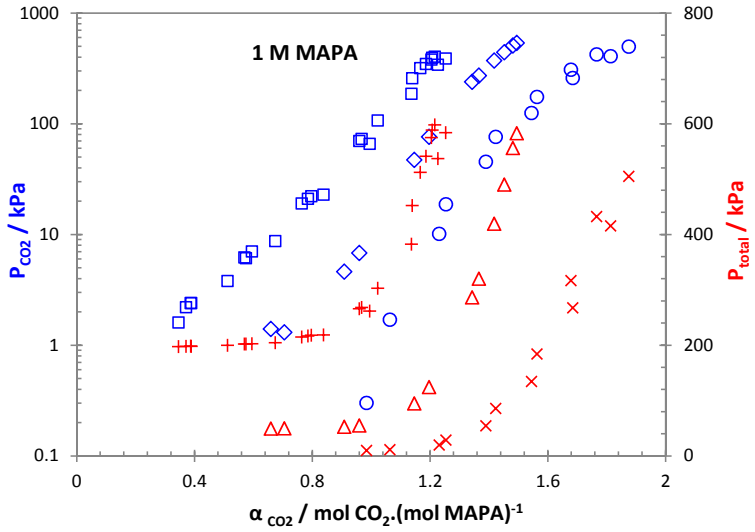

Figure 4.7: Total pressures and solubility of CO_2 in 1 M (~ 8.9 mass %) MAPA solutions as a function of CO_2 loading in this work. Total pressure (red points): X, 40 °C; Δ, 80 °C; and +, 120 °C. Partial pressure of CO_2 (blue points): O, 40 °C; ◊, 80 °C; and □, 120 °C.

4.3.3 H_2O-DEEA-MAPA-CO_2 Systems

In this study, two aqueous DEEA-MAPA mixtures, 5 M (~ 63.5 mass %) DEEA + 2 M (~ 19.1 mass %) MAPA and 5 M (~ 62 mass %) DEEA + 1 M (~ 9.3 mass %) MAPA, were examined in the temperature range of 40-120 °C. These mixtures, 5 M DEEA + 2 M MAPA and 5 M DEEA + 1 M MAPA, are respectively abbreviated as 5D2M and 5D1M. Both mixtures gave two liquid phases in a certain CO_2 loading range. The measured equilibrium total pressure and the estimated CO_2 partial pressure data in 5D2M and 5D1M are presented respectively in Table 4.5 and Table 4.6. The total pressure (right ordinate) and the CO_2 partial pressure (left ordinate) data as a function of CO_2 loading are also presented graphically in Figure 4.8 and Figure 4.9 for 5D2M and 5D1M, respectively.

MAPA (fast reaction kinetics), having primary and secondary amine functional groups, is expected to react first in the aqueous amine mixtures compared to that of DEEA (slow reaction kinetics), a tertiary alkanolamine. This can be observed in the results of CO_2 partial pressures against loading at 40 °C in Figure 4.8 for 5D2M. The isotherm is quite steep up to a certain CO_2 loading (~ 0.45 mol CO_2.(mol amine)$^{-1}$), showing a qualitative behavior similar to that of H_2O-MAPA-CO_2 systems, and then the slope of the line decreases, which shows a qualitative behavior similar to that of H_2O-DEEA-CO_2 system. Such a trend can also be seen for 5D1M at 40 °C in Figure 4.9. However, MAPA seems to be the dominating reacting component (with CO_2) in both amine mixtures at high temperatures, which can be observed from the steepness of the isotherms. This may be due to the reduced absorption capacity of DEEA at high temperatures e.g. the isotherm at 120 °C in Figure 4.5. Both the tested aqueous amine mixtures, 5D2M and 5D1M, gave liquid-liquid phase split in a certain CO_2 loading range. A detail description on the phase change behavior of these amine mixtures can be found in our previous work.[37]

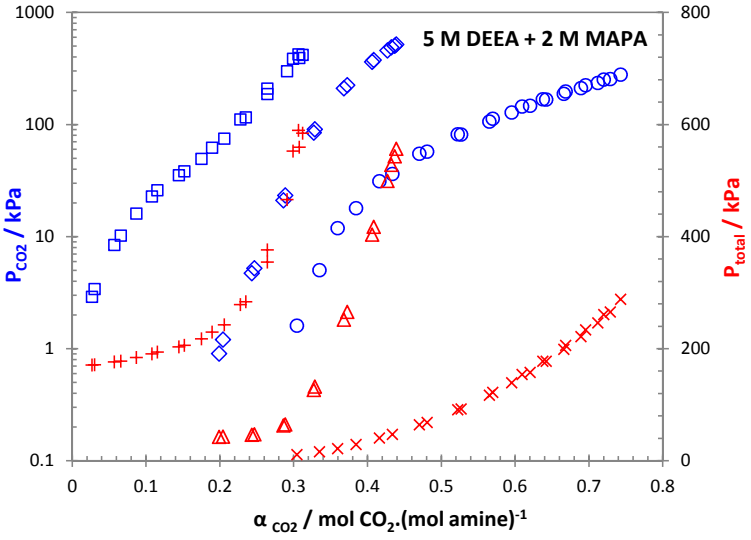

Figure 4.8: Total pressures and solubility of CO_2 in 5M (~ 63.5 mass %) DEEA + 2M (~ 19.1 mass %) MAPA solutions as a function of CO_2 loading in this work. Total pressure (red points): X, 40 °C; Δ, 80 °C; and +, 120 °C. Partial pressure of CO_2 (blue points): O, 40 °C; ◊, 80 °C; and □, 120 °C.

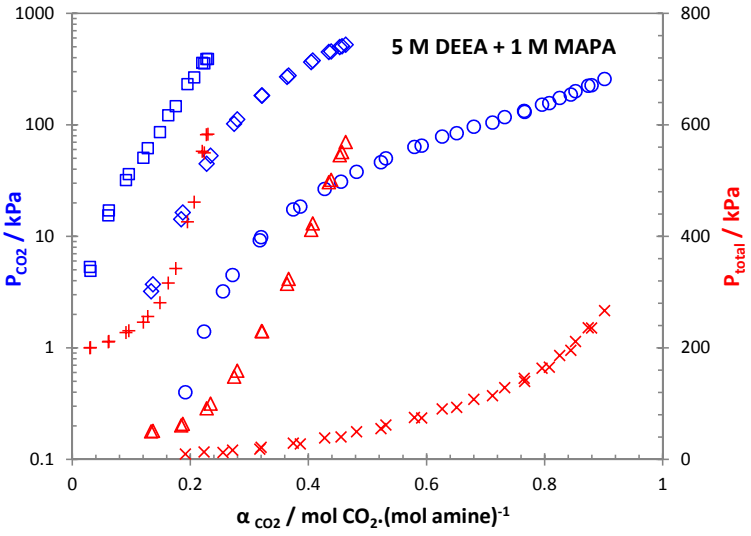

Figure 4.9: Total pressures and solubility of CO_2 in 5M (~ 62 mass %) DEEA + 1M (~ 9.3 mass %) MAPA solutions as a function of CO_2 loading in this work. Total pressure (red points): X, 40 °C; Δ, 80 °C; and +, 120 °C. Partial pressure of CO_2 (blue points): O, 40 °C; ◊, 80 °C; and □, 120 °C.

A comparison of CO_2 partial pressures as a function of loading for all the solvent systems studied in this work with 30 mass % MEA is given in Figure 4.10 for 40 °C and Figure 4.11 for 120 °C.

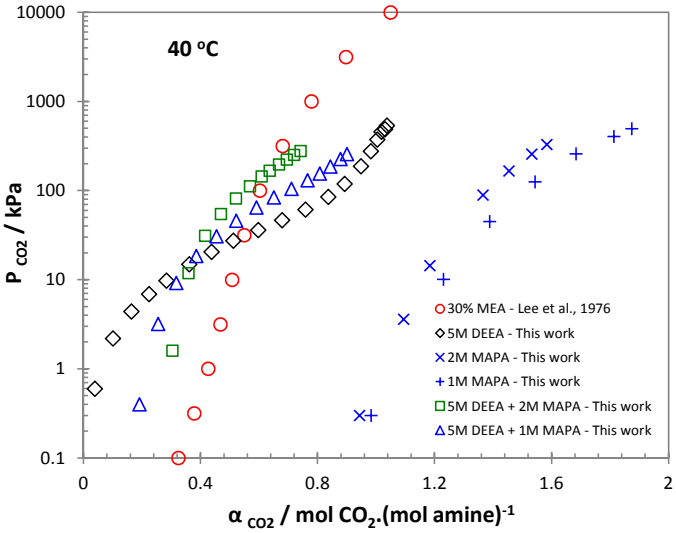

Figure 4.10: Comparison of CO_2 partial pressures as a function of loading for all the solvent systems studied in this work against the results of 30 mass % MEA at 40 °C.

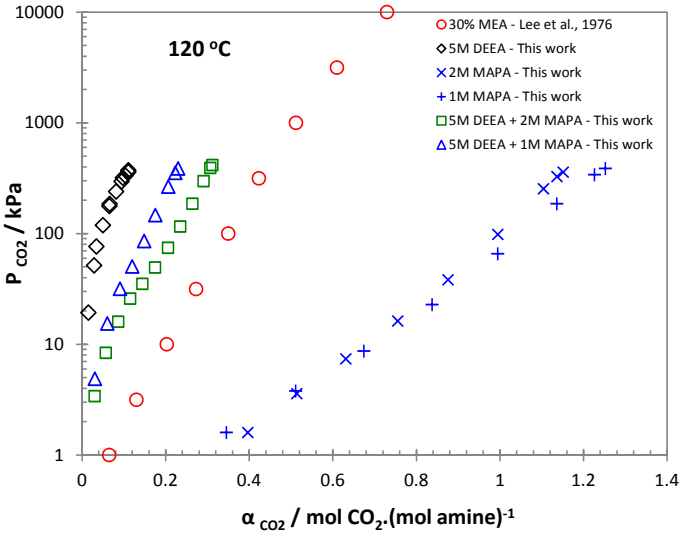

Figure 4.11: Comparison of CO_2 partial pressures as a function of loading for all the solvent systems studied in this work against the results of 30 mass % MEA at 120 °C.

Both 2 M and 1 M MAPA (diamine) solutions have shown very high CO_2 loading capacities at 40 and 120 ^oC compared to the results of 30 mass % MEA. The 5 M DEEA isotherms, on the other hand, show a very different behavior at 40 ^oC and also gave high CO_2 partial pressures at low loadings at 120 ^oC compared to the results of 30 mass % MEA. These kinds of isotherms of DEEA at 40 and 120 ^oC result in high equilibrium temperature sensitivity which can lead to the lower stripping steam requirements for solvent regeneration compared to that of 30 mass % MEA. Another advantage is the possibility of solvent regeneration at elevated pressures leading to high pressure CO_2 streams at the top of the desorber. This can reduce the cost of CO_2 compression during transportation to the storage site. The aqueous mixtures, 5D2M and 5D1M, show a kind of results similar to that of 5 M DEEA at 40 and 120 ^oC depending on the concentration of the promoter (MAPA). Heats of absorption of CO_2 in these mixtures are relatively lower than 30 mass % MEA.[37]

The differential enthalpy of absorption of CO_2 in aqueous amine solutions at constant CO_2 loading can be estimated from the equilibrium CO_2 solubility data by using following form of the Gibbs-Helmholtz equation.[40]

$$\frac{\Delta H_{abs}}{R} = \left(\frac{\partial \ln P_{CO_2}}{\partial (1/T)} \right)_x \tag{1}$$

where; ΔH_{abs} is the enthalpy of absorption, R is the gas constant, P_{CO_2} is the equilibrium CO_2 partial pressure, T is the temperature and x is the equilibrium CO_2 loading.

On the basis of Equation 1, the enthalpies of absorption were estimated at constant CO_2 loading from the slope of the linear plot between $\ln P_{CO_2}$ and $1/T$. The estimated enthalpies of absorption are 62.8 kJ.(mol CO_2)$^{-1}$, 84 kJ.(mol CO_2)$^{-1}$, 83.6 kJ.(mol CO_2)$^{-1}$, 70.1 kJ.(mol CO_2)$^{-1}$, and 69.7 kJ.(mol CO_2)$^{-1}$ for 5 M DEEA, 2 M MAPA, 1 M MAPA, 5D2M, and 5D1M, respectively, at constant CO_2 loadings of 0.1, 0.8, 0.72, 0.31, and 0.25 mol CO_2.(mol amine)$^{-1}$. These estimated values of enthalpy of absorption are almost similar to the values measured calorimetrically at 40 ^oC in our previous work at respective CO_2 loadings.[37] However, these values are significantly different from the values measured at 80 and 120 ^oC.

4.4 Conclusions

Equilibrium total pressures were measured and equilibrium CO_2 partial pressures were estimated from the total pressure measurements as a function of CO_2 loading in binary and ternary aqueous solutions of 2-(diethylamino)ethanol (DEEA) and 3-(methylamino)propylamine (MAPA). The measurements were performed isothermally in a reaction calorimeter used as an equilibrium cell. The tested systems were the binary aqueous solutions of 5 M DEEA, 2 M MAPA, and 1 M MAPA, and the ternary aqueous mixtures of 5 M DEEA + 2 M MAPA and 5 M DEEA + 1 M MAPA. The selected compositions of aqueous amine mixtures gave liquid-liquid phase split upon CO_2 absorption. The total pressures were measured and the CO_2 partial pressures were calculated as a function of CO_2 loading at three different temperatures 40, 80, and 120 ^oC. All experiments were reproduced with a good repeatability.

Measurements were also carried out in 30 mass % MEA solutions and compared with the literature data in order to validate the experimental method used in this work. All the measured data were compared with the results of 30 mass % MEA as a reference case. 5 M DEEA has shown high cyclic capacity. Both 2 and 1 M

MAPA showed high loading capacities at 40 and 120 ^{o}C. The aqueous amine blends, 5D2M and 5D1M, gave fairly good cyclic capacities and their results depend on concentration of the promoter (MAPA) in the amine blend. Due to high CO_2 partial pressure at low loadings, the studied mixtures can also allow the stripping process at elevated desorber pressures, thereby reducing the energy requirements for the CO_2 compression. Approximate enthalpies of absorption of CO_2 in all the tested aqueous amine systems were estimated from the CO_2 solubility data. The measured total pressure and the estimated CO_2 solubility data can be useful in thermodynamic modeling of the capture systems when aqueous DEEA-MAPA solutions are used as capture solvents.

4.5 References

(1) Metz, B.; Davidson, O.; Bosch, P.; Dave, R.; Meyer, L. (Eds.). *Climate Change 2007 – Mitigation of Climate Change*. Working Group III Contribution to the Fourth Assessment Report of the Intergovernmental Panel on Climate Change, Cambridge University Press, UK, 2007.

(2) Adams, D.; Davison, J. *Capturing CO_2*. IEA Greenhouse Gas R&D Programme, 2007 (ISBN : 978-1-898373-41-4).

(3) Metz, B.; Davidson, O.; de Coninck, H.; Loos, M.; Meyer, L. (Eds.). *Carbon Dioxide Capture and Storage*. Intergovernmental Panel on Climate Change (IPCC); Cambridge University Press, UK, 2005.

(4) *The Global Status of CCS: 2012*, Global CCS Institute: Canberra, Australia, 2012.

(5) Kohl, A. L.; Nielsen, R. B. *Gas Purification*, 5th ed.; Gulf Publishing Co.: Houston, TX, USA, 1997.

(6) Zhao, M.; Minett, A. I.; Harris, A. T. A review of techno-economic models for the retrofitting of conventional pulverised-coal power plants for post-combustion capture (PCC) of CO_2. *Energy Environ. Sci.* **2013**, 6, 25-40.

(7) Dillon, D.; Wheeldon, J.; Chu, R.; Choi, G.; Loy, C. A Summary of EPRI's Engineering and Economic Studies of Post Combustion Capture Retrofit Applied at Various North American Host Sites. *Energy Procedia* **2013**, 37, 2349-2358.

(8) Davidson, R. M. *Post-combustion Carbon Capture from Coal Fired Plants - Solvent Scrubbing*. IEA Clean Coal Centre: London, 2007; CCC/125.

(9) Wang, M.; Lawal, A.; Stephenson, P.; Sidders, J.; Ramshaw, C. Post-combustion CO_2 capture with chemical absorption: A state-of-the-art review. *Chem. Eng. Res. Des.* **2011**, 89, 1609-1624.

(10) Glasscock, D. A.; Critchfield, J. E.; Rochelle, G. T. CO_2 absorption/ desorption in mixtures of methyldiethanolamine with monoethanolamine or diethanolamine. *Chem. Eng. Sci.* **1991**, 46(11), 2829-2845.

(11) Bougie, F.; Iliuta, M. C. Sterically Hindered Amine-Based Absorbents for the Removal of CO_2 from Gas Streams. *J. Chem. Eng. Data* **2012**, 57, 635-669.

(12) Rochelle, G. T.; Chen, E.; Freeman, S.; Wagener, D. V.; Xu, Q.; Voice, A. Aqueous piperazine as the new standard for CO_2 capture technology. *Chem. Eng. J.* **2011**, 171, 725-733.

(13) Mehdizadeh, H.; Gupta, M.; Kim, I.; Da Silva, E. F.; Haug-Warberg, T.; Svendsen, H. F. AMP-CO_2-water thermodynamics, a combination of UNIQUAC model, computational chemistry and experimental data. *Int. J. Greenhouse Gas Control* **2013**, 18, 173-182.

(14) Le Tourneux, D.; Iliuta, I.; Iliuta, M. C.; Fradette, S.; Larachi, F. Solubility of carbon dioxide in aqueous solutions of 2-amino-2-hydroxymethyl-1,3-propanediol. *Fluid Phase Equilib.* **2008**, 268, 121-129.

(15) Bougie, F.; Iliuta, M. C. CO_2 Absorption in Aqueous Piperazine Solutions: Experimental Study and Modeling. *J. Chem. Eng. Data* **2011**, 56, 1547-1554.

(16) Brúder, P.; Grimstvedt, A.; Mejdell, T.; Svendsen, H. F. CO_2 capture into aqueous solutions of piperazine activated 2-amino-2-methyl-1-propanol. *Chem. Eng. Sci.* **2011**, 66, 6193-6198.

(17) Fosbøl, P. L.; Neerup, R.; Arshad, M. W.; Tecle, Z.; Thomsen, K. Aqueous Solubility of Piperazine and 2-Amino-2-methyl-1-propanol plus Their Mixtures Using an Improved Freezing-Point Depression Method. *J. Chem. Eng. Data* **2011**, 56, 5088-5093.

(18) Bougie, F.; Iliuta, M. C. CO_2 Absorption into Mixed Aqueous Solutions of 2-Amino-2-hydroxymethyl-1,3-propanediol and Piperazine. *Ind. Eng. Chem. Res.* **2010**, 49, 1150-1159.

(19) Zhu, D.; Fang, M.; Lv, Z.; Wang, Z.; Luo, Z. Selection of Blended Solvents for CO_2 Absorption from Coal-Fired Flue Gas. Part 1: Monoethanolamine (MEA)-Based Solvents. *Energy & Fuels* **2012**, 26, 147-153.

(20) Adeosun, A.; Abu-Zahra, M. R. M. Evaluation of amine-blend solvent systems for CO_2 post-combustion capture applications. *Energy Procedia* **2013**, 37, 211-218.

(21) Dubois, L.; Thomas, D. Postcombustion CO_2 capture by chemical absorption: screening of aqueous amine(s)-based solvents. *Energy Procedia* **2013**, 37, 1648-1657.

(22) Svendsen, H. F.; Hessen, E. T.; Mejdell, T. Carbon dioxide capture by absorption, challenges and possibilities. *Chem. Eng. J.* **2011**, 171, 718-724.

(23) Zhang, J.; Nwani, O.; Tan, Y.; Agar, D. W. Carbon dioxide absorption into biphasic amine solvent with solvent loss reduction. *Chem. Eng. Res. Des.* **2011**, 89, 1190-1196.

(24) Raynal, L.; Pascal, A.; Bouillon, P.-A.; Gomez, A.; le Febvre de Nailly, M.; Jacquin, M.; Kittel, J.; di Lella, A.; Mougin, P.; Trapy, J. The DMX^{TM} process: an original solution for lowering the cost of post-combustion carbon capture. *Energy Procedia* **2011**, 4, 779-786.

(25) Raynal, L.; Bouillon, P.-A.; Gomez, A.; Broutin, P. From MEA to demixing solvents and future steps, a roadmap for lowering the cost of post-combustion carbon capture. *Chem. Eng. J.* **2011**, 171, 742-752.

(26) Zhang, J.; Misch, R.; Tan, Y.; Agar, D. W. Novel thermomorphic biphasic amine solvents for CO_2 absorption and low-temperature extractive regeneration. *Chem. Eng. Technol.* **2011**, 34 (9), 1481-1489.

(27) Zhang, J.; Agar, D. W.; Zhang, X.; Geuzebroek, F. CO_2 absorption in biphasic solvents with enhanced low temperature solvent regeneration. *Energy Procedia* **2011**, 4, 67-74.

(28) Lee, J. I.; Otto, F. D.; Mather A. E. Equilibrium Between Carbon Dioxide and Aqueous Monoethanolamine Solutions. *J. Appl. Chem. Biotechnol.* **1976**, 26, 541-549.

(29) Shen, K.-P.; Li, M.-H. Solubility of Carbon Dioxide in Aqueous Mixtures of Monoethanolamine with Methyldiethanolamine. *J. Chem. Eng. Data* **1992**, 37, 96-100.

(30) Jou, F.-Y.; Mather, A. E.; Otto, F. D. The Solubility of CO_2 in a 30 Mass Percent Monoethanolamine Solution. *Can. J. Chem. Eng.* **1995**, 73, 140-147.

(31) Ma'mun, S.; Nilsen, R.; Svendsen, H. F. Solubility of Carbon Dioxide in 30 mass % Monoethanolamine and 50 mass % Methyldiethanolamine Solutions. *J. Chem. Eng. Data* **2005**, 50, 630-634.

(32) Aronu, U. E.; Gondal, S.; Hessen, E. T.; Haug-Warberg, T.; Hartono, A.; Hoff, K. A.; Svendsen, H. F. Solubility of CO_2 in 15, 30, 45 and 60 mass% MEA from 40 to 120°C and model representation using the extended UNIQUAC framework. *Chem. Eng. Sci.* **2011**, 66, 6393-6406.

(33) Anufrikov, Y. A.; Kuranov, G. L.; Smirnova, N. A. Solubility of CO_2 and H_2S in Alkanolamine-containing Aqueous Solutions. *Russ. J. Appl. Chem.* **2007**, 80(4), 515-527.

(34) Xu, Q.; Rochelle, G. T. Total Pressure and CO_2 Solubility at High Temperature in Aqueous Amines, *Energy Procedia* **2011**, 4, 117-124.

(35) Xu, Q. Thermodynamics of CO_2 Loaded Aqueous Amines. *Ph.D. Thesis*, The University of Texas at Austin, Austin, TX, **2011.**

(36) Arshad, M. W.; von Solms, N.; Svendsen, H. F.; Thomsen, K. Heat of Absorption of CO_2 in Aqueous Solutions of DEEA, MAPA and their Mixture. *Energy Procedia* **2013**, 37, 1532-1542.

(37) Arshad, M. W.; Fosbøl, P. L.; von Solms, N.; Svendsen, H. F.; Thomsen, K. Heat of Absorption of CO_2 in Phase Change Solvents: 2-(diethylamino)ethanol and 3-(methylamino)propylamine. *J. Chem. Eng. Data* **2013**, 58, 1974-1988.

(38) Kim, I.; Svendsen, H. F. Heat of absorption of carbon dioxide (CO_2) in monoethanolamine (MEA) and 2-(aminoethyl)ethanolamine (AEEA) solutions. *Ind. Eng. Chem. Res.* **2007**, 46, 5803-5809.

(39) Monteiro, J. G. M.-S.; Pinto, D. D. D.; Zaidy, S. A. H.; Hartono, A.; Svendsen, H. F. VLE data and modelling of aqueous N,N-diethyethanolamine (DEEA) solutions. *Int. J. Greenhouse Gas Control* **2013**, 19, 432-440.

(40) Sherwood, A. E.; Prausnitz, J. M. The heat of solution of gases at high pressure. *AIChE J.* **1962**, 8(4), 519-521.

4.6 Appendix

Table 4.1: Total Pressure and Solubility of CO_2 in 30 mass % MEA solutions (b_{MEA} = 7.017 mol MEA.(kg H_2O)$^{-1}$) at 40, 80, and 120 °C.[a]

α_{CO_2}	b_{CO_2}	P_{total}	P_{CO_2}	α_{CO_2}	b_{CO_2}	P_{total}	P_{CO_2}	α_{CO_2}	b_{CO_2}	P_{total}	P_{CO_2}
mol CO_2.(mol MEA)$^{-1}$	mol CO_2.(kg H_2O)$^{-1}$	kPa	kPa	mol CO_2.(mol MEA)$^{-1}$	mol CO_2.(kg H_2O)$^{-1}$	kPa	kPa	mol CO_2.(mol MEA)$^{-1}$	mol CO_2.(kg H_2O)$^{-1}$	kPa	kPa
	313.15 K				**353.15 K**				**393.15 K**		
0.497	3.485	9.6	8.9	0.353	2.476	48.4	4.2	0.068	0.480	178.1	2.1
0.582	4.086	36.0	35.3	0.435	3.054	56.3	12.1	0.138	0.967	181.4	5.4
0.663	4.650	142.8	142.1	0.496	3.478	82.0	37.8	0.207	1.452	187.6	11.6
0.729	5.115	336.7	336.0	0.556	3.901	176.6	132.4	0.272	1.909	199.2	23.2
0.780	5.474	586.6	585.9	0.593	4.159	303.1	258.9	0.315	2.209	212.3	36.3
				0.625	4.387	477.0	432.8	0.357	2.502	234.7	58.7
				0.637	4.472	551.5	507.3	0.398	2.790	270.7	94.7
				0.642	4.506	579.5	535.3	0.437	3.063	332.8	156.8
								0.477	3.348	434.6	258.6
								0.512	3.595	587.2	411.2

[a] The standard uncertainty for the temperature is *u(T)* = 0.03 K and the relative standard uncertainties for the CO_2 composition are $u_r(b)$ = 0.01 and $u_r(\alpha)$ = 0.01. The estimated uncertainty for the measured P_{total} is ± 1 % for the total pressure below 50 kPa (with corresponding uncertainty of ± 2 % for the calculated P_{CO_2}), ± 0.7 % for P_{total} ranging between 51-100 kPa (with corresponding uncertainty of ± 1.7 % for P_{CO_2}), and ± 0.5 % for P_{total} ranging between 101-600 kPa (with corresponding uncertainty of ± 1.5 % for P_{CO_2}).

Table 4.2: Total Pressure and Solubility of CO_2 in 5 M (61.087 mass %) DEEA solutions (b_{DEEA} = 13.392 mol DEEA.(kg H_2O)$^{-1}$) at 40, 80, and 120 °C.[a]

α_{CO_2}	b_{CO_2}	P_{total}	P_{CO_2}	α_{CO_2}	b_{CO_2}	P_{total}	P_{CO_2}	α_{CO_2}	b_{CO_2}	P_{total}	P_{CO_2}
mol CO_2.(mol DEEA)$^{-1}$	mol CO_2.(kg H_2O)$^{-1}$	kPa	kPa	mol CO_2.(mol DEEA)$^{-1}$	mol CO_2.(kg H_2O)$^{-1}$	kPa	kPa	mol CO_2.(mol DEEA)$^{-1}$	mol CO_2.(kg H_2O)$^{-1}$	kPa	kPa
	313.15 K (1)				**353.15 K (1)**				**393.15 K (1)**		
0.045	0.601	12.3	0.7	0.041	0.554	62.0	12.0	0.035	0.465	284.3	76.6
0.090	1.208	13.4	1.8	0.104	1.393	94.1	44.1	0.066	0.886	393.3	185.6
0.136	1.826	15.0	3.4	0.144	1.932	119.7	69.7	0.098	1.313	526.7	319.0
0.182	2.435	16.6	5.0	0.185	2.480	149.3	99.3	0.111	1.486	580.6	372.9
0.226	3.029	18.7	7.1	0.225	3.014	182.1	132.1		**393.15 K (2)**		
0.271	3.623	20.9	9.3	0.265	3.550	218.0	168.0	0.015	0.204	226.0	19.3
0.314	4.209	23.3	11.7	0.304	4.071	257.0	207.0	0.029	0.385	258.3	51.6
0.358	4.794	26.3	14.7	0.342	4.582	299.9	249.9	0.050	0.668	325.9	119.2
0.401	5.374	29.3	17.7	0.380	5.089	346.0	296.0	0.066	0.880	384.3	177.6
0.447	5.987	32.3	20.7	0.418	5.595	397.5	347.5	0.081	1.091	447.2	240.5
0.489	6.547	36.3	24.7	0.454	6.079	451.3	401.3	0.095	1.266	502.1	295.4
0.530	7.098	40.1	28.5	0.493	6.607	509.1	459.1	0.104	1.390	539.7	333.0
0.576	7.716	50.2	38.6	0.508	6.803	529.2	479.2	0.111	1.484	565.6	358.9
0.622	8.333	56.2	44.6	0.517	6.926	542.3	492.3		**393.15 K (3)**		
0.668	8.945	63.2	51.6	0.526	7.041	553.4	503.4	0.017	0.229	229.6	23.1
0.712	9.540	71.7	60.1		**353.15 K (2)**			0.032	0.430	271.3	64.8
0.755	10.112	82.2	70.6	0.038	0.510	60.7	10.6	0.050	0.670	332.7	126.2
0.798	10.691	97.0	85.4	0.077	1.035	78.1	28.0	0.069	0.926	407.2	200.7
0.840	11.246	119.6	108.0	0.134	1.793	111.3	61.2	0.088	1.175	490.2	283.7
0.880	11.783	155.1	143.5	0.189	2.529	151.2	101.1	0.100	1.339	545.0	338.5
0.918	12.289	218.1	206.5	0.243	3.256	197.6	147.5	0.107	1.436	575.6	369.1
0.954	12.773	330.5	318.9	0.296	3.969	249.8	199.7				
0.975	13.057	446.6	435.0	0.348	4.654	307.6	257.5				
0.987	13.213	527.7	516.1	0.398	5.326	370.5	320.4				
0.990	13.262	588.7	577.1	0.447	5.987	441.6	391.5				
	313.15 K (2)			0.485	6.500	496.3	446.2				
0.039	0.527	12.0	0.6	0.502	6.720	519.9	469.8				
0.101	1.359	13.6	2.2	0.515	6.892	537.7	487.6				
0.164	2.201	15.8	4.4	0.525	7.024	550.4	500.3				
0.224	3.006	18.3	6.9								
0.284	3.805	21.2	9.8								
0.362	4.845	26.3	14.9								
0.438	5.868	32.0	20.6								
0.513	6.869	38.9	27.5								
0.598	8.004	47.6	36.2								
0.679	9.098	58.0	46.6								
0.759	10.170	72.7	61.3								
0.837	11.212	96.6	85.2								
0.893	11.961	130.5	119.1								
0.949	12.708	199.2	187.8								
0.983	13.162	287.5	276.1								

1.005	13.460	385.6	374.2		
1.020	13.653	469.7	458.3		
1.031	13.811	500.1	488.7		
1.038	13.902	549.9	538.5		

[a] The standard uncertainty for the temperature is *u(T)* = 0.03 K and the relative standard uncertainties for the CO_2 composition are $u_r(b)$ = 0.01 and $u_r(\alpha)$ = 0.01. The estimated uncertainty for the measured P_{total} is ± 1 % for the total pressure below 50 kPa (with corresponding uncertainty of ± 2 % for the calculated P_{CO_2}), ± 0.7 % for P_{total} ranging between 51-100 kPa (with corresponding uncertainty of ± 1.7 % for P_{CO_2}), and ± 0.5 % for P_{total} ranging between 101-600 kPa (with corresponding uncertainty of ± 1.5 % for P_{CO_2}).

Table 4.3: Total Pressure and Solubility of CO_2 in 2 M (17.877 mass %) MAPA solutions (b_{MAPA} = 2.469 mol MAPA.(kg H_2O)$^{-1}$) at 40, 80, and 120 °C.[a]

α_{CO_2}	b_{CO_2}	P_{total}	P_{CO_2}	α_{CO_2}	b_{CO_2}	P_{total}	P_{CO_2}	α_{CO_2}	b_{CO_2}	P_{total}	P_{CO_2}
mol CO_2.(mol MAPA)$^{-1}$	mol CO_2.(kg H_2O)$^{-1}$	kPa	kPa	mol CO_2.(mol MAPA)$^{-1}$	mol CO_2.(kg H_2O)$^{-1}$	kPa	kPa	mol CO_2.(mol MAPA)$^{-1}$	mol CO_2.(kg H_2O)$^{-1}$	kPa	kPa
	313.15 K (1)				**353.15 K (1)**				**393.15 K (1)**		
0.943	2.330	10.1	0.3	0.696	1.720	47.7	1.2	0.397	0.979	192.4	1.6
1.094	2.703	13.4	3.6	0.813	2.008	48.7	2.2	0.514	1.269	194.4	3.6
1.184	2.924	24.2	14.4	0.935	2.308	52.3	5.8	0.631	1.558	198.2	7.4
1.365	3.372	99.2	89.4	1.079	2.666	73.0	26.5	0.755	1.866	207.1	16.3
1.455	3.593	176.3	166.5	1.200	2.964	153.4	106.9	0.876	2.163	229.2	38.4
1.532	3.784	266.6	256.8	1.273	3.144	264.9	218.4	0.995	2.457	289.6	98.8
1.584	3.912	338.3	328.5	1.327	3.277	388.1	341.6	1.104	2.726	445.2	254.4
	313.15 K (2)			1.359	3.357	473.7	427.2	1.137	2.807	518.4	327.6
0.988	2.440	10.6	0.4		**353.15 K (2)**			1.151	2.843	550.5	359.7
1.134	2.801	17.9	7.7	0.716	1.768	48.1	0.9		**393.15 K (2)**		
1.288	3.181	63.4	53.2	0.876	2.164	50.5	3.3	0.455	1.123	193.5	2.3
1.416	3.497	160.9	150.7	1.033	2.550	64.4	17.2	0.615	1.519	199.2	8.0
1.504	3.715	276.6	266.4	1.195	2.951	164.6	117.4	0.767	1.894	212.6	21.4
1.572	3.883	395.3	385.1	1.302	3.215	364.9	317.7	0.913	2.255	258.1	66.9
				1.351	3.337	504.9	457.7	1.066	2.632	434.7	243.5
								1.104	2.727	520.0	328.8
								1.121	2.768	558.2	367.0

[a] The standard uncertainty for the temperature is *u(T)* = 0.03 K and the relative standard uncertainties for the CO_2 composition are $u_r(b)$ = 0.01 and $u_r(\alpha)$ = 0.01. The estimated uncertainty for the measured P_{total} is ± 1 % for the total pressure below 50 kPa (with corresponding uncertainty of ± 2 % for the calculated P_{CO_2}), ± 0.7 % for P_{total} ranging between 51-100 kPa (with corresponding uncertainty of ± 1.7 % for P_{CO_2}), and ± 0.5 % for P_{total} ranging between 101-600 kPa (with corresponding uncertainty of ± 1.5 % for P_{CO_2}).

Table 4.4: Total Pressure and Solubility of CO_2 in 1 M (8.901 mass %) MAPA solutions (b_{MAPA} = 1.108 mol MAPA.(kg H_2O)$^{-1}$) at 40, 80, and 120 °C.[a]

α_{CO_2}	b_{CO_2}	P_{total}	P_{CO_2}	α_{CO_2}	b_{CO_2}	P_{total}	P_{CO_2}	α_{CO_2}	b_{CO_2}	P_{total}	P_{CO_2}
mol CO_2.(mol MAPA)$^{-1}$	mol CO_2.(kg H_2O)$^{-1}$	kPa	kPa	mol CO_2.(mol MAPA)$^{-1}$	mol CO_2.(kg H_2O)$^{-1}$	kPa	kPa	mol CO_2.(mol MAPA)$^{-1}$	mol CO_2.(kg H_2O)$^{-1}$	kPa	kPa
	313.15 K (1)				**353.15 K (1)**				**393.15 K (1)**		
0.984	1.091	9.7	0.3	0.705	0.781	49.5	1.3	0.345	0.383	197.2	1.6
1.231	1.364	19.5	10.1	0.959	1.063	55.0	6.8	0.512	0.567	199.4	3.8
1.389	1.540	54.6	45.2	1.196	1.326	124.1	75.9	0.674	0.747	204.3	8.7
1.544	1.712	134.6	125.2	1.365	1.513	320.0	271.8	0.838	0.929	218.4	22.8
1.684	1.867	267.6	258.2	1.452	1.610	490.0	441.8	0.995	1.103	261.5	65.9
1.813	2.010	415.6	406.2	1.495	1.657	582.7	534.5	1.136	1.260	382.1	186.5
1.875	2.078	505.0	495.6		**353.15 K (2)**			1.227	1.360	536.9	341.3
	313.15 K (2)			0.659	0.730	49.1	1.4	1.252	1.388	583.6	388.0
1.063	1.179	11.4	1.7	0.908	1.007	52.3	4.6		**393.15 K (2)**		
1.253	1.389	28.4	18.7	1.146	1.271	94.7	47.0	0.387	0.429	198.1	2.4
1.423	1.577	85.7	76.0	1.342	1.488	286.3	238.6	0.574	0.637	201.8	6.1
1.563	1.732	184.1	174.4	1.418	1.571	419.4	371.7	0.796	0.883	217.8	22.1
1.678	1.860	316.6	306.9	1.481	1.642	556.1	508.4	1.022	1.133	302.6	106.9
1.766	1.957	432.2	422.5					1.186	1.315	540.9	345.2
								1.216	1.348	597.8	402.1
									393.15 K (3)		
								0.370	0.411	197.9	2.2
								0.569	0.630	201.9	6.2
								0.764	0.847	214.7	19.0
								0.959	1.063	265.5	69.8
								1.139	1.262	452.3	256.6
								1.204	1.334	575.0	379.3
									393.15 K (4)		
								0.388	0.430	197.8	2.4
								0.594	0.659	202.4	7.0
								0.785	0.870	216.3	20.9
								0.967	1.072	268.2	72.8
								1.166	1.293	512.2	316.8
								1.206	1.337	588.6	393.2

[a] The standard uncertainty for the temperature is *u(T)* = 0.03 K and the relative standard uncertainties for the CO_2 composition are $u_r(b)$ = 0.01 and $u_r(\alpha)$ = 0.01. The estimated uncertainty for the measured P_{total} is ± 1 % for the total pressure below 50 kPa (with corresponding uncertainty of ± 2 % for the calculated P_{CO_2}), ± 0.7 % for P_{total} ranging between 51-100 kPa (with corresponding uncertainty of ± 1.7 % for P_{CO_2}), and ± 0.5 % for P_{total} ranging between 101-600 kPa (with corresponding uncertainty of ± 1.5 % for P_{CO_2}).

Table 4.5: Total Pressure and Solubility of CO_2 in 5 M (63.533 mass %) DEEA + 2 M (19.116 mass %) MAPA solutions ($b_{mixture}$ = 43.743 mol amine.(kg H_2O)$^{-1}$) at 40, 80, and 120 °C.[a]

α_{CO_2}	b_{CO_2}	P_{total}	P_{CO_2}	α_{CO_2}	b_{CO_2}	P_{total}	P_{CO_2}	α_{CO_2}	b_{CO_2}	P_{total}	P_{CO_2}
mol CO_2.(mol amine)$^{-1}$	mol CO_2.(kg H_2O)$^{-1}$	kPa	kPa	mol CO_2.(mol amine)$^{-1}$	mol CO_2.(kg H_2O)$^{-1}$	kPa	kPa	mol CO_2.(mol amine)$^{-1}$	mol CO_2.(kg H_2O)$^{-1}$	kPa	kPa
	313.15 K (1)				**353.15 K (1)**				**393.15 K (1)**		
0.335	14.651	16.1	5.0	0.199	8.695	42.5	0.9	0.027	1.160	170.5	2.9
0.385	16.821	29.0	17.9	0.243	10.633	46.3	4.7	0.066	2.872	177.8	10.2
0.434	18.973	47.2	36.1	0.286	12.517	62.6	21.0	0.108	4.709	190.3	22.7
0.481	21.025	68.2	57.1	0.327	14.311	126.0	84.4	0.152	6.638	205.7	38.1
0.527	23.032	92.5	81.4	0.372	16.285	265.6	224.0	0.189	8.282	229.5	61.9
0.565	24.720	116.9	105.8	0.408	17.859	417.2	375.6	0.228	9.963	278.5	110.9
0.595	26.042	139.2	128.1	0.432	18.904	527.7	486.1	0.264	11.560	376.2	208.6
0.620	27.121	157.7	146.6	0.439	19.199	556.6	515.0	0.299	13.085	552.4	384.8
0.642	28.084	177.5	166.4		**353.15 K (2)**			0.306	13.395	589.2	421.6
0.666	29.132	199.0	187.9	0.204	8.929	42.9	1.2		**393.15 K (2)**		
0.689	30.135	221.4	210.3	0.247	10.794	46.9	5.2	0.030	1.325	171.3	3.4
0.712	31.136	246.0	234.9	0.288	12.611	64.9	23.2	0.057	2.486	176.3	8.4
0.729	31.878	265.6	254.5	0.328	14.364	132.1	90.4	0.087	3.788	183.9	16.0
	313.15 K (2)			0.368	16.097	251.4	209.7	0.115	5.047	193.8	25.9
0.304	13.314	11.2	1.6	0.406	17.760	403.5	361.8	0.145	6.322	203.1	35.2
0.359	15.715	21.5	11.9	0.427	18.680	499.3	457.6	0.175	7.646	217.2	49.3
0.416	18.201	40.8	31.2	0.437	19.112	543.1	501.4	0.206	9.012	242.5	74.6
0.470	20.566	64.4	54.8					0.235	10.285	283.5	115.6
0.522	22.835	91.2	81.6					0.264	11.557	354.1	186.2
0.570	24.922	121.9	112.3					0.291	12.732	465.7	297.8
0.609	26.650	154.1	144.5					0.307	13.441	559.5	391.6
0.637	27.879	177.4	167.8					0.312	13.643	584.5	416.6
0.668	29.240	206.0	196.4								
0.695	30.411	233.7	224.1								
0.720	31.500	261.0	251.4								
0.743	32.496	288.1	278.5								

[a] The standard uncertainty for the temperature is *u(T)* = 0.03 K and the relative standard uncertainties for the CO_2 composition are $u_r(b)$ = 0.01 and $u_r(\alpha)$ = 0.01. The estimated uncertainty for the measured P_{total} is ± 1 % for the total pressure below 50 kPa (with corresponding uncertainty of ± 2 % for the calculated P_{CO_2}), ± 0.7 % for P_{total} ranging between 51-100 kPa (with corresponding uncertainty of ± 1.7 % for P_{CO_2}), and ± 0.5 % for P_{total} ranging between 101-600 kPa (with corresponding uncertainty of ± 1.5 % for P_{CO_2}).

Table 4.6: Total Pressure and Solubility of CO_2 in 5 M (62.025 mass %) DEEA + 1 M (9.331 mass %) MAPA solutions ($b_{mixture}$ = 22.173 mol amine.(kg H_2O)$^{-1}$) at 40, 80, and 120 °C.[a]

α_{CO_2}	b_{CO_2}	P_{total}	P_{CO_2}	α_{CO_2}	b_{CO_2}	P_{total}	P_{CO_2}	α_{CO_2}	b_{CO_2}	P_{total}	P_{CO_2}
mol CO_2.(mol amine)$^{-1}$	mol CO_2.(kg H_2O)$^{-1}$	kPa	kPa	mol CO_2.(mol amine)$^{-1}$	mol CO_2.(kg H_2O)$^{-1}$	kPa	kPa	mol CO_2.(mol amine)$^{-1}$	mol CO_2.(kg H_2O)$^{-1}$	kPa	kPa
	313.15 K (1)				**353.15 K (1)**				**393.15 K (1)**		
0.223	4.943	13.2	1.4	0.137	3.027	50.7	3.7	0.031	0.684	200.1	4.9
0.271	6.016	16.3	4.5	0.187	4.148	63.3	16.3	0.061	1.349	210.6	15.4
0.320	7.086	21.6	9.8	0.234	5.192	99.6	52.6	0.091	2.016	227.0	31.8
0.374	8.300	29.2	17.4	0.279	6.190	158.7	111.7	0.120	2.665	245.8	50.6
0.427	9.472	38.4	26.6	0.320	7.105	230.0	183.0	0.149	3.294	280.9	85.7
0.481	10.672	49.7	37.9	0.366	8.120	323.4	276.4	0.175	3.889	342.0	146.8
0.531	11.770	61.7	49.9	0.407	9.026	423.0	376.0	0.206	4.574	461.1	265.9
0.579	12.840	74.9	63.1	0.435	9.634	496.8	449.8	0.223	4.955	549.6	354.4
0.626	13.886	90.3	78.5	0.453	10.041	545.2	498.2	0.230	5.097	582.9	387.7
0.680	15.075	107.7	95.9	0.463	10.260	568.9	521.9		**393.15 K (2)**		
0.732	16.237	128.8	117.0		**353.15 K (2)**			0.030	0.663	199.7	5.3
0.765	16.963	145.2	133.4	0.133	2.957	49.8	3.2	0.062	1.370	211.4	17.0
0.795	17.635	163.3	151.5	0.184	4.087	60.8	14.2	0.096	2.126	230.4	36.0
0.825	18.298	186.2	174.4	0.227	5.043	91.2	44.6	0.128	2.835	256.1	61.7
0.852	18.896	211.6	199.8	0.274	6.071	148.3	101.7	0.163	3.604	315.8	121.4
0.873	19.366	235.9	224.1	0.321	7.127	229.6	183.0	0.195	4.324	425.7	231.3
	313.15 K (2)			0.364	8.064	314.7	268.1	0.220	4.878	552.3	357.9
0.191	4.245	9.6	0.4	0.405	8.972	411.4	364.8	0.227	5.034	582.3	387.9
0.255	5.658	12.4	3.2	0.438	9.716	501.3	454.7				
0.318	7.043	18.4	9.2	0.457	10.130	550.9	504.3				
0.386	8.559	27.7	18.5								
0.455	10.090	40.0	30.8								
0.522	11.584	55.3	46.1								
0.592	13.122	74.0	64.8								
0.651	14.432	93.3	84.1								
0.711	15.773	114.1	104.9								
0.766	16.985	139.7	130.5								
0.808	17.909	165.3	156.1								
0.844	18.720	195.7	186.5								
0.879	19.498	235.7	226.5								
0.901	19.984	266.9	257.7								

[a] The standard uncertainty for the temperature is *u(T)* = 0.03 K and the relative standard uncertainties for the CO_2 composition are $u_r(b)$ = 0.01 and $u_r(\alpha)$ = 0.01. The estimated uncertainty for the measured P_{total} is ± 1 % for the total pressure below 50 kPa (with corresponding uncertainty of ± 2 % for the calculated P_{CO_2}), ± 0.7 % for P_{total} ranging between 51-100 kPa (with corresponding uncertainty of ± 1.7 % for P_{CO_2}), and ± 0.5 % for P_{total} ranging between 101-600 kPa (with corresponding uncertainty of ± 1.5 % for P_{CO_2}).

5. Thermodynamic Modeling

5.1 Introduction

Thermodynamic models are essential for the process simulation and optimization of the CO_2 capture processes. When CO_2 (acid gas) is dissolved in the aqueous amine solutions, it forms electrolyte solutions. Two activity coefficient based models, e-NRTL (electrolyte Non-Random Two-Liquid) and Extended UNIQUAC, are the most commonly used local composition models applied for thermodynamic modeling of the electrolyte systems containing H_2O-Amine/Alkanolamine-Acid gas. The Extended UNIQUAC model has been adopted in this work for thermodynamic modeling of the de-mixing H_2O-DEEA-MAPA-CO_2 system. Previously, the Extended UNIQUAC model has been successfully applied to a variety of aqueous amine systems. Thomsen and Rasmussen[1] implemented the Extended UNIQUAC model to describe the vapor-liquid equilibria (VLE) and solid-liquid equilibria (SLE) in the H_2O-NH_3-CO_2 system. Darde et al.[2] further upgraded the model to a wide range of concentration, temperature, and pressure for its use in the aqueous ammonia process for CO_2 capture. Faramarzi et al.[3] implemented the Extended UNIQUAC to model the VLE in H_2O-MEA-CO_2, H_2O-MDEA-CO_2, and H_2O-MEA-MDEA-CO_2 systems and Sadegh, 2012[4] further improved the model by including more experimental data in the parameter estimation. Sadegh, 2012[4] also used the Extended UNIQUAC to model the H_2O-MDEA-H_2S and H_2O-MDEA-H_2S-CH_4 systems for acid gas removal from the sour natural gas streams.

The Extended UNIQUAC model is used in this work for thermodynamic modeling of the H_2O-DEEA-CO_2, H_2O-MAPA-CO_2, and H_2O-DEEA-MAPA-CO_2 systems. The last solvent system gives biphasic liquid-liquid phase split (de-mixing) when reacted with carbon dioxide. Only two thermodynamic modeling studies were found in the literature for these solvent systems. Hartono et al.[5] implemented the UNIQUAC framework to model the binary and ternary VLE in H_2O-DEEA-MAPA system (unloaded systems). No modeling study was found in the literature for the CO_2 loaded aqueous MAPA system. Monteiro et al.[6] reported the modeling results for the H_2O-DEEA-CO_2 system by using the e-NRTL model with only a small number of experimental data. The first complete (may be not perfect) modeling work of its kind is presented here for the H_2O-DEEA-CO_2, H_2O-MAPA-CO_2, and H_2O-DEEA-MAPA-CO_2 systems using the Extended UNIQUAC thermodynamic model. The type of experimental data used in this work are; pure amine vapor pressure, VLE (both unloaded and CO_2 loaded), SLE (freezing point depression data), LLE, excess enthalpy, and differential heat of absorption of CO_2 in aqueous amines. The developed model reproduces almost all the data points and describes all the data types satisfactorily with a single unique set of parameters.

The Gamma-Phi ($\gamma - \phi$) approach is used in this work for the phase equilibrium calculations. This means that the Extended UNIQUAC thermodynamic model is used to calculate the aqueous-phase activity coefficient (γ) and Soave-Redlich-Kwong (SRK) cubic equation of state (EoS) is used to determine the

vapor-phase fugacity coefficient (ϕ). The model only requires UNIQUAC volume (r) and surface area (q) parameters of each species for calculations of the combinatorial (or entropic) term and binary interaction energy parameters for each pair of species for calculations of the residual (or enthalpic) term. The Debye-Hückel term has no adjustable parameters and represents only the electrostatic interactions of the ionic species in the aqueous phase. Similarly, the SRK equation has no interaction parameters to be fitted for the gas phase. The SRK EoS is applied with classical mixing rules (quadratic mixing rule for the a parameter and linear mixing rule for the b parameter). A detail description of the Extended UNIQUAC model is given in the next section.

5.2 Chemical Potential and Activity Coefficient

The criterion for the vapor-liquid equilibrium (VLE), solid-liquid equilibrium (SLE) and liquid-liquid equilibrium (LLE) is that the chemical potential of each component is same in all the phases. The chemical potential of component i (μ_i) is the summation of standard state chemical potential (μ_i^0) and a term that describes the concentration and activity coefficient of that component i as given by

$$\mu_i = \mu_i^0 + RT \ln a_i = \mu_i^0 + RT \ln \left(x_i \gamma_i \right) \tag{1}$$

where, a_i is the activity, x_i is the mole fraction, and γ_i is the activity coefficient of component i. R is the gas constant (8.314 J.mol^{-1}.K^{-1}) and T is the temperature in Kelvin. The activity coefficient describes the non-ideal behavior of the component i and determined by the Extended UNIQUAC model. In this work, symmetrical convention is adopted for water (solvent) and unsymmetrical convention is adopted for remaining all the components (solute).

The chemical potential of water (μ_w), according to the symmetrical convention, can be written as

$$\mu_w = \mu_w^0 + RT \ln a_w = \mu_w^0 + RT \ln \left(x_w \gamma_w \right) \tag{2}$$

where, μ_w^0 is the standard state chemical potential of water, a_w is the activity of water, x_w is the water mole fraction, and γ_w is the rational symmetrical activity coefficient of water. The activity coefficient of water in its pure component state is unity at all temperatures, according to the symmetrical convention i.e. $\gamma_w = 1$ for $x_w = 1$.

According to unsymmetrical convention, the activity coefficient of component i is defined as

$$\gamma_i^* = \frac{\gamma_i}{\gamma_i^\infty} \tag{3}$$

where, γ_i^∞ is the activity coefficient at infinite dilution and γ_i^* is the rational unsymmetrical activity coefficient of solute i and has a value of unity at infinite dilution i.e. $\gamma_i^* = 1$ at infinite dilution. The term "unsymmetrical" is used due to the fact that this activity coefficient has a value of 1 at infinite dilution rather than in the pure component state. The infinite dilution activity coefficient of a component in water is

dependent on temperature and pressure. The rational unsymmetrical activity coefficient can be used in Equation 1 to derive an expression for the chemical potential of component (ion) i based on unsymmetrical convention.

$$\mu_i = \mu_i^* + RT \ln\left(x_i \gamma_i^*\right) \tag{4}$$

where, μ_i^* is the rational unsymmetrical standard state chemical potential defined as

$$\mu_i^* = \mu_i^0 + RT \ln\left(\gamma_i^\infty\right) \tag{5}$$

5.3 Extended UNIQUAC Model

Extended UNIQUAC model, an activity coefficient model for electrolyte systems,[1,7,8] is used in this work for thermodynamic modeling of H_2O-DEEA-MAPA-CO_2 system. The model has been described earlier by Sander et al.[9-11] and Nicolaisen et al.[12] It consists of short-range contribution from the original UNIQUAC model[13,14] combined with the Debye-Hückel long-range term which takes into account the electrostatic interactions of the ionic species present.

$$G^{Excess} = G^{Excess}_{Combinatorial} + G^{Excess}_{Residual} + G^{Excess}_{Debye-Hückel} \tag{6}$$

The first two terms, the combinatorial (or entropic) and the residual (or enthalpic) terms, are identical to the terms used in the UNIQUAC model. The expression of excess Gibbs energy for the entropic term of the model is given as:

$$\frac{G_C^E}{RT} = \sum_i x_i \ln\left(\frac{\phi_i}{x_i}\right) - \frac{z}{2}\sum_i q_i x_i \ln\left(\frac{\phi_i}{\theta_i}\right) \tag{7}$$

The combinatorial term is temperature independent and depends on the concentrations and relative sizes of the species. z is the co-ordination number of the lattice and assigned a values of 10 and x_i is the mole fraction of component i. ϕ_i and θ_i are, respectively, the volume and surface area fractions for the component i given by:

$$\phi_i = \frac{x_i r_i}{\sum_j x_j r_j} \tag{8}$$

$$\theta_i = \frac{x_i q_i}{\sum_j x_j q_j} \tag{9}$$

where, r_i and q_i are the volume and surface area parameters for the component i. These parameters are determined from the properties of non-electrolyte molecules in the classical application of UNIQUAC model.[13] However, these parameters are considered adjustable parameters in the Extended UNIQUAC

model due to the fact that this approach gave unsatisfactory results when the model was implemented to the multi component electrolyte systems.[15] The adjustable volume and surface area parameters are calculated by fitting to the experimental data.

The following expression of excess Gibbs energy is used for the temperature dependent residual term

$$\frac{G_R^E}{RT} = -\sum_i x_i q_i \ln\left(\sum_j \theta_j \psi_{ji}\right) \tag{10}$$

with ψ_{ji} parameter as

$$\psi_{ji} = \exp\left(\frac{u_{jj} - u_{ij}}{T}\right) \tag{11}$$

where, u_{ij} and u_{jj} are the interaction energy parameters. u_{ij} represents the interaction across a binary pair of different components and u_{jj} represents interaction across a binary pair of same component. These parameters are considered symmetrical and temperatures dependent as

$$u_{ij} = u_{ij}^0 + u_{ij}^T \left(T - 298.15\right) \tag{12}$$

where, u_{ij}^0 and u_{ij}^T are adjustable interaction parameters of the model determined by fitting to the experimental data.

The third term in the Extended UNIQUAC model is derived from the extended Debye-Hückel law. The following expression of excess Gibbs energy is used for the Debye-Hückel contribution to the model

$$\frac{G_{DH}^E}{RT} = -x_w M_w \frac{4A}{b^3}\left[\ln\left(1 + b\sqrt{I}\right) - b\sqrt{I} + \frac{b^2 I}{2}\right]^2 \tag{13}$$

where, x_w is the mole fraction and M_w (kg.mol^{-1}) is the molar mass of water. b parameter has a constant value of 1.50 (kg.mol^{-1})^{½}. I is the ionic strength of the electrolyte solution first defined by Lewis and Randall[16] as:

$$I = \frac{1}{2}\sum_i m_i Z_i^2 \tag{14}$$

where, m_i is the molality and Z_i is the charge number of the ionic species i. A is the Debye-Hückel parameter with a value of 1.1717 (kg.mol^{-1})^{½} at 25 °C.

$$A = \left(2\pi N_A d_0\right)^{1/2}\left(\frac{e^2}{4\pi\varepsilon_0\varepsilon_r kT}\right)^{3/2} \tag{15}$$

where, N_A is Avogadro's number (6.023 X 10^{23} mol^{-1}), d_0 is the density of water in $kg.m^{-3}$, e is the electron charge (1.60206 X 10^{-19} C), ε_0 is the permittivity in vacuum (8.8542 X 10^{-12} $C^2.J^{-1}.m^{-1}$), ε_r is the dielectric constant (or relative permittivity) of solvent (dimensionless) 78.4 for water at 298.15 K, k is the Boltzmann's constant (1.381 X 10^{-23} $J.K^{-1}$), and T is the temperature in Kelvin. Based on the density of pure water and the dielectric constant of water, the Debye-Hückel parameter can be approximated in the temperature range of 273.15 K < T < 473.15 K by

$$A = \left[1.131 + 1.335\times10^{-3}\left(T-273.15\right) + 1.164\times10^{-5}\left(T-273.15\right)^2\right]\left(kg.mol^{-1}\right)^{1/2} \tag{16}$$

The UNIQUAC excess Gibbs energy functions for the combinatorial and the residual terms are based on the rational symmetrical activity coefficient convention. However, the Debye-Hückel contribution to the excess Gibbs energy function is based on rational symmetrical convention for water and rational unsymmetrical convention for ions.

The rational symmetrical activity coefficients of the combinatorial and the residual UNIQUAC terms are obtained by partial molar differentiation of these terms

$$\ln\gamma_i^C = \ln\left(\frac{\phi_i}{x_i}\right) + 1 - \frac{\phi_i}{x_i} - \frac{z}{2}q_i\left[\ln\left(\frac{\phi_i}{\theta_i}\right) + 1 - \frac{\phi_i}{\theta_i}\right] \tag{17}$$

$$\ln\gamma_i^R = q_i\left[1 - \ln\left(\sum_j \theta_j\psi_{ji}\right) - \sum_j\left(\frac{\theta_j\psi_{ij}}{\sum_k \theta_k\psi_{kj}}\right)\right] \tag{18}$$

By setting $x_w = 1$ for Equations 17 and 18, the infinite dilution terms can be obtained as

$$\ln\gamma_i^{C\infty} = \ln\left(\frac{r_i}{r_w}\right) + 1 - \frac{r_i}{r_w} - \frac{z_i}{2}q_i\left[\ln\left(\frac{r_i q_w}{r_w q_i}\right) + 1 - \frac{r_i q_w}{r_w q_i}\right] \tag{19}$$

$$\ln\gamma_i^{R\infty} = q_i\left(1 - \ln\psi_{wi} - \psi_{iw}\right) \tag{20}$$

Similarly, by partial molar differentiation of the excess Gibbs energy function of the Debye-Hückel term, one can obtain the electrostatic contributions to the rational symmetrical activity coefficient of water and rational unsymmetrical activity coefficients of ions

$$\ln\gamma_w^{DH} = M_w\frac{2A}{b^3}\left[1 + b\sqrt{I} - \frac{1}{1+b\sqrt{I}} - 2\ln\left(1+b\sqrt{I}\right)\right] \tag{21}$$

$$\ln\gamma_i^{*DH} = -Z_i^2\frac{A\sqrt{I}}{1+b\sqrt{I}} \tag{22}$$

Finally, the activity coefficient of water in the Extended UNQUAC model is obtained by adding the three contributions as:

$$\ln \gamma_w = \ln \gamma_w^C + \ln \gamma_w^R + \ln \gamma_w^{DH} \tag{23}$$

And the activity coefficients of ion (or component) i are obtained by the summation of three terms and according to the definition of rational unsymmetrical activity coefficient as:

$$\ln \gamma_i^* = \ln\left(\frac{\gamma_i^C}{\gamma_i^{C\infty}}\right) + \ln\left(\frac{\gamma_i^R}{\gamma_i^{R\infty}}\right) + \ln \gamma_i^{*DH} \tag{24}$$

5.4 SRK EoS

In this work, the vapor-phase fugacity coefficients (describes non-ideality in the gas phase) were calculated from the SRK equation of state (EoS) by using classical mixing rule. SRK EoS has no interaction parameters to be fitted for the gas phase. Pure component properties (critical temperature, critical pressure and acentric factor) used for the calculations are tabulated in Table 5.1.

Table 5.1: Pure component properties used in SRK EoS.

Component	Critical Temperature, T_c / (K)	Critical Pressure, P_c / (bar)	Acentric factor ω
H_2O	647.1	220.64	0.345
CO_2	304.13	73.77	0.225
DEEA	619.41	26.37	0.732
MAPA	620.58	44.04	0.501

5.5 Chemical and Phase Equilibrium Calculations

5.5.1 Speciation Equilibria

When CO_2 in dissolved in the aqueous amine solutions, several reactions took place depending on the type of amine. The following speciation equilibria were considered for the thermodynamic modeling.

Dissociation of water: $$H_2O(l) \rightleftharpoons H^+(aq) + OH^-(aq) \tag{25}$$

Hydration of CO_2: $$CO_2(aq) + H_2O(l) \rightleftharpoons HCO_3^-(aq) + H^+(aq) \tag{26}$$

Bicarbonate dissociation: $$HCO_3^-(aq) \rightleftharpoons CO_3^{2-}(aq) + H^+(aq) \tag{27}$$

Protonation of DEEA: $$DEEA(aq) + H^+(aq) \rightleftharpoons DEEAH^+(aq) \tag{28}$$

Protonation of MAPA: $$MAPA(aq) + H^+(aq) \rightleftharpoons MAPAH^+(aq) \tag{29}$$

Di-protonation of MAPA: $MAPAH^{+}(aq) + H^{+}(aq) \rightleftharpoons {}^{+}HMAPAH^{+}(aq)$ (30)

MAPA carbamate (prim): $MAPA(aq) + HCO_3^{-}(aq) \rightleftharpoons MAPACOO^{-}(aq) + H_2O(l)$ (31)

When CO_2 is dissolved in the aqueous tertiary amine solutions like DEEA, it promotes the hydration of CO_2 to produce bicarbonate as suggested by Donaldson and Nguyen.[17]

$$DEEA(aq) + H_2O(l) + CO_2(aq) \rightleftharpoons DEEAH^{+}(aq) + HCO_3^{-}(aq) \quad (32)$$

It should be noted that the reaction given in Equation 32 is sum to the two reactions given in Equations 26 and 28.

On the other hand MAPA is a diamine containing a primary and a secondary amine functional group. It forms carbamate when reacted with CO_2 and there are possibilities of a large number of chemical reactions and formation of several different species. The complexity of the system is similar to that of aqueous 2-((2-Aminoethyl)amino)ethanol (AEEA), an alkanolamine with both primary and secondary amine groups.[18] There may be eight possible MAPA species present in the aqueous phase: $MAPA(aq)$, $MAPAH^{+}$, ${}^{+}HMAPAH^{+}$, $MAPACOO^{-}$ (both primary and secondary carbamate), ${}^{+}HMAPACOO^{-}$ (both primary and secondary protonated carbamate), and ${}^{-}OOCMAPACOO^{-}$. Ma'mun et al.[18] reported that the formation of secondary carbamate and dicarbamate of AEEA is very small in the whole CO_2 loading range of 0-1 mol CO_2.(mol AEEA)$^{-1}$. They also reported that the primary carbamate of AEEA is the dominating carbamate species present in the aqueous phase. Therefore, only four species of MAPA ($MAPA(aq)$, $MAPAH^{+}$, ${}^{+}HMAPAH^{+}$, and $MAPACOO^{-}$ (*prim*)) were considered for modeling in this work as shown in Equations 29-31.

For all the speciation equilibria given in Equations 25-31, the condition is that the summation of chemical potential of the reactants is equal to the summation of chemical potential of the products.

$$\sum_i \mu_{i,\,\text{Reactants}} = \sum_i \mu_{i,\,\text{Products}} \quad (33)$$

For equilibrium calculations Equation 33 is applied to, for example, hydration of CO_2 (Equation 26) by considering the symmetrical convention for water (Equation 2) and unsymmetrical convention for remaining species (Equation 4) to get following expression

$$-\frac{\left(\mu^{*}_{HCO_3^{-}(aq)} + \mu^{*}_{H^{+}(aq)}\right) - \left(\mu^{*}_{CO_2(aq)} + \mu^{0}_{H_2O(l)}\right)}{RT} = \ln\left(\frac{a^{*}_{HCO_3^{-}(aq)} a^{*}_{H^{+}(aq)}}{a^{*}_{CO_2(aq)} a_{H_2O(l)}}\right) \quad (34)$$

An expression similar to the Equation 34 can be obtained for all the equilibria given in Equations 25-31 and solved simultaneously for speciation calculations. Equation 34 can be written in a general form as

$$-\frac{\Delta G_j^{0}}{RT} = \sum_i v_i \ln a_i \quad (35)$$

where, ΔG_j^0 is the increment in standard state Gibbs energy for the reaction j. a_i is the activity of species i and v_i is the stoichiometric coefficient of species i, negative for the reactants and positive for the products.

5.5.2 Vapor-Liquid Equilibria

The following vapor-liquid equilibria were considered

$$H_2O(l) \rightleftharpoons H_2O(g) \tag{36}$$

$$CO_2(aq) \rightleftharpoons \mathrm{CO}_2(g) \tag{37}$$

$$DEEA(aq) \rightleftharpoons DEEA(g) \tag{38}$$

$$MAPA(aq) \rightleftharpoons MAPA(g) \tag{39}$$

The equilibrium condition is that the chemical potential of component i in the aqueous phase is identical to the chemical potential of component i in the gas phase at a given temperature and pressure.

$$\mu_{i(aq)} = \mu_{i(g)} \tag{40}$$

The chemical potential of component i in the gas phase at a temperature T and pressure P can be expressed as

$$\mu_{i(g)}(T,P) = \mu_i^{0,ig}(T,P_0) + RT\ln\left(\frac{y_i P\hat{\phi}_i}{P_0}\right) \tag{41}$$

where, $\mu_i^{0,ig}(T,P_0)$ is the standard state chemical potential of pure gas i at temperature T and pressure P_0 = 1 bar, y_i is the mole fraction of component i in the gas phase, and $\hat{\phi}_i$ is the fugacity coefficient of component i which describes the deviation from the ideal behavior just like the activity coefficient (γ_i) which describes the non-ideality in the solutions as described earlier.

The chemical potential of component i in the aqueous phase can be written as

$$\mu_{i(aq)}(T,P) = \mu_{i(aq)}^* + V_{i(aq)}(P-P_0) + RT\ln\left(x_{i(aq)}\gamma_{i(aq)}^*\right) \tag{42}$$

Equations 41 and 42 can be equated according to the criterion for vapor-liquid equilibrium as given in Equation 40 to get an expression given below

$$\frac{\mu_{i(aq)}^* - \mu_i^{0,ig}(T,P_0)}{RT} + \frac{V_{i(aq)}(P-P_0)}{RT} = \ln\left(\frac{y_i\hat{\phi}_i P}{x_i\gamma_i^* P_0}\right) \tag{43}$$

The second term on left hand side of the equation is the pressure correction to the aqueous phase chemical potential. This term can be ignored at low pressures.

The expression for the calculation of vapor pressure of pure components (only amines in this work, DEEA and MAPA) is given as

$$-\frac{\Delta G^0}{RT} = \ln\left(\frac{y_i \hat{\phi}_i P}{x_i \gamma_i^* P_0}\right) \tag{44}$$

The mole fraction of pure component i is same both in the liquid and the gas phases i.e. $x_i = y_i$. Also, the rational symmetrical activity coefficient of pure component i is unity i.e. $\gamma_i = 1$ at $x_i = 1$. Therefor by using the definition of rational unsymmetrical activity coefficient (Equation 3) for pure component, Equation 44 can be reduced to

$$-\frac{\Delta G^0}{RT} = \ln\left(\frac{\hat{\phi}_i \gamma_i^{\infty} P}{P_0}\right) \tag{45}$$

which is used in the calculation of vapor pressure of pure amines (DEEA and MAPA).

5.5.3 Solid-Liquid Equilibrium

The solid-liquid equilibrium considered in this work is

$$H_2O(s) \rightleftharpoons H_2O(l) \tag{46}$$

The criterion for the solid-liquid equilibrium is that the chemical potential is identical in the two phases. The activity of the solid compound in its phase is considered to be one. Therefore, the chemical potential of the solid compound is equal to its standard state chemical potential. Since ice is the only solid phase formed in the experimental freezing point depression data of both unloaded and CO_2 loaded aqueous amine solutions, Equation 35 can be reduced to

$$-\frac{\Delta G^0}{RT} = \ln a_w \tag{47}$$

where, $\Delta G^0 = \mu_w^0 - \mu_{ice}^0$ is the change in standard state chemical potential between the ice and liquid water and a_w is the activity of water.

5.5.4 Liquid-Liquid Equilibrium

An important characteristic of the aqueous DEEA-MAPA solutions is that they split into two liquid phases when reacted with CO_2. The equilibrium condition is that the chemical potential of component i is identical in the two liquid phases, I and II.

$$\mu_i^I = \mu_i^{II} \tag{48}$$

Since the same standard state is used for each independent component in the two phases, the standard state chemical potential on both sides of Equation 48 will cancel out each other and reduces to the following expression

$$a_i^I = a_i^{II} \tag{49}$$

where, a_i^I and a_i^{II} are the activity of component i in the liquid phases I and II, respectively. Therefore, the criterion for the LLE calculations is that the activity of each independent component is same in both liquid phases.

5.6 Excess Enthalpy Calculations

Thermal property data such as excess enthalpy are very useful for determination of the surface area parameter (q) because the UNIQUAC contribution to the excess enthalpy is proportional to the q parameter. Experimental excess enthalpy data for only water-DEEA system are available in the literature for modeling. The symmetrical excess enthalpy for the water-DEEA system can be calculated by using the Gibbs-Helmholtz equation.

$$\left(\frac{\partial\left(G^E/RT\right)}{\partial T}\right)_{P,x} = -\frac{H^E}{RT^2} = x_w\left(\frac{\partial \ln \gamma_w}{\partial T}\right)_{P,x} + x_{DEEA}\left(\frac{\partial \ln \gamma_{DEEA}}{\partial T}\right)_{P,x} \tag{50}$$

where, γ_{DEEA} is the symmetrical activity coefficient of DEEA which can be obtained from the unsymmetrical activity coefficient of DEEA by using Equation 3.

5.7 Heat of Absorption Calculations

The heat involved when CO_2 is absorbed in the aqueous amine solutions can be calculated from the energy balance of the absorption process.

$$\Delta H_{abs} = \frac{n_2 H_2 - n_1 H_1 - n_{CO_2} H_{CO_2}}{n_{CO_2}} \tag{51}$$

where, ΔH_{abs} is the heat of absorption per mole of CO_2 absorbed. H_1 and n_1 are the molar enthalpy and number of moles of solution before CO_2 absorption, H_2 and n_2 are the molar enthalpy and number of moles of solution after CO_2 absorption, and H_{CO_2} and n_{CO_2} are the molar enthalpy and number of moles of CO_2 absorbed in the solution.

At constant pressure and composition, the total enthalpy of formation of an electrolyte solution can be calculated as

$$nH = \tilde{n}_w H_w + \sum_i \tilde{n}_i H_i \tag{52}$$

where, H_w and H_i are the partial molar enthalpy of water and component (solute) i, respectively. $\tilde{n}_w$ and $\tilde{n}_i$ are the number of moles of water and component i, which is the equilibrium composition achieved after the establishment of speciation equilibrium.

The partial molar enthalpies of water and solute can be calculated from the temperature derivatives of the chemical potentials at constant pressure and composition. Therefore, the differentiation of Equation 2 (chemical potential of water) with respect to temperature at constant pressure and composition gives

$$\left(\frac{\partial\left(\mu_w/RT\right)}{\partial T}\right)_{P,x}=\left(\frac{\partial\left(\mu_w^0/RT\right)}{\partial T}\right)_{P,x}+\left(\frac{\partial \ln \gamma_w}{\partial T}\right)_{P,x} \tag{53}$$

$$\frac{H_w}{RT^2}=\frac{H_w^0}{RT^2}+\frac{H_w^{ex}}{RT^2} \tag{54}$$

where, H_w^0 is the standard state molar enthalpy of formation and H_w^{ex} is the partial molar excess enthalpy of water.

Similarly, the differentiation of chemical potential of solute (Equation 4) with respect to temperature at constant pressure and composition leads to

$$\left(\frac{\partial\left(\mu_i/RT\right)}{\partial T}\right)_{P,x}=\left(\frac{\partial\left(\mu_i^*/RT\right)}{\partial T}\right)_{P,x}+\left(\frac{\partial \ln \gamma_i^*}{\partial T}\right)_{P,x} \tag{55}$$

$$\frac{H_i}{RT^2}=\frac{H_i^*}{RT^2}+\frac{H_i^{ex}}{RT^2} \tag{56}$$

where, H_i^* is the standard state molar enthalpy of formation and H_i^{ex} is the partial molar excess enthalpy of solute i. By using Equations 54 and 56, the total enthalpy of formation of an electrolyte solution at constant pressure and composition (Equation 52) becomes

$$nH=\tilde{n}_w\left(H_w^0+H_w^{ex}\right)+\sum_i \tilde{n}_i\left(H_i^*+H_i^{ex}\right) \tag{57}$$

The molar enthalpy of absorbed CO_2 can be calculated as

$$H_{CO_2}=H_{CO_2}^0+\int_{T_0}^{T} C_{p,CO_2}^0\,dT \tag{58}$$

where, $H_{CO_2}^0$ is the standard state molar enthalpy of formation, $T_0=298.15\ K$ is the standard state temperature, and C_{p,CO_2}^0 is the standard state heat capacity of CO_2.

5.8 Standard State Properties

The standard state properties (Gibbs energy and enthalpy of formation, and heat capacity) of different components and species used in this work were taken from the NIST tables given at 25 °C. The values of chemical potential (Gibbs energy) at temperature of interest can be calculated from its values at 25 °C (298.15 K) by using Gibbs-Helmholtz equation.

$$-\frac{d\ln K}{dT}=\frac{d\left(\Delta G^{0}/RT\right)}{dT}=-\frac{\Delta H^{0}}{RT^{2}} \tag{59}$$

Equation 59 can be integrated from the standard state temperature ($T_0 = 298.15\ K$) to temperature T to get the following expression

$$\ln K_T - \ln K_{T_0} = \int_{T_0}^{T} \frac{\Delta H^{0}}{RT^{2}} dT \tag{60}$$

where, K_T and K_{T_0} are the equilibrium constants at temperatures T and $T_0 = 298.15\ K$, respectively. Temperature derivative of the enthalpy of formation of the process give the heat capacity of the species involved in the process as

$$\Delta C_p^0 = \frac{d\Delta H^{0}}{dT} \tag{61}$$

where, ΔC_p^0 is the increment in the standard state heat capacity. Three parameter temperature dependent heat capacity correlation used in the model[1,7] as suggested by Helgeson et al.[19] is given as

$$\Delta C_{p,i}^{*} = a_i + b_i T + \frac{c_i}{T - T_{\Theta,i}} \tag{62}$$

A constant value of 200 K is given to $T_{\Theta,i}$ for all the components. By combining Equations 61 and 62 and integrating leads to

$$\Delta H_T^0 = \Delta H_{T_0}^0 + \Delta a\left(T - T_0\right) + 0.5\Delta b\left(T^2 - T_0^2\right) + \Delta c \ln\left(\frac{T - T_\Theta}{T_0 - T_\Theta}\right) \tag{63}$$

ΔH_T^0 is the increment in standard state enthalpy at temperature T. Δa, Δb, and Δc are the increment in the heat capacity correlation parameters a, b, and c for the system considered.

Inserting Equation 63 in Equation 60 and integrating lead to the following form of the equilibrium constant

$$\begin{aligned} R\ln K_T = R\ln K_{T_0} - \Delta H_{T_0}^0\left(\frac{1}{T}-\frac{1}{T_0}\right) + \Delta a\left(\ln\frac{T}{T_0} - \frac{T_0}{T} - 1\right) \\ + 0.5\Delta b\left(\frac{\left(T-T_0\right)^2}{T}\right) + \frac{\Delta c}{T_\Theta}\left(\frac{T-T_\Theta}{T}\ln\frac{T-T_\Theta}{T_0-T_\Theta} - \ln\frac{T}{T_0}\right) \end{aligned} \tag{64}$$

This equation can be used to calculate the composition of the solution at the temperature T if the activity coefficients are known at this temperature.

5.9 Estimation of Model Parameters

The model parameters were estimated by performing a least-square minimization of the weighted sum of square residual (S) as

$$S = \sum_{P^{vap}\,data}\left(\frac{P^{vap}_{\text{calc}} - P^{vap}_{\text{exp}}}{0.0125P^{vap}_{\text{exp}}}\right)^2 + \sum_{VLE\ data}\left(\frac{P_{\text{calc}} - P_{\text{exp}}}{0.06\left(P_{\text{exp}} + 0.01\right)}\right)^2 + \sum_{SLE\ data}\left(\frac{\Delta G^0 + RT\sum_i v_i \ln a_i}{0.0015RT}\right)^2 + \sum_{H^E\ data}\left(\frac{H^E_{\text{calc}} - H^E_{\text{exp}}}{100Rx}\right)^2 + \sum_{H^{Abs}\ data}\left(\frac{H^{Abs}_{\text{calc}} - H^{Abs}_{\text{exp}}}{500Rx}\right)^2 + \sum_{LLE\ data}\sum_i\left(\frac{\ln a_i^{II} - \ln a_i^{I}}{0.5}\right)^2 \quad (65)$$

where, "calc" and "exp" represent the calculated values (by the model) and experimental data. The factors 0.0125, 0.06, 0.0015, 100, 500, and 0.5 are the weighting factors respectively used for the pure amine vapor pressure, vapor-liquid equilibrium (VLE), solid-liquid equilibrium (SLE), excess enthalpy (H^E), heat of absorption (H^{Abs}), and liquid-liquid equilibrium (LLE) data. These weighting factors were optimized on the basis of experience in modeling the H_2O-DEEA-MAPA-CO_2 and its sub-systems.

The term P^{vap} represents the pure amine vapor pressure (bar). The term *P* in the VLE data represents either the total pressure (bar) above the solutions or CO_2 partial pressure data in bar. In SLE data term, ΔG^0 is change in standard state Gibbs energy (J.mol^{-1}) between solid (ice in this case) and liquid phases, v_i is stoichiometric coefficient of component "i", a_i is activity of component "i", *R* is gas constant (8.314 J.mol^{-1}.K^{-1}) and *T* is temperature in Kelvin. x = 1 K is included to make both excess enthalpy and heat of absorption terms dimensionless. In liquid-liquid equilibrium (LLE) data term, a_i^I and a_i^{II} represent activity of component "i" in the two liquid phases I and II.

The weighting factor for vapor pressure data was chosen so that 1.25% difference between the calculated and experimental pressures would give a squared residual of 1. Similarly, the weighting factor was assigned to relatively high pressure VLE data so that 6% difference between the calculated and experimental total pressures or CO_2 partial pressures would give a squared residual of 1. It can be noticed that 0.01 bar is added to the experimental data in denominator in the VLE term in order not to give high weight to the very low pressure data. The addition of this number represents that an experimental pressure of 0.01 bar would lead to a square residual of 1 if the calculated pressure data deviate from the experimental pressures by 12%. The calculated pressures in the objective function (Equation 65) were the bubble point pressures. Only experimental total pressure data were used for the parameter estimations when both total pressure and CO_2 partial pressure data were available. The CO_2 partial pressure data were only used when total pressure data were not available.

The weighting factor for SLE data was chosen so that the solubility indexes of 1.0015 and 0.9985 would give a square residual of 1. Solubility index of a salt (ice in this work) is defined as the ratio of activity product of

a salt by its solubility product ($SI = \prod_i a_i^{\nu_i} \Big/ K_{\mathrm{sp}}$). The excess enthalpy and heat of absorption data were weighted so that an absolute difference of 831.4 J (for excess enthalpy) and 4157 J (for heat of absorption) between the calculated and experimental data would lead to a squared residual of 1 for each term. x = 1 K is included to make both excess enthalpy and heat of absorption terms dimensionless. The LLE data were weighted so that an absolute difference of 0.5 between the natural logarithm of activity of species "i" in the two liquid phases (I and II) at equilibrium would give a square residual of 1.

The parameter estimation was done by using two different routines: a modified Marquardt routine[20] and Nelder & Mead routine for function minimization.[21]

The modeling strategy consists of, firstly, the parameter estimation of the two sub-systems (H_2O-DEEA-CO_2 and H_2O-MAPA-CO_2) separately followed by the H_2O-DEEA-MAPA-CO_2 system where all the parameters were fitted to the experimental data simultaneously. The parameter estimation for the two sub-systems were started with the calculation of vapor pressures of pure amines followed by the binary CO_2 unloaded data (unloaded freezing point, excess enthalpy and unloaded VLE data) and then ternary CO_2 loaded data (loaded freezing point and VLE data and the heat of absorption data). Once a reasonable set of parameters were obtained for each of the H_2O-DEEA-CO_2 and H_2O-MAPA-CO_2 sub-systems, binary parameters across different species of DEEA and MAPA in the two sub-systems were estimated by using the ternary unloaded data (unloaded freezing point and VLE data). Then quaternary CO_2 loaded data (VLE and heat of absorption data) were introduced and all the pre-estimated parameters were refitted to the experimental data simultaneously to get a new set of parameters. Finally, the LLE data were introduced and a final set of parameters were estimated which can reproduce all data values and describe all data types (pure amine vapor pressure, excess enthalpy, VLE, SLE, LLE and heat of absorption of CO_2) with a single set of parameters.

The deviations between the model results and the experimental data are given in Equation 66 as absolute average relative deviation (AARD)

$$AARD = \frac{1}{n}\sum_{n}\left|\frac{\Phi_{\mathrm{calc}} - \Phi_{\mathrm{exp}}}{\Phi_{\mathrm{exp}}}\right| \times 100\% \tag{66}$$

where, Φ is the type of data and n is the number of data points. "calc" and "exp" represent the calculated data values (by the model) and experimental data respectively.

94 model parameters and 6 thermodynamic properties were fitted to approximately 1500 experimental data consisting of pure amine vapor pressure, vapor-liquid equilibrium, solid-liquid equilibrium, liquid-liquid equilibrium, excess enthalpy, and heat of absorption of CO_2. Out of 94 model parameters, volume (r) and surface area (q) parameters have 6 parameters each, the binary parameters u_{ij}^0 and u_{ij}^T have 41 parameters each for calculating the interaction energy parameters $u_{ij} = u_{ij}^0 + u_{ij}^T\left(T - 298.15\right)$, and 6 thermodynamic properties are the standard state Gibb's energy of formation and standard state enthalpy of formation for the three species $DEEA(l)$, $MAPA(l)$, and $MAPACOO^-$.

The Extended UNIQUAC model parameters of the aqueous phase H^+ and OH^- were taken from Thomsen et al.[7] and $CO_2(aq)$, CO_3^{2-}, and HCO_3^- from Thomsen and Rasmussen.[1] The r and q parameters, and the binary parameters u_{ij}^0 and u_{ij}^T for calculating the interaction energy parameters $u_{ij} = u_{ij}^0 + u_{ij}^T(T - 298.15)$ for the six species $DEEA(aq)$, $DEEAH^+$, $MAPA(aq)$, $MAPAH^+$, $^+HMAPAH^+$, and $MAPACOO^-$ were determined in this work by fitting to the experimental data.

The estimated r and q parameters are given in Table 5.2. The estimated binary parameters u_{ij}^0 and u_{ij}^T for each pair of species are given respectively in Table 5.3 and Table 5.4. Some of the u_{ij}^0 parameters were given a very high value of 10^{10} with corresponding values of 0 for the u_{ij}^T parameters. These values indicate that those pairs of species are most likely to have no interaction.

Table 5.2: UNIQUAC volume (r) and surface area (q) parameters fitted to the experimental data. Bold values are determined in this work.

	r	q
H_2O	0.92 [a]	1.4 [a]
$CO_2(aq)$	5.741 [c]	6.0806 [c]
$MAPA(aq)$	**11.96**	**8.845**
$DEEA(aq)$	**3.225**	**3.641**
H^+	0.13779 [b]	10^{-15} [b]
$MAPAH^+$	**4.499**	**9.664**
$^+HMAPAH^+$	**1.391**	**1.749**
$DEEAH^+$	**4.583**	**2.918**
OH^-	9.3973 [b]	8.8171 [b]
CO_3^{2-}	10.828 [c]	10.769 [c]
HCO_3^-	8.0756 [c]	8.6806 [c]
$MAPACOO^-$	**9.922**	**6.499**

[a] Abrams and Prausnitz[13]

[b] Thomsen et al.[7]

[c] Thomsen and Rasmussen[1]

Table 5.3: $u_{ij}^0 = u_{ji}^0$ **parameters for calculating UNIQUAC interaction energy parameters (**$u_{ij} = u_{ij}^0 + u_{ij}^T (T - 298.15)$**). Bold values are determined in this work.**

	H_2O	DEEA	MAPA	CO_2	H^+	$DEEAH^+$	$MAPAH^+$	$^+HMAPAH^+$	CO_3^{2-}	HCO_3^-	OH^-	$MAPACOO^-$
H_2O	0 [a]											
DEEA	**-4.3632**	**0**										
MAPA	**-125.7**	**106.25**	**0**									
CO_2	41.0717 [a]	**-311.22**	**287.39**	40.5176 [a]								
H^+	10^5 [a]	**10^{10}**	**10^{10}**	10^{10} [a]	0 [a]							
$DEEAH^+$	**-150.15**	**473.38**	**460.86**	**-178.08**	**10^{10}**	**0**						
$MAPAH^+$	**-455.55**	**-216.11**	**-13.017**	**113.99**	**10^{10}**	**-751.1**	**0**					
$^+HMAPAH^+$	**1256.2**	**2566.3**	**-64.801**	**552.76**	**10^{10}**	**7.0431**	**-292.5**	**0**				
CO_3^{2-}	361.388 [a]	**1581.9**	**612.11**	10^{10} [a]	10^{10} [a]	**1042.2**	**458.46**	**135.84**	1458.344 [a]			
HCO_3^-	577.050 [a]	**665.78**	**819.93**	651.045 [a]	10^{10} [a]	**799.14**	**419.3**	**1888.7**	800.008 [a]	771.04 [a]		
OH^-	600.495 [a]	**579.77**	**931.69**	10^{10} [a]	10^{10} [a]	**10^{10}**	**10^{10}**	**10^{10}**	1588.025 [a]	10^{10} [a]	1562.88 [a]	
$MAPACOO^-$	**-456.94**	**-250.18**	**379.78**	**10^{10}**	**10^{10}**	**-227.59**	**-646.89**	**2.9472**	**1121.9**	**342.24**	**592.19**	**1000**

[a] Thomsen and Rasmussen[1]

Table 5.4: $u_{ij}^T = u_{ji}^T$ **parameters for calculating UNIQUAC interaction energy parameters (**$u_{ij} = u_{ij}^0 + u_{ij}^T \left(T - 298.15\right)$**). Bold values are determined in this work.**

	H_2O	DEEA	MAPA	CO_2	H^+	$DEEAH^+$	$MAPAH^+$	$^+HMAPAH^+$	CO_3^{2-}	HCO_3^-	OH^-	$MAPACOO^-$
H_2O	0 [a]											
DEEA	**1**	**0**										
MAPA	**0.533**	**0.9511**	**0**									
CO_2	7.5184 [a]	**8.288**	**1.822**	13.629 [a]								
H^+	0 [a]	**0**	**0**	0 [a]	0 [a]							
$DEEAH^+$	**0.1918**	**1.816**	**-1.132**	**3.745**	**0**	**0**						
$MAPAH^+$	**-0.4654**	**-2.605**	**-8.025**	**7.793**	**0**	**-3.978**	**0**					
$^+HMAPAH^+$	**7.318**	**-9.42**	**3.532**	**6.816**	**0**	**-1.494**	**9.693**	**0**				
CO_3^{2-}	3.3516 [a]	**1.02**	**3.382**	**0**	0 [a]	**-3.486**	**1.476**	**4.128**	-1.3448 [a]			
HCO_3^-	-0.38795 [a]	**-0.3963**	**0.5863**	2.773 [a]	0 [a]	**2.277**	**-0.1296**	**1.33**	1.7241 [a]	-0.0198 [a]		
OH^-	8.5455 [a]	**9.2**	**-0.2957**	0 [a]	0 [a]	**0**	**0**	**0**	*2.7496* [b]	0 [a]	5.6169 [a]	
$MAPACOO^-$	**0.01686**	**2.825**	**-2.191**	**0**	**0**	**-3.352**	**-5.564**	**2.22**	**0.4127**	**3.809**	**7.164**	**0**

[a] Thomsen and Rasmussen[1]

[b] The value is corrected from the previous value (2.5176, an editing mistake) as reported in Thomsen and Rasmussen[1]

The values of standard state Gibbs energy and enthalpy of formation are given in Table 5.5. These values were taken from the NIST tables[22] for most of the components. For $DEEA(g)$ and $MAPA(g)$, these values were estimated from Marrero and Gani method by using ProPred (property prediction) tool in ICAS (Integrated Computer Aided System) software (Marrero and Gani[23]and CAPEC software[24]).

Table 5.5: Standard state thermodynamic properties estimated from experimental data in this work. Bold values are determined in this work.

	ΔG_f^0 / (kJ.mol^{-1})	ΔH_f^0 / (kJ.mol^{-1})
$H_2O(l)$	-237.129 [a]	-285.83 [a]
$H_2O(g)$	-228.572 [a]	-241.818 [a]
$H_2O(s)$	-236.5376 [a]	-292.6244 [a]
$CO_2(aq)$	-385.98 [a]	-413.8 [a]
$CO_2(g)$	-394.359 [a]	-393.509 [a]
H^+	0 [a]	0 [a]
OH^-	-157.2481 [a]	-230.2433 [a]
CO_3^{2-}	-527.81 [a]	-677.14 [a]
HCO_3^-	-586.77 [a]	-691.99 [a]
$DEEA(g)$	-29.36 [b]	-257.49 [b]
$MAPA(g)$	142.73 [b]	-37 [b]
$DEEA(l)$	**-44.903**	**-315.11**
$MAPA(l)$	**129.9**	**-88.227**
$DEEA(aq)$	**-55.999**	**-333.560**
$MAPA(aq)$	**112.659**	**-141.062**
$DEEAH^+$	**-111.2663**	**-370.92**
$MAPAH^+$	**52.299**	**-176.392**
$^+HMAPAH^+$	**3.139**	**-220.142**
$MAPACOO^-$	**-255.71**	**-577.52**

[a] NIST table[22]

[b] Determined from Marrero and Gani method by using ProPred (property prediction) tool in ICAS (Integrated Computer Aided System) software (Marrero and Gani[23] and CAPEC software[24])

The standard state Gibbs energy of formation for $DEEA(l)$ and $MAPA(l)$ were calculated from their corresponding values in the pure gas phase ($DEEA(g)$ and $MAPA(g)$) by using Equation 43. For $DEEA(aq)$ and $MAPA(aq)$, the standard state Gibbs energy of formation were estimated from their corresponding values in the pure liquid phase ($DEEA(l)$ and $MAPA(l)$) plus a contribution of activity coefficient at infinite dilution. Little et al.[25] and Hamborg and Versteeg[26] reported the dissociation constant ($\ln K_a$) of protonated DEEA as a function of temperature. These dissociation constant data were correlated to estimate the Gibbs energy of the dissociation reaction of protonated DEEA (Equation 28 in reverse order). The standard state Gibbs energy of formation of $DEEAH^+$ was then calculated from

$\Delta_r G^0 = \Delta_f G^0_{DEEA(aq)} - \Delta_f G^0_{DEEAH^+}$. Aronu et al.[46] reported the first and second dissociation constants for the mono and di protonated MAPA at different temperatures. These experimental data were correlated to calculate the Gibbs energy of reaction for the dissociation of protonated MAPA (Equation 29 in reverse order) and dissociation of di protonated MAPA (Equation 30 in reverse order). Similarly, the standard state Gibbs energy of formation of $MAPAH^+$ and $^+HMAPAH^+$ were estimated respectively from $\Delta_r G^0 = \Delta_f G^0_{MAPA(aq)} - \Delta_f G^0_{MAPAH^+}$ and $\Delta_r G^0 = \Delta_f G^0_{MAPAH^+} - \Delta_f G^0_{^+HMAPAH^+}$. No information was found in the literature about the thermodynamic properties or equilibrium constant of the MAPA carbamate reaction. A guess values for the standard state Gibbs energy and enthalpy of formation were used for the MAPA carbamate ($MAPACOO^-$) which then altered during the parameter estimation and fitted to all the experimental data in this work.

The a, b, and c parameters for the standard state three-parameters heat capacity correlation (Thomsen et al.[7]) presented in Equation 62 are given in Table 5.6.

Table 5.6: Parameters for the standard state heat capacity (Equation 62), fitted to the experimental data in this work. Bold values are determined in this work.

	a / (J.mol^{-1}.K^{-1})	b / (J.mol^{-1}.K^{-2})	c / (J.mol^{-1})
$H_2O(l)$	58.3695 [a]	0.03896 [a]	523.88 [a]
$H_2O(g)$	33.577 [b]	0	0
$H_2O(s)$	47.8996 [c]	0	0
$CO_2(aq)$	243 [d]	0 [d]	0 [d]
$CO_2(g)$	37.11 [b]	0	0
H^+	0 [a]	0 [a]	0 [a]
OH^-	1418.2 [a]	-3.446 [a]	-51473.13 [a]
CO_3^{2-}	894.688 [d]	-2.8272 [d]	-21149.44 [d]
HCO_3^-	-0.6771 [d]	0.27375 [d]	-10089.51 [d]
$DEEA(g)$	173 [e]	0	0
$MAPA(g)$	136 [e]	0	0
$DEEA(l)$	104.952 [f]	0.5936 [f]	0
$MAPA(l)$	147.111 [e]	0.2546 [e]	0
$DEEA(aq)$	**210.9899**	**0.35675**	**0**
$MAPA(aq)$	**485.4593**	**-0.49787**	**0**
$DEEAH^+$	**-32.1278**	**0**	**0**
$MAPAH^+$	**178.5593**	**0**	**0**
$^+HMAPAH^+$	**-114.9407**	**0**	**0**
$MAPACOO^-$	**358.2**	**-0.1178**	**-10613.4**

[a] Thomsen et al.[7] [b] Wagman et al.[27]
[c] Fosbøl et al.[28] [d] Thomsen and Rasmussen[1]

[e] Determined from Joback and Reid method by using ProPred (property prediction) tool in ICAS (Integrated Computer Aided System) software (Joback and Reid[29] and CAPEC software[24])

[f] Correlated from the experimental data reported by Maham et al.[30] and Rayer et al.[31]

The three parameters of the standard state heat capacity for the species $DEEA(g)$, $MAPA(g)$, and $MAPA(l)$ were estimated from Joback and Reid method by using ICAS software (CAPEC software[24] and Joback and Reid[29]). Maham et al.[30] and Rayer et al.[31] reported the molar heat capacity data of DEEA at different temperatures. These data were correlated to estimate the standard state heat capacity parameters for $DEEA(l)$. The standard state heat capacity parameters for $MAPACOO^-$ were estimated based on the assumption that the change in heat capacity of the MAPA carbamate reaction (Equation 31) is constant (and equal to zero i.e. $\Delta C_P = 0$). This is based on the "Principle of Balance of Identical Like Charges" as suggested by Murray and Cobble.[32] According to this principle, the ΔC_P is almost constant if there is a balance of ionic charge of similar species on both sides of the equilibrium reaction. This principle was applied to the equilibrium reaction in Equation 31 to estimate the parameters of the standard state heat capacity for the MAPA carbamate. The standard state heat capacity parameters of the remaining species were estimated by the model. The standard state heat capacity for $DEEAH^+$, $MAPAH^+$, and $^+HMAPAH^+$ were considered temperature independent.

5.10 Results and Discussion

To model the liquid-liquid DEEA-MAPA system, the model parameters were estimated first for the two sub-systems H_2O-DEEA-CO_2 and H_2O-MAPA-CO_2 followed by the H_2O-DEEA-MAPA-CO_2 system which give liquid-liquid split. The results of the two ternary sub-systems and the quaternary liquid-liquid systems are given in the following sections. As described earlier, the parameter estimation was done by starting with the simple system e.g. pure amine vapor pressure followed by the addition of binary and ternary data and finally the quaternary data. The data were systematically added and the relevant parameters were estimated. However, the results are presented here according to the data type for each system separately.

5.10.1 H_2O-DEEA-CO_2 System

The results of pure DEEA vapor pressure at different temperatures are given in Figure 5.1. Experimental data of vapor pressure of pure DEEA reported by several authors in the literature[5,33-35] are plotted along with the calculated curve. The model describes the vapor pressure data very well. However, some deviations at high temperatures can be observed. The absolute average relative deviations (AARD) between the model results and experimental data are 6.5 % for Steele et al.[33], 20.3 % for Kapteina et al.[34], and 5 % each for Klepáčová et al.[35] and Hartono et al.[5] The AARD for all the vapor pressure data together from all the literature sources is 9.9 %.

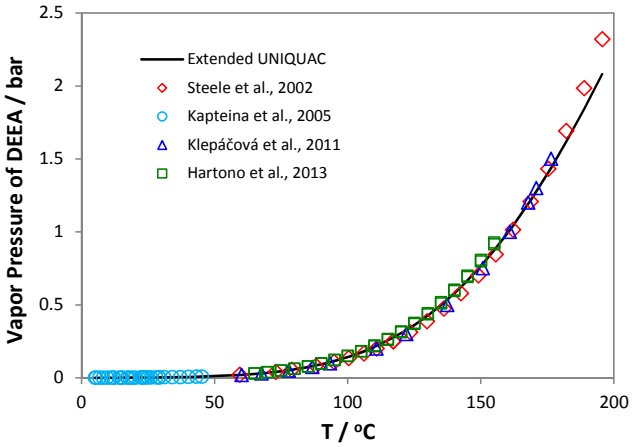

Figure 5.1: Vapor pressure of pure DEEA as a function of temperature.

Freezing point depression data have been reported by Arshad et al.[36] for both the unloaded and CO_2 loaded aqueous DEEA solutions and these data were included in the parameter estimation in this work. Such data are very important to compute the water activity, a key parameter to estimate the amount of water evaporation in stripping section during the solvent regeneration in the capture process. Freezing point depression data at different molal concentrations of aqueous DEEA solutions (H_2O-DEEA) are plotted with the calculated curve as shown in Figure 5.2. For H_2O-DEEA-CO_2 system (CO_2 loaded system), the freezing points are presented in Figure 5.3 for four different DEEA solutions (12, 20, 30, and 33 mass %) at a varying CO_2 concentration in the solutions. The model describes the freezing point data very well both in the unloaded (Figure 5.2) and the CO_2 loaded (Figure 5.3) DEEA solutions. However, there are some deviations in the CO_2 loaded solutions at high DEEA concentrations of 30 and 33 mass %. These two curves showed a decrease in the freezing points by increasing the CO_2 concentrations up to a certain point and then the freezing points became almost constant. The model calculated the trend lines very nicely with slightly higher calculated freezing points throughout the curves and the slightly lower calculated freezing points in the last couple of points in both the curves. The AARD between the calculated and the experimental freezing points are 4.2 % and 3.5 % respectively for the unloaded and the CO_2 loaded DEEA solutions.

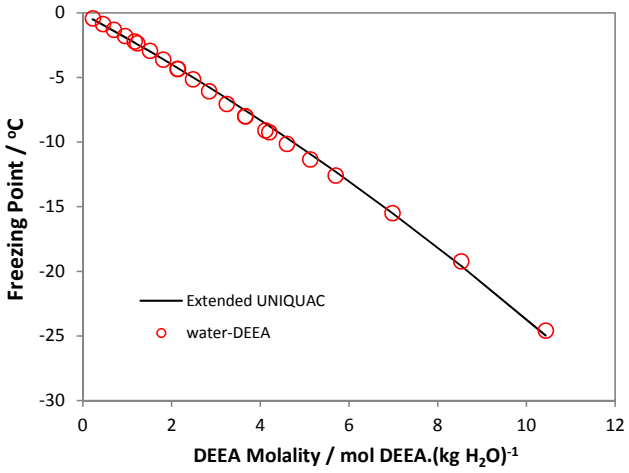

Figure 5.2: Freezing point depression of aqueous DEEA system. Experimental data from Arshad et al.[36]

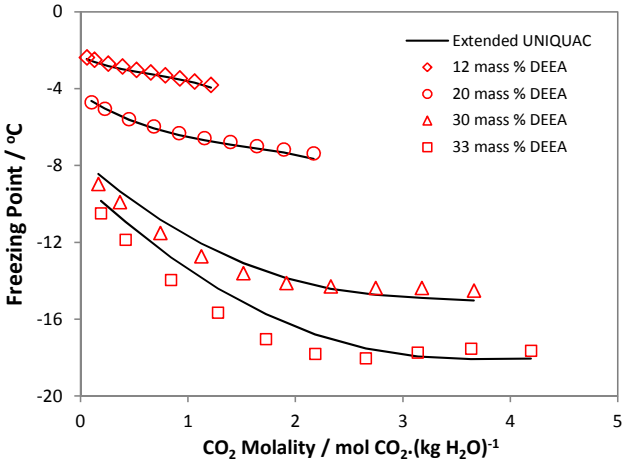

Figure 5.3: Freezing point depression of H_2O-DEEA-CO_2 systems at different compositions of DEEA and CO_2. Experimental data from Arshad et al.[36]

Vapor-liquid equilibrium data (both unloaded and CO_2 loaded aqueous amine solutions) are essential for the design and modeling of the unit operations in the capture process. The total pressure data are available from Hartono et al.[5] for the H_2O-DEEA system at different temperatures. The model results are given in Figure 5.4 together with the experimental data. The total pressure data are presented as a function of DEEA concentration in the liquid phase at different temperatures. The model represents the two isotherms at 323.15 K and 333.15 K quite well at lower DEEA concentrations but start deviating at higher concentrations

(the calculated total pressures are lower than the experimental data). These deviations are much larger in the isotherms at higher temperatures i.e., 353.15 K and 368.15 K. The AARD between the model results and the experimental data is 11 %. This is the only set of VLE data that have not been represented well by the model. On the other hand, the accuracy of this set of experimental data cannot be verified by comparing with other sources due to lack of such data for DEEA system in the literature.

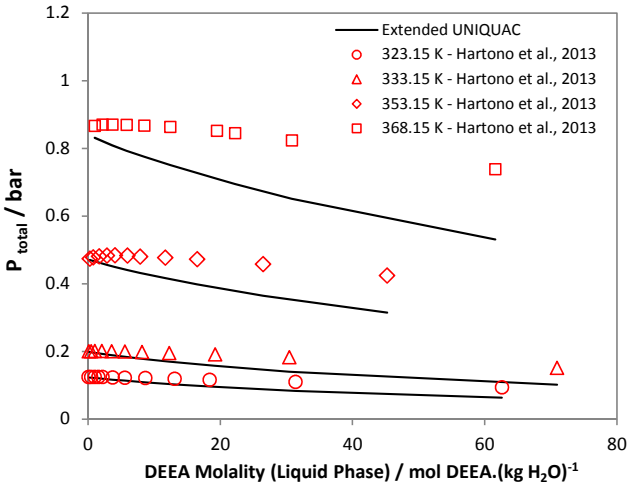

Figure 5.4: Total pressure of H_2O-DEEA system at different temperatures.

Vapor-liquid equilibrium data for the CO_2 loaded aqueous DEEA solutions (both total pressure and CO_2 partial pressure) were reported by Monteiro et al.[6] and Arshad et al.[37] The experimental total pressure data from both the literature sources along with the calculated curves for the 5M DEEA solutions are exhibited in Figure 5.5 as a function of CO_2 concentration at different temperatures. There is a good agreement between the experimental data and the model results. However, the model calculated total pressures are slightly higher for the 313.15 K isotherm and slightly lower for the two isotherms at 353.15 K and 393.15 K at high CO_2 concentrations. The estimated AARD between the model results and the experimental data are 7.6 % for Monteiro et al.[6] and 10.4 % for Arshad et al.[37] Similarly, Figure 5.6 presents the model results of the CO_2 partial pressure together with the experimental data in the 5M DEEA solutions as a function of the CO_2 concentration. It can be seen that the model represents the experimental CO_2 partial pressures well with the estimated AARD of 19.1 % for Monteiro et al.[6] and 22.4 % for Arshad et al.[37]

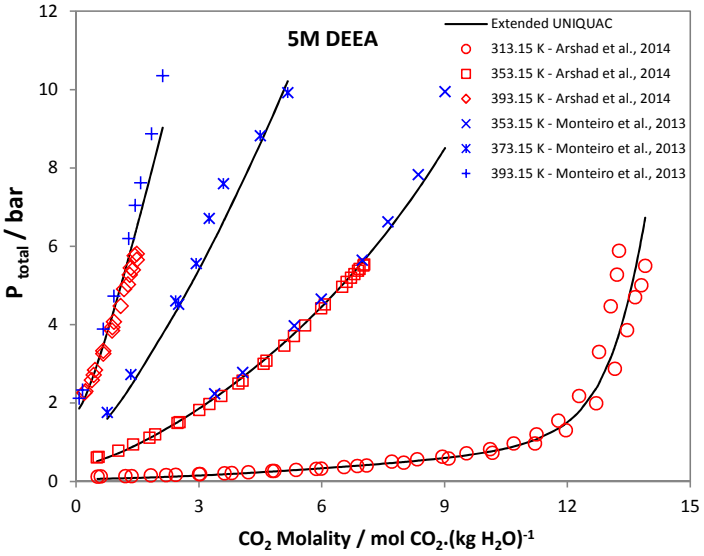

Figure 5.5: Equilibrium total pressure in 5M DEEA solutions as a function of CO_2 composition at different temperatures.

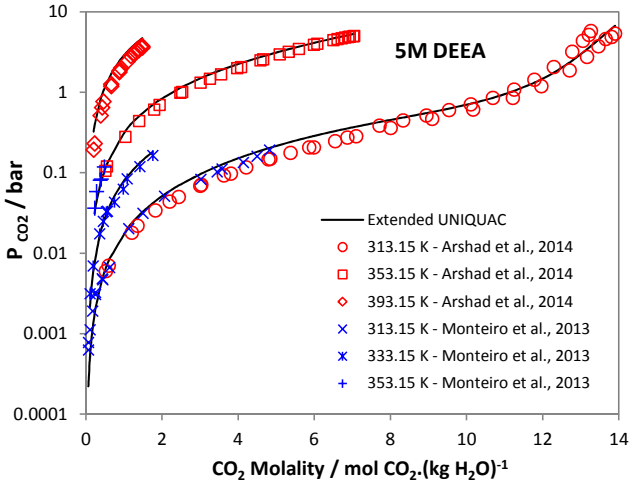

Figure 5.6: Partial pressure of CO_2 in 5M DEEA solutions at different temperatures.

The model results and the experimental data from Monteiro et al.[6] for the 2M DEEA solutions are given in Figure 5.7 for the total pressure and Figure 5.8 for the partial pressure (solubility) of CO_2 at three different temperatures. A good agreement between the experimental data and the calculated curves can be seen with some deviations in the total pressures at high CO_2 concentrations for the two isotherms at 353.15 K

and 373.15 K (Figure 5.7). The estimated AARD are 10.1 % and 14.1 % respectively for the total pressure and CO_2 partial pressure data.

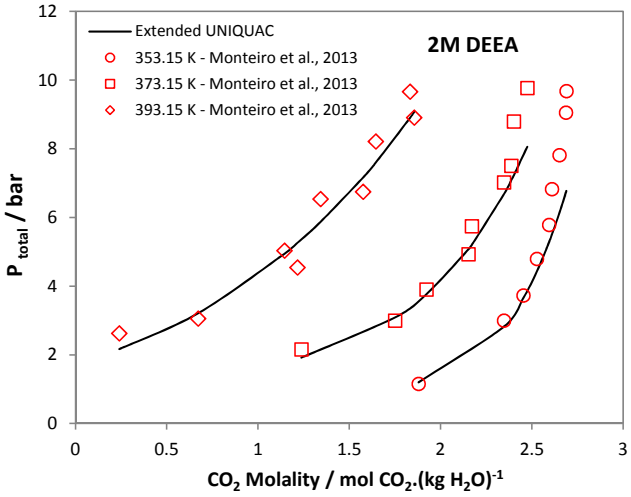

Figure 5.7: Equilibrium total pressure in 2M DEEA solutions as a function of CO_2 composition at different temperatures.

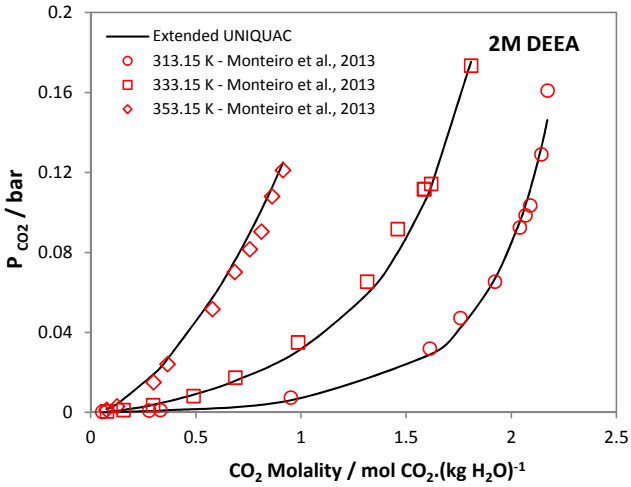

Figure 5.8: Partial pressure of CO_2 in 2M DEEA solutions at different temperatures.

Monteiro et al.[6] presented the experimental VLE measurements and the thermodynamic modeling of the H_2O-DEEA-CO_2 system using e-NRTL model. They reported that the large scatter in the experimental data at low CO_2 loadings have contributed greatly in the estimated deviations (AARD). This scatter in the data is inherited in the analytical method used for determining the CO_2 contents. This method gave high errors in the determined CO_2 amount when CO_2 contents are low in the solutions. By excluding the data below CO_2 loading of 0.02 mol CO_2.(mol amine)$^{-1}$ out of regression, they reported a lower numbers of AARD of 8.1 % for the total pressure (compared to the 10.2 % with all data included) and 15.5 % for CO_2 partial pressure (compared to the 18.6 % with all data included). However, the deviations reported in our work are obtained by including all the data in the parameter estimation. It can be seen that the deviations in this work are slightly higher than those reported by Monteiro et al.[6] But it should also be noted that the additional experimental VLE, heat of absorption and freezing point data were used in this work and more importantly the model describes and reproduces all the data sets and data types for H_2O-DEEA-CO_2 system together with H_2O-MAPA-CO_2 and H_2O-DEEA-MAPA-CO_2 systems with a single set of parameters.

Molar excess enthalpy and heat of absorption of CO_2 in the aqueous DEEA solutions were the thermal property data available for the thermodynamic modeling. Figure 5.9 presents the model results for the molar excess enthalpy in DEEA solutions together with the experimental data from Mathonat at al.[38] The model very well describes the excess enthalpy in the DEEA solutions with an AARD of 7.2 % between the experimental data and the calculated curve.

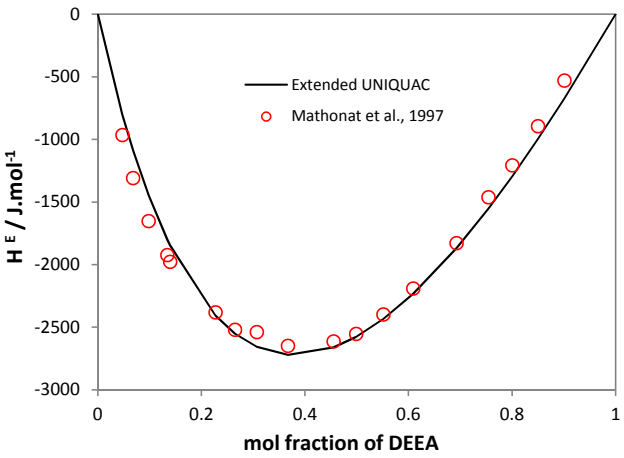

Figure 5.9: Excess enthalpy of DEEA as a function of mole fraction of DEEA.

Arshad et al.[39] reported the differential heat of absorption of CO_2 in 5M DEEA solutions in the temperature range of 40-120 ^{o}C and these data were included in the parameter estimation. The modeling results are shown in Figure 5.10. The model calculated the differential heats of absorption of CO_2 in 5M DEEA solutions reasonably well. However, the model calculated values are lower than the experimental data for the 80 and

120 °C isotherms especially at low CO_2 concentrations. The estimated deviation (AARD) is 14.9 % with major contribution from the data at 120 °C.

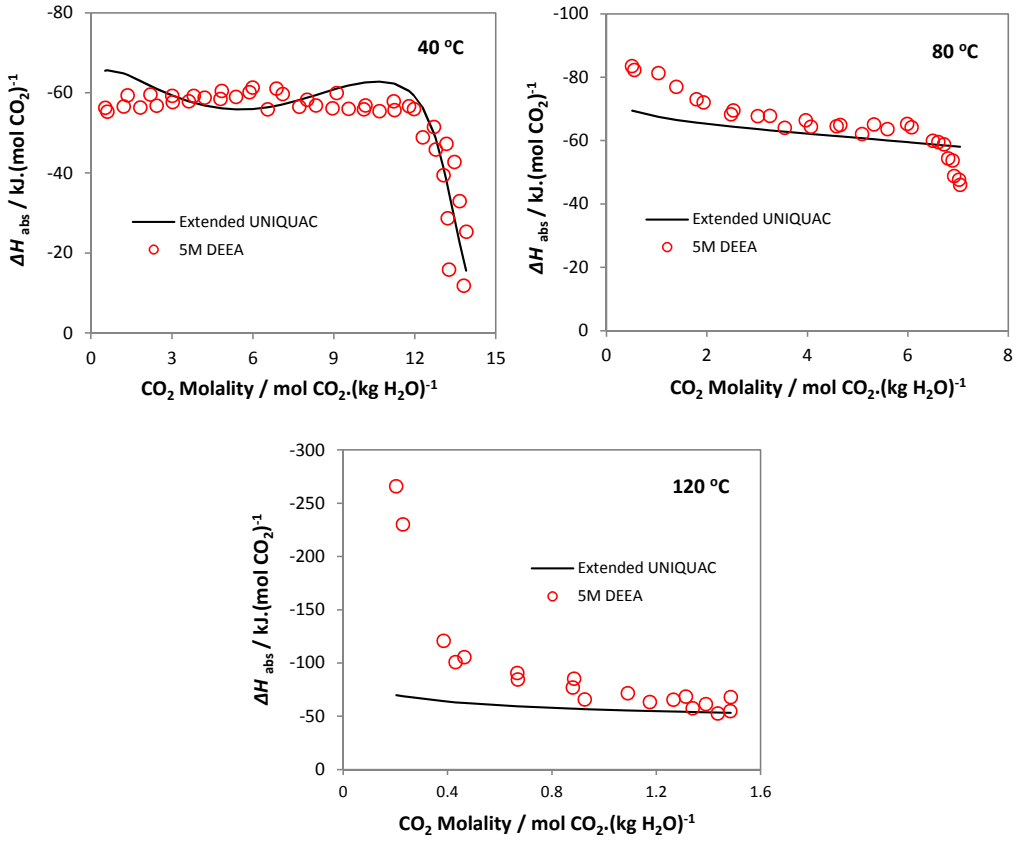

Figure 5.10: Differential heat of absorption of CO_2 in 5M DEEA solutions at 40, 80, and 120 °C. Experimental data from Arshad et al.[39]

The modeling results for the differential heat of absorption of CO_2 in 37 and 32 mass % DEEA solutions are presented in Figure 5.11. The experimental data were available from Kim, 2009.[40] It should be noted that these data were not included in the parameter estimation. A fairly good agreement between the experimental data and the model results can be seen in the isotherms at 40 and 80 °C for both the DEEA concentrations (37 and 32 mass %). However, the model results are too low for the data at 120 °C. The first experimental data point seems outlier in the 40 °C isotherm for the 37 mass % DEEA solutions. At low CO_2 concentrations, a large scatter can also be observed in the experimental data at 80 °C for both the DEEA concentrations. The estimated AARD are 20 % and 24.5 % respectively for the 37 mass % and 32 mass % DEEA solutions.

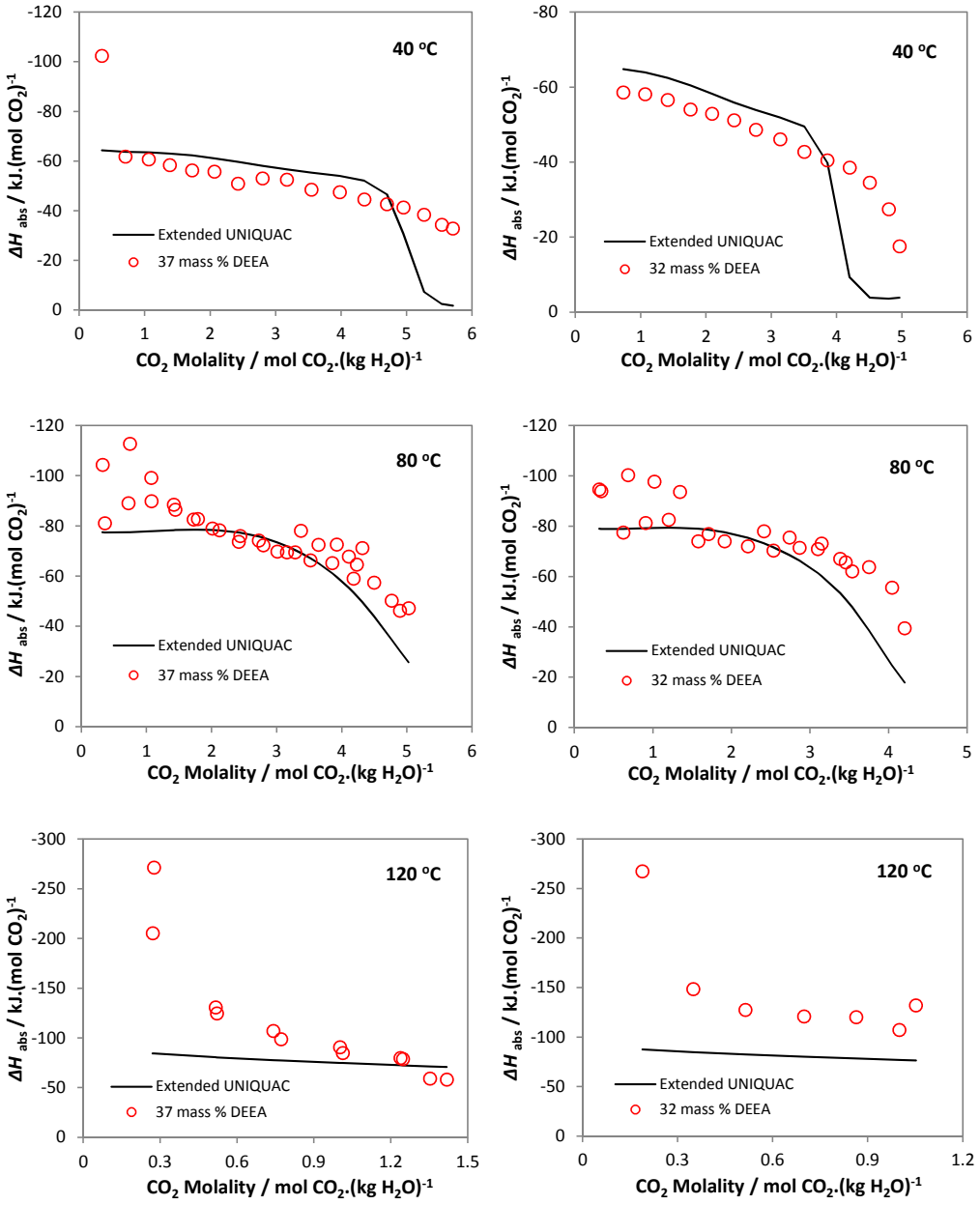

Figure 5.11: Differential heat of absorption of CO_2 in 37 mass % (left side images) and 32 mass % (right side images) DEEA solutions at 40, 80, and 120 °C. Experimental data from Kim, 2009[40] were not used in the parameter estimation.

5.10.2 H_2O-MAPA-CO_2 System

The experimental vapor pressures of pure MAPA as a function of temperature have been available from the literature[5,41,42] and included in the parameter estimation. The model results are plotted with the experimental vapor pressure data as shown in Figure 5.12. It can be seen that the calculated data are in very good agreement with the experimental data. The deviations (AARD) between the experimental data and the model results are 5.4 % for all the data together and individually 2.1 % for Kim et al.[41], 15.2 % for Verevkin and Chernyak [42], and 0.9 % for Hartono et al.[5]

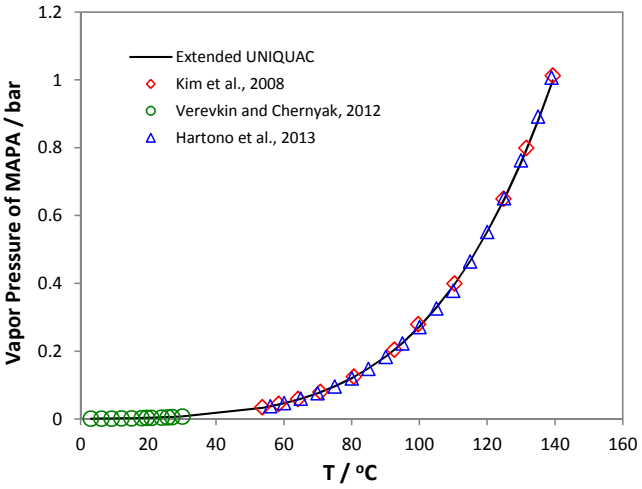

Figure 5.12: Vapor pressure of pure MAPA as a function of temperature.

Freezing point depression results for the unloaded and CO_2 loaded MAPA solutions are given in Figure 5.13 and Figure 5.14, respectively. The experimental freezing point data were available for the parameter estimation from Arshad et al.[36] Figure 5.13 exhibits the experimental and calculated freezing points for the aqueous MAPA solutions with different concentrations. A very good agreement can be observed between the experimental data and the model results with AARD of 3.4 %. For the CO_2 loaded aqueous MAPA solutions (H_2O-MAPA-CO_2), Figure 5.14 presents the calculated and experimental freezing points in different aqueous MAPA solutions (10, 20, and 27 mass %) at varying CO_2 concentrations. The model describes the wave like curves very well for all the three CO_2 loaded MAPA systems in the whole CO_2 concentration range with an AARD of just 3.1 %.

The total pressure data for the H_2O-MAPA system at different temperatures were included in the parameter estimation. The model results are presented in Figure 5.15 along with the experimental data available from Kim et al.[41] and Monteiro et al.[43] The total pressure data are presented as a function of MAPA concentration in the liquid phase at different temperatures. It can be seen that the model represents the three isotherms at 313.15 K, 333.15 K and 353.15 K very well. However, some deviations can be

observed in the isotherm at 373.15 K at high MAPA concentrations. It can also be noted that the experimental total pressures for the 373.15 K isotherm are only available from Kim et al.[41] and their accuracy cannot be cross checked with other sources due to lack of data for the H_2O-MAPA system. The estimated deviations (AARD) between the model results and the experimental data are 4.4 % and 3.7 % respectively for Kim et al.[41] and Monteiro et al.[43]

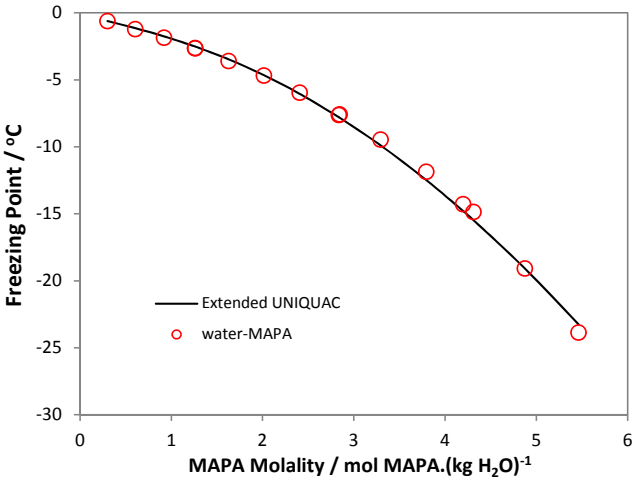

Figure 5.13: Freezing point depression in aqueous MAPA system. Experimental data from Arshad et al.[36]

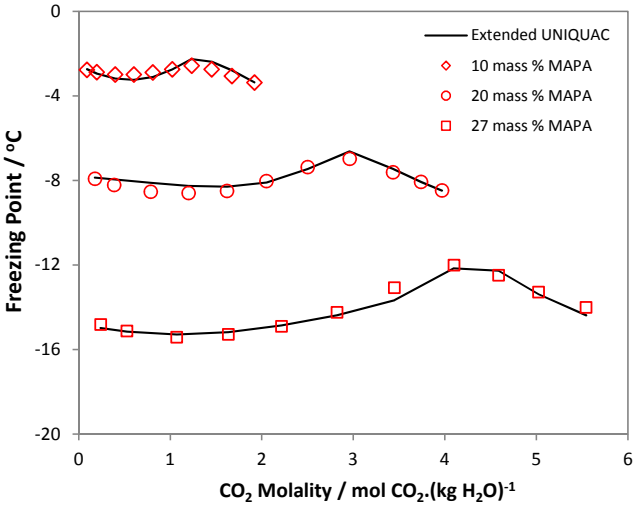

Figure 5.14: Freezing point depression of H_2O-MAPA-CO_2 systems at different compositions of MAPA and CO_2. Experimental data from Arshad et al.[36]

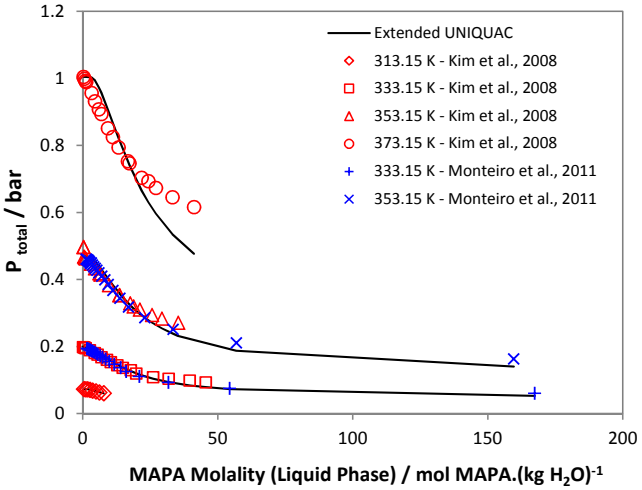

Figure 5.15: Total pressure of H_2O-MAPA system at different temperatures. Experimental data from Kim et al.[41] and Monteiro et al.[43]

The experimental equilibrium total pressure in 2M MAPA solutions at different temperatures from Arshad et al.[37] and the model calculated values are plotted in Figure 5.16. A fairly good agreement between the experimental and the calculated values can be seen at 313.15 K. The model also calculated the total pressures fairly good for 353.15 K isotherm at low pressures but deviate at pressures above 3 bar. Similar kind of deviations can also be observed at high pressures for the isotherm at 393.15 K. The ARRD between the experimental and the model calculated total pressures is 16.1 %.

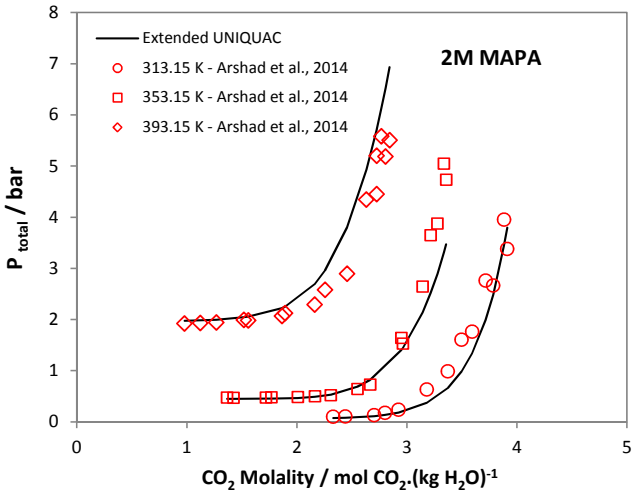

Figure 5.16: Equilibrium total pressure in 2M MAPA solutions as a function of CO_2 composition at different temperatures.

The Extended UNIQUAC model calculated solubility (partial pressure) of CO_2 in 2M MAPA solutions and the experimental data from Arshad et al.[37] and Pinto et al.[44] are compared in Figure 5.17 at the temperature ranging between 313.15 K and 393.15 K (40-120 ^{o}C). The model results are quite fair in the whole CO_2 concentration range for the 313.15 K and 353.15 K isotherms data from Arshad et al.[37] However, the model calculated results of CO_2 partial pressures are too high compared with the experimental data for the 393.15 K isotherm in the whole CO_2 concentration range which contributed the major part to the estimated deviation (AARD) of 55.1 % for Arshad et al.[37] Similarly, the model calculated values of CO_2 solubility have good agreement with the Pinto et al.[44] experimental data at 333.15 K. However, the model results show deviations for the two isotherms at 313.15 K and 353.15 K both at low and high CO_2 partial pressures. Some scatter in the experimental data can also be observed in both the isotherms at 313.15 K and 353.15 K. The estimated AARD value for the data set is 37.2 %.

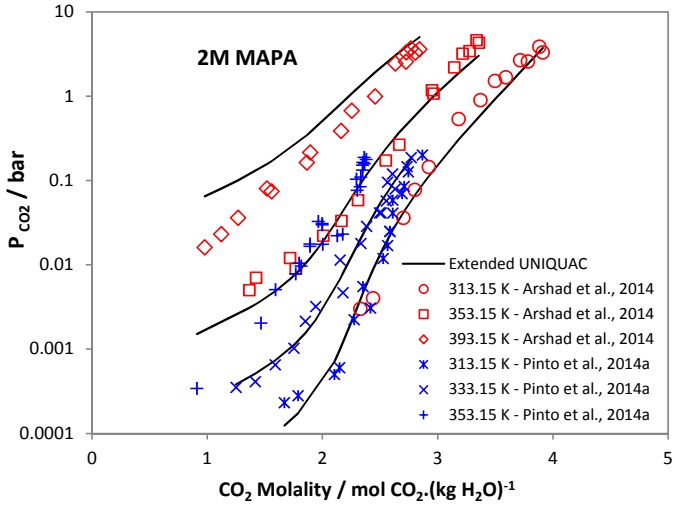

Figure 5.17: Partial pressure of CO_2 in 2M MAPA solutions at different temperatures.

The experimental total pressure and CO_2 partial pressure data as a function of CO_2 concentration for 1M MAPA solutions from Arshad et al.[37] are compared with the modeling results in Figure 5.18 and Figure 5.19, respectively. In Figure 5.18, the model describes the total pressures in 1M MAPA solutions fairly well with a few high calculated total pressure data points for the 313.15 K and 393.15 K isotherms and a few low calculated total pressure data points for the 353.15 K isotherm at high CO_2 concentrations. Similarly, Figure 5.19 exhibits a reasonably fair agreement between the experimental and model results with some deviations in all the three isotherms. The estimated deviations (AARD) are 15.2 % and 39 % respectively for the total pressure and CO_2 partial pressure data.

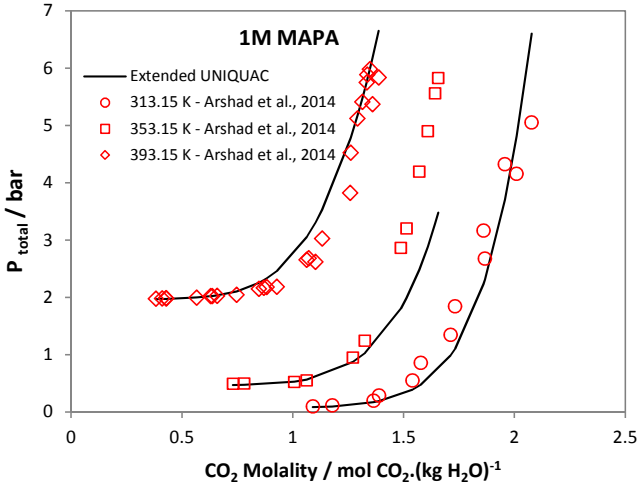

Figure 5.18: Equilibrium total pressure in 1M MAPA solutions as a function of CO_2 composition at different temperatures.

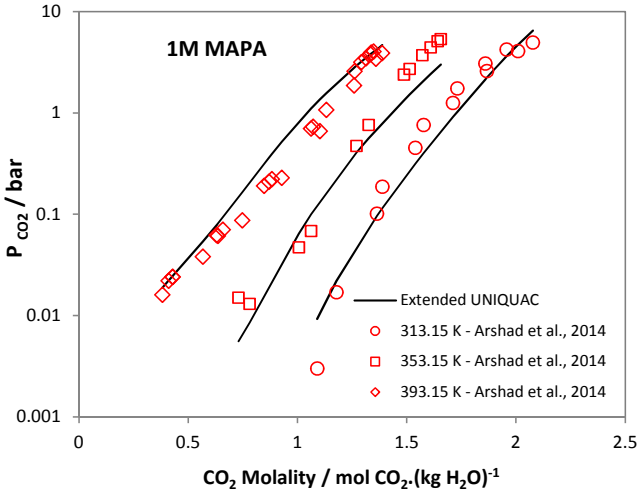

Figure 5.19: Partial pressure of CO_2 in 1M MAPA solutions at different temperatures.

The experimental total pressure in 5M MAPA solutions from Pinto et al.[44] are plotted with the modeling results in Figure 5.20. The modeling results look reasonable for the data at 353.15 K and 393.15 K with some deviations and deviate from the data at 373.15 K in the whole CO_2 concentration range. It can be observed that the experimental data points of the isotherms at different temperatures and crossing over each other reflecting inaccuracy in the experimental data. The estimated AARD between the model results and the experimental data is 35.2 %.

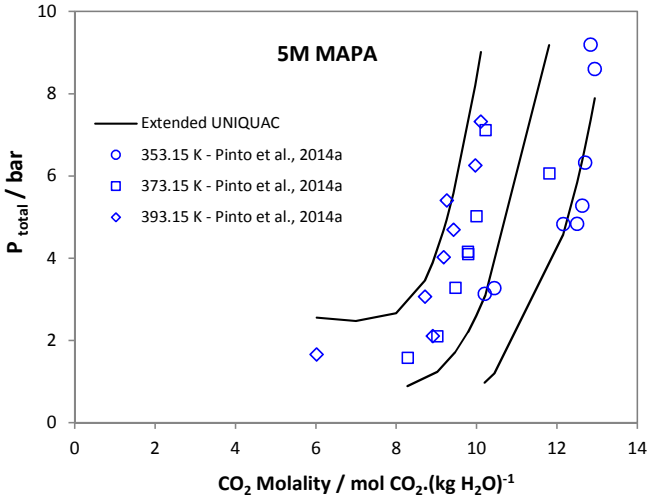

Figure 5.20: Equilibrium total pressure in 5M MAPA solutions as a function of CO_2 composition at different temperatures.

Pinto et al.[44] reported the solubility of CO_2 in 5M MAPA solutions at different temperatures. These experimental data are plotted with the calculated curves in Figure 5.21. Significant deviations between the experimental data and the modeling results can be observed for the data at 333.15 K and 353.15 K. However, a good agreement between the modeling results and the experimental data can be seen for the isotherm at 313.15 K. A magnified view of the results at low CO_2 partial pressures below 0.01 bar for the 313.15 K isotherm are shown in Figure 5.22 which also show some scatter in the experimental data.

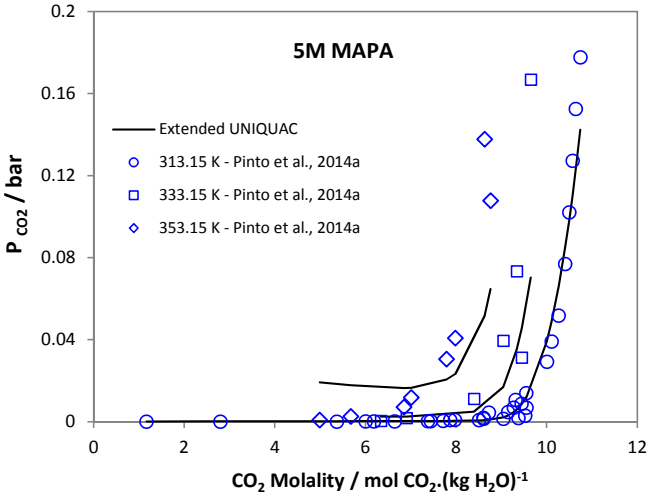

Figure 5.21: Partial pressure of CO_2 in 5M MAPA solutions at different temperatures.

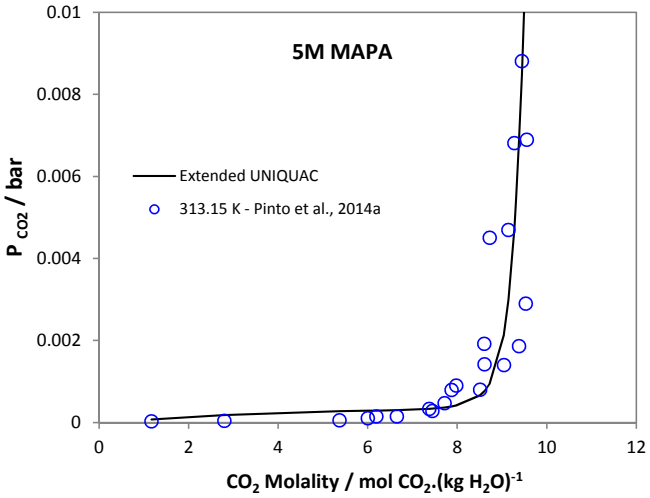

Figure 5.22: Magnified view of partial pressure of CO_2 in 5M MAPA solutions at 313.15 K below 0.01 bar.

Differential heats of absorption of CO_2 in the aqueous MAPA solutions were the only thermal property data available for thermodynamic modeling of the H_2O-MAPA-CO_2 system. The modeling results for the 2M and 1M MAPA solutions along with the experimental data from Arshad et al.[39] are given in Figure 5.23 (left side images for 2M MAPA and right side images for 1M MAPA). The model calculated the differential heat of absorption of CO_2 in 2M MAPA solutions very well at 40 ^{o}C. However, the model calculated results are slightly lower at 80 ^{o}C compared to the experimental data, and showed large deviations at low CO_2 concentrations for the 120 ^{o}C isotherm. Similar kind of results can also be seen for 1M MAPA solutions with slightly large deviations compared to the 2M MAPA results at respective temperatures. The estimated deviations (AARD) between the experimental data and the modeling results are 11.7 % and 15.6 % respectively for the 2M and 1M MAPA solutions with major contributions from the data at high temperatures.

The reported experimental data for differential heats of absorption of CO_2 in 8 mass % and 3 mass % MAPA solutions from Kim, 2009[40] and the modeling results are presented in Figure 5.24. The model very well describes the 8 mass % MAPA data at 40 ^{o}C and slightly lower calculated results for the 3 mass % MAPA data at the same temperature. However, there is a large scatter in the experimental data at 80 ^{o}C and 120 ^{o}C for both the MAPA systems (8 mass % and 3 mass %) and poorly represented by the model. The estimated deviations (AARD) are 34 % and 39.6 % respectively for the 8 mass % and 3 mass % MAPA solutions with largest contribution coming from the scattered experimental data at 80 ^{o}C and 120 ^{o}C. It should be noted that these data were not included in the parameter estimation.

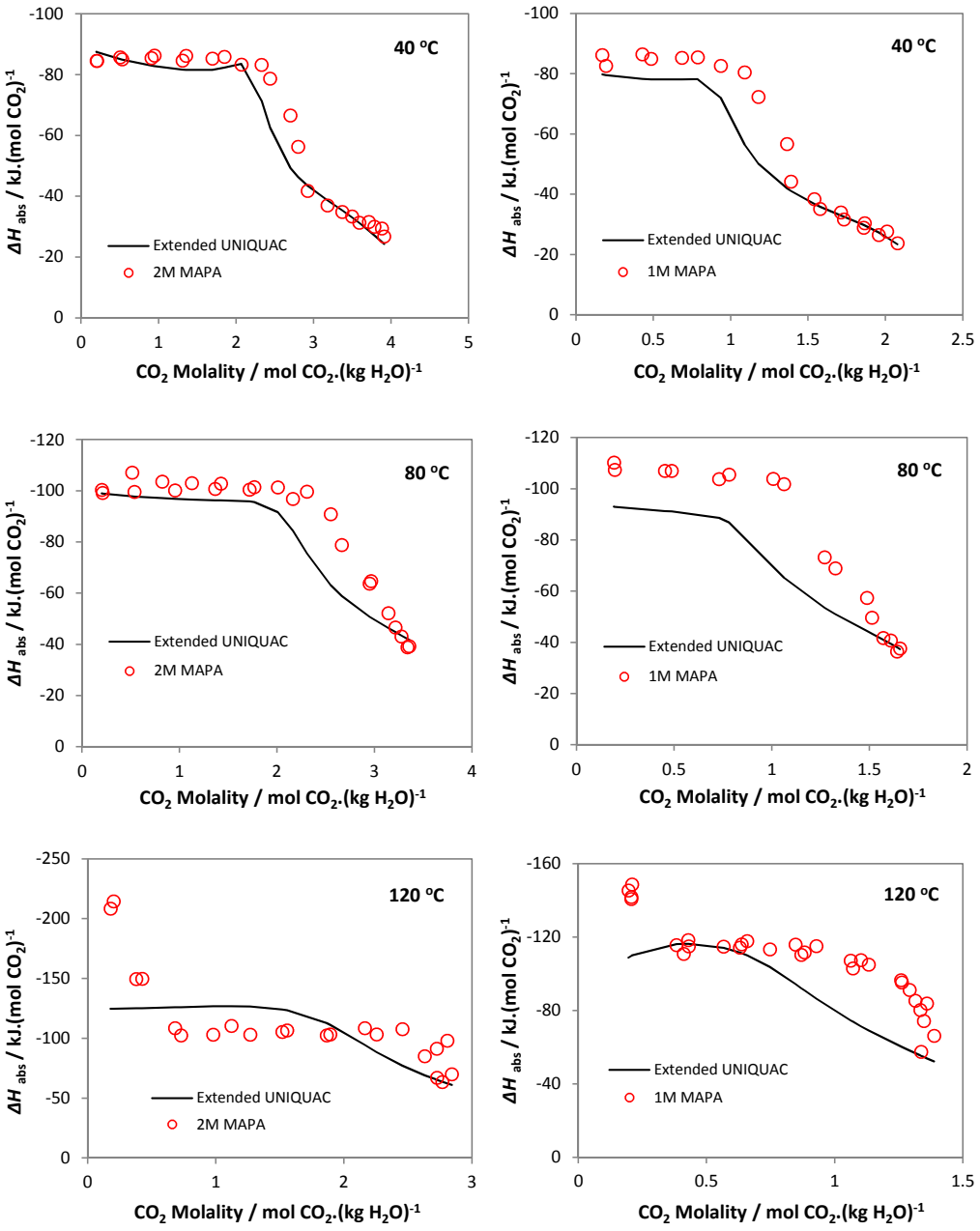

Figure 5.23: Differential heat of absorption of CO_2 in 2M (left side images) and 1M (right side images) MAPA solutions at 40, 80, and 120 °C. Experimental data from Arshad et al.[39]

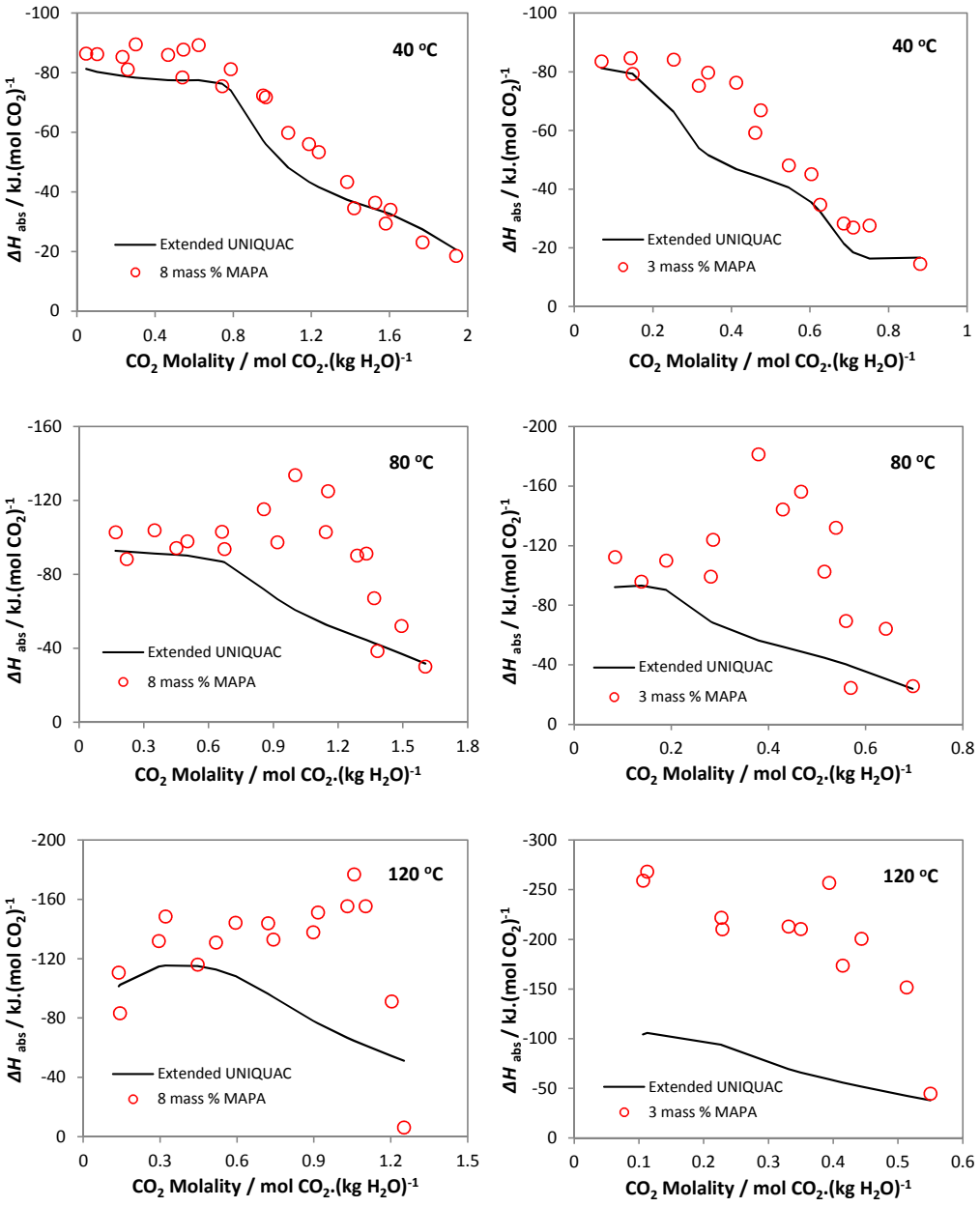

Figure 5.24: Differential heat of absorption of CO_2 in 8 mass % (left side images) and 3 mass % (right side images) MAPA solutions at 40, 80, and 120 °C. Experimental data from Kim, 2009[40] were not used in the parameter estimation.

It can be noticed that the modeling of the H_2O-MAPA-CO_2 system showed high deviations in the VLE and heat of absorption results. One possible reason may be the large scatter and low accuracy of some of the experimental data (e.g., VLE data of 5M MAPA system). Excluding those experimental data from the parameter estimation was not an option because these were the only available data for modeling of the system. Other reason may be lacking of one of the MAPA species in the modeling. This species may the protonated carbamate of MAPA ($^{+}HMAPACOO^{-}$). As mentioned earlier that the complexity of the MAPA system is similar to that of the aqueous AEEA as reported by Ma'mun et al.[18] They reported the formation of protonated carbamate species of AEEA at high CO_2 loadings. Due to unavailability of the standard state thermodynamic property data, it was difficult to include such a species in the parameter estimation. However, attempts were made in this work to model the MAPA system by including the protonated primary carbamate of MAPA with guess values for the standard state Gibbs energy and enthalpy of formation. These values were altered during the parameter estimation to fit to the experimental data. But the results did not show any improvements in the model. This might be due to inappropriate values for the standard state Gibbs energy and enthalpy of formation for the protonated primary carbamate of MAPA. Therefore, it was decided to exclude $^{+}HMAPACOO^{-}$ from the parameter estimation. It should be noted here that the standard state thermodynamic properties for the MAPA primary carbamate ($MAPACOO^{-}$) were also not available in the literature and were guessed initially and then these values were fitted to the experimental data. In case of MAPA primary carbamate, the results showed significant improvements and thus retained in the model.

5.10.3 H_2O-DEEA-MAPA-CO_2 System (Liquid-Liquid Split)

The parameter estimation for the blended aqueous DEEA-MAPA systems was started by calculating the freezing points and VLE (total pressure) for the H_2O-DEEA-MAPA solutions. The calculated freezing point data are illustrated in Figure 5.25 together with the experimental data from Arshad et al.[36] The freezing point data are plotted as a function of total amine concentration in the solutions for the 5:1, 3:1, 1:1, 1:3, and 1:5 molar ratios of DEEA/MAPA. A good agreement between the modeling results and the experimental data can be observed with an estimated AARD of 5.2 %. Figure 5.26 presents a comparison between the calculated and experimental (Hartono et al.[5]) total pressure data as a function of amine molality in the liquid phase at different temperatures. The model describes the total pressure data fairly well with an estimated AARD of 13.6 %.

The experimental VLE data (both total pressure and CO_2 partial pressure) for the 5M DEEA + 2M MAPA (5D2M) and 5M DEEA + 1M MAPA (5D1M) systems were reported by Arshad et al.[37] The results of 5D2M system are presented in the Figure 5.27 for the total pressure and Figure 5.28 for the CO_2 partial pressure. A fairly good agreement between the calculated and experimental total pressures can be seen in Figure 5.27 (AARD of 11.2 %) with some deviations in the results at 353.15 K and 393.15 K. It can be noticed that these deviations at 353.15 K and 393.15 K are similar to that of 2M MAPA results (Figure 5.16) which were probably reproduced also in the 5D2M system. These deviations are also reflected in the calculated CO_2 partial pressures for the same isotherm (at 353.15 K and 393.15 K) as can be seen in Figure 5.28. However, the model very well calculated the CO_2 partial pressures at 313.15 K.

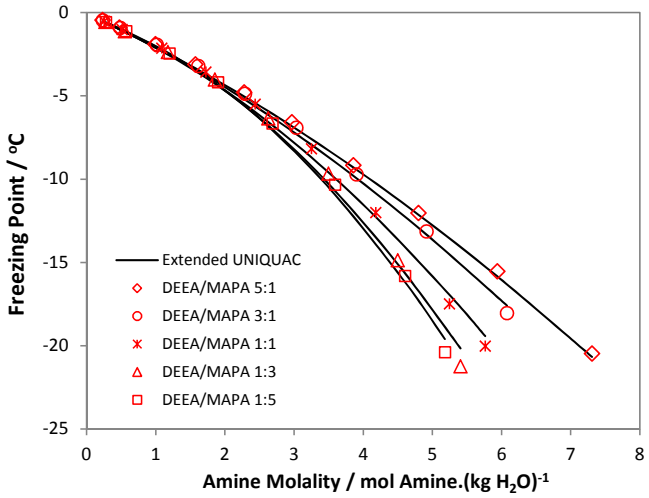

Figure 5.25: Freezing point depression in H_2O-DEEA-MAPA system. Experimental data from Arshad et al.[36]

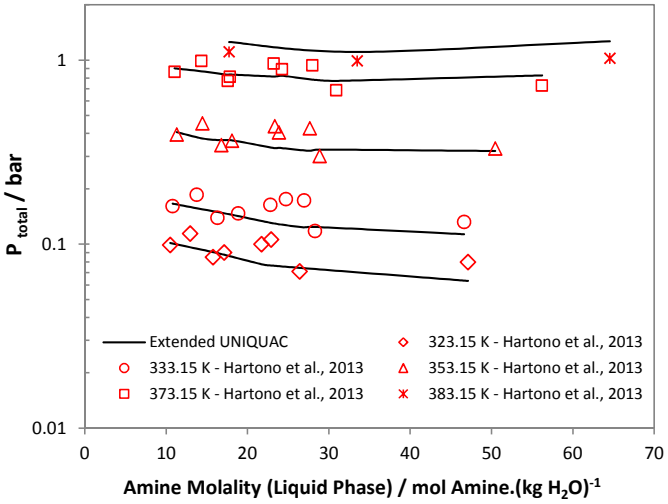

Figure 5.26: Total pressure of H_2O-DEEA-MAPA system at different temperatures.

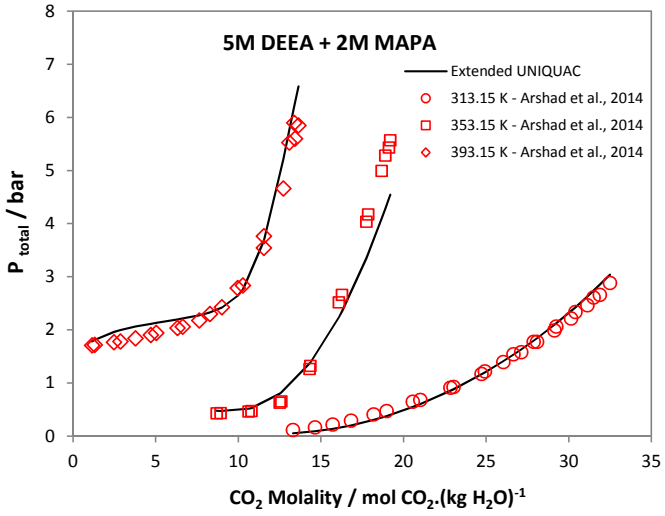

Figure 5.27: Equilibrium total pressure in 5M DEEA + 2M MAPA solutions as a function of CO_2 composition at three different temperatures.

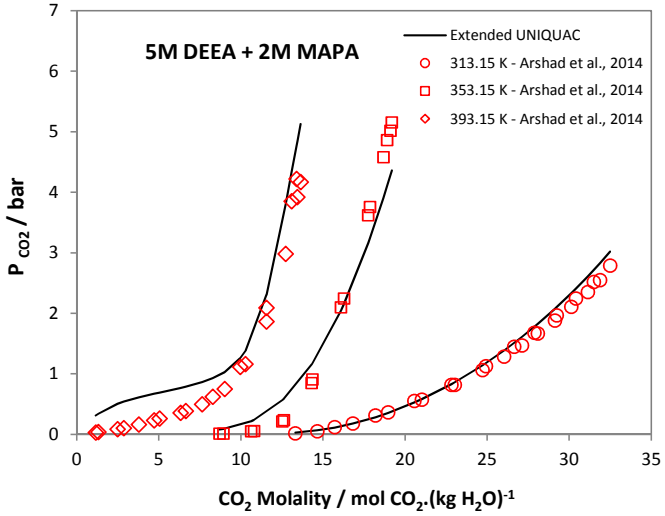

Figure 5.28: Partial pressure CO_2 in 5M DEEA + 2M MAPA solutions as a function of CO_2 composition at three different temperatures.

Similarly, for the 5D1M system, the total pressure results are shown in Figure 5.29 and the CO_2 partial pressure results are illustrated in Figure 5.30 along with the experimental data at three temperatures. The model describes the total pressure data very well in the whole CO_2 concentration range for all the three isotherms (Figure 5.29) with an estimated AARD of 8.2 %. Similar nice results can also be observed in Figure 5.30 for the CO_2 partial pressure data with a few high calculated data points for the 393.15 K isotherm at high CO_2 concentrations. The estimated AARD between the calculated and the experimental data set is 16.4 %, twice the AARD of total pressure data.

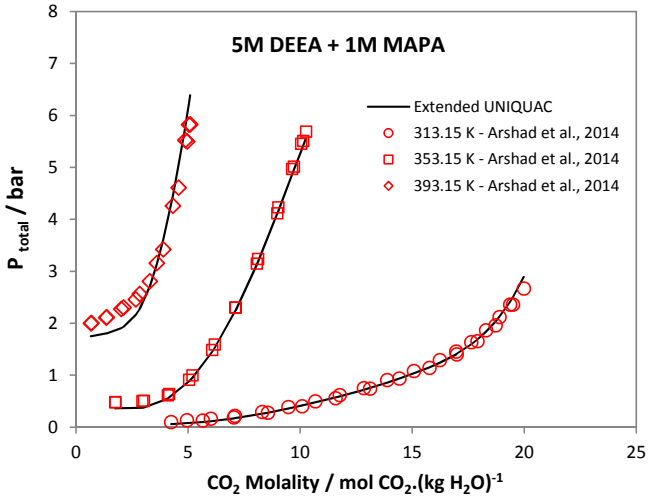

Figure 5.29: Equilibrium total pressure in 5M DEEA + 1M MAPA solutions as a function of CO_2 composition at three different temperatures.

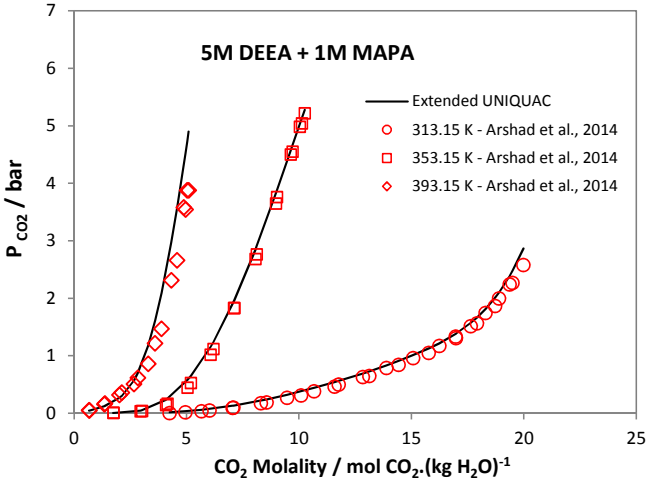

Figure 5.30: Partial pressure CO_2 in 5M DEEA + 1M MAPA solutions as a function of CO_2 composition at three different temperatures.

Figure 5.31 illustrates the calculated differential heats of absorption of CO_2 in 5D2M (left side images) and 5D1M (right side images) systems together with the experimental data from Arshad et al.[39] for the temperature range of 40-120 ^{o}C. The experimental and the calculated values present a good agreement for the 5D2M system in the whole range of temperature and CO_2 composition with an estimated AARD of 6.1 %. However, the 5D1M system shows higher deviations in all the three isotherms compared to that of the 5D2M systems. The estimated AARD for the 5D1M system is 8.3 %.

The experimental differential heat of absorption data available from Kim, 2009[40] for the aqueous blends of DEEA-MAPA are also compared with the calculated values as shown in Figure 5.32 for the 37 mass % DEEA + 3 mass % MAPA (left side images) and 32 mass % DEEA + 8 mass % MAPA (right side images) systems at 40, 80, and 120 ^{o}C. The results look satisfactory for both the systems at 40 and 80 ^{o}C. However, large deviations can be observed for both the systems at 120 ^{o}C. The estimated AARD between the model results and the experimental data is 18.1 % for the 37 mass % DEEA + 3 mass % MAPA system and 11.2 % for the 32 mass % DEEA + 8 mass % MAPA system. It should be noted that these experimental data were not included in the parameter estimation.

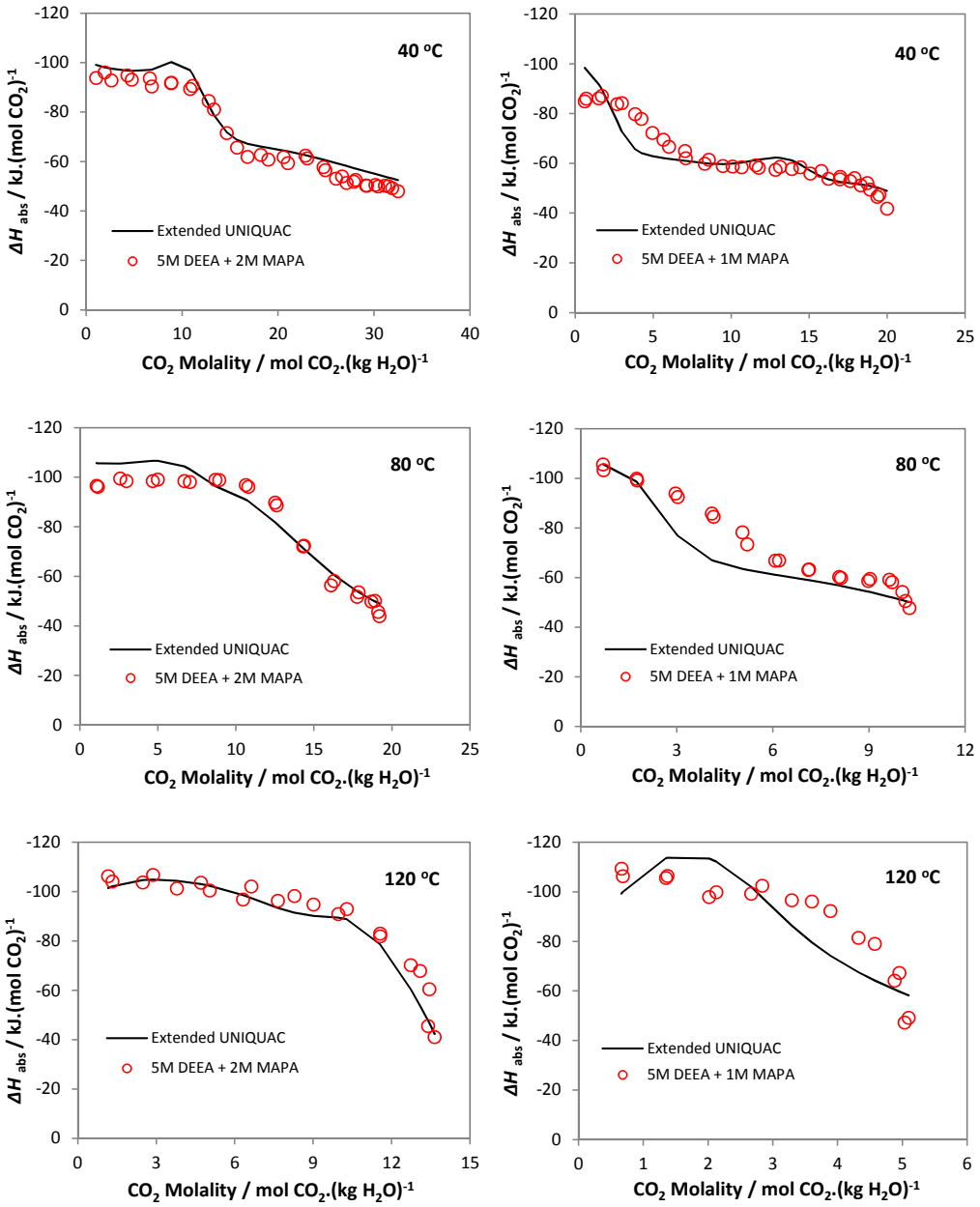

Figure 5.31: Differential heat of absorption of CO_2 in 5M DEEA + 2M MAPA (left side images) and 5M DEEA + 1M MAPA (right side images) solutions at 40, 80, and 120 °C. Experimental data from Arshad et al.[39]

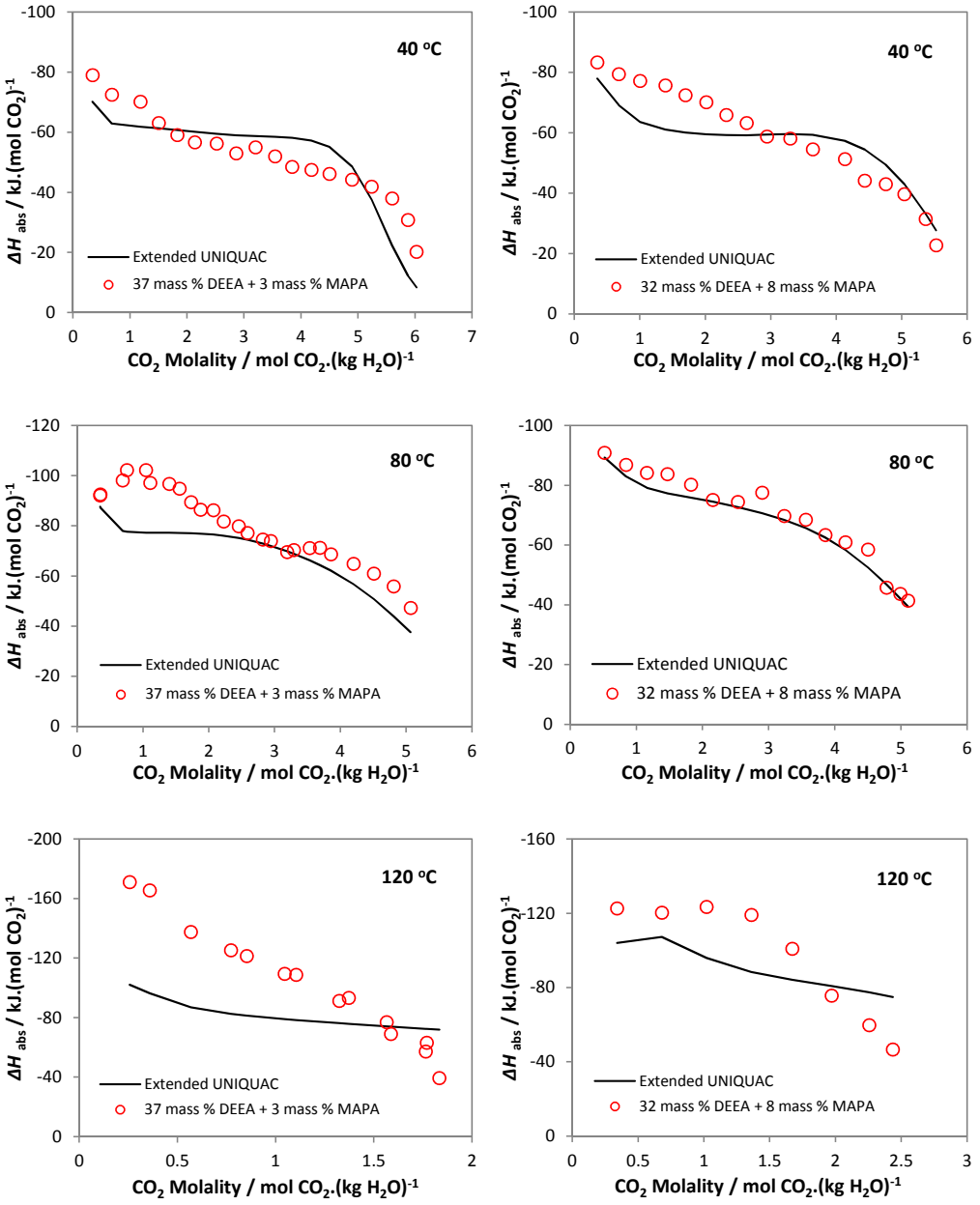

Figure 5.32: Differential heat of absorption of CO_2 in 37 mass % DEEA + 3 mass % MAPA (left side images) and 32 mass % DEEA + 8 mass % MAPA (right side images) solutions at 40, 80, and 120 °C. Experimental data from Kim, 2009[40] were not used in the parameter estimation.

As mentioned earlier, one of the main features of 5M DEEA + 2M MAPA mixture is that it gives liquid-liquid split upon CO_2 absorption. The upper phase, lean in CO_2 and rich in DEEA, is sent to the absorber without regeneration and only the CO_2 rich lower phase (also rich in MAPA) is regenerated in the stripper. It is essential that the model can predict the LLE in the mixed aqueous DEEA-MAPA system. Only 32 LLE data points were available for the parameter estimation from Pinto et al.[45] at three different temperatures. Figures 5.33 - 5.35 illustrate the LLE results in H_2O-DEEA-MAPA-CO_2 solutions at 40 °C, 60 °C, and 80 °C. The calculated results (binodal curves and tie lines) are plotted in comparison with the experimental data. Figure 5.33 shows the calculated values at 40 °C for the 6 molal MAPA solutions with a constant CO_2 concentration of 4.6 molal and varying DEEA concentrations. To keep the calculations simple and better visualization of the graphs, the model calculations were based on slightly different concentration conditions compared to the experimental data i.e., the MAPA and CO_2 concentrations were not constant in the experimental data but an almost averaged value was used for the model calculations. This simplification allowed the model to calculate the smooth binodal curves and the uniform tie lines which, otherwise, was not possible. Similarly, the model results at 60 °C for the 7.5 molal MAPA solutions with a constant CO_2 concentration of 4.5 molal are illustrated in Figure 5.34 and for the 7.5 molal MAPA solutions with a constant CO_2 concentration of 3.75 at 80 °C in Figure 5.35 together with the experimental data scattering around on the binodal curves.

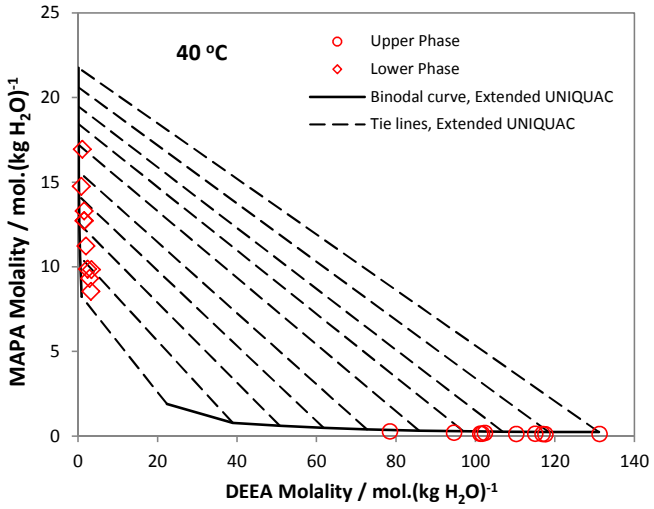

Figure 5.33: Modeling results of liquid-liquid equilibrium in H_2O-DEEA-MAPA-CO_2 solutions at 40 °C with experimental data from Pinto et al.[45] Calculated values are for 6 molal MAPA solutions with a constant CO_2 concentration of 4.6 molal and varying DEEA molality.

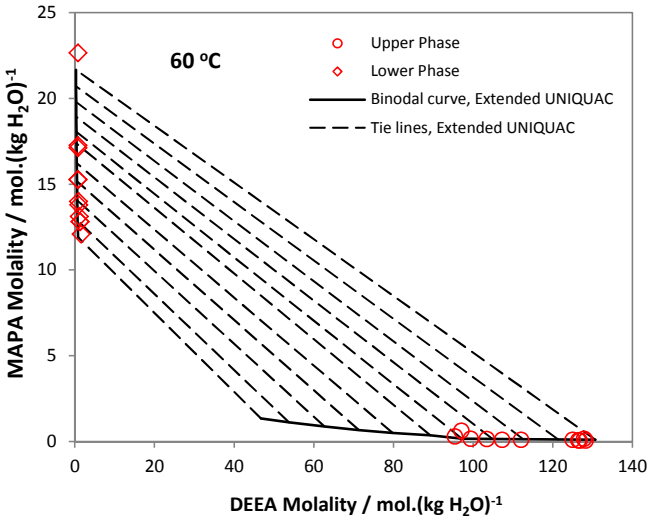

Figure 5.34: Modeling results of liquid-liquid equilibrium in H_2O-DEEA-MAPA-CO_2 solutions at 60 °C with experimental data from Pinto et al.[45] Calculated values are for 7.5 molal MAPA solutions with a constant CO_2 concentration of 4.5 molal and varying DEEA molality.

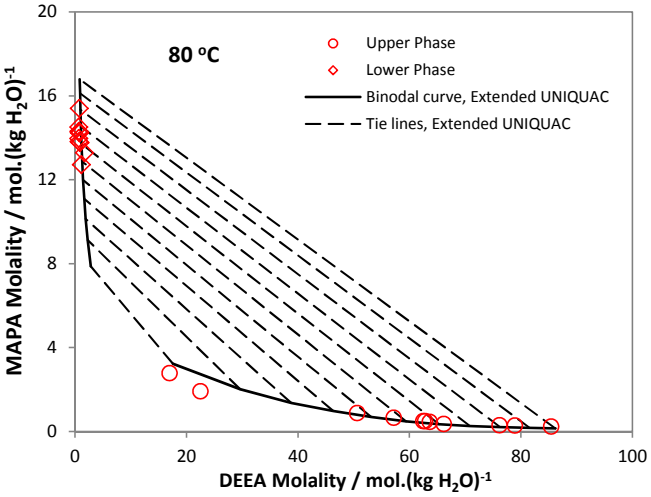

Figure 5.35: Modeling results of liquid-liquid equilibrium in H_2O-DEEA-MAPA-CO_2 solutions at 80 °C with experimental data from Pinto et al.[45] Calculated values are for 7.5 molal MAPA solutions with a constant CO_2 concentration of 3.75 molal and varying DEEA molality.

5.11 Deviations

In this section, all the calculated and experimental values of all the data type are presented graphically on parity plots to visualize the extent of agreement between the experimental data and the model calculations.

5.11.1 Pure Amine Vapor Pressure

Figure 5.36 presents a parity plot for the experimental and the calculated vapor pressure data of pure DEEA and MAPA. The *y* = *x* diagonal line (solid line) is used as a reference and dashed lines represents a ± 5 % deviation from the diagonal. It can be seen that all the points are randomly distribution on the diagonal line within ± 5 % deviation.

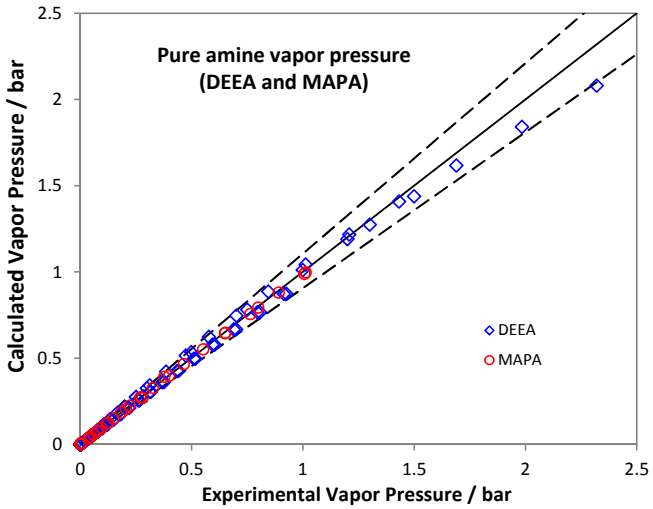

Figure 5.36: Parity plot with experimental and calculated values of the vapor pressure of pure amines (DEEA and MAPA) with ± 5 % deviation (dashed line) from the diagonal (solid line).

5.11.2 Excess Enthalpy

A parity plot is given in Figure 5.37 for the experimental and calculated values for molar excess enthalpy of DEEA. A diagonal line is drawn as a reference with ± 5 % deviation (dashed line) from the diagonal. The points are scattered around the diagonal line with only few points outside the ± 5 % deviation.

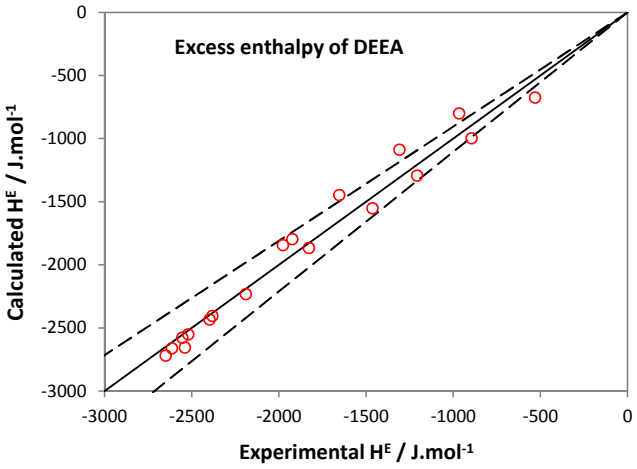

Figure 5.37: Parity plot with experimental and calculated values for molar excess enthalpy of DEEA with ± 5 % deviation (dashed line) from the diagonal (solid line).

5.11.3 Freezing Point Depression

Figure 5.38 represents the parity plot for the experimental and calculated freezing points for the binary and ternary aqueous amine systems (H_2O-DEEA, H_2O-MAPA, and H_2O-DEEA-MAPA) and Figure 5.39 illustrates the freezing point results for the CO_2 loaded systems (H_2O-DEEA-CO_2 and H_2O-DEEA-CO_2). All the points for both the unloaded and CO_2 loaded systems randomly scattered within ± 5 % deviation around the reference diagonal line.

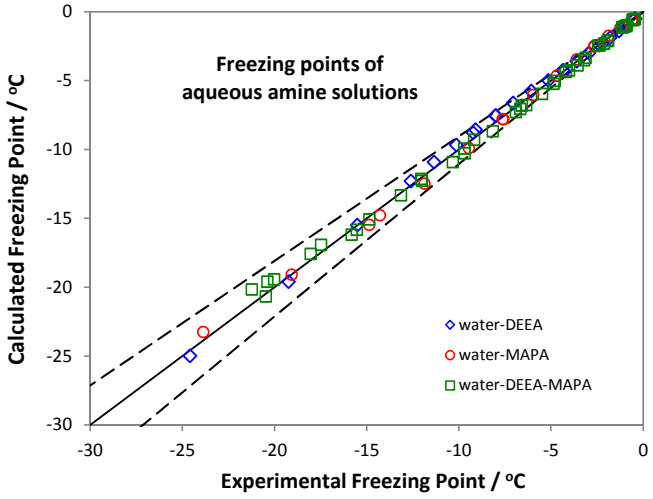

Figure 5.38: Parity plot with experimental and calculated values of the freezing points of the H_2O-DEEA, H_2O-MAPA, and H_2O-DEEA-MAPA systems with ± 5 % deviation (dashed line) from the diagonal (solid line).

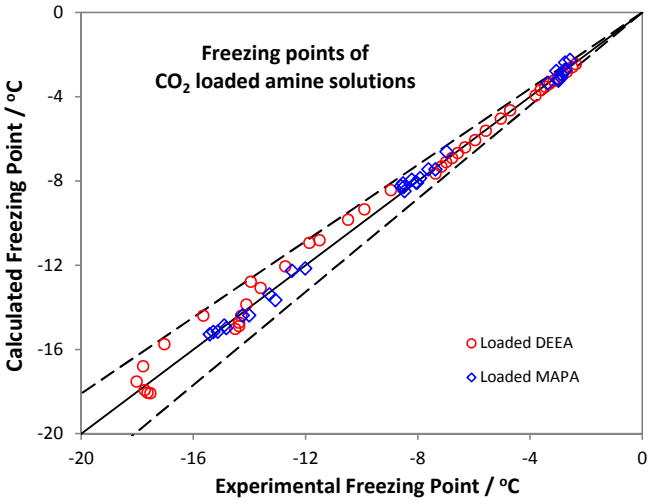

Figure 5.39: Parity plot with experimental and calculated values of the freezing points of the H_2O-DEEA-CO_2 and H_2O-MAPA-CO_2 systems with ± 5 % deviation (dashed line) from the diagonal (solid line)

5.11.4 Unloaded Vapor-Liquid Equilibrium

A parity plot is given in Figure 5.40 which presents the calculated and experimental total pressures in all the unloaded binary and ternary aqueous amine systems (H_2O-DEEA, H_2O-MAPA, and H_2O-DEEA-MAPA) in this work. The results are presented with ± 10 % deviation (dashed line) from the diagonal line.

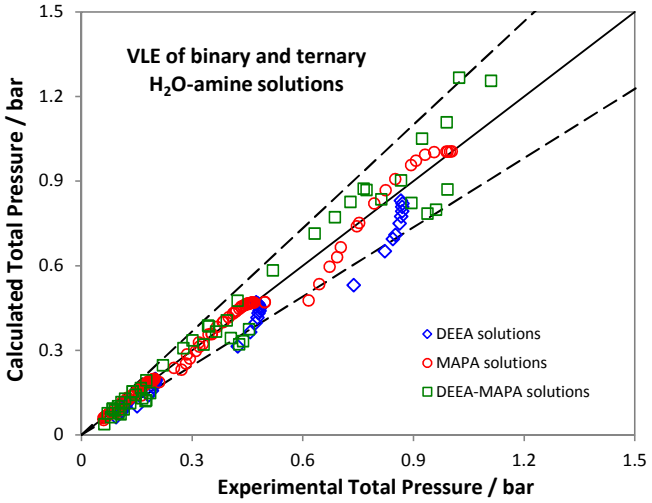

Figure 5.40: Parity plot with experimental and calculated values of the total pressure in H_2O-DEEA, H_2O-MAPA, and H_2O-DEEA-MAPA systems with ± 10 % deviation (dashed line) from the diagonal (solid line).

5.11.5 CO_2 Loaded Vapor-Liquid Equilibrium

The total pressure and CO_2 partial pressure data for the CO_2 loaded amine systems used in this work were available only from the two literature sources and presented here separately for Arshad et al.[37] and Monteiro et al.[6] and Pinto et al.[44] Figure 5.41 presents a parity plot for the calculated and experimental (Arshad et al.[37]) total pressures in CO_2 loaded ternary and quaternary systems (H_2O-DEEA-CO_2, H_2O-MAPA-CO_2, and H_2O-DEEA-MAPA-CO_2) with ± 10 % deviation envelopes (dashed line) from the diagonal. Similarly, a parity plot is illustrated in Figure 5.42 with the experimental data from Monteiro et al.[6] for DEEA solutions and Pinto et al.[44] for MAPA solutions, and the calculated results for the total pressures in CO_2 loaded ternary systems (H_2O-DEEA-CO_2 and H_2O-MAPA-CO_2) with ± 10 % error envelopes from the diagonal line. It can be noticed that several points of the ternary H_2O-MAPA-CO_2 system show more than ± 10 % deviations from the reference diagonal line in both Figure 5.41 and Figure 5.42 compared to only few points for the ternary H_2O-DEEA-CO_2 system and almost no point for the quaternary H_2O-DEEA-MAPA-CO_2 system.

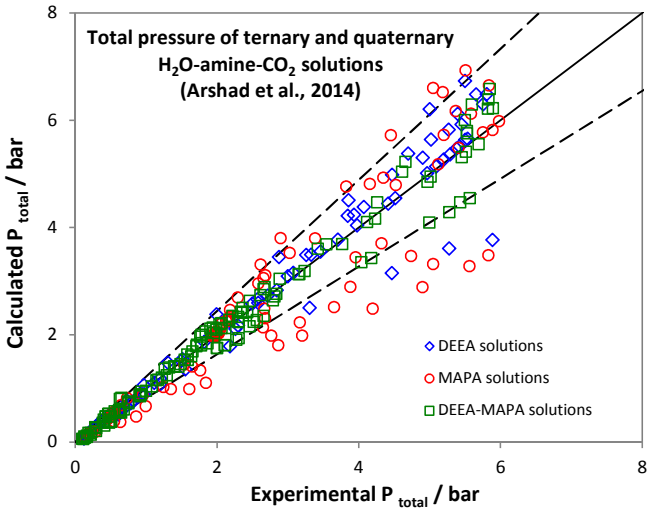

Figure 5.41: Parity plot with experimental and calculated values of the equilibrium total pressure in H_2O-DEEA-CO_2, H_2O-MAPA-CO_2, and H_2O-DEEA-MAPA-CO_2 systems (Arshad et al.[37]) with ± 10 % deviation (dashed line) from the diagonal (solid line).

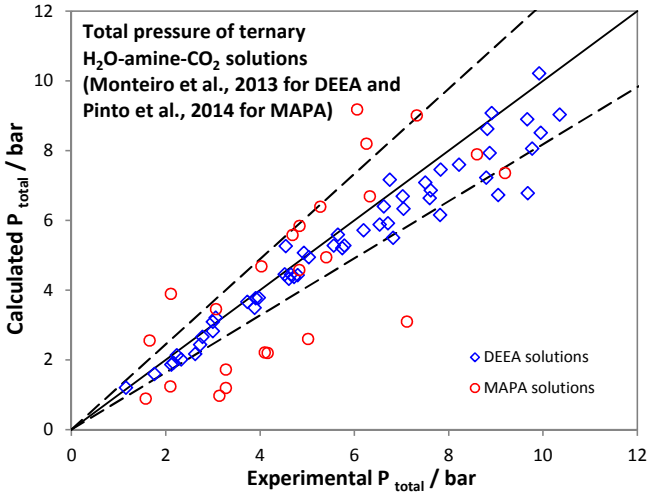

Figure 5.42: Parity plot with experimental and calculated values of the equilibrium total pressure in H_2O-DEEA-CO_2 and H_2O-MAPA-CO_2 systems (Monteiro et al.[6] for DEEA solutions and Pinto et al.[44] for MAPA solutions) with ± 10 % deviation (dashed line) from the diagonal (solid line).

A parity plot for the calculated and experimental (Arshad et al.[37]) CO_2 partial pressures in ternary and quaternary systems (H_2O-DEEA-CO_2, H_2O-MAPA-CO_2, and H_2O-DEEA-MAPA-CO_2) is shown in Figure 5.43 with ± 15 % error envelopes. Similar to the total pressure results (Figure 5.41), several points of the ternary H_2O-MAPA-CO_2 system show deviations higher than ± 15 %. The quaternary H_2O-DEEA-MAPA-CO_2 systems also show high deviation at low CO_2 partial pressures. Similarly, Figure 5.44 presents the parity plot with the experimental data from Monteiro et al.[6] for DEEA solutions and Pinto et al.[44] for MAPA solutions, and the calculated results for the partial pressures of CO_2 loaded ternary systems (H_2O-DEEA-CO_2 and H_2O-MAPA-CO_2) with ± 15 % error envelopes from the diagonal line. Again, the ternary H_2O-MAPA-CO_2 systems show the largest deviations.

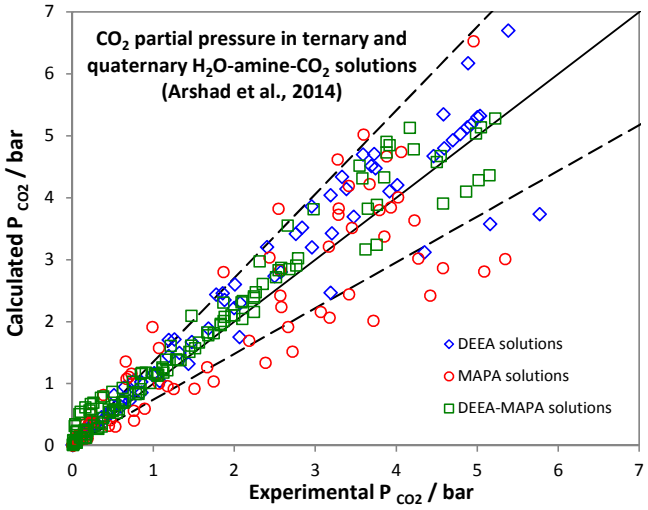

Figure 5.43: Parity plot with experimental and calculated values of the partial pressure of CO_2 in H_2O-DEEA-CO_2, H_2O-MAPA-CO_2, and H_2O-DEEA-MAPA-CO_2 systems (Arshad et al.[37]) with ± 15 % deviation (dashed line) from the diagonal (solid line).

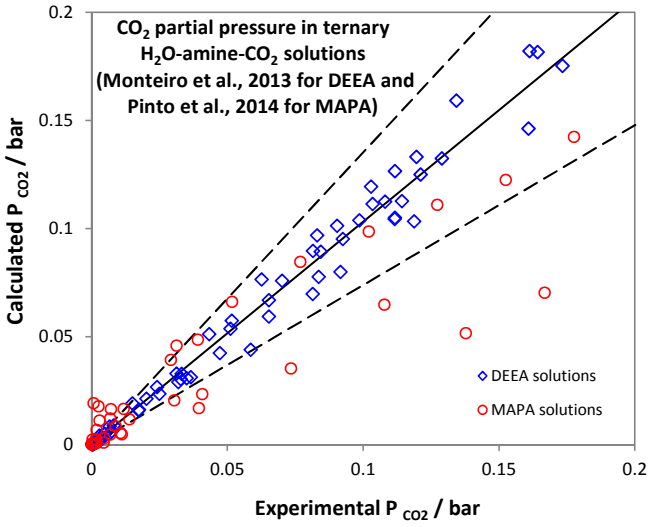

Figure 5.44: Parity plot with experimental and calculated values of the partial pressure of CO_2 in H_2O-DEEA-CO_2 and H_2O-MAPA-CO_2 systems (Monteiro et al.[6] for DEEA solutions and Pinto et al.[44] for MAPA solutions) with ± 15 % deviation (dashed line) from the diagonal (solid line).

5.11.6 Heat of Absorption of CO_2

Differential heats of absorption of CO_2 in aqueous amine solutions used in this work were available from Arshad et al.[39] and Kim, 2009[40] and their parity plots are presented here separately. The experimental data from Kim, 2009[40] were not used in the parameter estimation and results presented here were calculated from the model parameters estimated from the other data. Figure 5.45 presents the parity plot for the calculated and experimental (Arshad et al.[39]) differential heat of absorption of CO_2 in H_2O-DEEA, H_2O-MAPA, and H_2O-DEEA-MAPA systems and Figure 5.46 (with experimental data from Kim, 2009[40]) illustrates the parity plot in same aqueous amine systems as in Figure 5.45 but with different concentrations. Almost all the points in Figure 5.45 show deviations within ± 15 % from the diagonal except a few points of the aqueous DEEA and MAPA solutions. However, Figure 5.46 shows a much larger deviations for a large number of data points of all the aqueous amine systems compared to the results in Figure 5.45.

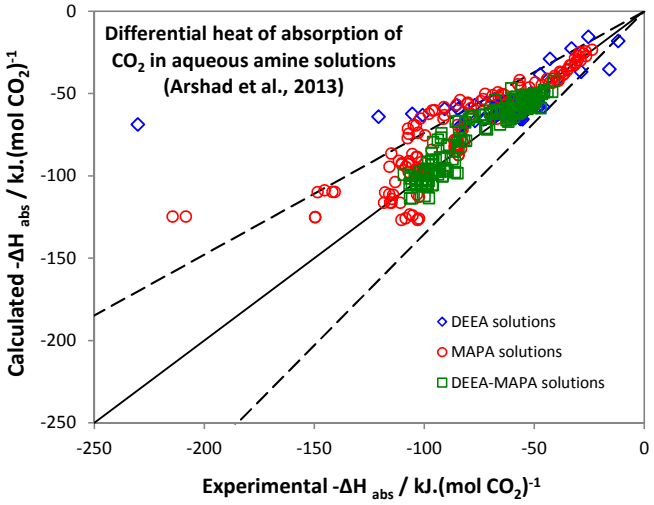

Figure 5.45: Parity plot with experimental and calculated values of differential heat of absorption of CO_2 in H_2O-DEEA, H_2O-MAPA, and H_2O-DEEA-MAPA systems (Arshad et al.[39]) with ± 15 % deviation (dashed line) from the diagonal (solid line).

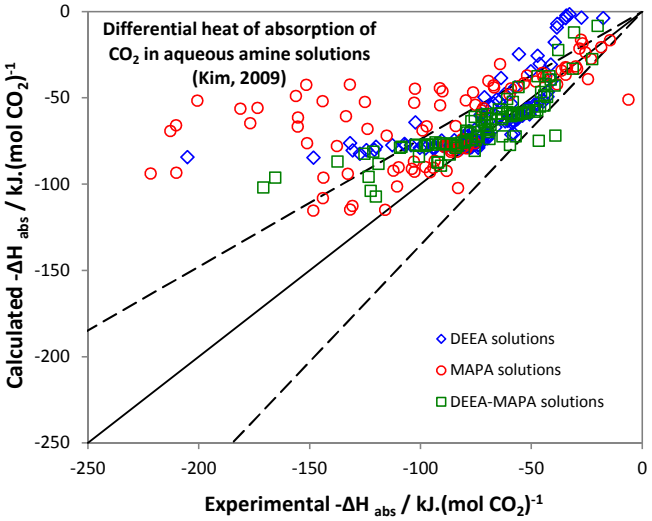

Figure 5.46: Parity plot with experimental and calculated values of differential heat of absorption of CO_2 in H_2O-DEEA, H_2O-MAPA, and H_2O-DEEA-MAPA systems (Kim, 2009[40]) with ± 15 % deviation (dashed line) from the diagonal (solid line).

5.12 Conclusions

The Extended UNIQUAC model was implemented in this work to describe the thermodynamics of the de-mixing aqueous DEEA-MAPA solvent systems for CO_2 capture. The two sub-systems, H_2O-DEEA-CO_2 and H_2O-MAPA-CO_2, were modeled first followed by the H_2O-DEEA-MAPA-CO_2 system which gives liquid-liquid split. Different types of experimental equilibrium and thermal property data were used for the parameter estimation. 94 model parameters and 6 thermodynamic properties were fitted to approximately 1500 experimental data consisting of pure amine vapor pressure, vapor-liquid equilibrium, solid-liquid equilibrium, liquid-liquid equilibrium, excess enthalpy, and heat of absorption of CO_2 in aqueous amine solutions. Out of 94 model parameters, volume (r) and surface area (q) parameters have 6 parameters each, the binary parameters u_{ij}^0 and u_{ij}^T have 41 parameters each for calculating the interaction energy parameters $u_{ij} = u_{ij}^0 + u_{ij}^T \left(T - 298.15\right)$, and 6 thermodynamic properties are the standard state Gibb's energy of formation and standard state enthalpy of formation for the three species $DEEA(l)$, $MAPA(l)$, and $MAPACOO^-$. The model developed in this work can reproduce almost all the data points and can describe all the data types satisfactorily with a single unique set of parameters.

5.13 References

(1) Thomsen, K., Rasmussen, P., 1999. Modeling of vapor-liquid-solid equilibrium in gas-aqueous electrolyte systems. Chemical Engineering Science 54, 1787-1802.

(2) Darde, V., van Well, W.J.M., Stenby, E.H., Thomsen, K., 2010. Modeling of carbon dioxide absorption by aqueous ammonia solutions using the Extended UNIQUAC model. Industrial & Engineering Chemistry Research 49, 12663-12674.

(3) Faramarzi, L., Kontogeorgis, G.M., Thomsen, K., Stenby, E.H., 2009. Extended UNIQUAC model for thermodynamic modeling of CO_2 absorption in aqueous alkanolamine solutions. Fluid Phase Equilibria 282, 121-132.

(4) Sadegh, N., 2012. Acid Gas Removal from Natural Gas with Alkanolamines: A Modeling and Experimental Study. Technical University of Denmark, DK-2800 Lyngby, Denmark.

(5) Hartono, A., Saleem, F., Arshad, M.W., Usman, M., Svendsen, H. F., 2013. Binary and ternary VLE of the 2-(diethylamino)-ethanol (DEEA)/ 3-(methylamino)-propylamine (MAPA)/ water system. Chemical Engineering Science 101, 401-411.

(6) Monteiro, J.G.M.-S., Pinto,D.D.D., Zaidy, S.A.H., Hartono, A., Svendsen, H.F., 2013. VLE data and modelling of aqueous *N,N*-diethyethanolamine (DEEA) solutions. International Journal of Greenhouse Gas Control 19, 432-440.

(7) Thomsen, K., Rasmussen, P., Gani, R., 1996. Correlation and prediction of thermal properties and phase behaviour for a class of aqueous electrolyte systems. Chemical Engineering Science, 51, 3675-3683.

(8) Thomsen, K., 1997. Aqueous electrolytes: model parameters and process simulation. Ph.D. Thesis, Technical University of Denmark, Kongens Lyngby, Denmark.

(9) Sander, B., Fredenslund, A., Rasmussen, P., 1986. Calculation of vapour-liquid equilibria in mixed solvent/ salt systems using an extended UNIQUAC equation. Chemical Engineering Science 41(5), 1171-1183.

(10) Sander, B., Rasmussen, P., Fredenslund, A., 1986. Calculation of vapour-liquid equilibria in nitric acid-water-nitrate salt systems using an extended UNIQUAC equation. Chemical Engineering Science 41(5), 1185-1195.

(11) Sander, B., Rasmussen, P., Fredenslund, A., 1986. Calculation of solid-liquid equilibria in aqueous solutions of nitrate salts using an extended UNIQUAC equation. Chemical Engineering Science 41(5), 1197-1202.

(12) Nicolaisen, H., Rasmussen, P., Sørensen, J.M., 1993. Correlation and prediction of mineral solubilities in the reciprocal salt system (Na^+, K^+)(Cl^-, SO_4^{2-})-H_2O at 0-100 ^oC. Chemical Engineering Science 48(18), 3149-3158.

(13) Abrams, D.S., Prausnitz, J.M., 1974. Statistical thermodynamics of liquid mixtures: A new expression for the excess Gibbs energy of partly or completely miscible systems. AIChE Journal 21 (1), 116-128.

(14) Maurer, G., Prausnitz, J.M., 1978. On the derivation and extension of the UNIQUAC equation. Fluid Phase Equilibria 2, 91-99.

(15) Thomsen, K., 2009. Electrolyte solutions: thermodynamics, crystallization, separation methods. Technical University of Denmark, DTU Chemical Engineering, Kongens Lyngby, Denmark.

(16) Lewis, G.N., Randall, M., 1921. The activity coefficient of strong electrolytes. Journal of the American Chemical Society 43, 1112-1154.

(17) Donaldson, T.L., Nguyen, Y.N., 1980. Carbon dioxide reaction kinetics and transport in aqueous amine membranes. Industrial and Engineering Chemistry Fundamentals 19, 260-266.

(18) Ma'mun, S., Jakobsen, J.P., Svendsen, H.F., 2006. Experimental and modeling study of the solubility of carbon dioxide in aqueous 30 mass % 2-((2-Aminoethyl)amino)ethanol solution. Industrial & Engineering Chemistry Research 45 (8), 2505-2512.

(19) Helgeson, H.C., Kirkham, D.H., Flowers, G.C., 1981. Theoretical prediction of the thermodynamic behavior of aqueous electrolytes at high pressures and temperatures: IV. Calculation of activity coefficients, osmotic coefficients, and apparent molal and standard and relative partial molal properties to 600 ^{o}C and 5 kbar. American Journal of Science 281, 1249-1516.

(20) Fletcher, R., 1971. A modified Marquardt subroutine for non-linear least squares, Harwell report. http://www.hsl.rl.ac.uk/ (accessed April 2013).

(21) StatLib-Applied Statistics Algorithms, Nelder-Mead routine (AS 47) http://lib.stat.cmu.edu/apstat/, or Nelder-Mead routine at http://lib.stat.cmu.edu/apstat/47 (accessed April 2013).

(22) NIST Chemical Thermodynamics Database Vesion 1.1, 1990. U.S. Department of Commerce, National Institute of Standards and Technology, Gaithersburg Maryland 20899.

(23) Marrero, J., Gani, R., 2001. Group-contribution based estimation of pure component properties. Fluid Phase Equilibria 183/184, 183-208.

(24) CAPEC Software, ProPed (pure component Property Prediction) tool in ICAS (Integrated Computer Aided System): http://www.capec.kt.dtu.dk/Software/CAPEC-Software

(25) Littel, R.J., Bos, M., Knoop, G.J., 1990. Dissociation constants of some alkanolamines at 293, 303, 318, and 333 K. Journal of Chemical and Engineering Data 35, 276-277.

(26) Hamborg, E.S., Versteeg, G.F., 2009. Dissociation constants and thermodynamic properties of amines and alkanolamines from (293 to 353) K. Journal of Chemical and Engineering Data 54, 1318-1328.

(27) Wagman, D.D., Evans, W.H., Parker, V.B., Schumm, R.H., Halow, I., Bailey, S.M., Kenneth, L.C., Nuttall, R.L., 1982. The NBS Tables of Chemical Thermodynamic Properties. Selected Values for Inorganic and C1 and C2 Organic Substances in SI Units. Journal of Physical and Chemical Reference Data 11, Supplement no. 2.

(28) Fosbøl, P.L., Thomsen, K., Stenby, E.H., 2009. Modeling of the mixed solvent electrolyte system CO_2-Na_2CO_3-$NaHCO_3$-monoethylene glycol-water. Industrial & Engineering Chemistry Research 48 (4), 4565-4578.

(29) Joback, K.G., Reid, R.C., 1987. Estimation of pure-component properties from group-contributions. Chemical Engineering Communications 57, 233-243.

(30) Maham, Y., Helper, L.G., Mather, A.E., Hakin, A.W., Marriott, R.A., 1997. Molar heat capacities of alkanolamines from 299.1 to 397.8 K. Group additivity and molecular connectivity analyses. Journal of Chemical Society, Faraday Transactions 93 (9), 1747-1750.

(31) Rayer, A.V., Henni, A., Tontiwachwuthikul, P., 2012. Molar heat capacities of solvents used in CO_2 Capture: a group additivity and molecular connectivity analysis. The Canadian Journal of Chemical Engineering 90, 367-376.

(32) Murray, R.C. Jr., Cobble, J.W., 1980. Chemical equilibria in aqueous systems at high temperatures. Annual Meeting - International Water Conference, 295-310.

(33) Steele, W.V., Chirico, R.D., Knipmeyer, S.E., Nguyen, A., 2002. Measurements of vapor pressure, heat capacity, and density along the saturation line for cyclopropane acid, *N,N*-diethylethanoalamine, 2,3-dihydrofuran, 5-hexen-2-one, perfluorobutanoic acid, and 2-phenylpropionaldehyde. Journal of Chemical and Engineering Data 47, 715-724.

(34) Kapteina, S., Slowik, K., Verevkin, S.P., Heinstz, A., 2005. Vapor pressures and vaporization of a series of ethnaolamines. Journal of Chemical and Engineering Data 50, 398-402.

(35) Klepáčová, K., Huttenhuis, P.J.G., Derks, P.W.J., Versteeg, G.F., 2011. Vapor pressures of several commercially used alkanolamines. Journal of Chemical and Engineering Data 56, 2242-2248.

(36) Arshad, M.W., Fosbøl, P.L., von Solms, N., Thomsen, K., 2013. Freezing point depressions of phase change CO_2 solvents. Journal of Chemical and Engineering Data 58 (7), 1918-1926.

(37) Arshad, M.W., Svendsen, H.F., Fosbøl, P.L., von Solms, N., Thomsen, K., 2014. Equilibrium Total Pressure and CO_2 Solubility in Binary and Ternary Aqueous Solutions of 2-(Diethylamino)ethanol (DEEA) and 3-(Methylamino)propylamine (MAPA). Journal of Chemical and Engineering Data 59 (3), 764-774.

(38) Mathonat, C., Maham, Y., Mather, A.E., Hepler, L.G., 1997. Excess molar enthalpies of (water + monoalkanolamine) mixtures at 298.15 K and 308.15 K. Journal of Chemical and Engineering Data 42, 993-995.

(39) Arshad, M.W., Fosbøl, P.L., von Solms, N., Svendsen, H.F., Thomsen, K., 2013. Heat of Absorption of CO_2 in Phase Change Solvents: 2-(diethylamino)ethanol and 3-(methylamino)propylamine. Journal of Chemical and Engineering Data 58 (7), 1974-1988.

(40) Kim, I., 2009. Heat of reaction and VLE of post combustion CO_2 absorbents. PhD Thesis. Norwegian University of Science and Technology, Trondheim, Norway.

(41) Kim, I., Svendsen, H.F., Børresen, E., 2008. Ebulliometric determination of vapor-liquid equilibria for pure water, monoethanolamine, *N*-methyldiethanolamine, 3-(methylamino)-propylamine, and their binary and ternary solutions. Journal of Chemical and Engineering Data 53 (11), 2521–2531.

(42) Verevkin, S.P., Chernyak, Y., 2012. Vapor pressure and enthalpy of vaporization of aliphatic propanediamines. Journal of Chemical Thermodynamics 47, 328-334.

(43) Monteiro, J.G.M.-S., Pinto,D.D.D., Hartono, A., Svendsen, H.F., 2011. Final report on liquid/ liquid solvents characterization. EU 7th Framework Program, iCap project. Deliverable number D 1.3.2.

(44) Pinto, D.D.D., Bruder P., Monteiro J.G.M-S., Jens C., Foss C., Hartono A., Svendsen H.F., 2014a. VLE data and modelling of aqueous N-methyl-1,3-diaminopropane (MAPA) solutions. To be submitted to Chemical Engineering Journal.

(45) Pinto, D.D.D., Zaidy, S.A.H., Hartono A., Svendsen H.F., 2014. Preliminary evaluation on a phase change solvent for CO_2 capture: Absorption and desorption tests. Submitted to International Journal of Greenhouse Gas Control.

(46) Aronu, U.E., Hartono, A., Svendsen, H.F., 2011. Kinetics of carbon dioxide absorption into aqueous amine amino acid salt: 3-(methylamino)propylamine/sarcosine solution. Chemical Engineering Science 66, 6109-6119.

6. Summary and Recommendations

6.1 Summary

A de-mixing solvent system for CO_2 capture is invetigated in this work consisting of 2-(diethylamino)ethanol (DEEA) and 3-(methylamino)propylamine (MAPA). To develop this advanced solvent system, different types of experimental measurements were performed in the binary and ternary solutions of DEEA and MAPA, both unloaded and CO_2 loaded. Based on the generated experimental data and other data available from the literature, a thermodynamic model was developed for the de-mixing H_2O-DEEA-MAPA-CO_2 system and the two sub-systems, H_2O-DEEA-CO_2 and H_2O-MAPA-CO_2. The main conclusions of this work are highlighted below.

Freezing point depression (FPD) measurements were performed by using a modified Beckmann apparatus for the binary aqueous DEEA and MAPA solutions at different concentrations of amine and for the ternary aqueous DEEA-MAPA solutions for different molar ratios of DEEA/MAPA. FPD measurements were also made for the CO_2 loaded systems of different concentration of DEEA and MAPA solutions at varying CO_2 loadings. The measured data were compared with the results of monoethanolamine (MEA) and methyl diethanolamine (MDEA) as a reference. The experimental results indicate that the non-ideal behavior of DEEA is almost similar to that of MEA. However, MAPA shows a stronger non-ideal behavior compared to DEEA and MEA. A correlation for the freezing points as a function of solution composition was formulated for the unloaded binary and ternary systems.

Differential heat of absorption of CO_2 in 5 M DEEA, 2 M MAPA, 1 M MAPA, 5 M DEEA + 2 M MAPA (5D2M), and 5 M DEEA + 1 M MAPA (5D1M) were measured as a function of temperature and CO_2 loading in a commercially available calorimeter. The last two mixtures were characterized as de-mixing solutions at certain concentrations of carbon dioxide. The measurements were performed isothermally at three different temperatures 40, 80, and 120 ^{o}C, and varying CO_2 loadings. The measured differential heat of absorption values were converted into integral values by integration. All the measured heats of absorption data were compared with 30 mass % MEA as a reference case. 5 M DEEA showed a lower heat of absorption compared to 30 mass % MEA. 2 M and 1 M MAPA solutions showed the heat of absorption values similar to that of 30 mass % MEA. Heats of absorption of CO_2 in the two de-mixing solutions, 5D2M and 5D1M, depend on CO_2 loading and composition of the constituent amines in the mixture.

Equilibrium total pressures were measured in binary aqueous solutions of 5 M DEEA, 2 M MAPA, and 1 M MAPA, and ternary aqueous solutions of 5D2M and 5D1M as a function of temperature and CO_2 loading by using a calorimeter as an equilibrium cell. The last two solvent mixtures were the de-mixing systems. For all the systems, equilibrium CO_2 partial pressures were calculated from the measured equilibrium total pressure data. All the measured data were compared with the results of 30 mass % MEA as a reference

case. 5 M DEEA showed a high CO_2 loading capacity at 40 ^oC and a very low loading capacity at 120 ^oC, thus giving a high CO_2 cyclic capacity. Both 2 M and 1 M MAPA showed high loading capacities at both 40 ^oC and 120 ^oC, thus giving a relatively lower cyclic capacity. The aqueous amine mixtures, 5D2M and 5D1M, gave fairly good cyclic capacities and their results depend on the concentration of the promoter (MAPA) in the mixtures.

Thermodynamic modeling of the de-mixing liquid-liquid phase change solvent system, H_2O-DEEA-MAPA-CO_2, and the two sub-systems, H_2O-DEEA-CO_2 and H_2O-MAPA-CO_2, was performed by using the Extended UNIQUAC thermodynamic model. Different types of experimental data measured in this work together with the data available from the literature were used to perform the parameter estimation. 94 model parameters and 6 thermodynamic properties were fitted to approximately 1500 experimental data consisting of pure amine vapor pressure, vapor-liquid equilibrium, solid-liquid equilibrium, liquid-liquid equilibrium, excess enthalpy, and heat of absorption of CO_2 in aqueous amine solutions. With a single unique set of parameters, the model developed in this work can reproduce almost all the binary, ternary, and quaternary data points and can describe all the data types satisfactorily for the H_2O-DEEA-CO_2, H_2O-MAPA-CO_2, and H_2O-DEEA-MAPA-CO_2 systems.

6.2 Recommendations

The work presented in this Ph.D. thesis is one of the initial studies conducted on the experimental measurements and thermodynamic modeling of the de-mixing CO_2 capture solvent systems consisting of DEEA and MAPA. Based on the experience of working with these solvent systems, this work can be extended further and several improvements in the current work and future developments can be made in different areas. Some of the recommendations related to the experimental and modeling work are briefly presented here.

As a starting point, the FPD measurements in the CO_2 loaded systems were only performed for the H_2O-DEEA-CO_2 and H_2O-MAPA-CO_2 systems at varying CO_2 loadings. These measurements can be extended to the de-mixing blends of H_2O-DEEA-MAPA-CO_2. It should be noted that these solvent systems have the de-mixing behavior only in a certain range of CO_2 loading and only for the aqueous amine blends in certain concentration ranges of DEEA and MAPA in the mixture. It would be of great worth if detailed investigations will be conducted to examine and understand the de-mixing behavior of these solvent systems. One way to conduct this study is to fully load the 5D2M system with CO_2 and then diluting this fully loaded solution with the original batch of the unloaded 5D2M solution to get samples with different CO_2 loadings. These samples can be examined for the two phases and freezing points can be measured. It can be a challenge to keep a homogeneous mixture of the two phases during freezing point measurements.

Since the DEEA-MAPA de-mixing system is a relatively new solvent system, only a small number of experimental data points were available for the thermodynamic modeling. Most of the VLE data in the loaded solutions are at high CO_2 partial pressures. The available CO_2 solubility data at low pressures has a large scatter in the data especially in the loaded MAPA solutions. For further development of this system as a potential candidate for CO_2 capture, it is suggested to generate more VLE data with high accuracy at low CO_2 partial pressures ranging between 1 to 20 kPa (CO_2 partial pressure in the flue gas at absorber conditions is approximately 3-15 kPa depending upon the source of flue gas). For the de-mixing solvent

systems, it is also very important to have VLE study of the lower CO_2 rich phase. Such data can help in improving the thermodynamic model used under the solvent regeneration conditions in the stripper.

Biphasic liquid-liquid phase split is a key property of the DEEA-MAPA de-mixing solvent but only a few LLE data points were available for the thermodynamic modeling. There was also a large scatter in the measured LLE data. It is essential to produce a reasonable number of experimental LLE data with a high accuracy. It is also important to check the accuracy of the experimental tie-lines. The two possible ways are to perform either the LLE measurements or the vapor-liquid-liquid equilibrium (VLLE) measurements in a setup which allows the collection of samples from the two phases without contaminating them by keeping all the phases in equilibrium at the given experimental conditions. The collected samples should be refrigerated to ensure no evaporation of any component from the collected sample, especially CO_2.

The UNIQUAC model parameters (r, q, u_{ij}^{0}, and u_{ij}^{T}) for the six species $DEEA(aq)$, $DEEAH^{+}$, $MAPA(aq)$, $MAPAH^{+}$, $^{+}HMAPAH^{+}$, and $MAPACOO^{-}$ were determined in this work by fitting to the experimental data. Thermodynamic modeling of the H_2O-MAPA-CO_2 system showed relatively higher deviations between the measured and the calculated results of VLE and heat of absorption of CO_2. This might be due to absence of the protonated carbamate of MAPA ($^{+}HMAPACOO^{-}$) from the parameter estimation due to unavailability of the standard state thermodynamic property data. It may be interested to include $^{+}HMAPACOO^{-}$ in the parameter estimation with known thermodynamic property data to see any improvements in the model. Molar excess enthalpy and molar heat capacity data of DEEA were available from the literature and used in the modeling. But these data were not available for the MAPA. Measuring such thermal property data and including them in the modeling can also improve the model performance. Speciation data for the DEEA-MAPA de-mixing system was not found in the literature. It will also be worth measuring the speciation data and comparing it with the model calculated data.

Besides the experimental measurements and the thermodynamic modeling, it is also essential to test the DEEA-MAPA de-mixing blends in the pilot plant to evaluate different operational parameters and the energy performance against the reference 30 mass % MEA. From a process simulation point of view, the thermodynamic model developed in this work can be tested in a commercial simulator like Aspen Plus to check the performance of the model. Based on the results, further improvements in the model can be made. The work presented in this Ph.D. study can be a stepping stone for future development of the de-mixing DEEA-MAPA solvent system as a potential CO_2 capture solvent.

List of Publications

Journal Articles

1) Arshad, M. W.; Svendsen, H. F.; Fosbøl, P. L.; von Solms, N.; Thomsen, K. Equilibrium Total Pressure and CO_2 Solubility in Binary and Ternary Aqueous Solutions of 2-(Diethylamino)ethanol (DEEA) and 3-(Methylamino)propylamine (MAPA). *J. Chem. Eng. Data* 2014, 59 (3), 764-774.

2) Arshad, M. W.; Fosbøl, P. L.; von Solms, N.; Svendsen, H. F.; Thomsen, K. Heat of Absorption of CO_2 in Phase Change Solvents: 2-(Diethylamino)ethanol (DEEA) and 3-(Methylamino)propylamine (MAPA). *J. Chem. Eng. Data* 2013, 58 (7), 1974-1988.

3) Arshad, M. W.; Fosbøl, P. L.; von Solms, N.; Thomsen, K. Freezing Point Depressions of Phase Change CO_2 Solvents. *J. Chem. Eng. Data* 2013, 58 (7), 1918-1926.

4) Hartono, A.; Saleem, F.; Arshad, M. W.; Usman, M.; Svendsen, H. F. Binary and ternary VLE of the 2-(diethylamino)-ethanol (DEEA)/ 3-(methylamino)-propylamine (MAPA)/ water system. *Chem. Eng. Sci.* 2013, 101, 401-411.

5) Fosbøl, P. L.; Randi, N.; Arshad, M. W.; Tecle, Z.; Thomsen, K. Aqueous Solubility of Piperazine and 2-Amino-2-methyl-1-propanol plus Their Mixtures Using an Improved Freezing-Point Depression Method. *J. Chem. Eng. Data* 2011, 56 (12), 5088-5093.

Articles in Proceedings

1) Arshad, M. W.; von Solms, N.; Svendsen, H. F.; Thomsen, K. Heat of Absorption of CO_2 in Aqueous Solutions of DEEA, MAPA and their Mixture, *Energy Procedia* 2013, 37, 1532-1542.

2) Arshad, M. W.; Fosbøl, P. L.; von Solms, N.; Svendsen, H. F.; Thomsen, K. Equilibrium Solubility of CO_2 in Alkanolamines, *Energy Procedia* 2014, 51, 217-223.

Conference Contributions

1) Arshad, M. W.; Fosbøl, P. L.; von Solms, N.; Svendsen, H. F.; Thomsen, K. Vapor-Liquid Equilibrium of CO_2 with Aqueous Solutions of DEEA, MAPA and their Mixture, 2nd Post Combustion Capture Conference (PCCC-2), Bergen, Norway, September 2013. (Oral)

2) Arshad, M. W.; Fosbøl, P. L.; von Solms, N.; Svendsen, H. F.; Thomsen, K. Equilibrium Solubility of CO_2 in Alkanolamines, 7th Trondheim CCS Conference (TCCS-7), Trondheim, Norway, June 2013. (Poster)

3) Hartono, A.; Fahad. S.; Arshad, M. W.; Svendsen, H. F. Binary VLE of DEEA/H_2O, MAPA/H_2O and DEEA/MAPA Systems, 7th Trondheim CCS Conference (TCCS-7), Trondheim, Norway, June 2013. (Oral)

4) Arshad, M. W.; von Solms, N.; Svendsen, H. F.; Thomsen, K. Thermodynamics of Phase Change Solvents, CCS Conference, Antwerp, Belgium, May 2013. (Oral)

5) Arshad, M. W.; von Solms, N.; Svendsen, H. F.; Thomsen, K. Heat of Absorption of CO_2 in Aqueous Solutions of DEEA, MAPA and their Mixture, GHGT-11, Kyoto International Conference Center, Japan, November 2012. (Poster)

6) Fosbøl, P. L.; Arshad, M. W.; Thomsen, K. Equilibrium. Measurement and Modelling of the Piperazine Potassium Carbonate Solutions for CO_2 Capture, 18th Symposium on Thermophysical Properties, Boulder, CO, June 2012. (Oral)

7) Arshad, M. W.; Thomsen, K. Freezing Point Depression of Aqueous Solutions of DEEA, MAPA and DEEA-MAPA with and without CO_2 Loading, 2nd ICEPE (International Conference on Energy Process Engineering), Frankfurt am Main, June 2011. (Oral)

Journal of chemical & engineering data

Article

pubs.acs.org/jced

Freezing Point Depressions of Phase Change CO_2 Solvents

Muhammad Waseem Arshad, Philip Loldrup Fosbøl, Nicolas von Solms, and Kaj Thomsen*

Technical University of Denmark, Department of Chemical and Biochemical Engineering, Center for Energy Resources Engineering (CERE), Søltofts Plads Building 229, DK-2800 Kongens Lyngby, Denmark

ABSTRACT: Freezing point depressions (FPD) in phase change solvents containing 2-(diethylamino)ethanol (DEEA) and 3-(methylamino)propylamine (MAPA) were measured using a modified Beckmann apparatus. The measurements were performed for the binary aqueous DEEA and MAPA solutions, respectively, in the concentration ranges of (0 to 55) mass percent and (0 to 32.5) mass percent of amine. For the ternary aqueous DEEA−MAPA solutions, freezing points were measured for 5:1, 3:1, 1:1, 1:3, and 1:5 molar ratios of DEEA/MAPA. The FPD method was extended for easy and accurate measurement of freezing points in the CO_2 loaded systems. It is based on saturation of the solution by CO_2 and then dilution by using a batch of the original unloaded solution in order to get the solutions with different CO_2 loadings. Freezing point measurements were then carried out for (12, 20, 30, and 33) mass percent DEEA solutions and (10, 20, and 27) mass percent MAPA solutions at different CO_2 loadings. The apparatus and the experimental method used showed good repeatability and accuracy. The measured freezing point data were compared with monoethanolamine (MEA) and methyl diethanolamine (MDEA) found in the literature. The experimental values indicate that the DEEA−water interaction is almost similar to that of MEA−water interaction. MAPA has shown a stronger nonideal behavior compared to DEEA. A correlation for the freezing points as a function of solution composition was formulated for the unloaded binary and ternary systems.

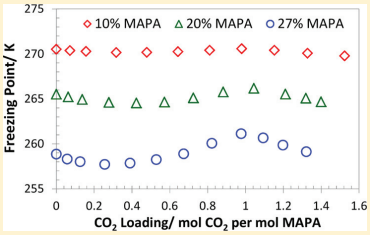

1. INTRODUCTION

Reactive absorption using amines is one of the most common industrial technologies available today for the postcombustion CO_2 capture. These processes have been considered as the most feasible route to capture CO_2 from power plant flue gases. This is due to their use in many industrial applications, such as CO_2 removal from reformer gases, acid gas removal from natural gas, etc.[1] The amine based scrubbing selectively removes CO_2 from the flue gases and releases a high-purity CO_2 offgas stream upon heating in a stripper column which is suitable for storage without any further treatment. However, the energy requirement for solvent regeneration is very high in these processes.[2,3] Therefore, the development of new solvent systems with improved energy efficiency, innovative process design, and technological improvements is necessary in order to reduce the high capital cost and energy requirements for the capture process.[4,5]

Primary and secondary amines are known for their fast reaction rates and high heat of reaction due to formation of carbamates with CO_2.[6] Consequently they require high energy for the reaction reversion. Tertiary amines, on the other hand, have low heat of reactions due to formation of bicarbonates by base catalysis of CO_2 hydration[7] and require relatively low energy for solvent regeneration. These amines generally have high CO_2 loading capacity and low reaction rate.[8,9] None of the amine types have ideal properties for CO_2 absorption, so mixed amine systems have become very popular in order to exploit the favorable properties of all types of amines.

A new set of solvents have recently emerged, which may be called phase change solvents. They have shown potential to reduce the energy requirements for solvent regeneration. These solvents either form precipitate, for example, the Alstom chilled ammonia (CAP) process[10] or form two liquid phases, for example, the DMX process[11] and thermomorphic biphasic solvents (TBS) systems.[12] The TBS solvent systems release the absorbed CO_2 in the desorber at a much lower temperature of 80 °C or even below, compared to the conventional aqueous alkanolamine solutions, which is typically 120 °C. They form two liquid phases during solvent regeneration and become one phase again during absorption and revert back to two phases upon heating and agitating in the desorber.[13−15] In the DMX process developed by IFP Energies nouvelles, on the other hand, the single phase solvent splits into two liquid phases after CO_2 absorption. The amine-rich phase with very low CO_2 loading recycles back to the absorber without regeneration and only the water-rich phase with very high CO_2 loading goes to the stripper for the thermal regeneration. Therefore, the energy consumption for solvent regeneration can be lowered due to reduced liquid flow rate in the stripper.[11]

Two different amines, 2-(diethylamino)ethanol (DEEA) and 3-(methylamino)propylamine (MAPA), are under investigation in this study. DEEA is a tertiary alkanolamine and MAPA has two amine functional groups, a primary and a secondary (see Figure 1). Therefore, we can exploit the favorable properties of amines by blending DEEA and MAPA. Their blends have an additional advantage of making liquid−liquid split when reacted

Received: December 12, 2012
Accepted: April 25, 2013
Published: May 22, 2013

dx.doi.org/10.1021/je3013167 | J. Chem. Eng. Data 2013, 58, 1918−1926

Journal of chemical & engineering data

Article

pubs.acs.org/jced

Heat of Absorption of CO_2 in Phase Change Solvents: 2-(Diethylamino)ethanol and 3-(Methylamino)propylamine

Muhammad Waseem Arshad,[†] Philip Loldrup Fosbøl,[†] Nicolas von Solms,[†] Hallvard Fjøsne Svendsen,[‡] and Kaj Thomsen[†,*]

[†]Department of Chemical and Biochemical Engineering, Center for Energy Resources Engineering (CERE), Technical University of Denmark, Søltofts Plads Building 229, DK-2800 Kongens Lyngby, Denmark

[‡]Department of Chemical Engineering, Norwegian University of Science and Technology (NTNU), NO-7491 Trondheim, Norway

ABSTRACT: Heat of absorption of CO_2 in phase change solvents containing 2-(diethylamino)ethanol (DEEA) and 3-(methylamino)propylamine (MAPA) were measured as a function of CO_2 loading at different temperatures using a commercially available reaction calorimeter. The tested systems were aqueous single amines (5 M DEEA, 2 M MAPA, and 1 M MAPA) and aqueous amine mixtures (5 M DEEA + 2 M MAPA and 5 M DEEA + 1 M MAPA) which give two liquid phases on reacting with CO_2. All parallel experiments have shown good repeatability. The measurements were taken isothermally at three different temperatures, (40, 80, and 120) °C. The measured differential heat of absorption values were converted into integral values by integration. Heats of absorption of CO_2 in aqueous single amines were affected by changing the solvent composition (large difference in concentrations) and CO_2 feed pressure simultaneously. In addition to these two parameters, it also depends on temperature and the type of amine used. Tertiary alkanolamine (DEEA) has shown greater dependency on these parameters compared to the diamine (MAPA) containing both primary and secondary amine functional groups. In aqueous amine mixtures, heats of absorption depend on CO_2 loading, temperature, and composition of the constituent amines in the mixture. All measured heat of absorption data were compared with 30 mass % MEA used as a base case.

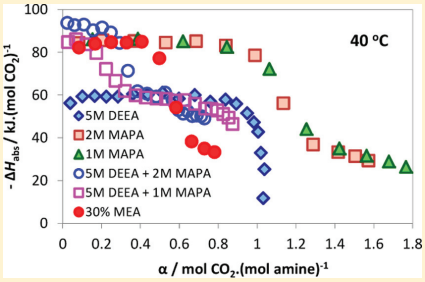

1. INTRODUCTION

Amine scrubbing is one of the most common postcombustion CO_2 capture technologies available today. Owing to its extensive use in different industrial applications, for example, CO_2 removal from reformer gases, natural gas sweetening etc.,[1] it has been considered as the most feasible route for the postcombustion capture. These amine scrubbing processes selectively absorb CO_2 from the flue gases and release a high-purity CO_2 offgas stream upon heating in a stripper which is suitable for storage without any further treatment. However, it is well-known that these processes are energy intensive.[2,3] Innovative process design and technological improvements are necessary in order to reduce the high capital cost and energy requirements for the capture processes.[4] Besides this, it is also essential to develop solvent systems with improved energy efficiency while retaining the desirable properties of fast reaction rate, high loading and cyclic capacities, low solvent degradation, low corrosiveness, and being environmental friendly, etc. For energy efficient solvent systems, besides reasonable heat of absorption, the equilibrium temperature sensitivity should also be high in order to reduce the need for stripping steam.[5]

Single amine solvent systems for CO_2 capture were extensively studied and reported in the open literature. Primary and secondary amines are very reactive toward CO_2 as they form carbamates. They have high heats of reaction and fast reaction rates.[6] Consequently, high energy is required for the solvent regeneration. Tertiary amines, on the other hand, form bicarbonates due to base catalysis of CO_2 hydration.[7] They have low heats of reaction leading to low energy requirements for the reaction reversion. These amines generally have high CO_2 loading capacity and a low reaction rate.[8,9] Each type of amine group is associated with its own merits and demerits. Therefore, amine blends have become an attractive choice to exploit the favorable properties of both amine types. Various amine blends (e.g., MEA + MDEA) have been studied and reported in the literature.[10,11]

Recently, a new class of mixed amine solvent systems is emerging, which may be called phase change solvents. They have shown a potential to reduce the solvent regeneration energy. These phase change solvents either form precipitates on CO_2 absorption such as the Alstom chilled ammonia process (CAP)[12] or make a liquid−liquid split, for example, the DMX process[13,14] and thermomorphic biphasic solvents (TBS) systems.[15] The TBS systems, after CO_2 absorption, regenerate at a relatively lower temperature of 80 °C compared to the regeneration temperature of conventional alkanolamine solutions (~120 °C).

Received: February 7, 2013
Accepted: May 30, 2013
Published: June 17, 2013

Journal of chemical & engineering data

Article

pubs.acs.org/jced

Equilibrium Total Pressure and CO_2 Solubility in Binary and Ternary Aqueous Solutions of 2-(Diethylamino)ethanol (DEEA) and 3-(Methylamino)propylamine (MAPA)

Muhammad Waseem Arshad,[†] Hallvard Fjøsne Svendsen,[‡] Philip Loldrup Fosbøl,[†] Nicolas von Solms,[†] and Kaj Thomsen*,[†]

[†]Department of Chemical and Biochemical Engineering, Center for Energy Resources Engineering (CERE), Technical University of Denmark (DTU), Søltofts Plads Building 229, DK-2800 Kongens Lyngby, Denmark

[‡]Department of Chemical Engineering, Norwegian University of Science and Technology (NTNU), NO-7491 Trondheim, Norway

ABSTRACT: Equilibrium total pressures were measured and equilibrium CO_2 partial pressures were calculated from the measured total pressure data in binary and ternary aqueous solutions of 2-(diethylamino)ethanol (DEEA) and 3-(methylamino)-propylamine (MAPA). The measurements were carried out in a commercially available calorimeter used as an equilibrium cell. The examined systems were the binary aqueous solutions of 5 M DEEA, 2 M MAPA, and 1 M MAPA and the ternary aqueous mixtures of 5 M DEEA + 2 M MAPA (5D2M) and 5 M DEEA + 1 M MAPA (5D1M), which gave liquid−liquid phase split upon CO_2 absorption. The total pressures were measured and the CO_2 partial pressures were calculated as a function of CO_2 loading at three different temperatures 40 °C, 80 °C, and 120 °C. All experiments were reproduced with good repeatability. The measurements were carried out for 30 mass % MEA solutions to validate the experimental method. All the measured data were also compared with the results of 30 mass % MEA as a reference case. 5 M DEEA has shown high cyclic capacity. Both 2 M and 1 M MAPA showed high loading capacities at 40 °C and 120 °C. The aqueous amine mixtures, 5D2M and 5D1M, gave fairly good cyclic capacities and their results depend on the concentration of the promoter (MAPA) in the mixture. Approximate enthalpies of absorption of CO_2 in all the tested aqueous amine systems were estimated from the CO_2 solubility data. The measured total pressure and the estimated CO_2 solubility data can be useful in thermodynamic modeling of the capture systems when aqueous DEEA−MAPA solutions are used as capture solvents.

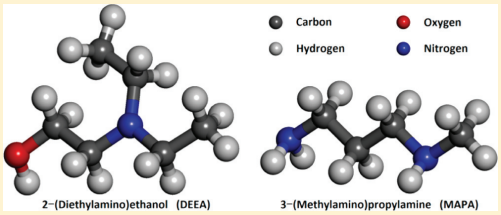

1. INTRODUCTION

Carbon dioxide (CO_2) is a well-known greenhouse gas and a major contributor to the global warming.[1] Fossil fuel based power generation is one of the major sources of CO_2 emissions worldwide.[2] The other large CO_2 emitting point sources are iron and steel industry, cement production plants, refineries, natural gas processing plants, and petrochemical production plants.[3] Carbon capture and storage (CCS) is considered as a potential solution to reduce the CO_2 emissions and to mitigate the climate change.[4] Among the available CCS technologies, the amine based absorption−desorption capture process is considered as the most mature technology due to its extensive use in different industrial application such as acid gas removal from natural gas.[5] This technology can be retrofitted to the existing power generation plants, and the techno-economic feasibility studies indicate that the technology will remain competitive in the coming future.[6,7] However, the major challenge with the amine scrubbing is the high energy requirements of the process.[8] Technical improvements in the capture process and improved process design are one way to reduce the high energy demand of the process, the other being the design of energy efficient solvent systems.[9]

On the basis of the characteristics of different groups of amines, several amine-based solvent systems have been studied and reported in the literature. A few examples are (a) aqueous single alkanolamine solutions such as primary (monoethanol-amine, MEA), secondary (diethanolamine, DEA), and tertiary (triethanolamine, TEA, and methyldiethanolamine, MDEA) alkanolamines,[5] (b) aqueous amine blends (tertiary amine blended with primary or secondary amines as a promoter such as MEA + MDEA and DEA + MDEA)[10] to exploit the favorable properties of different types of amines, and (c) sterically hindered amines[11] and cyclic amine (e.g., piperazine)[12] both as single aqueous solutions[13−15] or as a blend of both together[16−18] or a blend of each with other amines.[19−21] One of the basic purposes of these and many other studies reported in the literature is to get the best solvent system with the characteristics of high CO_2 loading and cyclic capacity, fast reaction kinetics, low heat of absorption, low thermal and chemical degradation, low corrosion tendency, environmentally benign, and possibility of operating at elevated

Received: October 4, 2013
Accepted: January 7, 2014
Published: February 3, 2014

Chemical Engineering Science 101 (2013) 401–411

Contents lists available at SciVerse ScienceDirect

Chemical Engineering Science

journal homepage: www.elsevier.com/locate/ces

Binary and ternary VLE of the 2-(diethylamino)-ethanol (DEEA)/3-(methylamino)-propylamine (MAPA)/water system

Ardi Hartono [a], Fahad Saleem [a], Muhammad Waseem Arshad [b], Muhammad Usman [a], Hallvard F. Svendsen [a,*]

[a] Department of Chemical Engineering, Norwegian University of Science and Technology, N-7491 Trondheim, Norway
[b] Technical University of Denmark, Søltofts Plads, 2800 Lyngby, Denmark

HIGHLIGHTS

- Binary, ternary VLE data measured for DEEA/H_2O, DEEA/MAPA and DEEA/MAPA/H_2O.
- Titration technique developed to quantify the DEEA/MAPA system.
- The UNIQUAC framework implemented and the parameters are fitted.
- Activity coefficients of DEEA/MAPA in ternary found lower than for binary systems.
- An inconsistency seen between water activity coefficients from VLE and SLE results.

ARTICLE INFO

Article history:
Received 22 April 2013
Received in revised form
21 June 2013
Accepted 28 June 2013
Available online 9 July 2013

Keywords:
VLE
Alkalinity
DEEA
MAPA
Absorption
Modeling

ABSTRACT

A mixed 2-(diethylamino)-ethanol (DEEA) and 3-(methylamino)-propylamine (MAPA) system could be an attractive alternative solvent to improve the performance of CO_2 capture for low partial pressure cases. This solvent has the advantages of forming two liquid phases upon CO_2 loading, one rich in CO_2 and the other very low in CO_2. Having a highly concentrated rich solvent improvements could be reached by reducing the sensible heat and improving the equilibrium sensitivity hence reducing the need for stripping steam. Also it is possible that the heat of absorption may change to the better.

To better understand this system in designing the separation unit requires substantial work on characterization of the solvent. One important aspect is to provide equilibrium data. In this work new ebulliometric VLE data for the binary DEEA/H_2O and DEEA/MAPA systems and the ternary DEEA/MAPA/H_2O system are reported at different temperatures and concentrations. Results show that pure MAPA is more volatile than DEEA, but in aqueous solution MAPA was found to be less volatile. A mix of DEEA and MAPA in aqueous solution tends to lower the volatility thus makes the system more advantageous by reducing volatility. The activity coefficients for the species in the ternary aqueous system are found to be lower than the activity coefficients obtained from the corresponding binary aqueous mixtures.

The UNIQUAC framework was implemented to represent the experimental data. The six UNIQUAC parameters were determined and were able to predict *P-T-x-y*, activity coefficient, excess enthalpy and freezing point depression for both the binary and ternary systems. However, a small inconsistency was observed between water activity coefficients determined from ebulliometer and freezing point depression measurements.

1. Introduction

Amine mixtures which potentially form two phases at higher CO_2 concentration have recently received attention as a CCS technology. The changes in technology comprises two major elements, solvent and process development. When two phases occur the regeneration heat requirement could be expected to be lower as only a lower phase, being a highly concentrated rich solvent is sent to the stripper and the sensible heat loss could be reduced. By forming a second phase the equilibrium temperature sensitivity could be improved thereby reducing the need for stripping steam and also the heat of absorption may be affected positively.

The DMX process by IFPEN is based on special solvents forming two immiscible phases and is now under testing in Italy (Raynal et al., 2011). This process is claimed to give a specific reboiler duty as low as 2.1 GJ/tonne CO_2 captured which is significantly lower than

* Corresponding author. Tel.: +47 73594100; fax: +47 73594080.
E-mail address: hallvard.svendsen@chemeng.ntnu.no (H.F. Svendsen).

0009-2509/$ - see front matter © 2013 Elsevier Ltd. All rights reserved.
http://dx.doi.org/10.1016/j.ces.2013.06.052

Available online at www.sciencedirect.com

SciVerse ScienceDirect

Energy Procedia 37 (2013) 1532 – 1542

Energy Procedia

GHGT-11

Heat of Absorption of CO_2 in Aqueous Solutions of DEEA, MAPA and their Mixture

Muhammad Waseem Arshad[a], Nicolas von Solms[a], Kaj Thomsen[a], Hallvard Fjøsne Svendsen[b,*]

[a]*Technical University of Denmark, Department of Chemical and Biochemical Engineering, Center for Energy Resources Engineering (CERE), Søltofts Plads Building 229, DK-2800 Kongens Lyngby, Denmark*
[b]*Norwegian University of Science and Technology (NTNU), Department of Chemical Engineering, NO-7491 Trondheim, Norway*

Abstract

A reaction calorimeter was used to measure the differential heat of absorption of CO_2 in phase change solvents as a function of temperature, CO_2 loading and solvent composition. The measurements were taken for aqueous solutions of 2-(diethylamino)ethanol (DEEA), 3-(methylamino)propylamine (MAPA) and their mixture. The tested compositions were 5M DEEA, 2M MAPA and their mixture, 5M DEEA + 2M MAPA which gives two liquid phases on reacting with CO_2. Experimental measurements were also carried out for 30% MEA used as a base case. The measurements were taken isothermally at three different temperatures 40, 80 and 120°C at a CO_2 feed pressure of 600 kPa. In single aqueous amine solutions, heat of absorption increases with increase in temperature and depends on the type of amine used. DEEA, a tertiary amine, has lower heat of absorption compared to MAPA being a diamine with primary and secondary amine functional groups. For amine mixtures, heat of absorption is a function of CO_2 loading and temperature. The heat of absorption against CO_2 loading depends on the composition of the amines in the mixture. All the measured data in this work were compared with 30% MEA at absorption (40°C) and desorption (120°C) conditions.

Selection and/or peer-review under responsibility of GHGT

Keywords: Heat of absorption; Calorimeter; Phase change solvents; CO_2 capture; DEEA; MAPA

1. Introduction

Carbon dioxide absorption using amines is the most common operation for CO_2 capture from power plant flue gases. The amine-based absorption processes selectively absorb CO_2 and release a high-purity

* Corresponding author. Tel.: +47 7359 4100; fax: +47 7359 4080.
E-mail address: hallvard.svendsen@chemeng.ntnu.no.

1876-6102
Selection and/or peer-review under responsibility of GHGT
doi:10.1016/j.egypro.2013.06.029

JOURNAL OF CHEMICAL & ENGINEERING DATA

ARTICLE

pubs.acs.org/jced

Aqueous Solubility of Piperazine and 2-Amino-2-methyl-1-propanol plus Their Mixtures Using an Improved Freezing-Point Depression Method

Philip Loldrup Fosbøl,* Randi Neerup, Muhammad Waseem Arshad, Zacarias Tecle, and Kaj Thomsen

Department of Chemical and Biochemical Engineering, Center for Energy Resources Engineering (CERE), Technical University of Denmark (DTU), Søltofts Plads, Building 229, DK-2800 Kongens Lyngby, Denmark

ABSTRACT: In this work the solid−liquid equilibrium (SLE) and freezing-point depression (FPD) in the electrolytic binary aqueous systems piperazine (PZ, CAS No. 110-85-0) and aqueous 2-amino-2-methyl-1-propanol (AMP, CAS No. 124-68-5) were measured. The FPD and solubility were also determined in the ternary AMP−PZ−H_2O system. A method was developed by which solubility can be determined at higher temperatures using the FPD setup. A total of 86 data points are listed in the full concentration range from (−35 to 90) °C. The solid phases piperazine hexahydrate ($PZ \cdot 6H_2O$), piperazine hemihydrate ($PZ \cdot 1/2H_2O$), and anhydrous PZ precipitated during the experiments. The data can be used in the formulation, prevention, or intentional formation of slurries in piperazine solvents for promoting CO_2 capture using absorption and desorption.

1. INTRODUCTION

CO_2 capture is an openly debated topic for carbon emission reduction to reduce pollution by greenhouse gases. Process streams containing carbon dioxide can be cleaned by absorption in aqueous liquid solvents. Amines, strong bases, or combination of the two are typically used as active components. The low heats of absorption and desorption are design criteria that reduce the cost of energy in regeneration of the solvent. This is obtained by using sterically hindered amines. The result is often slow reaction kinetics between the solvent and CO_2. Consequently piperazine (PZ) is being used in solution formulation to create an enhanced CO_2 capture solvent. PZ can be used with both amine and potash solutions (K_2CO_3) to increase the rate of absorption and thereby promote the CO_2 capture.

A lower PZ concentration was typically used in literature. Recently the scope has changed, and PZ is now being used at higher concentrations. On increasing the concentration, the solubility limit of PZ is being reached, especially during winter temperatures and even up to room temperature. The unexpected formation of slurries and solids downstream may create unforeseen process conditions, decrease efficiency, and create clogging which will result in unfortunate hazardous operations. In general it could be interesting to provoke the formation of CO_2 containing solids and thereby facilitate and increase the capacity of the capture solvent. CO_2 deprived solids are rarely preferable in terms of CO_2 capture.

The aim of this work is to determine the solid−liquid phase boundary in the two binary PZ−H_2O and AMP−H_2O systems and also in the ternary AMP−PZ−H_2O system. 2-Amino-2-methyl-1-propanol (AMP) is a sterically hindered amine. CO_2 absorption in AMP solutions can be promoted by adding PZ.

An additional goal of this work was to enhance the utilization of freezing-point depression (FPD) equipment developing a method for the purpose of studying solid−liquid equilibrium (SLE) behavior in solutions precipitating solids other than ice.

PZ is a compound which has a variety of applications; for example, it has been used for animal and human intake in the treatment of roundworm infections as an anthelmintic.[1,2]

The SLE phase boundaries of the aqueous PZ system were examined very early by Berthelot,[3] further by Rosso and Carbonnel,[4] and in summary by Carbonnel and Rosso.[5] Berthelot[3] stated the existence of the hexahydrate $PZ \cdot 6H_2O$, the hemihydrate $PZ \cdot 1/2H_2O$, and possibly a monohydrate. The differential scanning calorimetry (DSC) analysis by Rosso and Carbonnel[4] confirmed the formation of the following PZ solid hydrate phases, hexahydrate, hemihydrate, and anhydrous PZ with the equilibrium reactions:

$$PZ \cdot 6H_2O(s) \rightleftarrows PZ(aq) + 6H_2O(l) \quad (1)$$

$$PZ \cdot \frac{1}{2}H_2O(s) \rightleftarrows PZ(aq) + \frac{1}{2}H_2O(l) \quad (2)$$

$$PZ(s) \rightleftarrows PZ(aq) \quad (3)$$

Rosso and Carbonnel especially note that the system has two eutectic points, at −1 °C between ice and hexahydrate and at 33 °C between hexahydrate and hemihydrate, including a peritectic point at 58 °C at the intersection between hemihydrate and anhydrous PZ. The hexahydrate melts at 44 °C, and anhydrous PZ melts at 104 °C, as determined by Berthelot,[3] Schwarzenbach,[6] and Rosso and Carbonnel.[4] A more accurate anhydrous melting point was estimated by Witschonke[7] of (111.4 and 111) °C by Hetzer et al.,[8] which is in line with the chemical supplier of this work. Rosso and Carbonnel[4] present a

Special Issue: Kenneth N. Marsh Festschrift

Received: September 5, 2011
Accepted: November 8, 2011
Published: November 14, 2011

Available online at www.sciencedirect.com

ScienceDirect

Energy Procedia 51 (2014) 217 – 223

Energy Procedia

7th Trondheim CCS Conference, TCCS-7, June 5-6 2013, Trondheim, Norway

Equilibrium Solubility of CO_2 in Alkanolamines

Muhammad Waseem Arshad[a], Philip Loldrup Fosbøl[a], Nicolas von Solms[a], Hallvard Fjøsne Svendsen[b], Kaj Thomsen[a,*]

[a]*Technical University of Denmark, Department of Chemical and Biochemical Engineering, Center for Energy Resources Engineering (CERE), Søltofts Plads Building 229, DK-2800 Kongens Lyngby, Denmark*

[b]*Norwegian University of Science and Technology (NTNU), Department of Chemical Engineering, NO-7491 Trondheim, Norway*

Abstract

Equilibrium solubility of CO_2 were measured in aqueous solutions of Monoethanolamine (MEA) and *N,N*-diethylethanolamine (DEEA). Equilibrium cells are generally used for these measurements. In this study, the equilibrium data were measured from the calorimetry. For this purpose a reaction calorimeter (model CPA 122 from ChemiSens AB, Sweden) was used. The advantage of this method is being the measurement of both heats of absorption and equilibrium solubility data of CO_2 at the same time. The measurements were performed for 30 mass % MEA and 5M DEEA solutions as a function of CO_2 loading at three different temperatures 40, 80 and 120°C. The measured 30 mass % MEA and 5M DEEA data were compared with the literature data obtained from different equilibrium cells which validated the use of calorimeters for equilibrium solubility measurements.

Selection and peer-review under responsibility of SINTEF Energi AS

Keywords: Equilibrium CO_2 solubility; Vapor-liquid equilibrium; Calorimeter; Post-combustion capture; Alkanolamines; Monoethanolamine (MEA); *N,N*-diethylethanolamine (DEEA)

* Corresponding author. Tel.: +45 4525 2860; fax: +45 4588 2258.
E-mail address: kth@kt.dtu.dk

Selection and peer-review under responsibility of SINTEF Energi AS
doi:10.1016/j.egypro.2014.07.025

Center for Energy Resources Engineering
Department of Chemical and
Biochemical Engineering
Technical University of Denmark
Søltofts Plads, Building 229
DK-2800 Kgs. Lyngby
Denmark

Phone: +45 4525 2800
Fax: +45 4525 4588
Web: www.cere.dtu.dk

ISBN : 978-87-93054-55-4